UNIVERSITY OF HAWAI'I AT MĀNOA

School of Ocean and Earth Science and Technology
Hawai'i Natural Energy Institute

January 10, 2007

Dr. Michele L. Anderson
Code 331
Office of Naval Research
875 N. Randolph Street
One Liberty Center
Arlington, VA 22203-1995

Dear Dr. Anderson:

Re: Final Technical Report: HEET Initiative: Grant N00014-04-1-0682

Enclosed you will find a copy of the Final Technical Report for the subject grant, titled Hawaii Energy and Environmental Technologies (HEET) Initiative. Also enclosed is a completed form SF 298.

The DD 882 Report of Inventions and Subcontracts is being sent to appropriate parties under separate cover.

Thank you for your support of this work.

Sincerely yours,

Richard E. Rocheleau
Principal Investigator

Enclosure: Final Technical Report (with 4 Appendices/Attachments)
SF 298

c: Defense Technical Information Center (report + SF 298) ✓
Naval Research Laboratory, Code 5227 (report + SF 298)
ONR Regional Office Seattle (DD 882)
Office of Naval Research, Attn: ONR 00CC (DD 882)

REPORT DOCUMENTATION PAGE

Form Approved
OMB No. 0704-0188

The public reporting burden for this collection of information is estimated to average 1 hour per response, including the time for reviewing instructions, searching existing data sources, gathering and maintaining the data needed, and completing and reviewing the collection of information. Send comments regarding this burden estimate or any other aspect of this collection of information, including suggestions for reducing the burden, to Department of Defense, Washington Headquarters Services, Directorate for Information Operations and Reports (0704-0188), 1215 Jefferson Davis Highway, Suite 1204, Arlington, VA 22202-4302. Respondents should be aware that notwithstanding any other provision of law, no person shall be subject to any penalty for failing to comply with a collection of information if it does not display a currently valid OMB control number.

PLEASE DO NOT RETURN YOUR FORM TO THE ABOVE ADDRESS.

1. REPORT DATE *(DD-MM-YYYY)*	2. REPORT TYPE	3. DATES COVERED *(From - To)*
08-31-2006	Final Technical Report	06-15-04 to 06-30-06

4. TITLE AND SUBTITLE

Hawaii Energy and Environmental Technologies (HEET) Initiative
Phase 4

5a. CONTRACT NUMBER

5b. GRANT NUMBER

N00014-04-1-0682

5c. PROGRAM ELEMENT NUMBER

6. AUTHOR(S)

Rocheleau, Richard E.

5d. PROJECT NUMBER

05PR10625-00

5e. TASK NUMBER

5f. WORK UNIT NUMBER

7. PERFORMING ORGANIZATION NAME(S) AND ADDRESS(ES)

University of Hawaii
2530 Dole Street, Sakamaki D200
Honolulu, HI 96822

8. PERFORMING ORGANIZATION REPORT NUMBER

9. SPONSORING/MONITORING AGENCY NAME(S) AND ADDRESS(ES)

Office of Naval Research
Reeional Office Seattle
1107 NE 45th Street, Suite 350
Seattle, WA 98105-4631

10. SPONSOR/MONITOR'S ACRONYM(S)

ONR

11. SPONSOR/MONITOR'S REPORT NUMBER(S)

12. DISTRIBUTION/AVAILABILITY STATEMENT

Approved for public release; distribution is unlimited.

13. SUPPLEMENTARY NOTES

In addition to the primary Final Technical Report with 64 pages, attached are four Appendices with 192 pages total.

14. ABSTRACT

This report summarizes work conducted by the Hawaii Natural Energy Institute of the University of Hawaii under the Hawaii Energy and Environmental Technologies (HEET) Initiative funded through the Office of Naval Research. This initiative focused on critical technology needs associated with the exploration and utilization of seabed methane hydrates and the development and testing of advanced fuel cells and fuel cell systems. The efforts in methane hydrates comprised four primary components: laboratory and analytical investigations of hydrate destabilization phenomena, characterization of the microbial community in marine hydrate beds, engineering development of subsea power generation systems utilizing seafloor methane, and promotion of international R&D partnerships. In the fuel cell area, the major accomplishment was the addition of three new fuel cell test cells to the Hawaii Fuel Cell Test Facility to augment existing capabilities to include fuels purity studies and hardware-in-the-loop testing. In addition, simulation work encompassed evaluation of a fuel cell energy/power system for propulsion of an unmanned underwater vehicle.

15. SUBJECT TERMS

Fuel Cells, Fuel Cell Testing, Fuel Processing and Gas Conditioning for Hydrogen Production, Fuels Purity, Methane Hydrates

16. SECURITY CLASSIFICATION OF:			17. LIMITATION OF ABSTRACT	18. NUMBER OF PAGES	19a. NAME OF RESPONSIBLE PERSON
a. REPORT	b. ABSTRACT	c. THIS PAGE			Yaa-Yin Fong, Director of Research Services
U	U	U	UU	256	19b. TELEPHONE NUMBER *(Include area code)* (808) 956-9081

FINAL TECHNICAL REPORT

Hawaii Energy and Environmental Technologies (HEET) Initiative – Phase 4

Office of Naval Research

Grant Number N00014-04-1-0682

For the period June 15, 2004 to June 30, 2006

Hawaii Natural Energy Institute

HNEI
HAWAII NATURAL ENERGY INSTITUTE

School of Ocean and Earth Science and Technology
University of Hawaii at Manoa

August 2006

Table of Contents

Final Technical Report for the Hawaii Energy and Environmental Technologies (HEET) Initiative – Phase 4
Grant Number N00014-04-1-0682
(June 15, 2004 to June 30, 2006)

1. Executive Summary

This report summarizes work conducted under Grant Number N00014-04-1-0682, the Hawaii Energy and Environmental Technologies (HEET) Initiative, funded through the Office of Naval Research to the Hawaii Natural Energy Institute (HNEI) of the University of Hawaii. The work reported here under this initiative, focused on critical technology needs associated with the development and testing of advanced fuel cells and fuel cell systems, and the exploration and utilization of seabed methane hydrates, represents the second award of this title.

Major accomplishments under the first award, Grant Number N00014-01-1-0928, included the planning, design and construction of the Hawaii Fuel Cell Test Facility, which opened in May 2003 with three full-size test stands for PEM fuel cells. Under the first award, HNEI, in partnership with industry, established test protocols and conducted a variety of long-term durability studies. HNEI also procured subscale fuel cells for use in the characterization of the effects of hydrogen fuel contaminants on fuel cell performance. The methane hydrates activities under the first agreement included studies to characterize hydrate thermochemistry and kinetics, hydrate microbiology and development of international collaborations.

Under this agreement (N00014-04-1-0682), HNEI expanded its test capabilities with the addition of three new fuel cell test stands at the Hawaii Fuel Cell Test Facility (HFCTF). Two of the new test stands were Greenlight Power Technologies G50 units for use in the fuels purity studies. Detailed test protocols to assess the effects of trace contaminants on PEM fuel cell performance were developed and validated using subscale hardware provided by GM and Ballard Power Systems. A high resolution GC with automated sampling was implemented to allow in-situ analysis of gases into and out of the fuel cell. Initial testing was conducted using aromatic hydrocarbons (benzene and toluene) as well as CO. The remaining test stand was a specialized FuelCon Systems Inc. C100 Evaluator with dynamic capabilities for use in developing the Hardware-in-the-Loop testing system.

In addition to installation and commissioning of the test stands, HNEI also developed and validated an MEA fabrication laboratory to support the existing fuel cell assembly laboratory.

Hardware-in-the-Loop (HiL) development at HNEI was launched with installation of the FuelCon C100 fuel cell test station. This test stand was utilized in testing a 100 cm^2 fuel cell via a fuel cell vehicle simulation program in the HiL mode. Refinement and modification of the test stand is continuing, to improve performance and yield better dynamic operation. Simulation efforts were advanced with the modeling and simulation of a fuel cell energy/power system (FCEPS) for use in an Unmanned Underwater Vehicle (UUV). The simulation tool was run using a duty cycle from the Japanese UUV, the URASHIMA. In addition, an evaluation and technical screening was conducted, for

application of an FCEPS to the propulsion of a UUV. This assessment supports the expectation that an FCEPS has the potential to significantly increase the energy storage in a UUV, compared with battery-based propulsion systems.

In support of finding alternative fuel supplies, HNEI has expended continuing efforts in the area of fuel processing and gas conditioning for hydrogen production. This work was based on the potential use of crude glycerin, a byproduct of biodiesel production. The automated lab-scale fuel processing system completed earlier was used to investigate the conversion of glycerin into hydrogen. Work was done with crude and chemical-grade glycerin as well as chemical-grade glycerin doped with contaminants representative of the biodiesel production process. A test stand for removal of sulfur contaminants from gas streams was designed and fabricated.

In addition to work with traditional PEM fuel cells, HNEI has also continued research on novel fuel cell components. One area involves the use of biocarbons (carbonized charcoal produced from biomass) in fuel cell bipolar plates. Specialized biocarbons were prepared from a wide variety of biomass substrates, including some doped with boron and phosphorous. These prepared biocarbons were characterized with a host of analysis methods. One method, in particular, revealed (for the first time) the existence of two classes of biocarbons, those that evolve CO at high temperatures and those that do not. Another area is enzymatic bio-fuel cells. Such fuel cells can complement traditional cells that use expensive platinum-based catalysts. Currently, bio-fuel cells suffer low power generation and short life in enzyme stability. To better understand these limitations, we focused on development and utilization of a suite of characterization techniques to analyze cell performance and facilitate optimization of power generation. Results of these efforts have led to paper publications, invited presentations, and extension of collaborations with other laboratories and industries, in leveraging two extramurally funded projects by the U.S. Air Force Office of Scientific Research (AFOSR) Multi-University Research Initiative (MURI) and the Director of Central Intelligence Postdoctoral Research Program, respectively.

HNEI's activities in the area of methane hydrates comprised four primary components: laboratory and analytical investigations of hydrate destabilization phenomena, characterization of the microbial community in marine hydrate beds, engineering development of subsea power generation systems utilizing seafloor methane, and promotion of international R&D partnerships.

During the present reporting period, the first phase of experiments employing the new hydrate destabilization facility were completed. The objective of these experiments was to explore the mechanism of hydrate decomposition induced by chemical reagents. The data were interpreted with a one-dimensional time-domain model of hydrate sample dissociation that we developed applying the concept of an intrinsic dissociation rate proposed previously by other researchers. An initial comparison raises questions about the underlying formalism of the model. These questions, along with improvements to the experiment and additional tests, will be pursued in the future. The destabilization kinetics studies are being supplemented by thermochemistry experiments performed with the Calvet-Tien calorimeter. The major accomplishment during the present reporting period was the design and fabrication of a novel fiberoptic probe and associated components that will be used to identify the phases or compounds existing within the

calorimeter sample cell using Raman spectroscopy. This information will be correlated with the thermograms. Assembly and testing of the fiberoptic probe system will begin in September 2006.

In cooperation with the Naval Research Laboratory, the molecular biological studies of hydrate sediments were continued. Our primary interest lies in identifying the microbial consortium and metabolic pathways responsible for the sudden depletion of porewater methane just below the seafloor. This has significant environmental implications, since it controls the leakage of methane into the water column. Push core samples from the Gulf of Mexico and offshore New Zealand were collected and are undergoing analysis.

The engineering development of subsea power generation systems focused on investigations of sulfur to sulfite and sulfite to sulfate oxidation reactions. These reactions are critical to the operation of a seafloor sedimental microbial fuel cell. Re-analysis of our existing microbial fuel cell data and new calculations indicate that an alternative electrolyte system of seawater and Nafion membrane could reduce inter-electrode resistance by a factor of 30, with an associated improvement in performance. Reactors testing this seawater/Nafion electrode system are being fabricated.

Finally, HNEI was again a sponsor and member of the organizing committee of the 4th International Workshop on Methane Hydrates that took place in Victoria, British Columbia, Canada on 9-11 May 2005. This conference was attended by approximately sixty participants from the U.S., Canada, Japan, the UK, Norway, Chile, Germany, and New Zealand. One outcome of this workshop was a collaboration that resulted in an oceanographic research cruise in late June 2005 to explore hydrates on the Hikurangi Margin offshore the North Island of New Zealand. HNEI researchers participated in this cruise and collected samples for analysis. The 5th International Workshop is scheduled for 9-12 October 2006 in Edinburgh, Scotland.

This page is intentional blank

2. Introduction

The Hawaii Energy and Environmental Technologies (HEET) Initiative, funded to the Hawaii Natural Energy Institute (HNEI) of the University of Hawaii through the Office of Naval Research (ONR), was initiated in the summer of 2001 under Grant Number N00014-01-1-0928 to address critical technology needs associated with the exploration and utilization of seabed methane hydrates and the development and testing of advanced fuel cells and fuel cell systems. During the first three years of operation, the focal point of our activity was development of the Hawaii Fuel Cell Test Facility (HFCTF) which houses dual facilities for fuel cell testing and for the synthesis and characterization of methane hydrates. This program ended March 31, 2005.

Concurrently, a new program under Grant Number N00014-04-1-0682 was initiated (June 15, 2005) with an end date of June 30, 2006. This Final Technical Report covers the work accomplished under the latter award during the period June 15, 2004 through June 30, 2006.

The efforts covered in this phase are for the task areas of fuel cell systems and methane hydrates. Within the fuel cell systems area were four major subtasks: PEM fuel cell testing and component development; fuel cell Hardware-in-the-Loop (HiL) and system simulation development; fuel processing and gas conditioning for hydrogen production; and novel fuel cell and component development. The area of methane hydrates included four major subtasks: continued international partnership development; seafloor methane hydrate destabilization studies; microbial characterization; and seafloor methane hydrate analysis for *in situ* power generation.

The remaining two sections of this report focus on each of the major areas covered within the HEET initiative. Section 3 is on fuel cell systems, with subsections for each of the associated subtasks for this area. Section 4 covers methane hydrates, including subsections for the subtasks of this area.

This page is intentional blank

3. Fuel Cell Systems

3.1 Objectives

Under this Grant, HNEI expanded on the testing and research capabilities of the Hawaii Fuel Cell Test Facility. Specific focus areas for the fuel cell systems task included infrastructure to allow accelerated life testing of PEM fuel cells under H_2/O_2 operating conditions; infrastructure to allow characterization of the effects of trace impurities; continuing effort in the area of novel fuel cells; development of Hardware-in-the-Loop (HiL) capabilities for evaluating fuel cells under simulated real-world operating conditions; and continuing work on fuel processing and gas conditioning research.

This task area was organized into four major subtasks: PEM fuel cell testing and component development; fuel cell HiL and system simulation development; fuels processing and gas conditioning for hydrogen production; and novel fuel cell and component development. Details for the activities conducted under each of these subtasks are given below.

3.2 PEM Fuel Cell Testing and Component Development

Primary activities in this area included the installation and validation of two Greenlight GLP 50 test stands, modification of the existing UTC XT-800 test stands, installation and operation of the FuelCon Hardware-in-the-Loop apparatus, and improvement of the infrastructure (ventilation, gas lines, etc) to accommodate the expanded testing.

3.2.1 Test Stands/Infrastructure Upgrades

Under the prior agreement, specifications were developed for purchase of two Greenlight GLP 50 Fuel Cell Test Stands (see Final Technical Report Grant No. N00014-01-1-0928). Under the current agreement, these stands were purchased, installed into the facility, and the performance validated against in-house and commercial fuel cell tests. Since final validation, these stands have largely been used to conduct studies to characterize the effects of trace impurities on the performance of PEM fuel cells.

With increased use of the subscale fuel cells, we also found it valuable to modify one of the UTC XT-800 test stands to allow subscale (50 to 100 cm^2) testing. Modifications included installation of a parallel lower-capacity humidifier compatible with reduced gas flows, additional lower-capacity flow-meters, and a back pressure regulation system to allow operation from ambient up to 60 psig outlet from the fuel cell.

Finally, the remaining XT-800 test stands were modified to increase their capability for transient testing for durability studies. In one stand, the software was modified to allow quick load changes to simulate transient vehicle operation such as bus cycles. In the final test stand, additional cooling was installed, allowing transient temperature operation between 10 °C and 80 °C. This latter protocol was established as part of an accelerated test program on advanced seals funded under a separate Navy effort (via UTC Fuel Cells).

As part of the effort to increase the number and type of test stands, it was also necessary to upgrade certain features of the facility. Modifications to the infrastructure included expansion of the ventilation (following the same design rules as used for the initial design), installation of additional gas lines to each of the new test stands, and upgrades to the air conditioning to maintain the laboratory environment with the increased load.

During installation of the test stands and infrastructure, we also upgraded our gas analysis capabilities in anticipation of increased emphasis on the role of trace impurities under real-world operating conditions. The gas analyzer selected was a custom-built instrument configured according to specifications identified by HNEI. The analyzer consists of two Varian Model CP-3800 Gas Chromatographs™, fully automated valving and an automated stream selector valve allowing sampling from 31 different ports. The fully automated valving and use of the Varian® Star Workstation™ enable continuous unattended process sampling.

The gas sample is introduced into fixed-volume sample loops and then directed towards separation columns for the required chromatography before entering the detectors. The set-up is as shown in Figure 3.2-1 below.

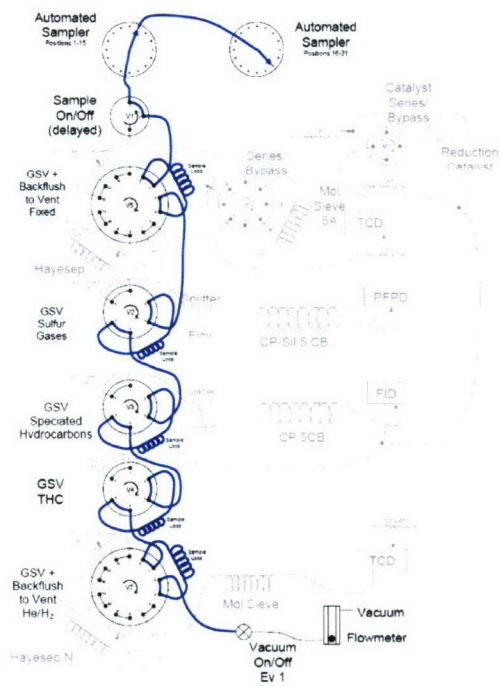

Figure 3.2-1. Upgraded gas analysis set-up.

The detectors include two thermal conductivity detectors (TCDs), a pulsed flame photometric detector (PFPD), a flame ionization detector (FID) and a pulsed Helium discharge ionization detector (PDID) that can be operated either in a universal or

selective mode. The analyzer is designed to load one sample and analyze the sample either simultaneously with all five detectors or only with a user-selected detector. For additional analysis an Agilent® Gas Chromatography / Mass Spectrometer (HP 6890 GC & 5972 MS) is also available. The GC/MSD is comprised of a HP 6890 GC interfaced to a HP 5972 Mass Selective Detector Quadrupole Mass Spectrometer. The system uses electron impact (EI) ionization and is capable of performing full mass scans or selective ion monitoring (SIM) to allow detailed chemical analysis including isotope labeling experiments.

3.2.2 Cell and Component Testing

Cell testing during this period mainly involved efforts to validate protocols for testing of the effects of trace contaminants in fuel cells and collection of initial data on two different aromatic hydrocarbons and CO at several levels.

During this program, HNEI developed test protocols for characterizing impurities which were based, in large part, on the single cell test protocols published by the US Fuel Cell Council. Figure 3.2-2 shows schematically the approach for contaminant introduction and gas sampling.

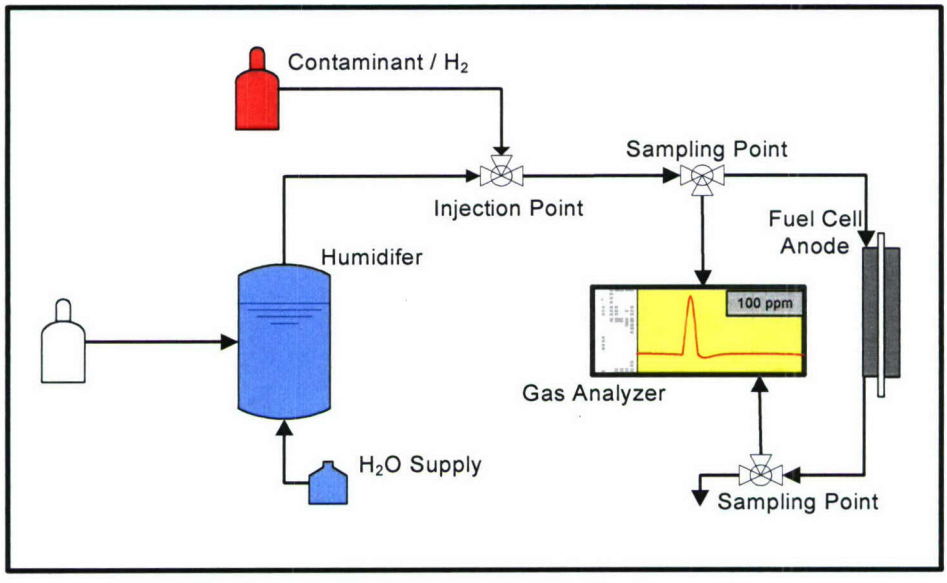

Figure 3.2-2. Schematic of contaminant injection and sampling.

During contaminant testing, hydrogen with a well-defined concentration of contaminant is introduced into a high purity hydrogen stream downstream from the humidifier. Introduction of the contaminant downstream of the humidifier minimizes the potential for absorption of the contaminant in the water at the humidifier. Humidifier temperature is adjusted to insure the desired value in the mixed stream. Fuel composition is sampled just prior to introduction into the cell (to confirm the mix ratio) and again at the outlet of

the cell to characterize adsorption or reaction of the impurity in the fuel cell. A standard test consists of:

Beginning-of-test diagnostics to define fuel cell characteristics,
Short term testing with pure hydrogen to characterize daily degradation,
Short- or long-term testing with contaminant in the fuel stream, and
End-of test diagnostics to characterize changes in fuel cell performance.

During this period there was substantial effort to insure that HNEI cell build procedures were consistent with industry. Figure 3.2-3 shows one such comparison. These results, obtained using subscale test hardware provided by Ballard Power Systems (BPS), compares performance of a fuel cell built by BPS personnel (Cell A) with an identical cell build by HNEI personnel (Cell B).

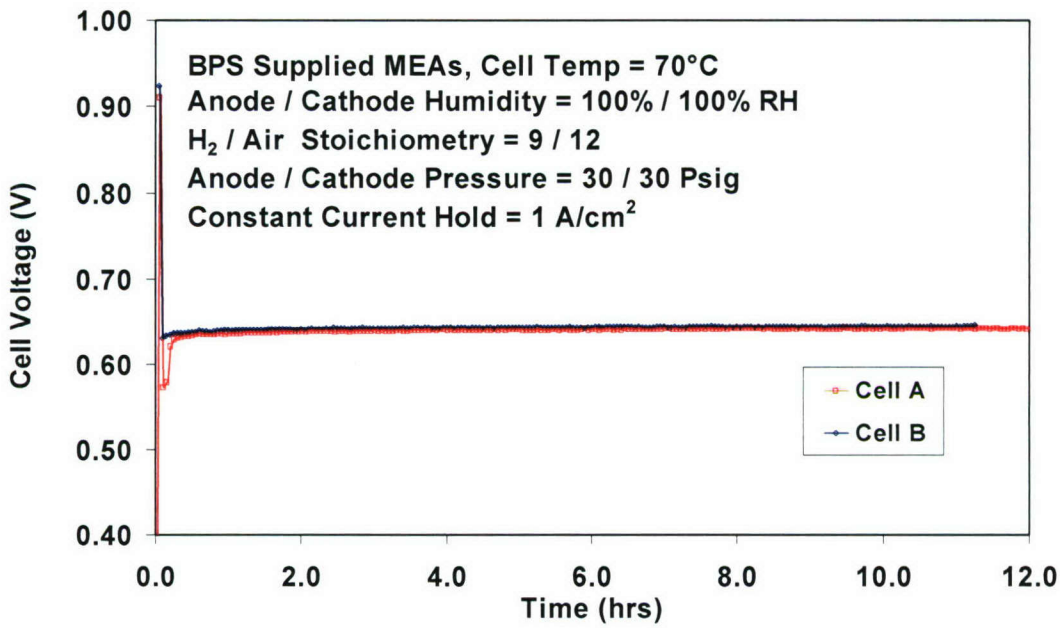

Figure 3.2-3. Comparison of cells built by OEM and HNEI.

During development of the protocols, various tests were also conducted to insure that partial bypass of the hydrogen stream did not, by itself, affect cell performance. Figure 3.2-4 (on the next page) shows results of one such test, comparing the degradation of the cell during the initial phase of the test, with and without a portion of the hydrogen bypassing the humidifier. These tests have been conducted using various sets of hardware. The results shown in Figure 3.2-4 were obtained using the BPS hardware.

During the period covered by this Grant, a number of tests were conducted to validate the test protocols and our ability for on-line sampling during extended runs. These initial validations were conducted with contaminants introduced through the fuel side. A number of 'typical results are presented below.

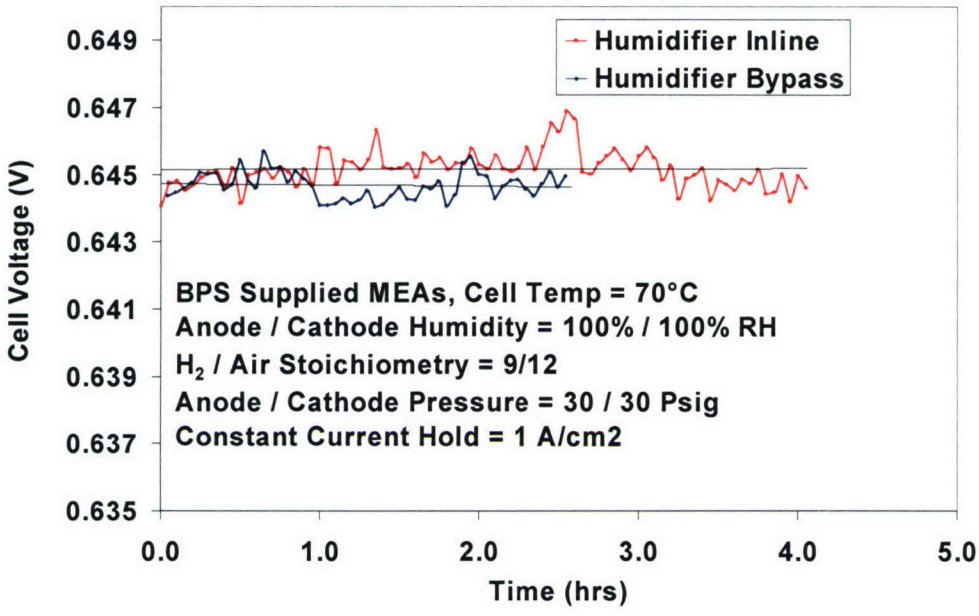

Figure 3.2-4. Cell performance with and without partial hydrogen bypass.

Figure 3.2-5 shows the effect of various concentrations of CO on cell performance. As expected, the rate and magnitude of the degradation increased with increasing CO concentration. These tests, conducted using subscale cells provided by GM, include a 10-hour period with no contaminant to validate the build and performance of this specific cell.

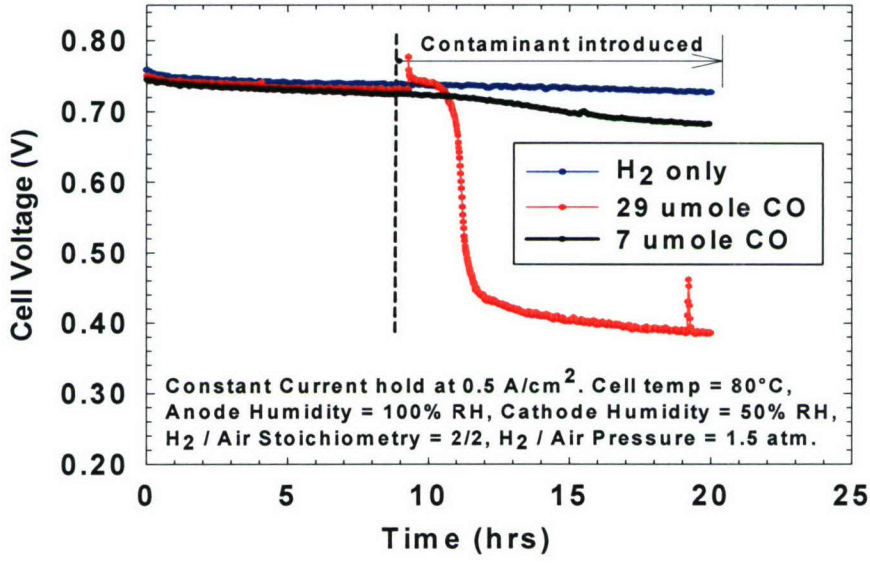

Figure 3.2-5. Effect of CO on fuel cell performance.

Figure 3.2-6 shows similar behavior with 29 ppm CO introduced into a BPS cell. This figure also shows the rapid recovery of the cell once the contaminant introduction is stopped.

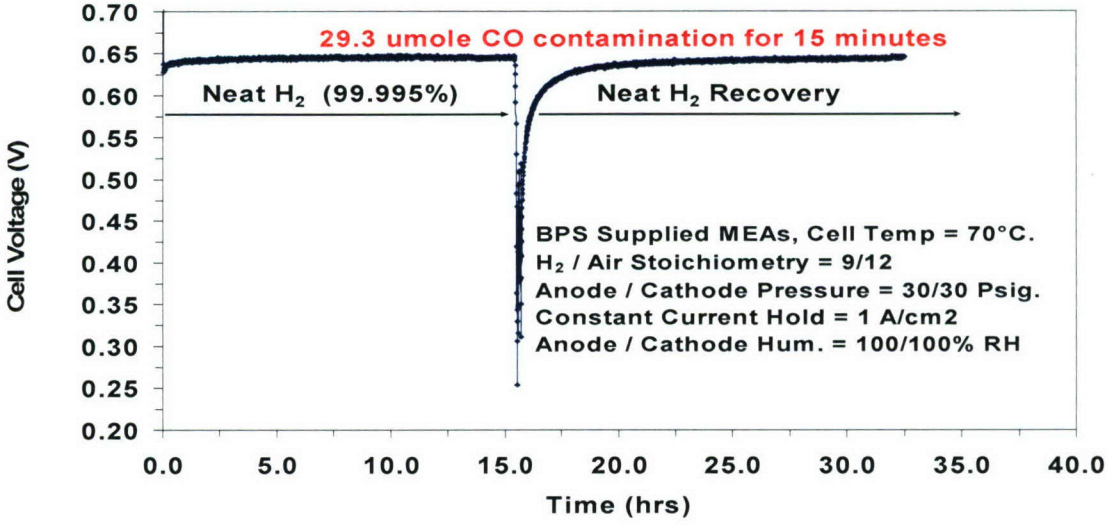

Figure 3.2-6. Effect of CO on performance of BPS subscale fuel cell.

Figure 3.2-7 shows results with even lesser amounts of CO, 1 ppm introduced into the cell. Significantly, this test which was conducted for over 100 hours includes on-line analysis of the fuel stream composition before (inlet) and after (outlet) the fuel cell. Efforts are currently underway to determine the cause of the relatively high CO^2 concentrations and to close the mass balances.

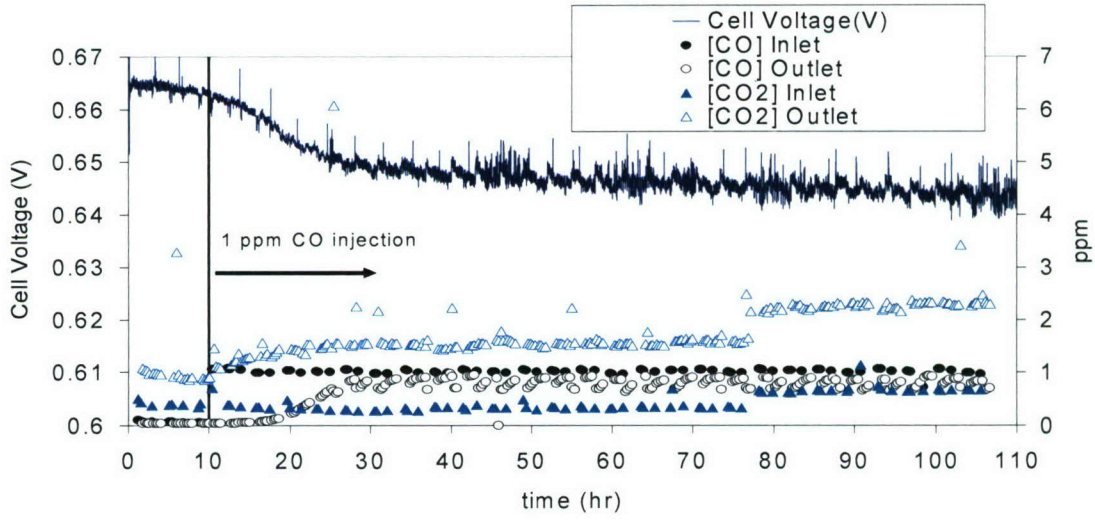

Figure 3.2-7. Effect of 1 ppm CO, with inlet and outlet measurements.

The U.S. Department of Energy has also now established a program to characterize the effect of fuel side contaminants. HNEI expects to receive funding under this program. In the future, funds from the HEET award will be used primarily to develop and maintain infrastructure and to characterize the effects of air (cathode) contaminants. This work will begin under our new agreement which has been awarded.

3.2.3 MEA Fabrication Laboratory

During the past year, HNEI has successfully established the capacity to produce membrane electrode assemblies (MEAs). The model for the chosen MEA production process at HNEI was the MEA fabrication technology as used and developed at Los Alamos National Laboratory (LANL).

This technology entails the creation of a catalyst ink mixture. Standard ink composition used at HNEI for polymer electrolyte fuel cell (PEFC) applications contains 20% platinum on carbon (Pt/C) and 5% Nafion solution (1100 EW) in a weight ratio of 5:2, and tetrabutylammonium hydroxide (TBA-OH). The catalyst ink mixture is coated on a hot press transfer substrate, which is an intermediate carrier material referred to as a 'decal.' Presently, HNEI applies the catalyst layers by hand painting. This coating technique allows for minimal material waste, flexible choice of electrode size and shape, and the application of a very broad range of adjustable catalyst loadings. The target catalyst ink loading of this technology can be adjusted from approximately 0.05 - 0.8 mg Pt/cm^2. The desired loading is reached by stepwise manual application of the ink with subsequent drying and weighing of the catalyst material. A successive hot pressing step permanently transfers the created electrode layer on a Nafion membrane. See Figure 3.2-8 on the next page for a view of the MEA formed after hot pressing. Final steps in this production process is a proton exchange step of the MEA in sulfuric acid of low molarity, and an MEA drying step on a vacuum hotplate. See Figure 3.2-9 on the next page for the overall fabrication process.

Establishing the MEA fabrication laboratory at HNEI involved supplementation of the existing laboratory setup. Several pieces of equipment were either purchased according to stringent specifications or designed and machined in house, considering the specific needs of the desired operation. The laboratory now possesses equipment and material to produce MEAs for PEFC applications ranging from 5 – 600 cm^2. The list of equipment includes: (i) a manual 50-ton hot press with 18.5" x 18.5" precision platens of high parallelism (see Figure 3.2-9 on the page following the next one), (ii) a manual 12-ton hot press with 12" x 12" platen size, (iii) a precision balance with 0.1 mg accuracy, (iv) a high-volume convection oven (5.4 cu.ft.), (v) a fume hood, (vi) two vacuum hotplates, (vii) several single and a multiple stir plates, and (viii) a DI-water system.

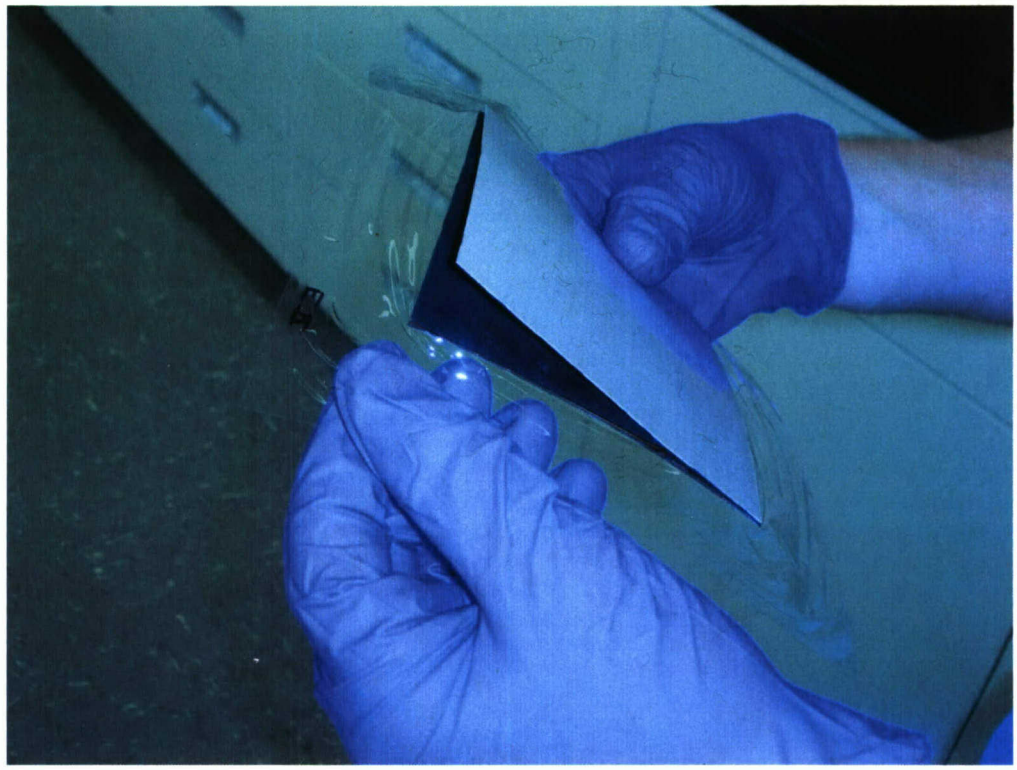

Figure 3.2-8. During the hotpressing step, the catalyst layer is transferred to the membrane, forming an MEA. The decal material is carefully removed from the assembly of electrodes and membrane.

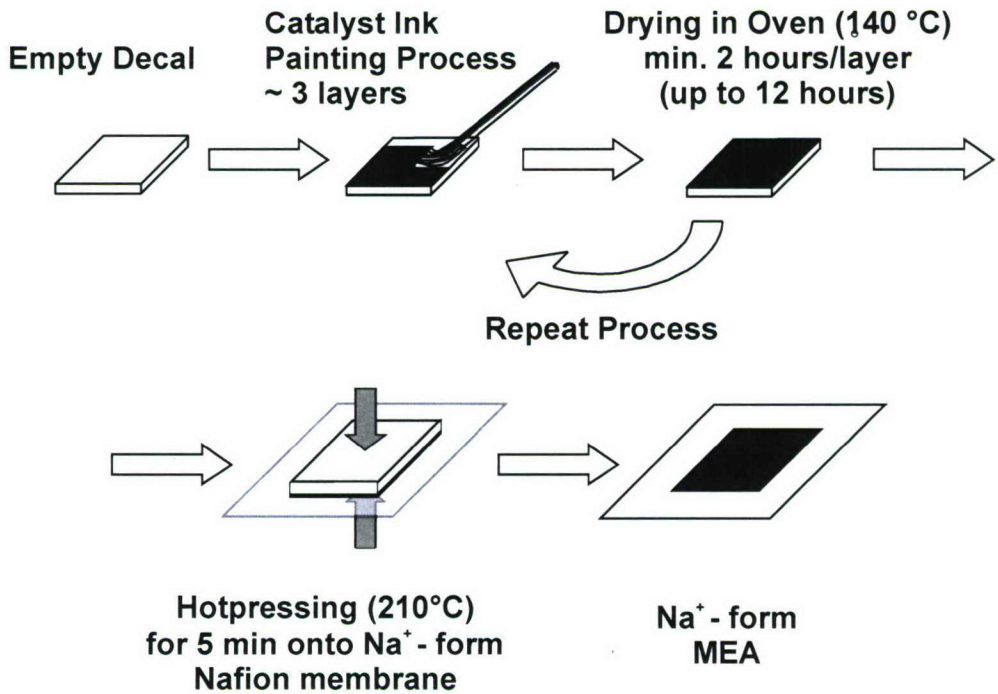

Figure 3.2-9: Schematic of HNEI MEA fabrication method.

Figure 3.2-10: Manually operated hotpress of 50 ton pressing capacity.

Production of 50 and 100 cm^2 cells have been demonstrated using the above described setup. In the following months, these cells will be tested and analyzed using the capacities at HNEI's Hawaii Fuel Cell Test Facility (HFCTF). A cooperation with LANL is in preparation to compare the achieved results at HNEI with standard MEAs created and operated at LANL. This cooperation may involve the exchange of MEAs to establish a common baseline for future work of the two labs. Furthermore, HNEI intends to expand the currently established MEA fabrication technique by implementation of a semi-automated catalyst ink coating setup. This knife-spreading apparatus will be designed and built in house. It increases the speed of the coating process for an MEA to less than 2.5 hours, while allowing for loading deviations of less than 4%, and very high catalyst homogeneities. This semi-automated technique is specifically useful when highly reproducible MEA production of repetitive cell sizes and loadings are key to successful research and development.

3.3 Fuel Cell Hardware-in-the-Loop and System Simulation Development

The objectives of this subtask were divided between two major activities: a) development of Hardware-in-the-Loop (HiL) testing capabilities, and b) development of fuel cell system simulation tools. The HiL capability and simulation tools are intended to contribute towards providing a Rapid Prototyping System (RPS) for Naval application of fuel cell systems. Both of these topics will be discussed in the following paragraphs.

3.3.1 Scope of Work and Approach

HiL Development

The plan included procurement of a fuel cell test stand allowing measurement of cell performance under dynamic conditions such as variable gas flow, gas saturation, cooling water flow, and dynamic loads. In order to use this test stand, a set of electronic controls (including a dynamic software model) is required, along with a suitable PEM fuel cell plus data acquisition and analysis capabilities. After installation of the test stand and associated equipment, testing needed to be conducted for determining the actual usefulness of the overall system for HiL testing purposes. The overall HiL system as initially defined includes the linking of an existing fuel cell system to a dynamic software model via a vendor-supplied fuel cell test stand.

Simulation Tool Development

Development efforts were aimed at assembly of fuel cell simulation tools to provide diagnostic capability for understanding dynamic cell performance and aiding evaluation of design enhancements. Simulation would also be valuable in the implementation of HiL and RPS capabilities, especially for fuel cell systems intended for Naval applications. One focus of such applications would be unmanned underwater vehicles.

3.3.2 Technical Accomplishments

HiL Development

Acquisition of HiL testing capability at HNEI involved a series of activities resulting in the assembly of the first level system, called the HiL #1 System. The intention is that this first step will lead to the next generation unit, the HiL #2 System, with higher-level capabilities. The HiL #1 System consists of a specialized fuel cell test stand (the HiL #1 test stand), a 100 cm^2 PEM fuel cell for testing within the test stand, control and data acquisition systems (including dynamic software modeling), and the facilities necessary for fuel cell operation (as provided by HNEI's HFCTF).

Purchase of the HiL #1 test stand was preceded by a number of steps including specification determination, vendor evaluation, a request-for-quotation process, and evaluation of the quotations received. Once the order was placed (with FuelCon Systems Inc.) and the HiL #1 test stand was constructed (at the vendor's factory in Germany), factory acceptance testing was conducted initially at the factory in Germany and again at the HFCTF, upon installation after shipment. Concurrent with the above steps, a Lynntech 100 cm2 PEM fuel cell was purchased, tested, and used in the HiL #1 test stand during acceptance testing and subsequent operations.

The basic elements of the HiL #1 System include two interconnected personal computer units (PC 1 and PC 2) and a special connection between PC 2 and the HiL #1 test stand with a fuel cell installed. PC 1 is for modeling or simulation (including MATLAB®/Simulink®) and PC 2 is for real time operation, including a controller area network (CAN) connection for providing rapid communication between the controller of the test stand and simulation. Figure 3.3-1 on the next page is a graphical representation of the basic elements in the HiL #1 System. Figure 3.3-2 on the next page shows the actual installed HiL #1 test stand during operation. The capabilities and limitations of the

HiL #1 test stand are discussed in the following sections. To assist in overcoming some of the limitations as delineated below, HNEI has proceeded with a variety of modifications to yield better performance of the HiL #1 System. Initial modifications are proving valuable and additional modifications are continuing to be in progress. A report delineating all aspects of installation of the HiL #1 System is included as and attachment and is designated as Appendix A.

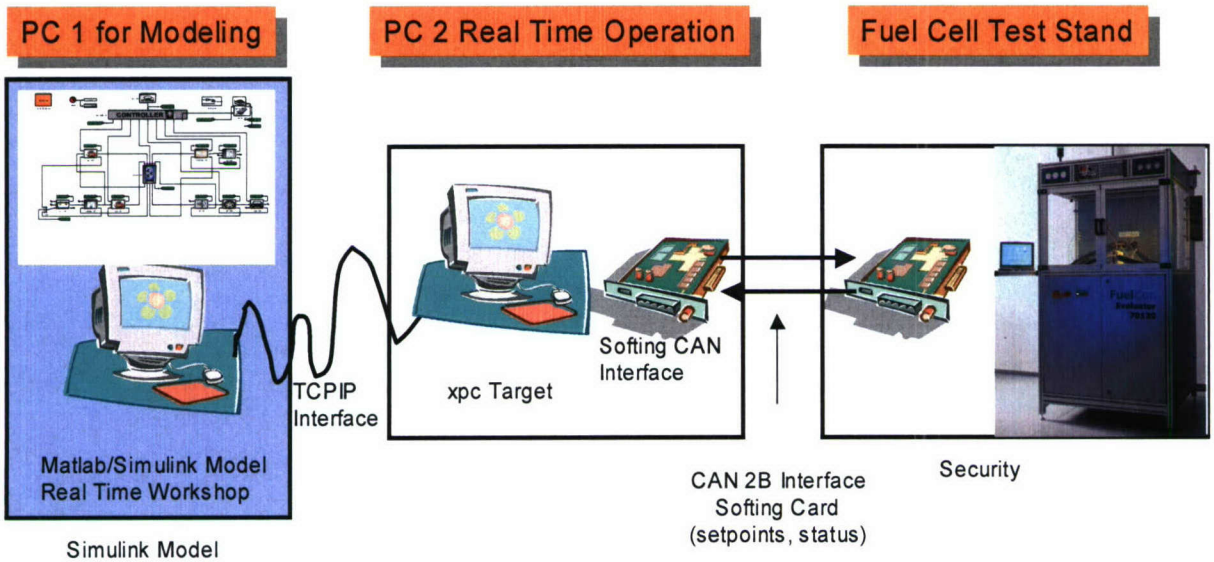

Figure 3.3-1. Sketch of the Overall HiL #1 System Setup.

Figure 3.3-2. The HiL #1 System during acceptance testing.

HiL #1 Test Stand Capabilities: The HiL #1 test stand has a wide spectrum of capabilities. In a general way, the fuel cell test station is capable of 24-hour automatic, unattended operation, and can accommodate a single fuel cell. Such operation can be carried out in two different operational modes, either operating as an independent tester (with the CAN interface inactive) or in HiL operation (with an active HiL interface).

The test stand has a closed test cabin and an integrated ventilation system with LEL hydrogen detectors to safeguard the operators and facility. It includes direct-injection humidification technology plus electronic flow control, temperature and pressure control, nitrogen purge and electronic load management. The control software permits operation of the fuel cell on hydrogen and either with air or oxygen. The test station can operate in a power range of 0 to 200 W. The maximum anode and cathode flow ranges are 0-2 slpm (standard liters per minute) and 0 to 10 slpm, respectively. The maximum inlet gas temperature for both the anode and cathode is 150 °C, and the relative humidity range is from dry to 100% at 90 °C. The back pressure control range is 1.1 to 5.0 bar(a). An optional feature of the test stand is an AC impedance measurement system. This analytical tool provides full impedance spectroscopy in a wide frequency range for cell characterization and performance analysis.

One mode of operation for the test station is as an independent fuel cell tester. In this case, it would basically be working as a static test stand. Operation is controlled from the keyboard and monitor system of the FuelCon control PC. Various scripts could be run using this arrangement, some of which could be approximations of dynamic testing for a fuel cell. Such operation would be very limited, however, and for true dynamic testing with full simulations, HiL operation would be required.

The more important method of operation is, of course, in the HiL mode. In this configuration, complete simulations can be utilized, including, for example, use of the fuel cell vehicle simulation model developed earlier, allowing operation of the fuel cell in a great variety of ways, including all the dynamism of the various drive cycles that have been formulated.

HiL #1 Test Stand Limitations: In summary, the HiL #1 test stand has limitations regarding control features, electronic communications, data flow, and lack of ability to modify features of the FuelCon tester FuelWork software (the software system of the test stand's integral controller system).

One basic feature of HiL #1 system is the long chain of controllers employed during system operation. The pathway includes the simulation within PC 1, PC 2, the CAN interface, the FuelCon PC with FuelWork, the actual FuelCon tester controller, and finally, the fuel cell being tested. Furthermore, this pathway includes the flow of setpoints towards the electronic load/fuel and actual data returning.

Another control feature presenting problems is the use of off-the-shelf, stand-alone pressure and flow controllers within the FuelCon tester. This control strategy, designed and built into the tester by FuelCon, contributed to the inability to achieve the rapid transients of pressure and flow required for good HiL operations, especially where vehicle simulation calls for stringent drive cycles.

A final control issue is that the tester controller does have the ability to adjust PID (proportional-integral-derivative) parameters (as adapted by the RS232 slow serial data interface) to be optimum for a particular operating condition, but such settings remain fixed during any test session. As operating conditions change during a single test, no parameter changes can be made "on-the-fly" and parameters are optimum for only a portion of the test.

Ideally, data flow during any dynamic fuel cell test would utilize the highest possible data transfer rate. Due to the oscillations and data corruption obtained, it became necessary to operate at the slow rate of 300 ms. This unsatisfactory operating method is caused by the data input/output passing through the Microsoft Windows-based FuelCon PC (with its FuelWork operating software).

Whereas HNEI had specified the requirement for the uncompiled development version of the tester operating software (FuelWork), FuelCon was unable to fulfill this specification. This has meant that HNEI personnel have not been able to write any adjustment codes for the software, in order to optimize operation of the tester for HNEI purposes, especially to help achieve better transient performance. Another element was the graphical user interface (GUI) portion of the software. The arrangement of GUI components and window-sizing capability were both fixed items. It was not possible to change any of the software code for these features and the embedding of add-ons was also not possible.

Simulation Tool Development

Whereas Unmanned Underwater Vehicles (UUVs) are primarily run with battery power systems, a Fuel Cell Energy/Power System (FCEPS) could be used and has already been demonstrated in a developmental Japanese UUV, the URASHIMA. We have developed a PEM FCEPS design concept and from this formulated a schematic model of an FCEPS suitable for a UUV. The specific system modeled included compressed hydrogen and oxygen tanks, gas pressure regulation and mass flow control, a PEM fuel cell, anode and cathode humidification control, temperature control, and DC/CD converter (see Figure 3.3-3 on the next page). This model was then simulated within a MATLAB®/Simulink® environment to yield a PEM FCEPS simulation tool.

The initial testing of this FCEPS Simulation tool was accomplished using a dynamic duty cycle, specifically the URASHIMA current load cycle. A full set of system performance results was obtained under this dynamic duty cycle. These results verified the transient and steady state performance of the FCEP system within reasonable performance ranges. Details of modeling, simulation, and performance data results are presented in a report included as an attachment and designated as Appendix B. In future work, HNEI intends to develop a UUV simulation tool (UUVSi) to be used under various UUV mission profiles involving vehicle speed, propeller speed, motor speed or torque, etc.

To assist in considerations for using fuel cell technology in UUV applications, HNEI conducted a technology assessment to provide an initial evaluation and technology screening for the use of an FCEP system in propulsion of a UUV. This work included hydrogen-oxygen FCEP system designs for UUVs. For the range of hydrogen/oxygen storage options considered, the FCEP system option compares favorable with the Navy threshold requirements. Therefore, the initial technology assessment supports the

expectation that an FCEP system has the potential to significantly increase the energy storage in a UUV, when compared to other refuelable air-independent propulsion energy/power systems. A report covering the results of this work is included as an attachment and designated as Appendix C.

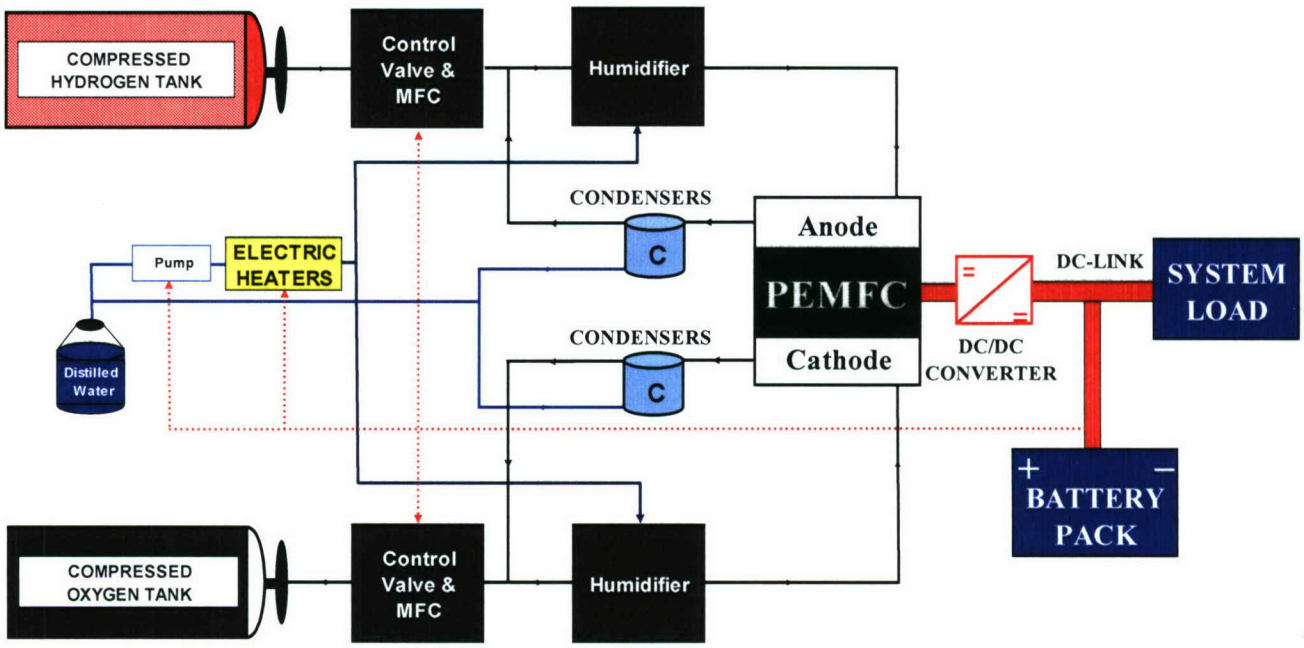

Figure 3.3-3. Schematic representation of the FCEP system.

3.3.3 Summary of Papers, and Presentations Resulting from Efforts

PAPERS

Sundaresan, M. and R.M. Moore, "PEM Fuel Cell Stack Cold Start Thermal Model," Fuel Cells, V. 5 (4), 476-485, December 2005.

Sundaresan, M., R.M. Moore, "Polymer Electrolyte Fuel Cell Stack Thermal Model to Evaluate Sub-Freezing Startup," Journal of Power Sources, V. 145, 534-545, April 2005.

Moore, R.M., K.H. Hauer, D. Friedman, J. Cunningham, P. Badrinarayanan, S. Ramaswamy, and A. Eggert, "A Dynamic Simulation Tool for Hydrogen Fuel Cell Vehicles," Journal of Power Sources, V. 141 (2), 272-285, March 2005.

PRESENTATIONS

Moore, R.M., "Fuel Cell and Stack Models for Dynamic System Simulation," invited Keynote Paper, 1st European Fuel Cell Technology and Application Conference (EFC05) ASME & ENEA, Rome, Italy 13-15 December 2005.

Virji, M., "Modelling of an Indirect Diesel Proton Exchange Membrane Fuel cell (PEMFC) System for a Marine Application," 1st European Fuel Cell Technology and Application Conference (EFC05) ASME & ENEA, Rome, Italy 13-15 December 2005.

Moore, R.M., "Research Issues and Opportunities for PEMFCs," invited seminar Chemical Engineering Department, University of Cambridge, 7 December 2005.

Moore, R.M., "FCEPS Simulation, HiL, and UUVSim & UUV Mission Profiles," University of Southampton-UK National Oceanographic Centre, Southampton, England, 5 December 2005.

Moore, R.M., "Fuel Cell System Simulation and Hardware-in-Loop," ECS 207, Quebec, Canada, 15-20 May 2005.

Moore, R.M., "FCSystemSim – A dynamic Simulation, HiL, and RP tool for fuel cell systems," EVS 21, Monaco, April 2005.

3.4 Fuel Processing and Gas Conditioning for Hydrogen Production

Task objectives were to develop experimental capabilities and perform research on fuel processing and gas conditioning for hydrogen production. Eventually, the hydrogen from the fuel processing unit is expected to be tested at the Hawaii Fuel Cell Test Facility, as a step forward from pure bottle hydrogen and hydrogen produced via electrolysis.

3.4.1 Scope of Work and Approach

Due to the lack of naturally occurring hydrogen (H_2), successful fuel cell implementation will require H_2 production based on highly efficient fuel processing in which fuels are converted to H_2, and contaminants and pollutants are removed.

With the heightened interest in renewable biofuels, the increased production of biodiesel has created a growing, and underutilized, supply of crude glycerin, a byproduct of biodiesel production. This resource has the potential to be used for the production of renewable hydrogen via catalytic reforming.

Under Phase 1, an automated fuel processing testbed was designed, fabricated, and tested. As shown in Figure 3.4-1, it consists of a lab-scale fixed-bed reactor, gas sampling and analysis capability, a control and data acquisition system, and a safety system.

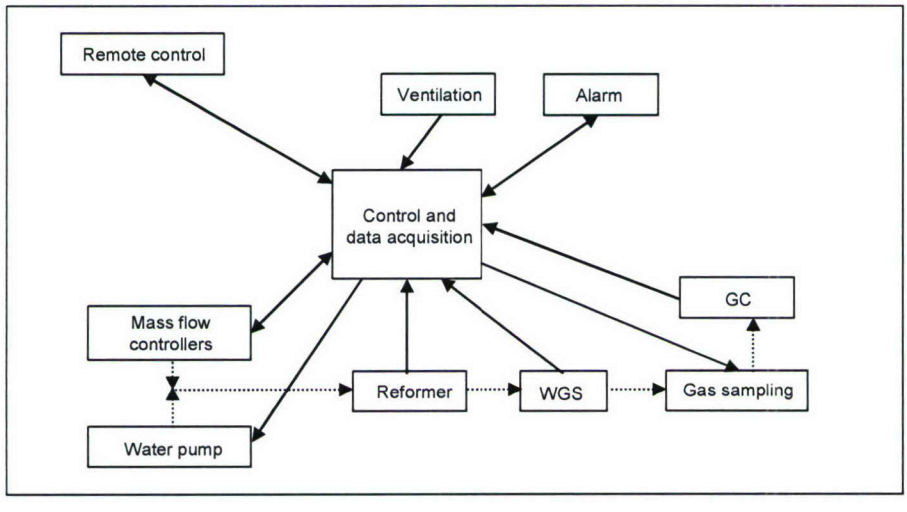

Figure 3.4-1. Conceptual design of the automated fuel processing testbed. (WGS = water gas shift; GC = gas chromatograph).

LabVIEW™ is used for control and data acquisition. Feed rates of fuel, oxidizer, and steam, processing conditions, gas conditioning, and gas analysis are automated. Safety measures are installed so that the system can be run unattended. The system can also be accessed and controlled remotely.

Under this agreement, the following work was carried out.

- Using the automated lab-scale fuel processing system, a study was conducted to investigate optimal reformer conditions for converting chemical-grade glycerin into hydrogen.
- Based on the results of the chemical-grade glycerin investigation, a study of crude glycerin reforming was conducted.
- Based on the results of the crude glycerin reforming, chemical-grade glycerin was doped with contaminants representative of the biodiesel production process and contaminant effects were determined.
- A test stand for the removal of sulfur contaminants from gas streams was designed and fabricated.

3.4.2 Technical Accomplishments

3.4.2.1 Chemical-grade glycerin reforming

Method. A 2^3 factorial experimental design was used to study the effects of oxygen to carbon ratio (O), steam to carbon ratio (S), reformer temperature, T, and the interaction of the three variables on hydrogen yield and hydrogen concentration produced from reforming glycerin. Initial reforming conditions were chosen based on literature review and thermochemical equilibrium calculations. The initial condition for the three variables under study were O = 1.05 (mole O_2/mole C), S = 2.35 (mole H_2O/mole C) and T = 810 °C. S was changed by ±0.35 to 2.0 and 2.7, O was changed by ±0.15 to 0.9 and 1.2, and the temperature was changed by ±40 °C to 770 and 850 °C. Note that the three oxygen atoms in the glycerin molecule are included in the definition of O and thus a minimum value for O is 0.5. Table 3.4-1 on the next page shows the value of the original test conditions including two center points (conditions 9 and 10). Coding was used to make the statistical analysis easier. In coded units, X_1, X_2 and X_3 represent O, S and T, respectively. A zero value represents the center point for the variable, and +1 and -1 represent the upper and lower values for the three variables under study. The performance of the experiment is defined primarily by studying the H_2 yield (mole H_2/mole glycerin), and also yields of CO, CO_2 and CH_4. Based on results from these initial experiments, response surface methodology was used to improve the process performance by varying S, O, and T. The reformer was initially used without the water gas-shift shift reactor. For each condition (1 through 10), the reformate gas was analyzed for the predominant gases N_2, H_2, CO, CO_2 and CH_4, and the trace gases, C_2H_6 and C_2H_4.

After optimizing reforming, a water gas shift reactor was added downstream to investigate its effect on H_2 production. Employed was a monolithic WGS catalyst on a nano-particle, ceria-based, mixed oxide support (NexTech Materials, Ltd., Lewis Center, OH). The gas stream exiting flowed immediately to the shift reactor, the two being in series. Temperature was the only variable changed in tests of the shift reactor performance and the reformer was operated at the optimum conditions identified earlier.

Table 3.4-1. Initial reformer conditions in real and coded units.

Condition	Variable Values			Coded Values		
Number	O	S	T, °C	X_1	X_2	X_3
1	0.9	2.0	770	-1	-1	-1
2	1.2	2.0	770	1	-1	-1
3	0.9	2.7	770	-1	1	-1
4	1.2	2.7	770	1	1	-1
5	0.9	2.0	850	-1	-1	1
6	1.2	2.0	850	1	-1	1
7	0.9	2.7	850	-1	1	1
8	1.2	2.7	850	1	1	1
9	1.05	2.4	810	0	0	0
10	1.05	2.4	810	0	0	0

Results. Results of the initial 2^3 factorial design are presented in Table 3.4-2. H_2 yield ranged from 1.2 to 3.5 mole H_2 per mole glycerin. CO and CO_2 yields ranged from 0.5 to 1.0 moles per mole glycerin and 1.9 to 2.3 moles per mole glycerin, respectively. CH_4 yields were less than 0.04 mole per mole glycerin for all test conditions. From the results, a mathematical model describing the hydrogen yield Y_{H2} as a function of the coded units for S, O, and T was derived.

$$Y_{H2} = 2.3 - 0.93X_1 + 0.034X_2 - 0.02X_3 + 0.06X_1X_2 - 0.18X_1X_3 - 0.047X_2X_3 - 0.08X_1X_2X_3 \quad (3.4\text{-}1)$$

Table 3.4-2. Reformate gas component yields.

Condition	mole/mole glycerin (Average ± Standard Deviation)			
Number	H_2	CO	CO_2	CH_4
1	3.2±0.1	1.0±0.03	2.0±0.01	0.03±0.001
2	1.5±0.5	0.5±0.2	2.3±0.3	0.02±0.006
3	3.1±0.1	0.8±0.03	2.0±0.02	0.027±0.001
4	1.9±0.2	0.5±0.3	2.4±0.2	0.008±0.001
5	3.5±0.1	1.2±0.03	1.9±0.02	0.04±0.001
6	1.3±0.1	0.7±0.07	2.2±0.02	0.03±0.002
7	3.5±0.3	1.0±0.1	2.0±0.1	0.04±0.003
8	1.2±0.1	0.6±0.05	2.3±0.05	0.03±0.003
9	2.1±0.1	0.8±0.1	1.9±0.02	0.04±0.006
10	2.1±0.05	0.8±0.04	2.2±0.04	0.04±0.008

Equation (3.4-1), shows that X_1 (i.e., O in coded units) has the most effect on hydrogen yield, followed by the interaction between O and T. The steam to carbon ratio had very little effect on the hydrogen yield. Following surface response methodology, equation (3.4-1) was used to determine new values of O, S, and T (see Table 3.4-3) predicted to improve Y_{H2} along a path of steepest ascent. Equation (3.4-1) shows that to improve Y_{H2}, O had to be decreased while almost keeping S and T at their center point values from the original test conditions. O = 0.5 (mole O_2/mole C) is the lowest oxygen to carbon ratio attainable due to the inherent oxygen content of glycerin. Table 3.4-4 shows the gas yields for reforming experiments conducted at conditions 11 and 12. By minimizing the oxygen input (a reduction of 52% from the center point), the hydrogen yield was improved from ~2 to 4.5 mole H_2/mole glycerin, i.e., 65% of the theoretical yield (7 mole H_2/mole). 1.4 moles of CO were also produced, which could theoretically produce another 1.4 mole of H_2. The amount of carbon monoxide increased in comparison to conditions 1 through 10, showing that the reforming process produced more CO instead of CO_2. Figure 3.4-2 on the next page shows the reformate hydrogen and carbon monoxide concentrations for each condition. The experimental results were compared against the equilibrium composition predicted using FactSage™, a thermochemical software and database package. At the values of O, S, and T used for condition 12, equilibrium predicted 5.4 mole H_2/mole glycerin. The experimental value of 4.5 moles H_2/mole glycerin thus achieved 83% of equilibrium.

Table 3.4-3. Experimental conditions determined from response surface analysis.

Condition	Variables		
Number	O	S	T (°C)
11	0.8	2.3	807
12	0.5	2.2	804

Table 3.4-4. H_2, CO, and CO_2 yields from conditions along path of steepest ascent.

Condition	mole/mole glycerin		
Number	H_2	CO	CO_2
11	3.8±0.07	1.0±0.03	1.9±0.02
12	4.5±0.08	1.4±0.04	1.4±0.02

Water gas shift. The water gas shift optimal temperature was reached following the same surface response approach used to improve reformer operation. Figure 3.4-3 on the next page shows the H_2 gas yields obtained by operating the reformer and the water gas shift in series. The hydrogen yield per mole of glycerin increased from 4.5 mole H_2/mole glycerin using only the reformer to 5.3 mole H_2/mole glycerin when the WGS was used, an improvement of 18%. Also, the amount of CO_2 rose from 1.4 to 2.2 mole H_2/mole glycerin, and the CO decreased from 1.4 to 0.5 mole H_2/mole glycerin. These results are in keeping with the water gas shift reaction since the CO_2 and H_2 production each increased by 0.8 moles and the CO production decreased by 0.9, showing that approximately all the CO is converted to CO_2. If the water gas shift was the only reaction

taking place in the shift reactor, an additional 0.1 mole of CO_2 should have been produced to complete the carbon balance. The gas analysis showed that 0.065 mole of C_2H_6 was produced per mole glycerin, compared to 0.01 moles per mole glycerin at the reformer exit for condition 12. This could account for the 0.1 difference between CO and CO_2 yields. The carbon balance computed for the final condition was 97.6%, indicating that the measurement of system inputs and outputs are in close agreement. The addition of the shift reactor to the reformer improved hydrogen yield from 64% to 75% of the maximum theoretical yield.

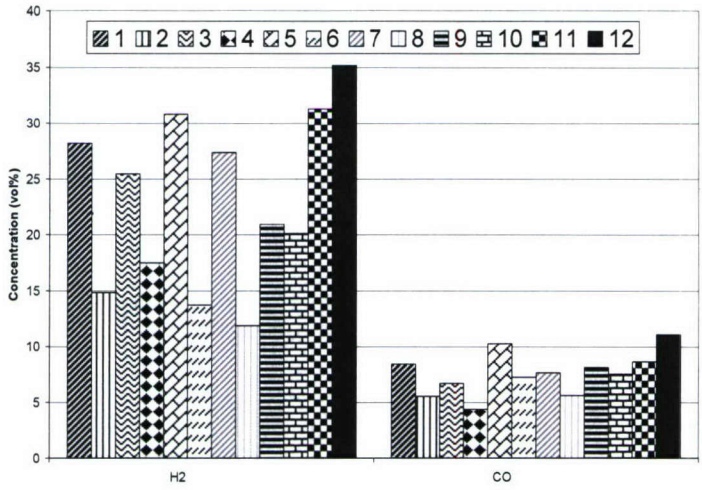

Figure 3.4-2. H_2 and CO concentrations (vol %, dry basis) in reformate gas for conditions 1 through 12.

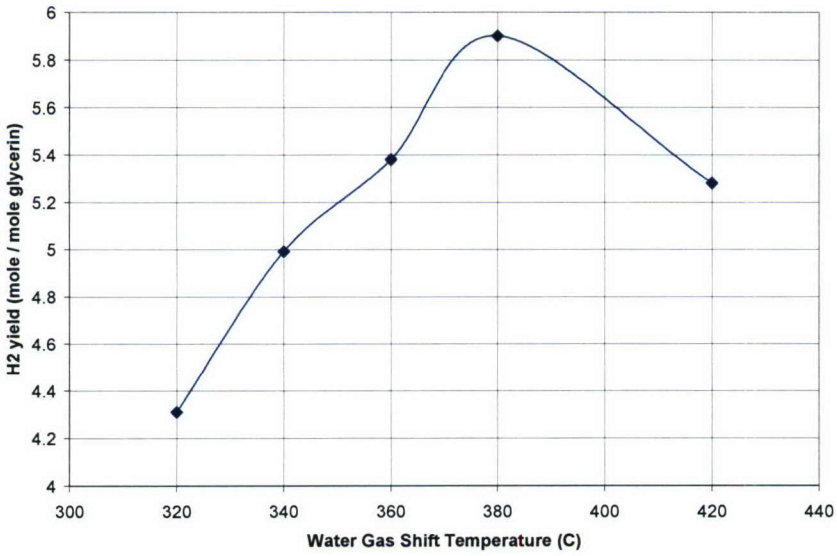

Figure 3.4-3. Hydrogen yield as a function of water-gas shift temperature with the reformer operated at condition 12.

Catalyst deactivation. Catalyst deactivation occurs over time mainly due to coking, and results in a lower hydrogen yield. An indicator of catalyst deactivation is an increase in methane production, and to a lesser extent, ethane. The decrease in reformer performance was noticeable after a few hours of testing. For condition 12 (i.e., best reforming condition), the hydrogen yield decreased from 4.8 to 4.5 moles H_2 per mole glycerin during the first three hours, a reduction of at 0.6% / hr. During the same time period, the methane production increased from 0.1 to 0.16 moles CH_4 per mole glycerin, or 24%/hr. The effects of S and O on methane production (and catalyst deactivation) were studied using the data from the original design (i.e., conditions 1 through 8). Similar levels of methane production were found for both low and high S values. Comparing the methane production for the low and high O values showed a 30% lower methane production for the high oxygen input, For O = 0.9, Y_{CH4} = 0.033 mole CH_4/mole glycerin and for O = 1.2, Y_{CH4} = 0.023. At condition 12, where O = 0.5 and no external O_2 was supplied, methane production is even higher at 0.1 mole/mole glycerin. Methane yield was modeled as a function of X_1, X_2, and X_3.

$$Y_{CH4} = 0.027 - 0.0054(X_1) - 0.0011(X_2) + 0.006(X_3) \qquad [3.4\text{-}2]$$

The lower methane production at higher oxygen to carbon ratio is explained by the fact that supplemental oxygen helps prevent carbon deposition on the catalyst surface, thereby maintaining catalyst activity. Carbon deposits were readily apparent on the catalyst pieces closest to the reformer inlet when they were recovered after a test was completed. Catalyst pieces farthest downstream kept their original, grayish color. The amount of carbon recovered from the reformer and the filter after each test was small (0.36 g to 1.0 g), accounting for less than 1% of the total carbon contained in the glycerin feed. A secondary impact of carbon formation was an increase of reformer operating pressure over the test duration. A higher S/C could be expected to reduce coking and slow the catalyst deactivation. From the amount of carbon collected in the reformer and the pressure recorded in the reformer, it was not possible to determine a clear effect of S/C on the carbon formation for the duration of these tests.

3.4.2.2 Crude Glycerin Tests

Crude glycerin reforming tests were conducted at the same conditions used for reagent-grade glycerin, i.e., O = 0.5, S = 2.21, T_{set} = 804 °C. The process worked well for the first hours with Y_{H2} = 4.4 mole H_2/mole glycerin, compared to 4.5 with reagent grade glycerin (although the crude glycerin contained impurities, the hydrogen yield values were computed based on pure glycerin). Methane yield (0.23 mole CH_4/mole glycerin) was more than twice the amount observed when reforming reagent-grade glycerin and the yields of CO and CO_2 were markedly lower, each at ~1 mole per mole glycerin. In addition, C_2H_4 was produced at levels equal to methane, where previously it was negligible in all runs performed using reagent-grade glycerin. The hydrogen yield decreased quickly after the second sample (-0.41 mole H_2 per mole glycerin per hour) and the amount of CH_4 and C_2H_4 increased (+0.072 mole /hr), indicating rapid catalyst deactivation and poor system performance. The pressure quickly increased past 69 kPa (the limit for the pressure sensor) and the experiment was terminated. After the reformer cooled down and was opened to be cleaned and to recover the used catalyst, it was found that the reformer tube was filled with sintered deposits. It was not possible to tell how

much carbon was in the reformer because it could not be removed. The carbon balance on this test showed that only 2.5 mole of C were recovered in the gas phase per mole of glycerin (83% recovery). This test showed that crude glycerin can be reformed with high hydrogen yield, but that contaminants can cause severe coking during the reforming process. The major contaminants known to be present in crude glycerin are sulfur (present in the waste cooking oil), potassium/sodium cations (from either the potassium or sodium hydroxide base used as catalyst in biodiesel manufacture), free fatty acids (present in the cooking oil from animal-fat-based oil), and methanol (reacts with the oil and replaces the glycerin to form biodiesel). NaCl, NaOH and C_3H_3OH were used to contaminate reagent-grade glycerin and determine their effects on the reforming process. The contaminants were introduced at a concentration of 0.5% by weight. It was found that methanol had no effect on the process, but that the compounds containing sodium both caused problems similar to those encountered with crude glycerin, such as rapid pressure built-up in the system due to coke and deposit formation and associated higher methane yield.

3.4.2.3 Sulfur Removal Test Stand

A Shimadzu 2014 gas chromatograph equipped with a Sievers sulfur chemiluminescent detector capable of quantifying low level sulfur concentrations, on the order of 50 ppb, was purchased and installed in the fuel reforming lab. This instrument is being incorporated into a recently designed test stand for evaluating sulfur removal techniques for gas phase fuels.

3.4.3 Summary of Papers Resulting from Efforts

Douette, A., S. Turn, W. Wang, and V. Keffer, Hydrogen production from glycerin reforming, presented at the 14th European Biomass Conference and Exhibition: Biomass for Energy, Industry, and Climate Protection, Paris, October 17-21, 2005.

Douette, A., Hydrogen production from glycerin reforming, College of Tropical Agriculture and Human Resources Student Symposium, University of Hawaii, Honolulu,HI, May, 2006.

Douette, A., S. Turn, W. Wang, and V. Keffer, An experimental investigation of hydrogen production from glycerin reforming. Manuscript in review, *Energy & Fuels*.

3.5 Novel Fuel Cell and Component Development

3.5.1 Objectives

The effort to develop novel fuel cell components included two major activities: a) biocarbons for use in fuel cell bipolar plates, and b) enzymatic bio-fuel cells. Both of these topics are addressed in the following paragraphs.

Biocarbons for use in fuel cell bipolar plates

Graphite is an important component of the bipolar plate assembly that is employed in many fuel cells. Graphite also plays a critical role in many batteries and capacitors. Graphite is desired for these applications because it is an excellent conductor of electricity and it is inert. Unfortunately, because it is inert it is not a good support for

catalysts. Likewise, it has a very low porosity and surface area. High surface areas can be desirable for some catalytic applications.

The electrical conductivity of many biocarbons (carbonized charcoal produced from biomass) approaches that of graphite. These biocarbons can be inert. Unlike graphite, biocarbons can possess very high surface areas and easily can be loaded with catalysts. In spite of these attractive features, virtually no attention has been given to the use of biocarbons as replacements for graphite in fuel cell bipolar plates, capacitors, and batteries.

The objective of this work was to characterize the electrical and physical properties of a wide range of biocarbons in order to facilitate their use in improved fuel cell bipolar plates, capacitors, and batteries.

Enzymatic bio-fuel cells

Enzymatic bio-fuel cells (EBFC) are a promising alternative that can complement the conventional fuel cell technologies which rely upon transitional metal oxides or noble metal catalysts for conversion of chemical energy, typically stored in hydrogen, to useful electrical energy. Some of the more promising aspects of the EBFC include:

- Catalyst regeneration (via chemical or biological means) – a unique characteristic that conventional Pt-based counterparts lack and something that promises potentially low cost production and unlimited supply. It also offers new approaches to overcome degradation on system performance for long-duration applications, especially at remote locations (covert operations, deep ocean deployment, or space travel), where catalysts might be repaired or replenished on site;
- Selectivity – Enzyme catalysts are reactant specific and therefore less prone to competing reactions, which can simplify fuel logistics or cell design.
- Tolerance to impurity – Due to their selectivity, enzymes are generally more tolerant (relative to noble metals such as platinum) to contaminants which could reduce the impact of dirty fuels.
- Adaptability – Enzymes, if appropriately isolated from target organisms, can potentially retain activity at extreme conditions (e.g., temperature extremes). If the gene coding for the enzyme is obtained, a suite of directed evolution techniques exist to create more effective enzymes.
- Self-assembly – possibly *in situ* in biological systems to simplify fabrication processes for micro-devices.

This work has been focused on elucidating the fundamentals underlying charge transfer limitations in enzyme catalyzed electrodes, and transferring this knowledge into the engineering design of practical *bio-fuel cells.* To reach this goal, the following specific tasks have been pursued for systems employing both gas- and liquid-phase fuels:

- The establishment of an array of quantitative *in situ* characterization techniques, test cells, and modeling capabilities to determine limitations to bioelectrocatalysis [1-4], and to construct a bio-electrochemical test bed that will allow us to refine such techniques in microbial or enzyme based bioelectrocatalysis operation [5], and

- To develop a technology base with know-how to improve performance (e.g., catalyst lifetime, current density) with respect to important process variables such as choice of catalyst, choice of mediators, immobilization matrix, and mode of immobilization (e.g., direct attachment versus entrapment of enzyme).

3.5.2 Scope of Work and Approach

Biocarbons for use in fuel cell bipolar plates

- Biocarbons were produced by the Flash Carbonization™ process from a variety of biomass feedstocks. Dopants and catalytic materials were added to some biomass feedstocks prior to carbonization.
- Various properties of the biocarbons were measured by gas sorption analysis, XRD, FTIR, elemental analysis, etc. The effects of these properties on the electrical resistivity of the biocarbons were inferred.

Enzymatic bio-fuel cells

To execute the specific objectives, a number of specific tasks have been pursued. In development of a prototype bio-fuel test cell, prototypes are continuously being constructed and tested. We currently employ a modular stacked-cell design to facilitate integration of component testing and cell construction, transfer of knowledge from component fabrication to cell performance characterization, and collection of data that is cross-platform and interchangeable from one configuration to another. To aid in advancing enzyme fuel cell design, we developed a suite of characterization techniques to analyze cell performance and facilitate optimization of power generation. These include the coupling of spectrophotometry with electrochemical techniques to determine charge transfer efficiency of bound enzyme [2] and immobilized enzyme activity in the absence of mass transfer effects [3], the use of fluorescence to estimate spatial distribution of enzyme [4], and the coupling of imaging ellipsometry with cyclic voltammetry to estimate film thickness with cycle number [1]. With respect to specific technique utilization, we believe we are one of the first groups to estimate charge transfer efficiency of bound enzyme and to use imaging ellipsometry to observe film thickness growth with deposition conditions *in situ*.

3.5.3 Technical Accomplishments

Biocarbons for use in fuel cell bipolar plates

- Carbon materials cannot be shipped by air unless they have been tested and certified according to certain UN test procedures. During 2004 we purchased a furnace and other equipment needed to execute the UN tests, and we developed the necessary procedures to accomplish the tests. Because our biocarbons failed one of the tests, there are some restrictions placed on their shipment by air. Fortunately, because our biocarbons passed all the other tests, these restrictions are not onerous.
- We prepared charcoals and carbonized charcoals (biocarbons) from a wide variety of biomass substrates using the Flash Carbonization™ process developed at HNEI. Model biocarbons were synthesized from sucrose, glucose, fructose, inulin, and Kraft lignin. Commercial biocarbons were synthesized from oak wood, corncob, and demineralized corncob.

- Biocarbons doped with boron and phosphorous were also prepared.
- These prepared biocarbons were characterized by methods including XRD, NMR, ICP-MS, SEM, and TG-MS, and their properties were compared to those of graphite. The TG-MS analyses revealed (for the first time) that there are two classes of biocarbons: those that persistently evolve CO at temperatures approaching 1000 °C, and those that do not. The presence of certain catalytic species in the ash of these biocarbons appears to be responsible for the different behaviors.
- We are preparing two papers that describe the above results. They will be submitted for peer review and publication soon.

Enzymatic bio-fuel cells

Prototype Bio-fuel Test Cell: Several prototype cells have been constructed to deliver gas fuels. A final version of the working enzymatic bio-fuel cell was constructed and tested. Design considerations and test applications were described in the June 2005 Final Technical Report. Complete details on this work have been published [2]. From this work we have determined that the use of gaseous fuels is limited by the solubility of the gaseous fuel in the aqueous buffer that is required to maintain enzyme activity.

Suite of Characterization Techniques: The complement of methods utilized included potentiostatic DC polarization, dynamic potentiometry, and electrochemical impedance spectroscopy (EIS) combined with spectrophotometric detection of enzyme activity in order to characterize electrode performance, and to differentiate between the relative contributions towards charge transfer efficiency. Among the results of our efforts, in particular, we believe we were one of the first groups to report charge transfer efficiency for bound enzyme. Much of this has been summarized in a book chapter to be published in 2006 [6]. An additional mass transport modeling effort that can be combined with DC-polarization data to yield information valuable for future electrode development has been completed. Detailed description of the technique application, data and results can be found in the literature [3].

The technique of fluorescence has been applied to study the interaction between enzyme and polymer for its effect on the immobilization process. Specifically, we have tagged ethanol-oxidizing enzymes with various fluorescent probes and then used confocal microscopy to image the spatial distribution of the enzyme. We have also used polarization measurement to quantify the effect of charge-charge interactions between the enzyme and polymer, and to question whether this affects the spatial distribution. The results of this work have been submitted for publication [4].

To evaluate film thickness during electrochemical deposition of electrode immobilization matrix or mediator film on electrode surface, we have combined the technique of imaging ellipsometry with cyclic voltammetric deposition technique to track the thickness of the deposited film with cycle number. This very valuable technique has contributed new information regarding the fundamental reaction kinetics and mechanisms underlying the electrochemical deposition of conductive films onto electrode surfaces. The initial work has been submitted for publication [1].

Outcomes from this HEET-funded work has been used to leverage two extramurally funded projects. The first one is a grant from the Director of Central Intelligence

Postdoctoral Fellow Research Program to support development of bio-fuel cells for micro-power source applications (B.Y. Liaw, PI). The second is a sub-award from the AFOSR Multi-University Research Initiative (MURI) program (M. Cooney, PI) awarded to the lead institution, the University of New Mexico (P. Atanassov, PI). Both awards lend national recognition of this EBFC program and promise future collaborations with national and international premier research institutions to expand the scope and level of competency in this field.

Finally, this work has resulted in authorship of one book chapter and eight invited presentations at national and international conferences.

3.5.4 Summary of Awards, Books, Papers, and Presentations Resulting from Efforts

Biocarbons for use in fuel cell bipolar plates

AWARDS

Finalist, 2005 Frank Annunzio Award in the field of Alternative Energy Sources offered by the Christopher Columbus Fellowship Foundation.

PAPERS

Varhegyi, G., E. Meszaros, J. J. Antal, Jr., J. Bourke, and E. Jakab, "Combustion Kinetics of Corncob Charcoal and Partially Demineralized Corncob Charcoal in the Kinetic Regime," *Ind. Eng. Chem. Res.*, V. 45 (14), 4962-4970, 2006.

Wade, S.R., T. Nunoura, ***and M.J.*** Antal, Jr., "Studies of the Flash Carbonization Process. 2. Violent Ignition Behavior of Pressurized Packed Beds of Biomass: A Factorial Study," *Ind. Eng. Chem. Res.*, V. 45 (10), 3512-3519, 2006.

Two more papers with ONR support will be submitted for publication before the end of this year.

Enzymatic bio-fuel cells

BOOKS

Cooney, M. J., and B. Y. Liaw. In situ characterization techniques for design and evaluation of micro and nano enzyme-catalyzed power sources. In *Nano-scale Science and Technology in Biomolecular Catalysis*, P.S Wang and J. B. Kim, editors, American Chemical Society, expected to be published in Winter 2006.

PAPERS

Johnston, W.J., M.J. Cooney, and B. Y. Liaw, "In situ measurement of effective diffusion coefficients in enzyme immobilized electrodes," Enzyme and Microbial Technology, V. 39, 131-140, 2006.

Johnston, W.A., B.Y. Liaw, R. Sapra, M.W.W. Adams, and M.J. Cooney, "Design and Characterization of Redox Enzyme Electrodes: New Perspectives on Established Techniques with Application to An Extremeophilic Hydrogenase," *Enzyme and Microbial Technology*, V. 36 (4), 540-549, 2005.

Liaw, B. Y., F. L. Quinlan, and M. J. Cooney, Microstructure and Morphology of Polypyrrole Films Electrochemically Deposited onto Nickel Electrode Surface, submitted to Electrochimica Acta., 2006.

Konash, A., M. J. Cooney, B. Y. Liaw, and D. M. Jameson, Characterization of Enzyme-Polymer Interactions using Fluorescence, submitted to the Journal of the American Chemical Society, 2006.

Svoboda, V., C. Rippolz, M.J. Cooney, and B. Y. Liaw, Characterization of electrochemically polymerized methylene green films on platinum and vitreous carbon supports, submitted to Journal of Electrochemical Society, 2006.

PRESENTATIONS

Liaw, B.Y., M.J. Cooney, B.Y. Liaw, V. Svoboda, A. Konash, and D.M. Jameson, *In situ* Characterization of Polymer Matrices for Bio-electrode Applications, 17th International Symposium on Fine Chemistry and Functional Polymers (FCFP-XVII) & 3rd IUPAC International Symposium on Novel Materials and their Synthesis (NMS-III), Shanghai, China, October 18-20, 2007.

Svoboda, V., M.J. Cooney, C. Rippolz, and B. Y. Liaw, Development of an Enzymatic Ethanol Bio-Fuel Cell for Micro-Power Generation, Fuel Cell Seminar, Honolulu, HI, November 13-17, 2006.

Konash, A. M.J. Cooney, B.Y. Liaw, and D. Jameson, Enzyme-polymer interaction study using fluorescence probes, Symposium on Nano-scale Science and Technology in Biomolecular Catalysis, 232nd ACS National Meeting, San Francisco, CA, September 10-14, 2006.

Cooney, M. J., Building Instrumentation Support Facility to Support Fundamental Study of Enzyme Fuel Cells, AFOSR MURI symposium on Fundamentals and Bioengineering of Enzyme Fuel Cells, Washington, DC, September 6-7, 2006

Cooney, M. J, Svoboda, V., Rippolz, C., and B. Y. Liaw, *In situ* Characterization of Methylene Green Modified Enzyme Electrodes, 209th ECS Meeting, Denver, CO, May 7-12, 2006.

Svoboda, V., M.J. Cooney, C. Rippolz, and B. Y. Liaw, Design Considerations and Characterization of Enzymatic Ethanol Fuel Cells, 209th ECS Meeting, Denver, CO, May 7-12, 2006.

Svoboda, V., M.J. Cooney, C. Rippolz, and B.Y. Liaw, Design Consideration and In-situ Characterization of Bio-Anode for Enzymatic Ethanol Fuel Cell Application, IBA – HBC 2006 Meeting, Waikoloa, HI, January 9-12, 2006.

Quinlan, F., V. Svoboda, M.J. Cooney and B.Y. Liaw, Deposition and Characterization of Controlled Conductive Polymer Framework for Power Generation, national meeting of the American Institute of Chemical Engineers, Cincinnati, OH, October 31-November 4, 2005.

Liaw, B.Y. F Quinlan, and M.J. Cooney, "Polypyrrole Deposition in Aqueous Solutions: Film Characteristic Dependence on Deposition Conditions," 208th Meeting of the Electrochemical Society, Los Angeles, California, Oct. 16-21, 2005.

Liaw, B.Y., V. Svoboda, and M.J. Cooney, "Morphological Study of Conducting Polymer via Electrochemical Deposition Using Imaging Ellipsometry and RQCM Technique," 208th Meeting of the Electrochemical Society, Los Angeles, California, Oct. 16-21,2005.

Cooney, M.J., B.Y. Liaw, W. Johnston, V. Svoboda, F. Quinlan, and N. Maynard, "Design of macropore structure for enzyme fuel cells operation," Fuel Division: Biofuel cells, 230th ACS National Meeting, Washington, DC, Aug 28-Sept 1, 2005.

Liaw, B.Y., V. Svoboda, F. Quinlan, and M.J. Cooney, "Understanding Conductive Polypyrrole Deposition Via Micro- and Nano-Scale Observations," Division of Colloid and Surface Chemistry, 230th ACS National Meeting, Washington, DC, Aug 28-Sept 1, 2005.

Cooney, M.J., B.Y. Liaw, and W. Johnston, "Comparative effects of reaction kinetics and mass transfer limitation in micro enzyme fuel cell bioreactors," Biochemical Engineering XIV: Frontiers and Advances in Biotechnology, Biological and Biomolecular Engineering, Harrison Hot Springs, BC, Canada, July 10-14, 2005.

Liaw, B.Y., M.J. Cooney, F. Quinlan, V. Svoboda, and N. Maynard, "Engineering Effective Bioelectrocatalysis Electrodes for Power Generation," Second International Conference on Polymer Batteries and Fuel Cells (Fuel Cells), Las Vegas, Nevada, June 12-17, 2005.

3.5.5 References

Enzymatic bio-fuel cells

1. Svoboda, V. M.J. Cooney, C. Rippolz and B.Y. Liaw, *In situ* Characterization of Electrochemically Polymerized Methylene Green Films on Platinum Electrodes, submitted to the Journal of the Electrochemical Society, 2006.

2. Johnston, W.A., M.J. Cooney, B.Y. Liaw, R. Sapra, and M.W.W. Adams, Design and Characterization of Redox Enzyme Electrodes: New Perspectives on Established Techniques with Application to an Extremeophilic Hydrogenase, Enzyme and Microbial Technology, V. 36 (4), 540-549, 2005.

3. Johnston, M. Maynard, B.Y. Liaw, and M.J. Cooney, *In situ* Measurement of Activity and Mass Transfer Effects in Enzyme Immobilized Electrodes, Enzyme and Microbial Technology, V. 39 (1), 131-140, 2006.

4. Konash, S., M.J. Cooney, B.Y. Liaw, and D. Jameson, Characterization of Polymer-Enzyme Interactions using Fluorescence, submitted to the Journal of Materials Chemistry, 2006.

5. Svoboda, V., M.J. Cooney, C. Rippolz, and B.Y. Liaw, *In situ* Characterization of an Enzyme Catalyzed Bio-Fuel Cell, in preparation.

6. Cooney, M.J. and B.Y. Liaw, *In situ* Characterization Techniques for Design and Evaluation of Micro and Nano Enzyme-Catalyzed Power Sources, in Nano-Scale

Sciences and Technology in Biomolecular Catalysis, P.S. Wang and J.B. Kim, editors, American Chemical Society.

4. Methane Hydrates

4.1 Objectives

Methane hydrates in ocean sediments constitute an enormous energy reservoir that is estimated to exceed the energy content of all known coal, oil, and conventional natural gas resources. Located on continental margins throughout the world, methane hydrates offer unique opportunities as an onsite source of fuel for various marine applications and are believed to play a major role in seafloor stability and global climate.

National R&D programs on methane hydrates were initiated in Japan and India in the mid-1990s with the goal of commercial gas production within a 20-year time horizon. The U.S. established its own program in May 2000. The Methane Hydrate Research and Development Act of 2000 (Public Law 106-193) included seven technical areas of focus: (1) identification, exploration, assessment, and development of methane hydrate as a source of energy; (2) technology development for efficient and environmentally sound recovery of methane from hydrates; (3) transport and storage of methane produced from methane hydrates; (4) education and training related to methane hydrate resource R&D; (5) assessment and mitigation of environmental impacts of natural and purposeful hydrate degassing; (6) development of technologies to reduce the risks of drilling through methane hydrates; and (7) support of exploratory drilling projects. Public Law 106-193 was reauthorized for an additional five years in 2005.

The objectives of the Methane Hydrates Task of the HEET Initiative, which began in 2001, reflect most of the priorities of P.L. 106-193, but emphasize those areas of particular relevance to the Office of Naval Research (ONR) and which are consistent to the overall goals of the HEET Initiative. Specifically, the development of hydrates and related sources of seafloor methane as logistical fuels for Naval applications or for specialized subsea power applications, and related marine environmental issues, are principal areas of interest; exploratory drilling projects and seafloor stability/safety have received limited attention. Task objectives were devised to fully leverage hydrate R&D expertise and infrastructure that had been developed at HNEI during previous research programs on CO_2 ocean sequestration and deep oil spills.

During the present reporting period (2005-2006), the specific goals of the HEET Methane Hydrates Task were:

- Conduct experiments and analyses of hydrate destabilization for methane fuel recovery.
- Continue the characterization of the microbial assemblage that modulates levels of methane in the seafloor sediment and leakage into the water column.
- Continue the development of subsea power systems based on seafloor methane and hydrates.
- In cooperation with the Naval Research Laboratory (NRL) and ONR Global (previously ONR-IFO), promote international collaborative research on methane hydrates.

4.2 Scope of Work and Approach

Pursuant to the goals identified in the preceding section, the scope of work (SOW) of the Methane Hydrates Task comprised four primary components which are described below.

Development of the International Partnership

In cooperation with NRL, HNEI will participate in organizing the 4th International Workshop on Methane Hydrates to be held in Victoria, British Columbia, Canada in May 2005 and the 5th International Workshop on Methane Hydrates to be held in Edinburgh, Scotland in October 2006. These workshops have served as a forum for the international exchange of research results and have promoted collaborative field and laboratory studies.

Studies of Seafloor Methane Hydrate Destabilization

In previous Phases of the HEET Initiative, studies of methane hydrate thermochemistry and kinetics were initiated, utilizing two primary facilities: the hydrate destabilization facility and a Calvet-Tien calorimeter (Setaram model BT2.15). Descriptions of these facilities were provided in the Final Technical Report (2005) for ONR Grant N00014-01-1-0928 (i.e., the report on HEET Phases 1-3). During the present reporting period, the SOW for this research component comprised the development of an instrument to perform simultaneous Raman spectroscopy and calorimetry with the BT2.15, and investigation of strategies for hydrate decomposition using the hydrate destabilization facility and the calorimeter.

Microbial Characterization

During the present reporting period, HNEI proposed to continue its efforts to characterize the unique microbial assemblage associated with methane hydrates. The goal of this effort is to understand how methane levels in the sediment are modulated by microbial methanogenic and methanotrophic processes.

Subsea Power Generation

The SOW for this research component consisted of developing conceptual process designs of subsea power systems utilizing seafloor methane hydrates.

4.3 Technical Accomplishments

The principal technical accomplishments of the HEET Methane Hydrates Task for each of the four components identified in the previous section are summarized below.

4.3.1 International Partnerships

The 4th International Workshop on Methane Hydrates was held in Victoria, British Columbia, Canada on 9-11 May 2005. HNEI once again was a sponsor and participated in organizing this workshop. There were approximately sixty attendees from the U.S., Canada, Japan, the UK, Norway, Chile, Germany, and New Zealand. Participants included leading researchers in methane hydrates, and representatives from government agencies and the private sector. As in the preceding three workshops, a primary goal was to promote international collaborative research on methane hydrates.

The Victoria workshop focused on four topics: ***methane hydrate resource characterization and distribution; methane hydrates kinetics, dissociation and biogeochemistry; environmental concerns, seabed stability and ecosystem health; and***

methane hydrate future development. The workshop included technical presentations, breakout sessions, panel discussions, and a poster session. As of 31 August 2006, the workshop report was still being prepared. The website for the meeting is:

http://web.uvic.ca/ceor/hydrates/2005.html

Planning for the 5th International Workshop on Methane Hydrates commenced immediately after the conclusion of the 4th Workshop. It is scheduled for 9-12 October 2006 in Edinburgh, Scotland. HNEI is a sponsor and a member of the organizing committee, which is being led by colleagues in the UK. The website for the 5th workshop is:

http://www.noc.soton.ac.uk/CHD/fluidflow/fiery_ice/index.html

One outcome of the Victoria workshop was a collaboration that resulted in an oceanographic research cruise in late June 2006 (20 June – 3 July) to survey hydrate deposits on the Hikurangi Margin offshore of New Zealand. Participants in this cruise included the Institute of Geological and Nuclear Sciences and the National Institute of Water and Atmospheric Research of New Zealand, the University of Otago (New Zealand), the Marine Biogeochemistry Section of the U.S. Naval Research Laboratory, the University of Rochester, and HNEI. The main objective of this investigation was to locate gas-hydrates that might serve as a future energy resource for New Zealand. Toward this end, seismic profiling was performed and sediment piston cores and heatflow data were collected. HNEI was tasked to perform molecular biological analyses and microbial culturing of the piston-core sediment samples.

It was reported previously that two foreign graduate students were engaged to pursue their studies of marine methane hydrates and to conduct collaborative experiments at the HNEI laboratories. Both returned to their home institutions prior to the present reporting period. Ms. Kana Kuroda, the M.S. student from the Department of Marine System Engineering of Osaka Prefecture University in Japan, received her degree in March 2006. Her thesis was based on the studies of hydrate destabilization conducted during her stay at HNEI.

4.3.2 Methane Hydrate Destabilization

During the present reporting period, the primary accomplishments of this subtask were: (1) collection and analysis of a preliminary data set on hydrate destabilization arising from the injection of chemical inhibitors; (2) continuation of methane hydrate calorimetry experiments; and (3) completion of the design and initiation of the fabrication of an instrument to perform simultaneous Raman spectroscopy and calorimetry. Details of these three accomplishments are provided below.

Reagent Destabilization of Methane Hydrates

The hydrate destabilization facility and initial shakedown experiments performed with this facility were described in the Final Technical Report for ONR Grant N00014-01-1-0928. During the present reporting period, a suite of experiments was conducted in which synthetic methane hydrate samples were destabilized by injection of warm water or methanol-water solutions, or by depressurization. Some of the data from these tests were presented in Kuroda *et al.* (2005). The injection experiments involved spraying liquid reagents over a cylindrical hydrate sample inside a high pressure reactor (i.e., the

hydrate synthesis vessel) and monitoring the evolved methane gas. In order to interpret the experimental data, a model following the approach of Jamaluddin *et al.* (1989) was developed. This one-dimensional time-domain algorithm allows the simultaneous determination of the location of the hydrate decomposition front (i.e., the location of the receding hydrate-liquid boundary) and temperatures inside the hydrate sample at selected nodes. In the model, hydrate decomposition is presumed to be governed by an intrinsic rate (Clarke & Bishnoi, 2001), but the decomposition thermodynamic conditions (e.g., hydrate-liquid boundary temperature in constant-pressure experiments) are affected by heat transfer between the hydrate sample and the bulk liquid phase. Bulk liquid phase temperature is therefore an additional variable in the model, with heat transfer represented by a simple convective term. In contrast, Jamaluddin *et al.* (1989) treated cases with constant heat flux. A description of the model is provided as an attachment and is designated as Appendix D.

Results from three of the experiments conducted with different concentrations of methanol in water injected over the hydrate samples were selected for comparison with the model which was coded into a computer program. These data records were corrected to account for the displaced gas (due to injection of the liquid into the constant volume synthesis vessel) following the protocol described in Appendix D. The raw and corrected data and the corresponding test conditions are included in this Appendix.

The model requires a number of parameters. Some of these parameters (e.g., s_0, T_0 and T_{inj}; definitions provided in the Nomenclature in the Appendix) are known from the test conditions presented in Table 1 of Appendix D. The initial length of the cylindrical hydrate sample, L_0, can be estimated from the quantity of ice used to synthesize the hydrate, but is not known precisely, since the synthesis and reagent injection take place in a closed pressure chamber with no visual access and the synthesis process entails melting the ice to form the hydrate. For these initial model comparisons, L_0 was assumed to be 0.5 m. Other physical parameters of the model were assigned values taken from the technical literature. With little loss of generality, the methane hydrate sample was assumed to have a guest-molecule occupancy given by $n = 5.75$ (i.e., 5.75 molecules of O_2 per molecule of CH_4).

The three-phase equilibrium pressure $p_{eq}(T; s)$ depends on the methanol mass fraction s in the liquid. This dependency was parameterized by including a temperature offset δT in the formula of Handa (1990) for $p_{eq}(T; 0)$:

$$\begin{cases} p_{eq} = p_{atm} \exp\{-1205.907 + \dfrac{44097}{T + \delta T} + 186.7594 \log(T + \delta T)\} \\ \text{where } \delta T = 5\left(\dfrac{s}{0.1}\right)^{1.2} \end{cases} \tag{4-1}$$

Figure 4-1 shows a reasonable fit between Equation (4-1) and available data (compiled from Sloan, 1998, *p. 404, Ch. 6*).

The methanol solution injection function q_{inj} was simplified as well into a step function, as illustrated in Figure 4-2. This reflects the selected experimental protocol accurately

while eliminating noise from the data; also, time integrals of q_{inj} then become straightforward. A value of 1.7 g/s was adopted and the injection time was prorated in inverse proportion to the initial methanol volume fraction, from 188 s with Record # 051028 (corresponding to injection of 25% MEOH solution; see Table 1 in Appendix D for the other test conditions).

The hydrate dissociation formalism discussed in Appendix D represents the baseline for the present comparisons. Corresponding results are labeled 'Clarke Bishnoi,' with the values K_0 = 36000 mol/m^2-Pa-s and E = 81000 J/mol for the Arrhenius-type kinetics taken from Clarke & Bishnoi (2001). For the time being, the turbulent convective heat transfer coefficient H was kept constant, with sample values of 1000 and 3000 W/m^2-K.

A simpler hydrate dissociation kinetic model, labeled 'Equilibrium,' was also considered. It assumes that the decomposing surface temperature T_s is equal to the equilibrium value at ambient pressure p. In this case, δf is zero and the kinetic constant K_d must be infinite. Mathematically, Equation (5) in Appendix D is replaced by $p_{eq}(T_s; s) = p$, or, by obvious definition of T_{eq}, $T_s = T_{eq}$.

Figures 4-3 through 4-5 show calculated results of gas flow rate and load cell change for the three experiments under consideration.

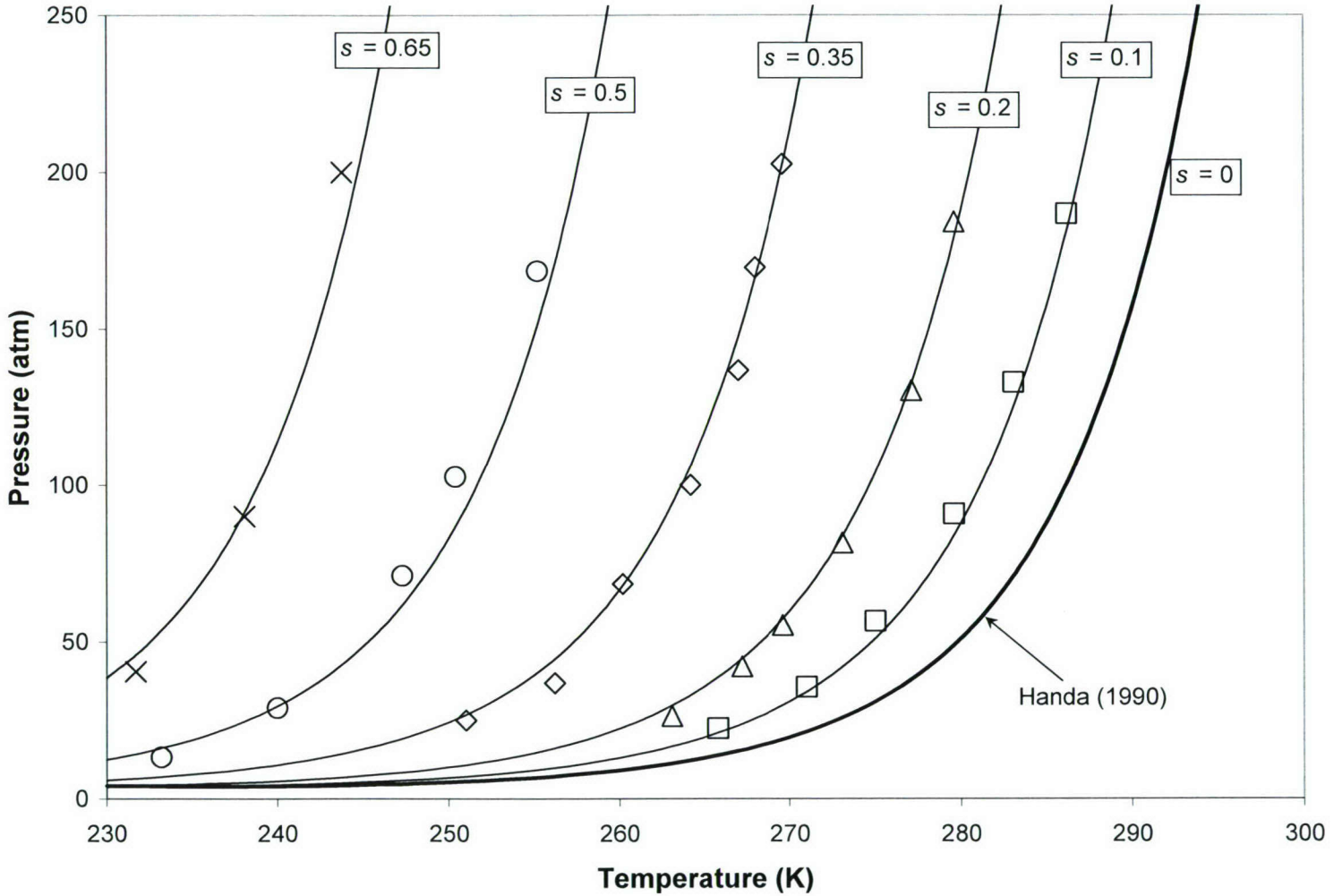

Figure 4-1. Three-phase equilibrium pressure p_{eq} as s varies: Equation (4-1) (thin lines); data (symbols).

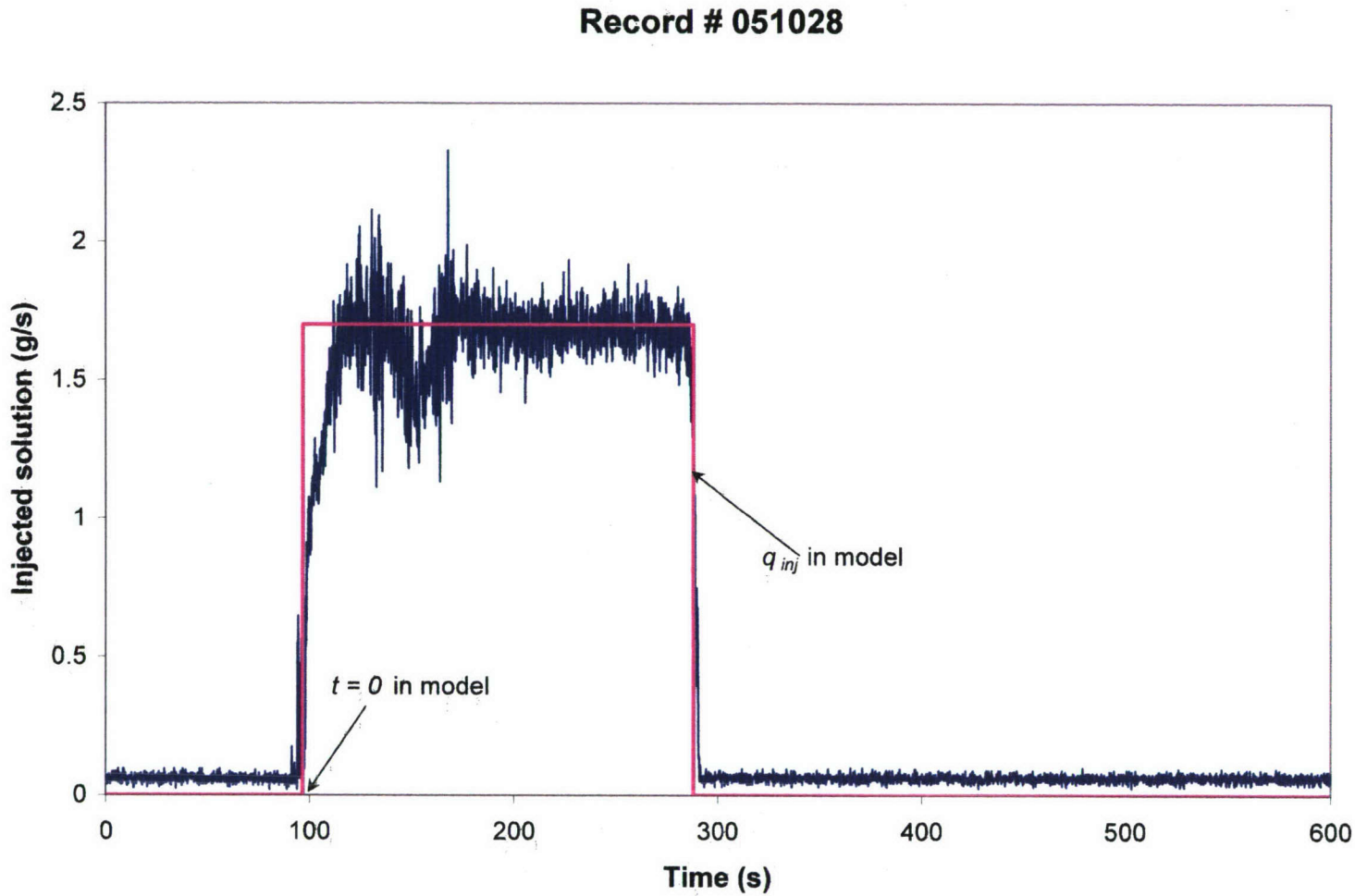

Figure 4-2. Sample representation of q_{inj} in computer model.

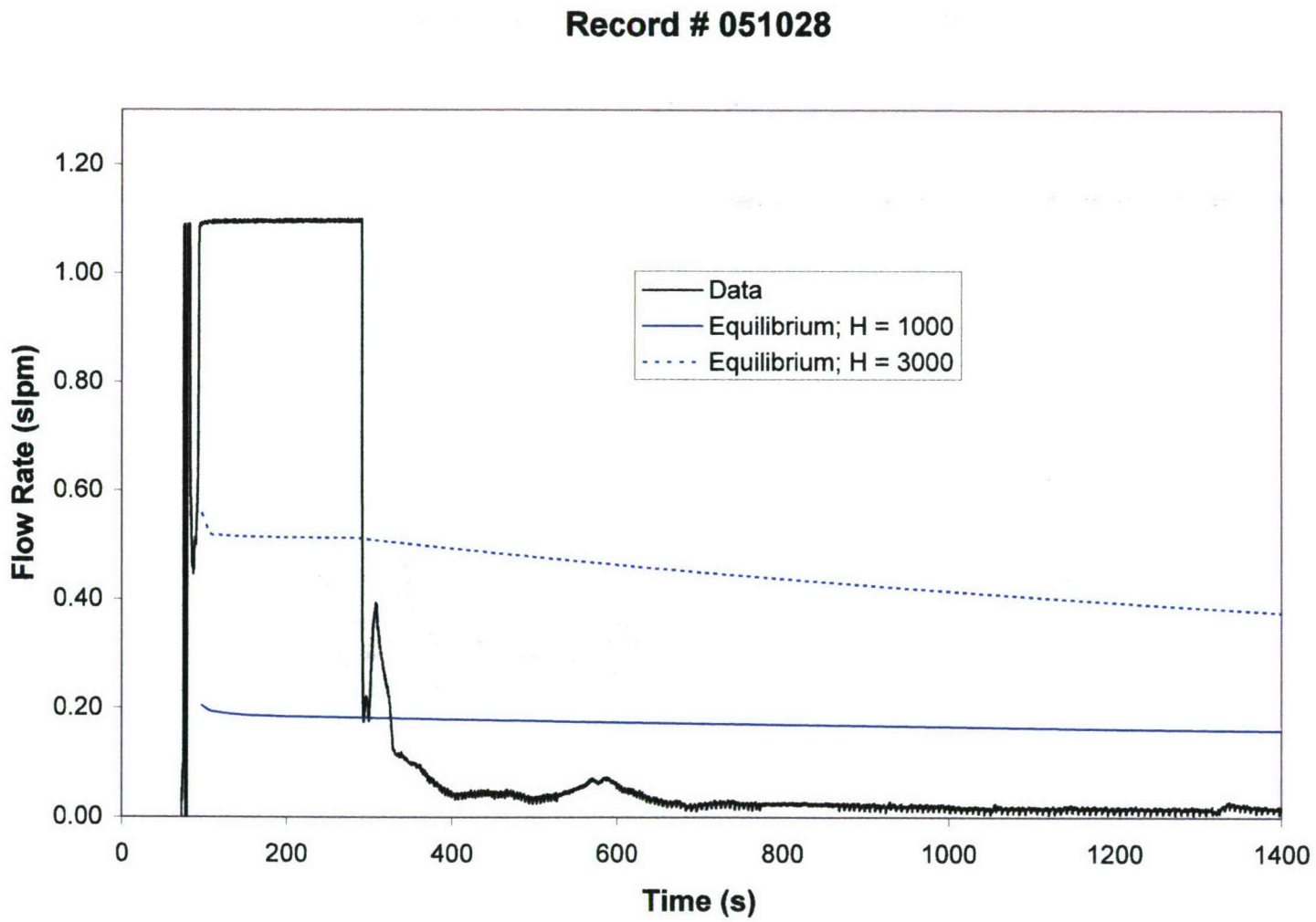

Figure 4-3a. Comparison of model predictions and experimental data on gas production for injection of 25% (by volume) MeOH in DI water at 4 °C and nom. 5.13 MPa over synthetic methane hydrate.

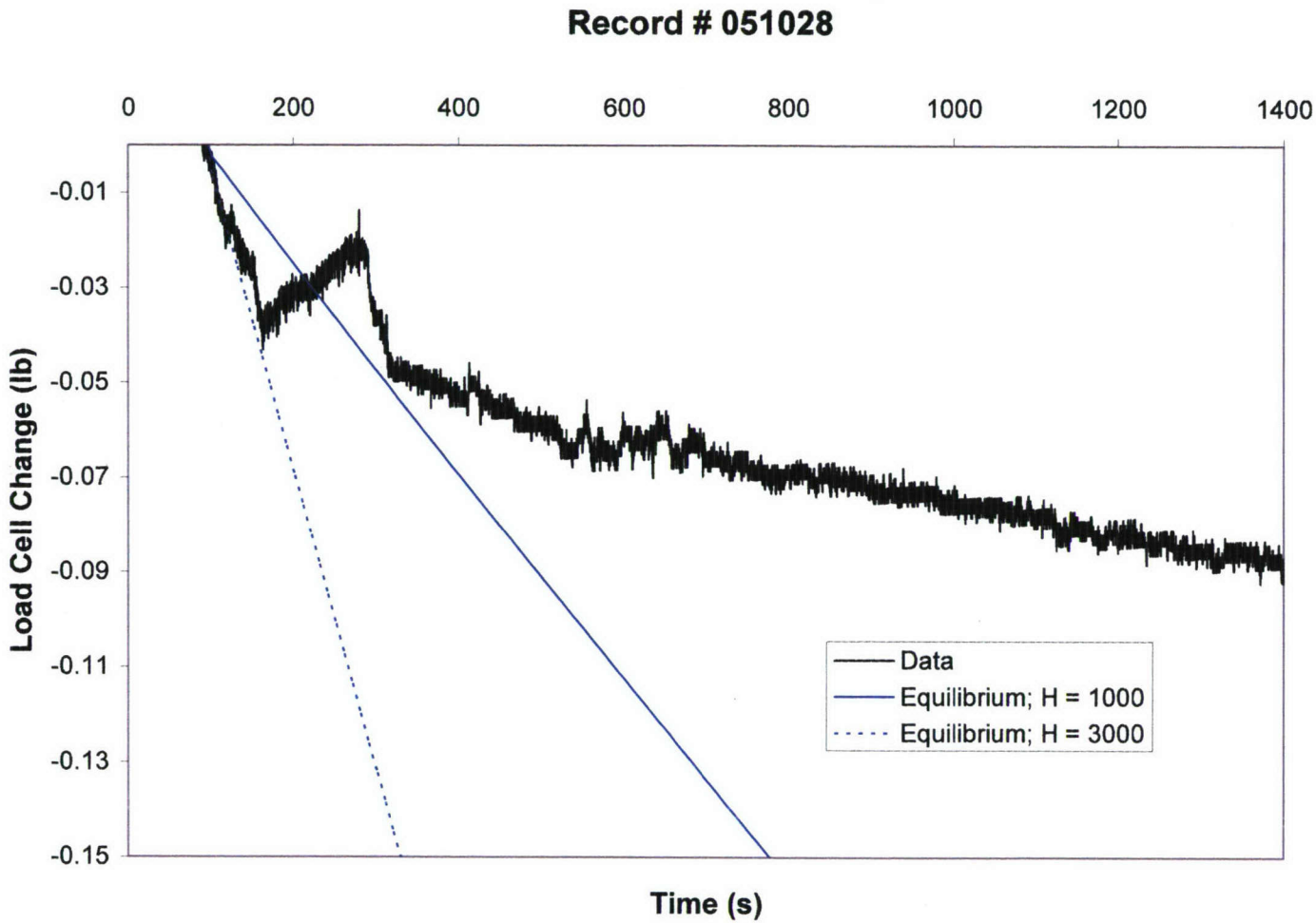

Figure 4-3b. Comparison of model predictions and load cell data on gas production (weight of water displaced by gas flowing into Torricelli tube device) for injection of 25% (by volume) MeOH in DI water at 4 °C and nom. 5.13 MPa over synthetic methane hydrate.

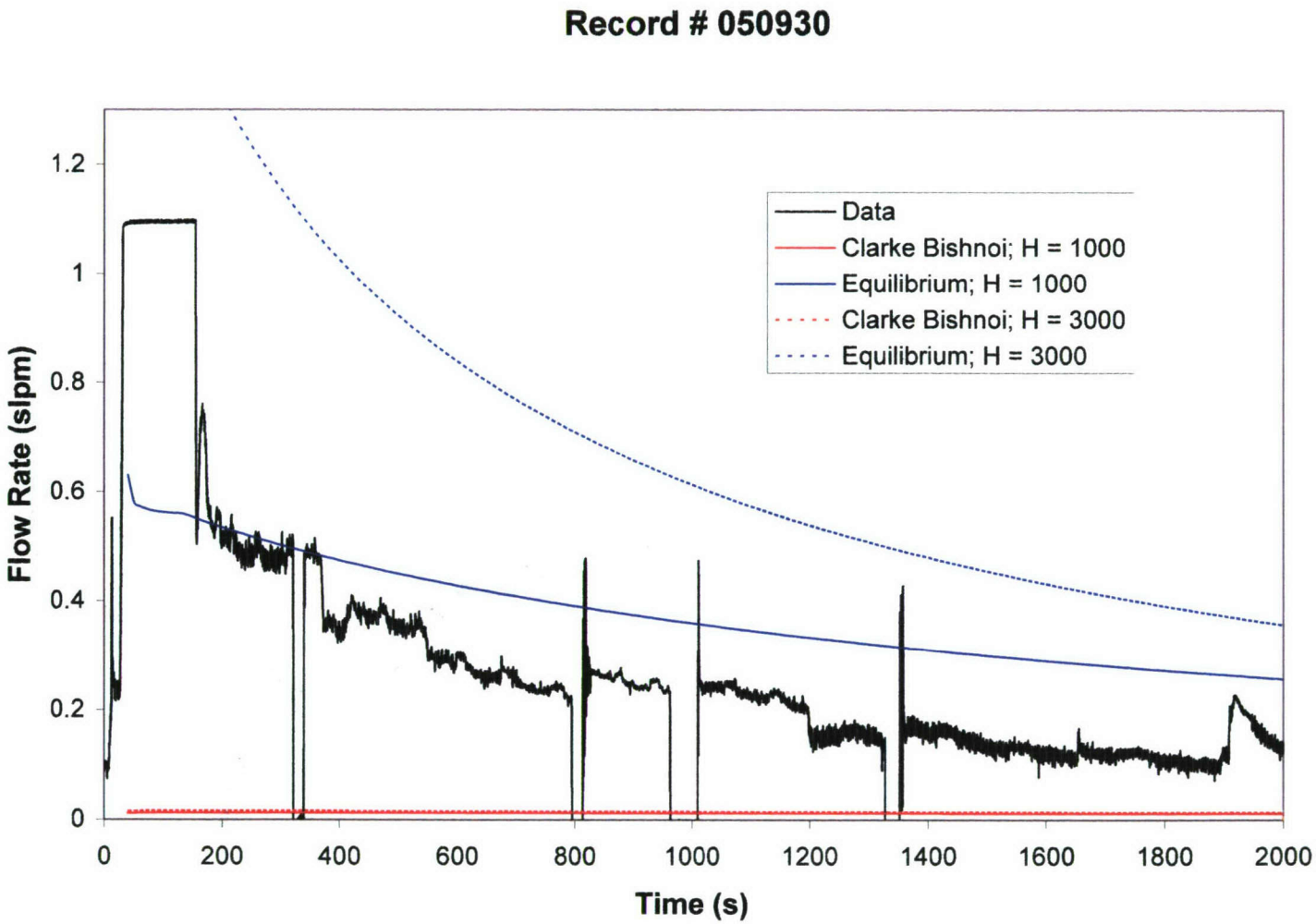

Figure 4-4a. Comparison of model predictions and experimental data on gas production for injection of 50% (by volume) MeOH in DI water at 7 °C and nom. 5.13 MPa over synthetic methane hydrate.

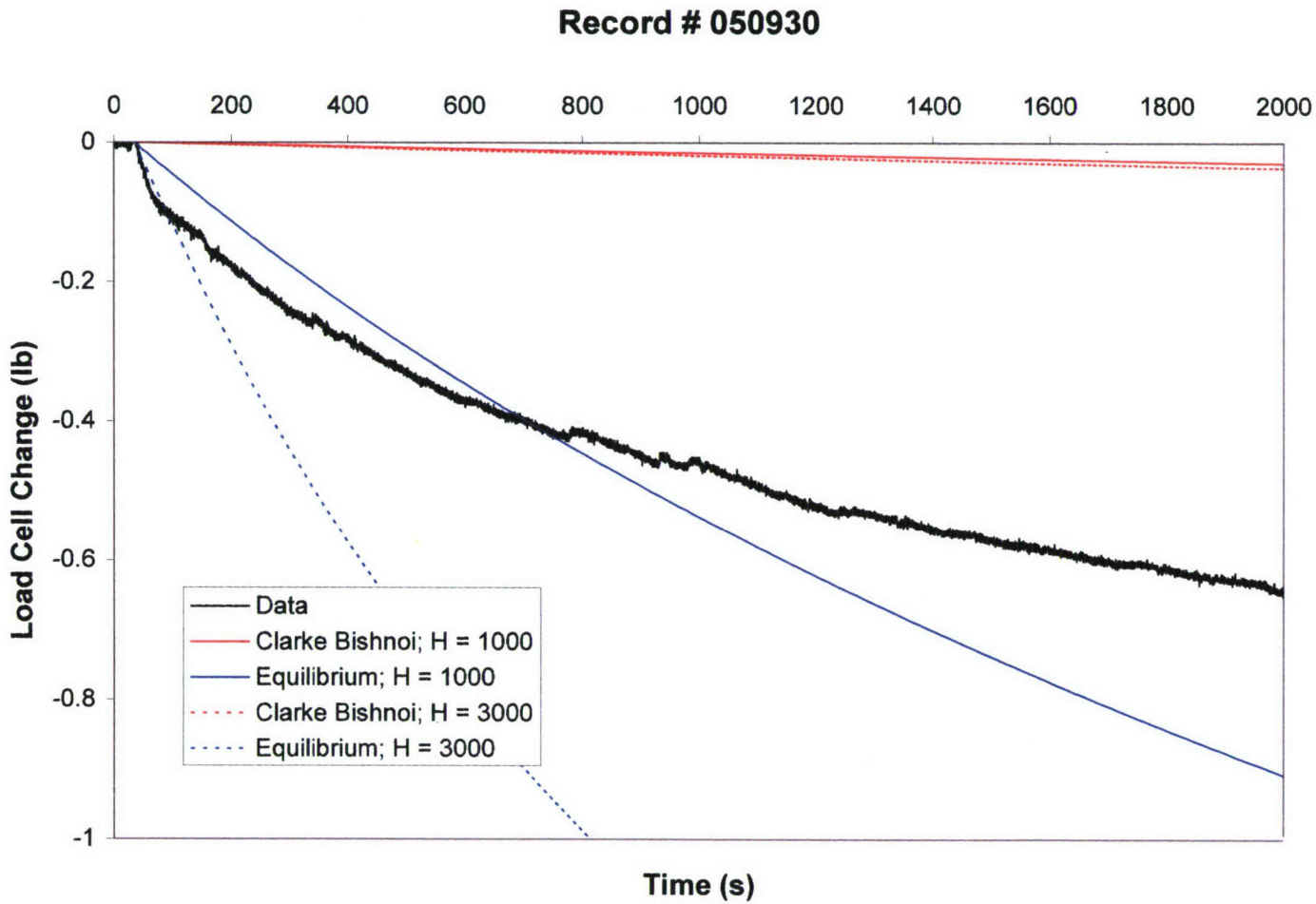

Figure 4-4b. Comparison of model predictions and load cell data on gas production (weight of water displaced by gas flowing into Torricelli tube device) for injection of 50% (by volume) MeOH in DI water at 7 °C and nom. 5.13 MPa over synthetic methane hydrate.

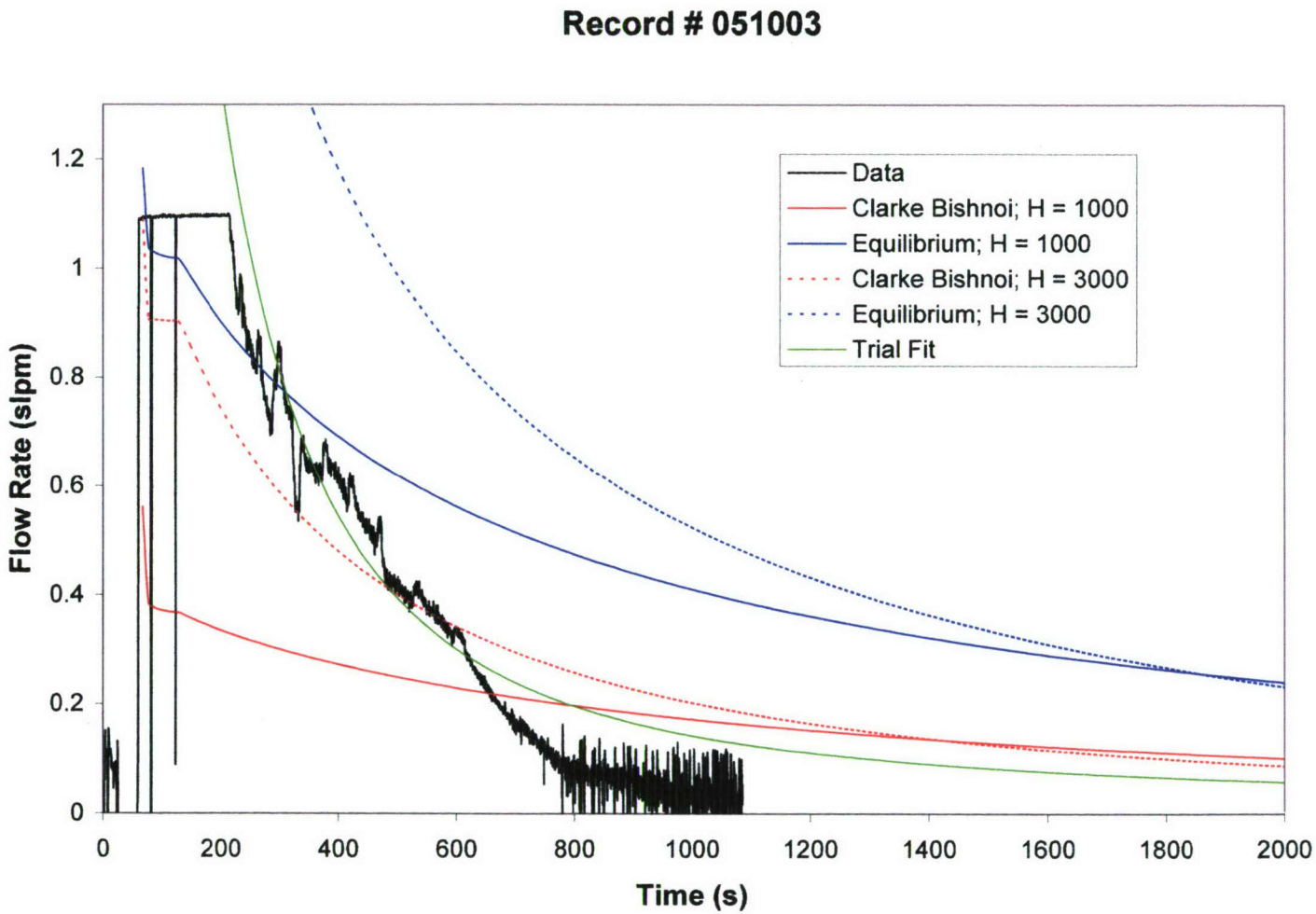

Figure 4-5a. Comparison of model predictions and experimental data on gas production for injection of 75% (by volume) MeOH in DI water at 10 °C and nom. 5.13 MPa over synthetic methane hydrate.

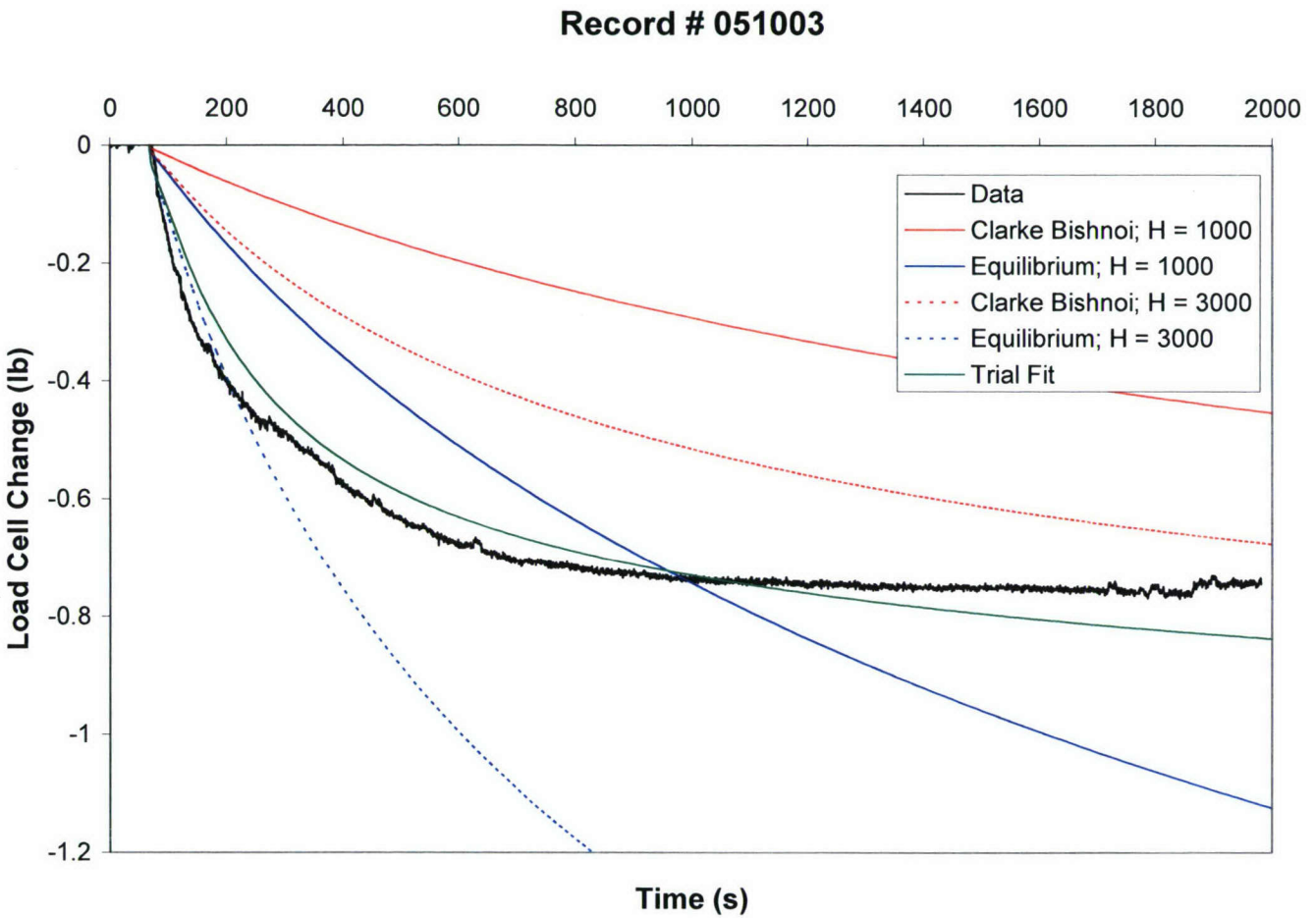

Figure 4-5b. Comparison of model predictions and load cell data on gas production (weight of water displaced by gas flowing into Torricelli tube device) for injection of 75% (by volume) MeOH in DI water at 10 °C and nom. 5.13 MPa over synthetic methane hydrate.

Gas flow rate data in Figures 4-3a, 4a and 5a are only relevant when they are below about 1.1 slpm, the maximum reading from the Coriolis flow meter. Fortunately, physical phenomena taking place during higher gas release, especially when the liquid inhibitor solution is injected, may be explored using the load cell time histories.

For Record # 051028 (injection of 25% MEOH solution by volume), baseline parameters using the intrinsic dissociation kinetics of Clarke & Bishnoi (2001) result in negligibly small hydrate dissociation rates to the extent that the corresponding calculations do not appear in Figures 4-3a and 3b. Results in Figure 4-3b with a dissociation surface instantaneously at equilibrium suggest that much faster kinetics may hold, at least for a minute or two.

These observations essentially are corroborated with Record # 050930 (injection of 50% MEOH solution by volume). Here again, equilibrium kinetics seem relatively more successful in representing the data. While a higher heat transfer coefficient H of 3000 W/m^2-K still does well immediately following injection, a more moderate value of about 1000 W/m^2-K provides reasonable predictions over 10 to 20 minutes. Since the 'Equilibrium' approach essentially is a one-parameter model (H), a possible approach to improve predictions would be to consider H variable with time; this would be relatively intuitive since the more gas is released per unit dissociation area, the more turbulence occurs in the liquid phase contacting the hydrate surface. This approach will be pursued in the future.

Record # 051003 (injection of 75% MEOH solution by volume) finally shows substantial hydrate dissociation even with the 'Clarke-Bishnoi' kinetics. 'Equilibrium; H = 3000' results still do quite well matching the data at small times of a couple of minutes. As conceived, the one-dimensional model using Equation (1) of Appendix D has three fundamental parameters (K_0, E and H), while only H must be set when equilibrium kinetics are used. There likely are different ways to fit these model parameters to match the data, although it is doubtful that a given parametric choice may hold for all data records. To illustrate this point, the selection K_0 = 36 mol/m^2-Pa-s (one thousandth of the baseline value), E = 81,000 J/mol (unchanged) and H = 10,000 W/m^2-K was used ('Trial Fit'); as can be appreciated, results match this particular data set quite well.

More work obviously needs to be done. A balance should be found between practical algorithms of potential engineering value and modeling based on as much physics as possible (versus mere curve fitting). While established on well written publications, the Clarke-Bishnoi hydrate dissociation formalism already has proved itself difficult to use with hydrate dissociation mechanisms other than depressurization without substantial *ad hoc* modifications of the kinetic constants (Moridis *et al.*, 2005; Nihous & Masutani, 2006). This is believed to reflect a fundamental ambiguity in using the fugacity driving force δf as a metric ('distance' from equilibrium) for all hydrate dissociation mechanisms. In the case of experiments at constant pressure, for example, a more natural choice for such a metric would be (T_s - T_{eq}). A preliminary exploration of this concept was attempted in the present model, and the new kinetic formalism did not appear to fare any worse than the Clarke Bishnoi equation. Such an approach, however, only shifts the problem from one thermodynamic variable to another, since one ultimately would have to consider cases of hydrate dissociation under *simultaneous* depressurization and heating.

In summary, during the present reporting period we have completed a suite of preliminary experiments of hydrate destabilization utilizing the facility constructed during previous Phases of the HEET Initiative. A model has been developed based on the concept of an intrinsic

dissociation rate to interpret the data from these experiments. An initial comparison raises questions about the underlying formalism of the model. These questions, along with improvements to the experiment and additional tests, will be pursued in the future.

Calorimetry

Differential Scanning Calorimetry (DSC) is commonly used for thermal characterization of physico-chemical transformations. The technique monitors the heat exchange between a sample and its surrounding versus time and/or temperature. It has been used to study the thermodynamic conditions of stability, dissociation enthalpies, and heat capacities of various gas hydrates (Koh *et. al.*, 2002; Kharrat & Dalmazzone, 2003; Dalmazzone *et. al.*, 2004). Methane hydrate measurements need to be studied at high pressures and low temperatures. The BT2.15 calorimeter has these capabilities and was procured in 2003. During the present reporting period, we continued our experiments with the BT2.15 calorimeter on the thermodynamics of stability of various hydrates including THF, methane, and ethane.

Kharrat & Dalmazzone (2003) performed DSC measurements of dissociation temperatures of methane hydrate in pure water. Figure 4-6 shows the thermogram corresponding to the heating at 6.00 MPa of a sample of pure liquid water under methane gas from 270 K to 285 K.

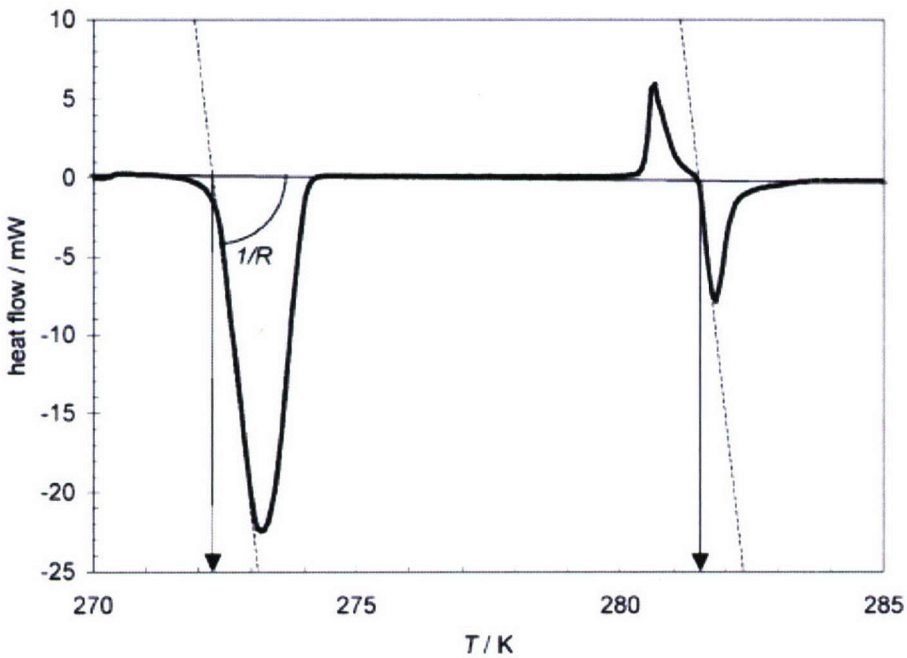

Figure 4-6. DSC thermogram of water-methane system initially cooled to 270 K at 6.00 MPa. From Kharrat & Dalmazzone (2003).

The thermogram shows ice melting at 272.3 K, then hydrate formation at about 280.5 K, followed by dissociation of the hydrate at about 281.5 K. It is important to note that Kharrat & Dalmazzone only observed the formation of hydrate upon heating, after ice melting, and never upon cooling as would be expected. Stern *et al.* (2000) studied the synthesis of high purity methane hydrate by slowly heating and cooling small ice crystals in the presence of methane at elevated pressures just below the stability boundary. Several cycles of warming and freezing

were required to produce methane hydrate crystals of high purity. They observed a shell of hydrate forming on ice grains at low temperatures in the ice subsolidus field immediately after exposure to methane gas. This formation virtually halts after the initial surface reaction unless the solid is vigorously agitated (to expose new surface area) or the temperature is raised. The process of converting the unreacted ice core to hydrate by raising the temperature is not well understood. Although there is evidence of some melting of the cores as the system is warmed through the melting point of ice, it is apparent that complete melting does not take place, since particle morphology can be maintained through this process.

It has been posited that hydrate nucleation follows the formation of labile clusters (Sloan, 1998) or structured water, which implies that the history of the H_2O phase can be significant (e.g., liquid water from melted ice could contain residual structured water). Understanding the mechanisms that underlie the genesis of hydrates from ice or liquid water therefore is significant, probably more so for permafrost scenarios than for marine sediments.

Calorimetry studies conducted during the present reporting period have examined the effect of the history of the water phase (ice or liquid) during hydrate formation and decomposition. Figure 4-7 is a typical thermogram of slow heating of pure ice crystals (<200 μm) in the presence of methane gas at 6.00 MPa. Note that the calorimeter allows the user to control the temperature of the sample. Melting of ice is observed at about 0 °C. A small hydrate formation peak may be observed during the 8 hour hold at 3 °C, and a large dissociation peak is observed at about 8 °C, which is the expected dissociation temperature for methane hydrate at 6.00 MPa. It is unclear why the formation peak is so much smaller than the dissociation peak. If, as we believe, the peaks correspond to methane hydrate formation and dissociation, then the areas under each should be equal (cf. Figure 4-7 on the next page). Additional experiments are underway to rigorously investigate differences in the formation and dissociation of methane hydrate from ice crystals and liquid water. In these tests, Raman measurements, which can detect and differentiate between hydrate, ice, and liquid water, would provide valuable information to interpret the thermograms. Toward this end, we have pursued development of a probe that provides optical access to the interior of a high-pressure calorimeter sample cell to perform Raman and other spectroscopic measurements.

4.3.3 Simultaneous Spectroscopy and Calorimetry

DSC is a powerful tool to investigate methane hydrate thermochemistry; however, commercially available DSC instruments do not provide any means to identify the phases or compounds that exist within the sample cell in order to relate an observed absorption or emission of thermal energy to a particular reaction or phase change. It was determined that a high pressure gas circulation cell for our BT2.15 calorimeter, shown in Figure 4-8 on the next page, could be modified to accommodate a fiberoptic link to the interior of the cell. The fiberoptic link would be coupled to an external light source (e.g., laser or lamp) to illuminate the sample and would collect and transmit scattered light out of the cell to a detection system.

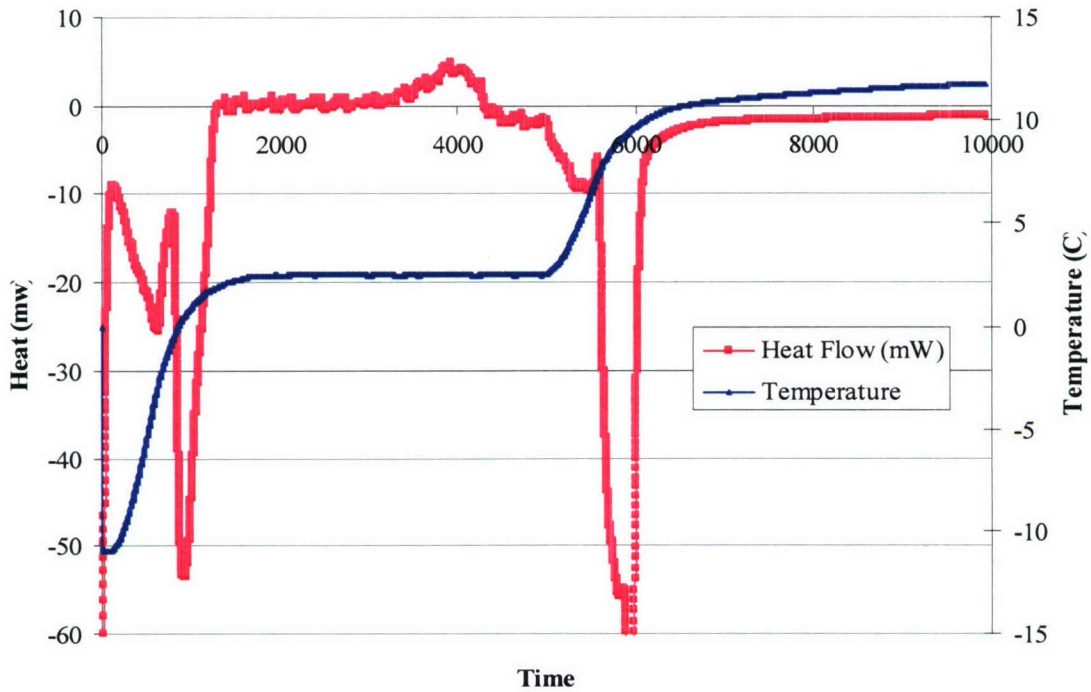

Figure 4-7. Thermogram showing temperature and heat flow histories (over 10^4 s) of fine ice crystals under methane gas at 6.00 MPa.

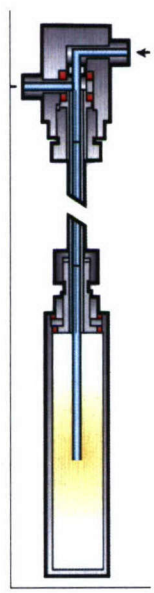

Figure 4-8. Schematic drawing of the standard high pressure gas circulation cell for the Setaram BT2.15 calorimeter (from http://thermal-analysis.setaram.com/fichiers/produit/bt215-lien4-a200394832161739.pdf).

In the standard Setaram circulation cell, gas or liquid can be injected into the sample volume via a small diameter (approx. 1/16 in. o.d.) tube enclosed within a larger tube (approx. 1/8 in. o.d.).

Fluid is removed through the annulus between the two tubes. To provide access for the fiberoptic link, the cell closure and gas tubes were redesigned as shown in Figure 4-9 on the next page. A ¼ inch o.d., 0.028 in. wall stainless steel tube was substituted for the original 1/8 inch tube to provide enough room for both a fiberoptic probe and the 1/16 in. o.d. fluid injection tube. Fluid can still be withdrawn through the open spaces between these components and the inner walls of the ¼ inch tube.

A number of options were considered for the fiberoptic link. The primary constraints in the present application were size (i.e., the fiberoptics needed to be threaded through the ¼ inch tube along with the fluid injection tube) and operating pressure. Pressure in the sample cell and ¼ inch tube could be as high as 100 bar and the fiberoptics would have to transition to ambient pressure outside the calorimeter well. A pressure-sealed, small diameter shielded probe appeared to be appropriate and an acceptable design was identified after consultations with several potential suppliers. Figure 4-10 on the page after the next one shows a drawing of the probe.

The fiberoptic probe comprises seven 200 μm core UV silica fibers encased in epoxy (as a pressure seal) within a 0.125 inch o.d. 316 stainless steel sleeve. Radiation is transmitted into the cell via a single fiber positioned at the center of the probe. This transmitting fiber is surrounded by the remaining six receiving fibers which collect the Raman-shifted light and bring it out to be coupled into a spectrograph. Commercial fiberoptic Raman probes generally include filters and micro focusing optics at the ends of the fibers to minimize unwanted radiation and improve spatial resolution; however, including these component was not feasible since they could not be configured to fit within the maximum allowable 0.125 inch o.d. of the probe. Analyses indicated that fluorescence from the silica fibers induced by the excitation laser light would not be significant due to the relatively short length of the fibers. Lacking focusing optics, the spatial resolution of the probe is determined by the overlap of the fields of view (acceptance cones) of the transmitting and receiving fibers.

The modified gas circulation cell and the fiberoptic probe have been procured along with a 100 mW diode pumped solid state CW laser (532 nm frequency doubled Nd:YAG) and the optics required to couple the two fiberoptic cables (i.e., transmitting and receiving) to the laser and spectrograph. A custom transition section (i.e., pressure seal) for the fiberoptic probe and gas supply tubes has been designed using the ANSYS® software package and fabricated at one of the UH machine shops. Assembly and testing will commence in September 2006, on completion of electronics to monitor the radiant power input into the sample cell. Since calorimetry generally entails the measurement of small energy transfers to and from a sample arising from some physical process such as phase change, reaction, or mixing, the radiant energy supplied by the excitation laser light and the radiant energy removed by the receiving fibers need to be accounted for in the analysis of the calorimeter heat flow data. In our experiments, there will be a number of methods to quantify the energy transfers associated with the Raman measurements. Since the measurements do not need to be performed continuously, the laser will be shuttered most of the time. To estimate the net radiant energy input during a Raman measurement, we will unshutter the laser and perform a measurement at a point in the process when the sample is stable, i.e., the heat flow is zero. The heat flow spike registered by the calorimeter associated with this measurement can be used to estimate the net radiant energy contribution for a "typical" Raman measurement. This estimate can then be applied when measurements are performed when heat flow is not zero due to phase change.

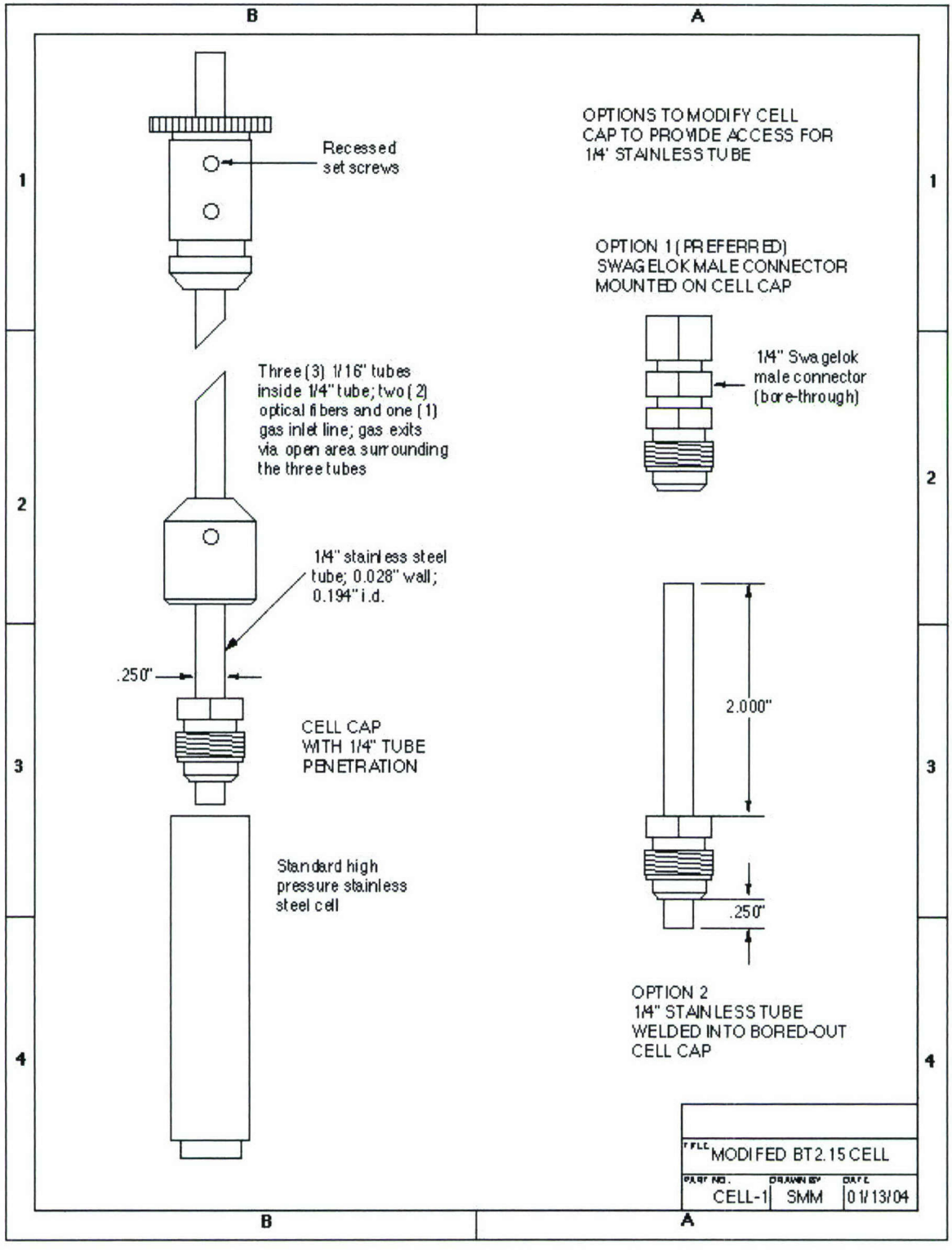

Figure 4-9. Modifications to high pressure gas circulation calorimeter cell.

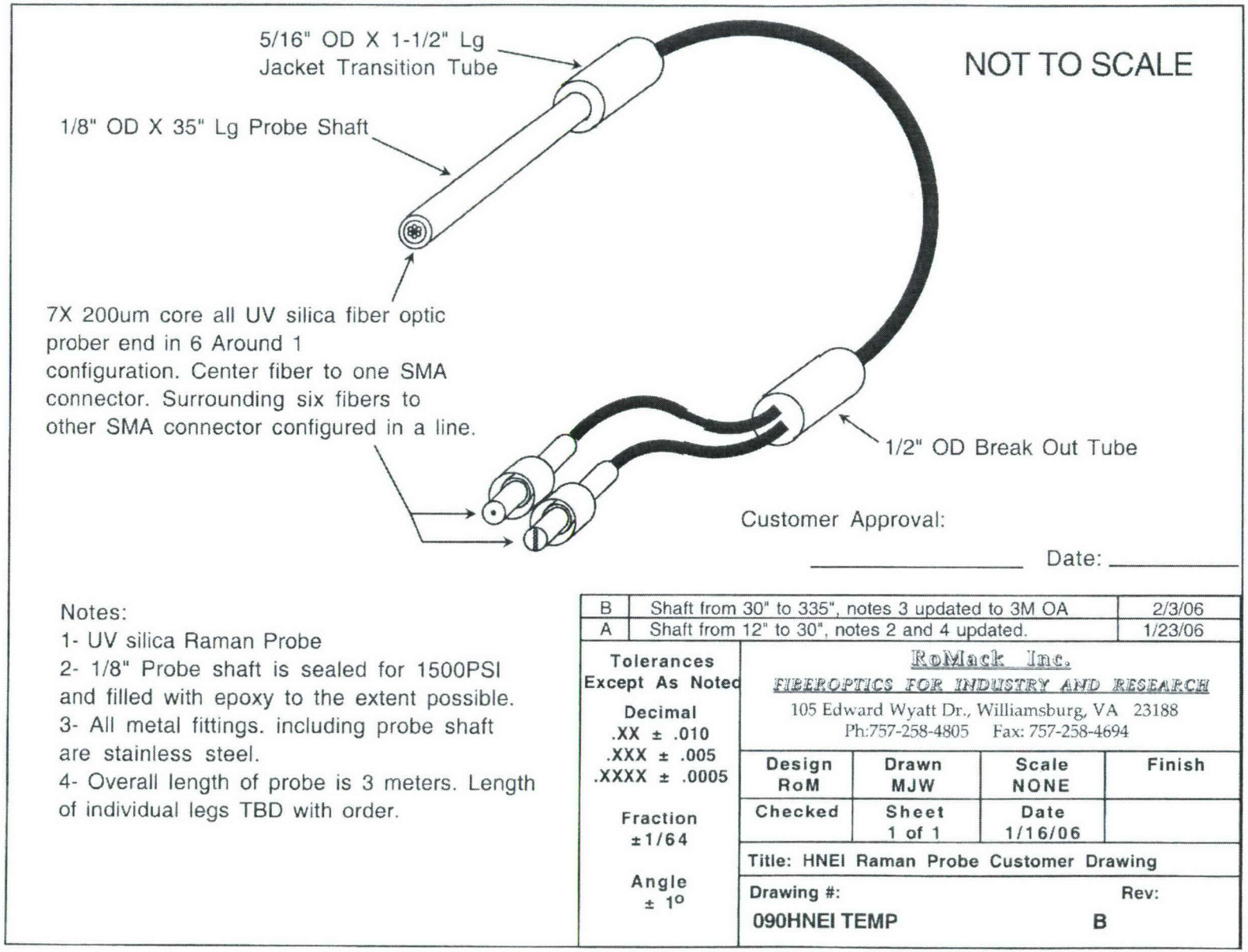

Figure 4-10. Fiberoptic probe.

Since it is anticipated that the laser radiation entering the cell will constitute the primary energy contribution of the Raman instrument, and since there can be small temporal fluctuations in the laser output power, a portion of the beam (~5%) will be split off prior to coupling into the receiving fiber using a pellicle beamsplitter and directed through a narrow band (3 nm FWHM) laser line filter onto a silicone photodetector. The photodetector signal will be input into the data acquisition system used with the calorimeter to provide a continuous time record (via calibration) of the laser power entering the sample cell. The conditioning electronics for the photodetector currently are being constructed.

In addition to the immediate objective of conducting Raman measurements of hydrates during calorimetric tests, the fiberoptic link can also be employed in other applications that are amenable to different diagnostic techniques such as emission or fluorescence spectroscopy. Our collaborators at NRL are particularly interested in utilizing the system to investigate photocatalyzed reactions of importance to marine biochemistry. In this case, the fiberoptic probe would irradiate a sample with UV light.

4.3.4 Hydrate Microbiology

Levels of methane in the majority of ocean sediments are biologically mediated. Microorganisms (*Archaea* and bacteria) determine the production, consumption, and distribution of methane and therefore play a critical role in hydrate formation and transfers between carbon pools (Kvenvolden, 1998; Kennicutt *et al.*, 1993). Hydrate microbiology is an important component of the methane hydrates task of the HEET Initiative from both the pure science and practical perspectives. Specifically, recovery of methane fuel from seafloor hydrates at any significant scale will demand assurances to the public that associated impacts on the marine environment will not be significant. This will require a thorough understanding of the affected sediment and seafloor microbial ecology and the linkages between these microorganisms and higher trophic levels in the food web. Furthermore, there is a growing body of evidence that leakage of methane from the sediment into the oceanic water column is limited by a consortium of bacteria and *Archea* in the top few meters of the seafloor. Changes in the methane flux resulting from purposeful or inadvertent hydrate destabilization during methane recovery could overwhelm the capacity of these organisms to contain leakage. During the present reporting period, efforts have focused on continuing activities initiated during the earlier Phases of HEET to characterize the microbial consortium—particularly with respect to developing effective protocols for molecular biological analysis and culturing—and cooperative investigations with NRL of methane depletion immediately adjacent to the seafloor.A six inch push core sediment sample collected by an ROV from the top of a hydrate mound in Barkley Canyon in the Gulf of Mexico was received from NRL to identify the microbiological community. Molecular biological techniques applied previously to other samples were employed to analyze this material. The generation of genomic preparations from microbial communities initially involves the extraction of nucleic acids from environmental samples and the quantification of the nucleic acids, especially double stranded DNA. Quantification of DNA in such samples can be hampered by the co-extraction or co-purification of humic substances (Bachoon *et al.*, 2001). Humic acids are chemically complex and polydisperse mixtures of microbiologically decomposed and transformed organic materials. There are several subclasses of humic acids that include tannins, lignins and fulvic acids. Structurally, humic materials are constructed from relatively small bio-organic supramolecular components that are self-assembled, mainly by weak dispersive forces such as van der Waals attractions, into larger molecules. DNA extractions for sediments and porewater previously were performed using commercially available kits and the same procedure initially was employed with the push core sample. It was determined, however, that in this case, the

purity of the recovered DNA was not acceptable. DNA extracts were visually tinted, indicating contamination by humic acids. Furthermore, PCR amplifications were poor. PCR amplification is sensitive to co-extracted substances such as heavy metals, pigments, and humic acids (Holben *et al.*, 1988, Juniper *et al.*, 2001, Rochelle *et al.*, 1992).

Extraction of DNA derived from soil (or sediment) microorganisms is based either on *in situ* cell lysis (More *et al.*, 1994; Ogram *et al.*, 1987; Picard *et al.*, 1992; Smalla *et al.*, 1993; Tebbe *et al.*, 1993; Tsai *et al.*,1991; Van Elsas *et al.*, 1998) or extraction from cells previously separated from soil (Holben *et al.*; 1988, Jacobson and Rasmussen 1992; Torsvic 1980). The latter strategy specifically targets prokaryote DNA and minimizes the extraction of higher concentration extracellular DNA from terrestrial sources. This generally results in higher purity; however, recovered cellular fractions only correspond to about 25-35% of the total number of bacteria present in the soil (Bakken 1985; Holben *et al.*, 1988; Steffan *et al.*,1988). Direct *in situ* lysis attempts to avoid representation problems, but different bacterial populations are not lysed in equal proportions. Furthermore, DNA from lysed organisms can become adsorbed to soil colloids that are not recovered by extraction, leading to under-representation of the total DNA concentration or specific DNA targets. The extraction of DNA is particularly difficult from sediments with high clay content (Frostegard *et al.*, 1999).

To reduce contamination, a manual method that separately extracts intracellular and extracellular DNA (Corinaldesi *et. al.*, 2005) and removes humic acids was attempted. Parallel analyses of both DNA pools currently are being conducted. Due to the limitations mentioned previously, total DNA (extracellular and intracellular) cannot accurately be determined from these samples. DNA extraction, however, does not differentiate between different sources. Therefore, the principal challenge is to secure sufficient quantities of DNA for microbiological species that are in very low concentrations. The visually high clay content of the push core sample exacerbates recovery problems. DNA extracted by the manual method was PCR amplified using the group specific primers given in Table 4-1. Qualitative amplification results presented in Table 4.2 need to be verified with cloning data. While it has been posited that methane is oxidized in anaerobic environments at the sulfate-methane interface near the seafloor by a consortium of methanogenic *Archea* and sulfate-reducing bacteria (SRB) (Claypool & Kvenvolden, 1983; Aharon & Fu, 2000), the PCR analysis of the sample to date indicates a lack of SRB in the mid core but the presence of aerobic methanotrophic bacteria (Table 4-2). The role of methanotrophic bacteria in the methane hydrate community is not well documented in current literature (Yan *et al.*, 2006).

Table 4-1. Primers for specific microbial groups associated with methane hydrates.

Microbial Group	Forward	Reverse
Bacteria (Lane *et al.*, 1991)	27F	1492R
Sulfate-Reducing Bacteria (Wagner *et al.*, 1998)	Dsr1F	Dsr4R
Methanogen (Marchesi *et al.*, 2001)	146F	1324R
Methanotroph I (Wise *et al.*, 1999)	MethT1bR	MethT1dF
Methanotroph II (Wise *et al.*, 1999)	27F	MetT2R

Table 4.2. PCR results for Barkley Canyon push core sample.

Core section DNA extracts from cellular fraction (c) and extracellular fraction (ex)

Primer Type	38c/ex	39c/ex	40c/ex	41c/ex	42c/ex	43c/ex
16s rDNA	X / X	X / X	X / X	X / X	X / X	X / X
Methanogen	X / O	X / X	X / X	X / X	X / X	X / X
SRB	X / O	X / X	O / O	O / O	X / O	X / O
Methanotroph Type I	O / O	O / O	X / O	X / O	O / O	O / O
Methanotroph Type II	O / O	O / O	O / O	O / O	O / O	O / O

*DNA extraction performed by method described by Corinaldesi *et al.*, 2005; fractions separated into whole cellular components and free extra-cellular DNA; PCR using various primer sets that target specific microorganism groups; positive amplification (X) and negative amplification (O).

To obtain relative microorganism group populations for the different sediment stratifications and mixed communities, DNA concentrations were normalized and applied toward the optimization of real time PCR. Real time PCR has the ability to quantify differences between starting materials; a theoretical relationship exists between the amount of starting target sample and the amount of PCR product at any given cycle. For equal concentrations of starting DNA, it is possible to compare relative concentrations of specific starting DNA templates between the different stratifications in the sediment. Spectrofluorometry using SYBR green I fluorescent dye was employed to determine and adjust DNA concentrations (Zipper *et al.*, 2003). Analyses presently are being optimized for initial DNA concentrations and primer annealing temperatures, using different primers pairs. Real time PCR is being performed at the University of Hawaii Biotech Core Facility.

In addition to the Gulf of Mexico push core, samples also have been collected recently during the joint research cruise on the Hikurangi margin offshore the North Island of New Zealand. Alternating 15 cm sections from two piston cores were shipped back to the University of Hawaii for microbiological analysis. The cores were selected based on a clearly defined sulfate-methane interface (SMI), where anaerobic methane oxidation occurs. Figure 4-11 on the following page presents the results of geochemical analyses of these cores, conducted onboard the research vessel during the cruise, which clearly show the concurrent depletion of sulfate and methane in the sediment at the SMI. DNA has been extracted for molecular phylogenic analysis from the core sections employing the same manual technique as the Barkley Canyon push core. Sub-samples currently are being enriched in culture medium in an attempt to perform pure culture isolation of methanogenic *Archea*, methanotrophic bacteria, and sulfate-reducing bacteria.

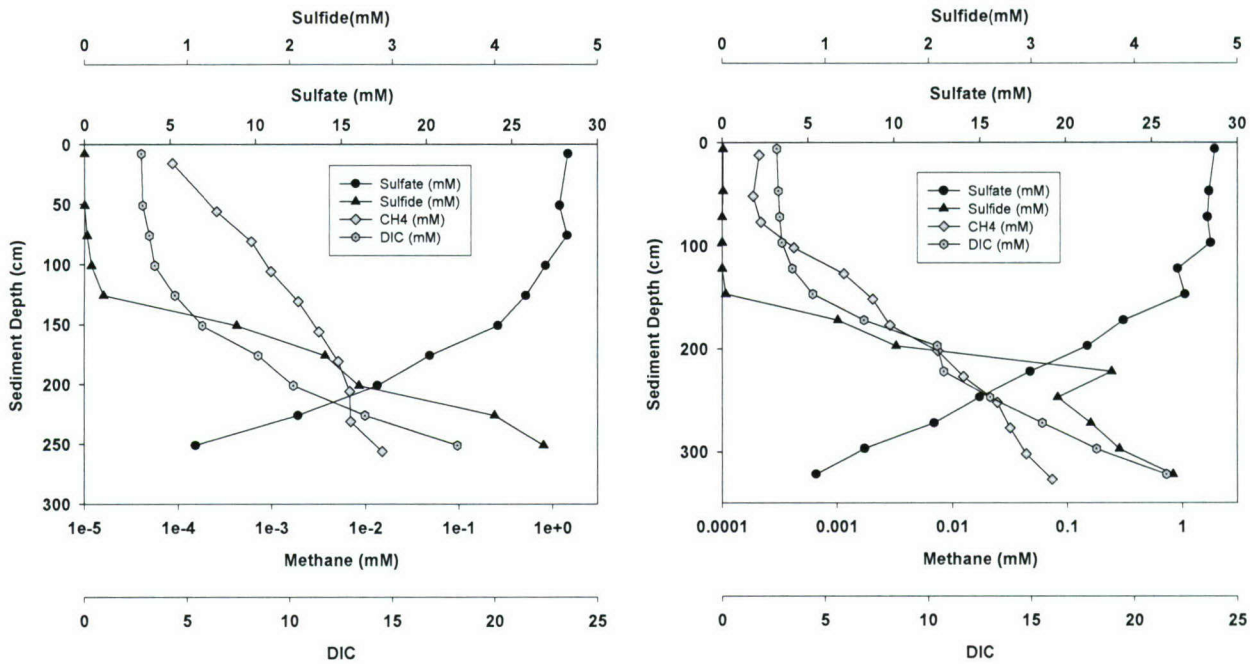

Unpublished data property of NRL Biogeochemistry group.

Figure 4-11. Geochemical analysis of pore water from piston core samples obtained on the Hikurangi Margin, New Zealand. A) Piston core # 11, B) Piston core # 14.

4.3.5 Subsea Power Generation

The original plan for the present reporting period was to continue to explore low-power microbial fuel cells for seafloor instrument power applications and to initiate analyses of higher power systems based on solid oxide, PEM, or alkaline fuel cells utilizing hydrates as an energy source. We were awarded a one-year grant from DARPA in May 2005 that provided the necessary resources to assess feasibility and complete a conceptual design study of a system that could produce approximately 100 W of net electrical power from seafloor methane and dissolved oxygen. As a result, we postponed the work on these types of systems under this grant until the completion of the DARPA project. The results of that study will be leveraged when the effort is resumed in the future.

During years 1-3 of the HEET Initiative, microbial fuel cells were tested in sediments samples collected from methane hydrates sites on the Cascadia Margin, Blake Ridge, and Gulf of Mexico. It was demonstrated that, at least in the short term, these microbial fuel cells performed similarly to those that had been tested previously by other researchers in shallow estuarine sediments. Typical power densities were about 0.01 W/m^2. This power density would require graphite electrodes with approximately 100 m^2 of external surface area to produce 1 W of power. Fuel cells of this size probably are not feasible due to difficulties in deployment and the cost of materials per unit power generated. Significant technical advances appear to be required if this approach is to be practicable.

Based on earlier results, power density appears to be limited by the transport of sulfide and oxygen reactants to the electrodes and the resistance of the porewater/seawater electrolyte to proton transfer. Understanding these limitations is essential to devise solutions; hence, experimental investigation of these phenomena was a focus of the subsea power generation subtask over the past year. The degree to which sulfide is oxidized to sulfate at the microbial fuel cell electrodes also was explored. This is important from a performance perspective since full oxidation of sulfide by a three reaction process yields four times the current per mole of sulfide as the initial conversion of sulfide to sulfur.

During previous Phases of HEET, voltammetry techniques were applied to bacteria cultured from sediment samples taken from methane hydrate sites in the Gulf of Mexico. These tests served both as a tool to identify which reactants were present in the sediment as a result of bacterial metabolism and to measure the reaction rates of these reagents. Over the past year, voltammetry experiments were performed in a solution of sodium sulfide dissolved in synthetic seawater and also in a sodium chloride electrolyte having the same chloride concentration as seawater. The results indicated that the electrolytes contributed minimal amounts of current and would not interfere with the measurement of sulfide oxidation reactions.

Figure 4-12 on the next page compares oxidation of dissolved sulfide in a NaCl solution to a voltagram of the same solution without sulfide. Subsequent tests were able to resolve the large peak with the extended tail into two different peaks as shown in Figure 4-13, on the following page. The major peak is likely to be sulfide oxidation to elemental sulfur. A similar peak, though slightly offset in potential, was observed in earlier experiments performed with the metabolites of sulfate-reducing bacteria in growth media. The second peak located around 400 mV in the present tests may be associated with the oxidation of the elemental sulfur to sulfite. This electrochemical reaction has a standard potential of 449 mV. Future experiments will investigate this reaction and how it may contribute to current production in the fuel cell. Refinements are being made to the voltammetry protocols and equipment to search for evidence of a sulfite to sulfate oxidation reaction.

Data from the original microbial fuel cell experiments were re-analyzed and the resistance of the porewater/seawater electrolyte was calculated to be around 600 Ω for the 35 cm^2 electrodes, or 21 $k\Omega \cdot cm^2$. An alternative electrolyte system could consist of seawater and a Nafion membrane that limits diffusion between the electrodes to proton transfer. Seawater resistivity typically is around 20 $\Omega \cdot cm$ with a resistance of 23 Ω for a similar-sized seawater electrolyte system. Nafion 117 membranes have a resistivity of 0.16 $\Omega \cdot cm^2$ and when scaled to the same area have a resistance of 4.6 mΩ. Resistance between the electrodes could therefore be reduced by about a factor of 30, which would decrease the voltage drop across the portion of power curve that is governed by Ohm's Law. Reactors currently are being fabricated to test the seawater/Nafion electrolyte system.

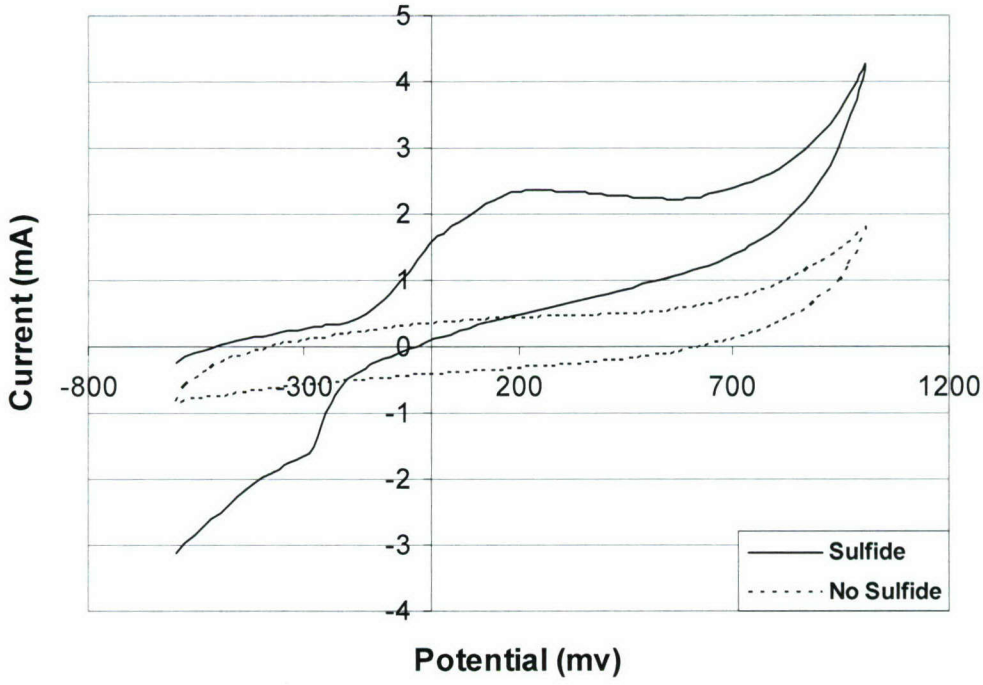

Figure 4-12. Voltagram of NaCl electrolyte before and after the addition of sulfide.

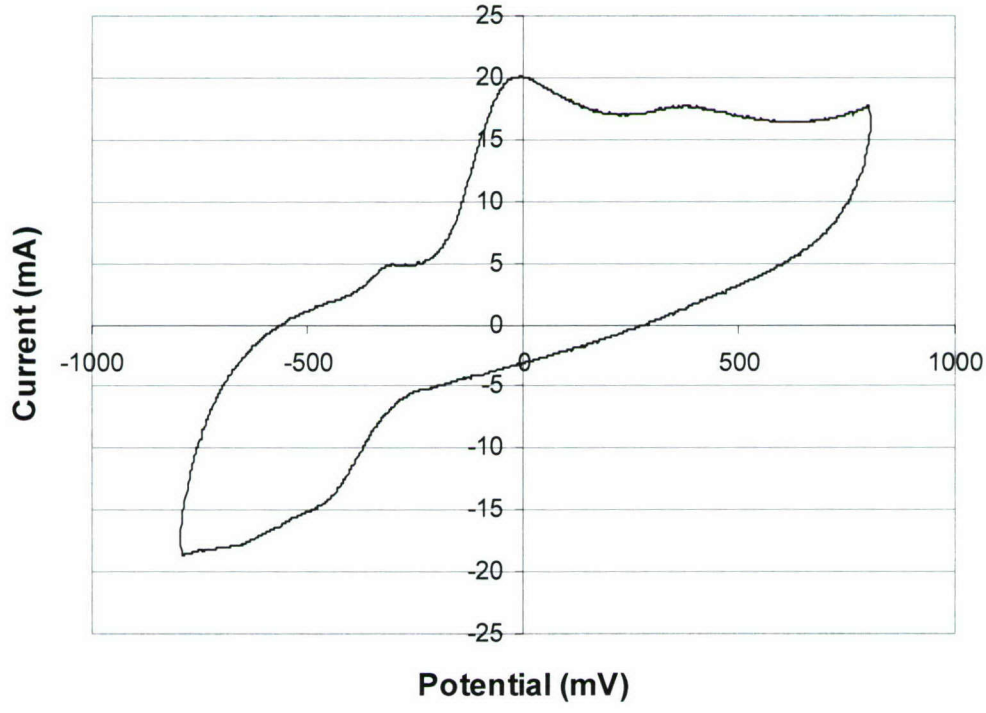

Figure 4-13. Voltagram of sulfide dissolved in NaCl solution.

4.4 Summary of Papers and Presentations Resulting from Efforts

R&D conducted as part of the HEET Methane Hydrates Task has produced the following thesis, papers, and presentations.

THESIS

Kurasaki, R., "Investigation of a Biological Fuel Cell in Methane Hydrate Marine Sediment," M.S. Thesis, Bioengineering, Department of Molecular Biosciences and Bioengineering, University of Hawaii, December 2004.

PAPERS

Nihous, G.C. and S.M. Masutani, "Theoretical Considerations Concerning the Dissolution Rate of Gas Hydrates in Undersaturated Water," submitted to *Chem. Eng. Sci.*, June 2005, under review.

Nihous, G.C. and S.M. Masutani, "A Model of Methane Concentration Profiles in the Open Ocean," submitted to *Global Biogeochem. Cycles*, February 2005, under revision.

Masutani, S.M., "Greenhouse Gas Hydrates in the Ocean," in Carbon Dioxide Utilization for Global Sustainability, (S.E. Park, J.S. Chang, and K.W. Lee, eds.), pp. 487-494, Elsevier Science, 2005.

Masutani, S.M. and R.B. Coffin, "Laboratory and Field Studies of Marine Methane Hydrates," in Proc. 5th International Symposium on CO_2 Fixation and Efficient Utilization of Energy, pp. 78-82, Tokyo Institute of Technology, Tokyo, Japan, 2002.

Uchida, T., J.A. Ripmeester, S.M. Masutani, and E.D. Sloan, Jr., "Database on Hydrate Properties: Influence of Kinetic and Thermodynamic Parameters on Formation and Stability," in Proc. 4th International Conference on Gas Hydrates, 2002.

PRESENTATIONS

Kuroda, K., S.M. Masutani, and G.C. Nihous, "Laboratory Experiments to Investigate Hydrate Destabilization," presented at ISOPE 2005, Seoul, Korea, 19-24 June 2005.

S.M. Masutani and R.B. Coffin, "Methane Hydrates," invited talk presented at the International Mechanical Engineering Congress and R&D Expo, Anaheim, CA, November 2004.

Kurasaki, R.J., B.A. Yoza, and S.M. Masutani, "Benthic Methane Fuel Cells," presented at the 32nd International Geological Congress, Florence, Italy, August 2004.

4.5 References

Aharon, P. and B. Fu, "Microbial sulfate reduction rates and sulfur and oxygen isotope fractionations at oil and gas seeps in deepwater Gulf of Mexico," *Geochim. Cosmologica Acta*, **64**, 233-246, 2000.

Bachoon, D.S., E. Otero, and R.E. Hodson, "Effects of humic substances on fluorometric DNA quantification and DNA hybridization," *J. Microbiol. Methods,* **47**(1), 73-82, 2001.

Bakken L.R., "Separation and purification of bacteria from soil," *Appl. Environ. Microbiol.*, **49**(6), 1482-1487, 1985.

Circone, S., Stern, L.A., Kirby, S.H., Pinkston, J.C., and W.B. Durham, "Methane hydrate dissociation rates at 0.1 MPa and temperatures above 272 K," *New York Academy of Science*, 544-555, 2000.

Clarke, M. and P.R. Bishnoi, "Determination of the activation energy and intrinsic rate constant of methane gas hydrate decomposition," *Canadian Journal of Chemical Engineering*, **79**, 143-147, 2001.

Claypool, G.E. and K.A. Kvenvolden, "Methane and other hydrocarbon gases in marine sediments," *Annu. Rev. Earth Planet Sci.*, **11**, 299-327, 1983.

Corinaldesi C., R. Danovary, A. Dell Anno, "Simultaneous recovery of extracellular and intracellular DNA suitable for molecular studies from marine sediments," *Appl. Environ. Microbiol.*, **71**(1), 46-50, 2005.

Dalmazzone, D., D. Clausse, C. Dalmazzone, B. Herzhaft, "The stability of methane hydrates in highly concentrated electrolyte solutions by differential scanning calorimetry and theoretical computation," *Am. Mineral.*, **89**, 1183-1191, 2004.

Frostegard, A., S. Courtois, V. Ramisse, S. Clerc, D. Bernillon, F. Le Gall, J. Pascale, X. Nesme, and P. Simonet, "Quantification of bias related to the extraction of DNA directly from soils," *Appl. Environ. Microbiol.*, **65**(12), 5409-5420, 1999.

Gao, S., "The decomposition of gas hydrates," http://www.owlnet.rice.edu/~sqgao/c602.pdf, 24 p., 2004.

Handa, Y.P., "Effect of hydrostatic pressure and salinity on the stability of gas hydrates," *Journal of Physical Chemistry*, **94**, 2652-2657, 1990.

Holben, W.E., J.K. Jansson, B.K. Chelm, and J.M. Tiedje, "DNA probe method for the detection of specific microorganisms in the soil bacterial community," *Appl. Environ. Microbiol.*, **54**(3), 703-711, 1988.

Jacobson, C.S. and O.F. Rasmussen, "Development and application of a new method to extract bacterial DNA from soil based on separation of bacteria from soil with cation exchange resin," *Appl. Environ. Microbiol.*, **58**(8), 2458-2462, 1992.

Juniper, S.K., M.A. Cambron, F. Lesongeur, and G. Barbier, "Extraction and purification of DNA from organic rich subsurface sediments (ODP Leg 169S)," *Mar. Geol.*, **174**(1), 241-247, 2001.

Kharrat, M., Dalmazzone, D., "Experimental determination of stability conditions of methane hydrate in aqueous calcium chloride solutions using high pressure differential scanning calorimetry," *J. Chem. Thermodynamics*, **35**, 1489-1508, 2003.

Koh, C.A., Westacott, R.E., Zhang, W., Hirachand, K., Creek, J.L., Soper, A.K. "Mechanisms of gas hydrate formation and inhibition," *Fluid Phase Equilibria*, **194-197**, 143-151, 2002.

Kuroda, K., S.M. Masutani, and G.C. Nihous, "Laboratory Experiments to Investigate Hydrate Destabilization," presented at ISOPE 2005, Seoul, Korea, 19-24 June 2005.

Jamaluddin, A.K.M., Kalogerakis, N., and P.R. Bishnoi, "Modelling of decomposition of a synthetic core of methane gas hydrate by coupling intrinsic kinetics with heat transfer rates," *Canadian J Chem. Eng.*, **67**, 948-954, 1989.

Kennicutt, M.C., J.M. Brooks, and H.B. Cox, "The origin and distribution of gas hydrates in marine sediments," in Engel M.H. and S.A Macko (eds.) *Organic Geochemistry*, Plenum Press, New York, pp. 535-544, 1993.

Kvenvolden K.A., "A primer on the geological occurrence of gas hydrate," in J.P. Henriet and J. Mienert (eds.), *Gas hydrates: Relevance to world margin stability and climate change*, The Geological Society, London, pp.39-80, 1998.

Kim, H.C., Bishnoi, P.R., Heidemann, R.A., and S.S.H. Rizvi, "Kinetics of methane hydrate decomposition," *Chem. Eng. Sci.*, **42**(7), 1645-1653, 1987.

Lane, D.J., "16S/23S rRNA sequencing," in E. Stackebrandt and M. Goodfellow (eds.), *Nucleic Acid Techniques in Bacterial Systematics*, pp. 115–175, Chichester, Wiley, 1991.

Marchesi, J.R., Weightman, A.J., Cragg, B.A., Parkes, R.J., Fry, J.C. "Methanogen and bacterial diversity and distribution in deep gas hydrate sediments from the Cascadia Margin as revealed by 16S rRNA molecular analysis," *FEMS Microbiol. Ecol.* **34**(3), 221-228, 2001

More, M.I., Herrick, J.B., Silva, M.C., Ghiorse, W.C., Madsen, E.L. "Quantitative cell lysis of indigenous microorganisms and rapid extraction of microbial DNA from sediment," *Appl. Environ. Microbiol.* **60**(5), 1572-1580, 1994

Moridis, G.J., Y. Seol, and T. Kneafsey, "Studies of reaction kinetics of methane hydrate dissociation in porous media," Lawrence Berkeley Laboratory Report LBNL-57298, 2005 (also in the Proceedings of the 5th International Conference on Gas Hydrates, Trondheim, Norway, June 13-16, 2005).

Nihous, G.C. and S.M. Masutani, "Notes on the dissolution rate of gas hydrates in undersaturated water," *Chemical Engineering Science*, in press, 2006.

Ogram, A.V., Sayler, S., Barkay, T. "The extraction and purification of microbial DNA from sediments," *J. Microbiol. Methods.* **7**, 57-66, 1987

Picard, C., Ponsonnet, C.,Nesme, X., Somonet, P. "Detection and enumeration of bacteria in soil by direct DNA extraction and polymerase chain reaction," *Appl. Environ. Microbiol.* **58**(9), 2717-2722, 1992

Rochelle, P.A., Fry, J.C., Parkes, R.J., Weightman, A.J. "DNA extraction for 16S gene analysis to determine genetic diversity in deep sediment communities," *FEMS Microbiol. Lett.* **100**, 59-66, 1992

Sloan, E.D., Jr., Clathrate Hydrates of Natural Gases (2nd ed.), Marcel Dekker, New York, 730 p., 1998.

Smalla, K., Cresswell, N., Mendonca-Hagles, L., Wolters, A., Van Elsas, D.J. "Rapid DNA extraction protocol from soil for polymerase chain reaction mediated amplification," *J. Appl. Bacteriol.* **74**, 78-85, 1993

Steffan, R. J., Goksoyr, J., Bej, A.K., Atlas, R. "Recovery of DNA from soils and sediments," *Appl. Environ. Microbiol.* **54**(12), 2908-2915, 1988

Stern, L.A., Kirby, S. H., Durham, W. B., Circone, S., and W.F. Waite, "Laboratory synthesis of pure methane hydrate suitable for measurement of physical properties and decomposition behavior," *In* Max, M.D. (ed.) Natural gas hydrate in oceanic and permafrost environments. Kluwer Academic Publishers, Netherlands, 245-261, 2000.

Tebbe, C.C., and Vahjen, W. "Interference of humic acids and DNA extracted directly from soil in detection and transformation of recombinant DNA from bacteria and a yeast," *Appl. Environ. Microbiol.* **59**(8), 2657-2665, 1993

Torsvic, V. L. "Isolation of bacterial DNA from soil," *Soil.Biol. Biochem.* **12**, 15-21, 1980

Tsai, Y.L., Olson, B. "Rapid method for direct extraction of DNA from soil and sediments," *Appl. Environ. Microbiol.* **57**(4), 1070-1074, 1991

Van Elsas, J.D., Duarte, G.F., Rosando, A.S. Smalla, K. "Microbiological and molecular biological methods for monitoring microbial innoculants and their effects in the soil environment," *J. Microbiol. Methods.* **32**(2), 133-154, 1998

Wagner, M., Roger, A.J., Flax, J.L., Brusseau, G.A., Stahl, D.A. "Phylogeny of dissimilatory sulfite reductases supports an early origin of sulfate respiration," *J. Bacteriol.* **180**(11), 2975-82, 1998

Wise, M.G., McArthur, J.V., Shimkets, L.J. "Methanotroph diversity in landfill soil: isolation of novel type I and type II methanotrophs whose presence was suggested by culture-independent 16S ribosomal DNA analysis," *Appl. Environ. Microbiol.* **65**(11), 4887-97, 1999

Yan, T., Ye, Q., Zhou, J., Zhang, C.L. "Diversity of functional genes for methanotrophs in sediments associated with gas hydrates and hydrocarbon seeps in the Gulf of Mexico," *FEMS Microbial. Ecol.* **57**(2), 251-259, 2006

Zipper, H., Buta, C., Lammle, K., Brunner, H., Bernhagen, J., Vitzthum, F. "Mechanisms underlying the impact of humic acids on DNA quantification by SYBR green I and consequences for the analysis of soils and aquatic sediments," *Nucleic acids Res.* **31**(7), e39, 2003

APPENDICES

Here attached to this Final Technical Report are four Appendices, as called out within the text of the primary report. These Appendices have individual, independent page numbers, distinct from the page numbering of the primary report, and are as indicated below:

Appendix A Complete installation of the initial Hardware-in-the-Loop Fuel Cell Test System (HiL #1) at the Hawaii Fuel Cell Test Facility
[76 pages]

Appendix B Gen 0 Fuel Cell Energy/Power System Simulation for an Unmanned Underwater Vehicle
[20 pages]

Appendix C UUV FCEPS Technology Assessment and Design Process
[80 pages]

Appendix D One-Dimensional Time-Domain Model of Hydrate Sample Dissociation
[16 pages]

This page is intentional blank

APPENDIX A

Technical Milestone Report

Complete installation of the initial Hardware-in-the-Loop Fuel Cell Test System (HiL #1) at the Hawaii Fuel Cell Test Facility

Hawaii Energy and Environmental Technologies (HEET) Initiative
Phase 4

Office of Naval Research
Grant Number N00014-04-1-0682
For the period June 15, 2004 to June 30, 2006

April 2006

TABLE OF CONTENTS

LIST OF FIGURES

LIST OF FIGURES (continued)

TECHNICAL MILESTONE REPORT
Task 1, Subtask 2, Year 1
Complete installation of initial Hardware-in-Loop Cell Test System (HiL #1)
at the Hawaii Fuel Cell Test Facility

1. Introduction

This milestone report covers the various elements involved in the installation of the first Hardware-in-Loop (HiL) dynamic test system (HiL #1) at the Hawaii Natural Energy Institute (HNEI) Hawaii Fuel Cell Test Facility (HFCTF). HiL in this context means the linking of an existing fuel cell system to a dynamic software model via a vendor-supplied fuel cell test stand or test station. The purpose is to evaluate the characteristics of the fuel cell system in an appropriate application, e.g., passenger vehicle, ship, airplane, or stationary power station, prior to the integration of the system. Among others, key parameters of interest are performance degradation, lifetime, efficiency and the development of control patterns for optimal operation of the fuel cell in specific applications. Figure 1 is a graphical representation of the basic elements in the HiL #1 system.

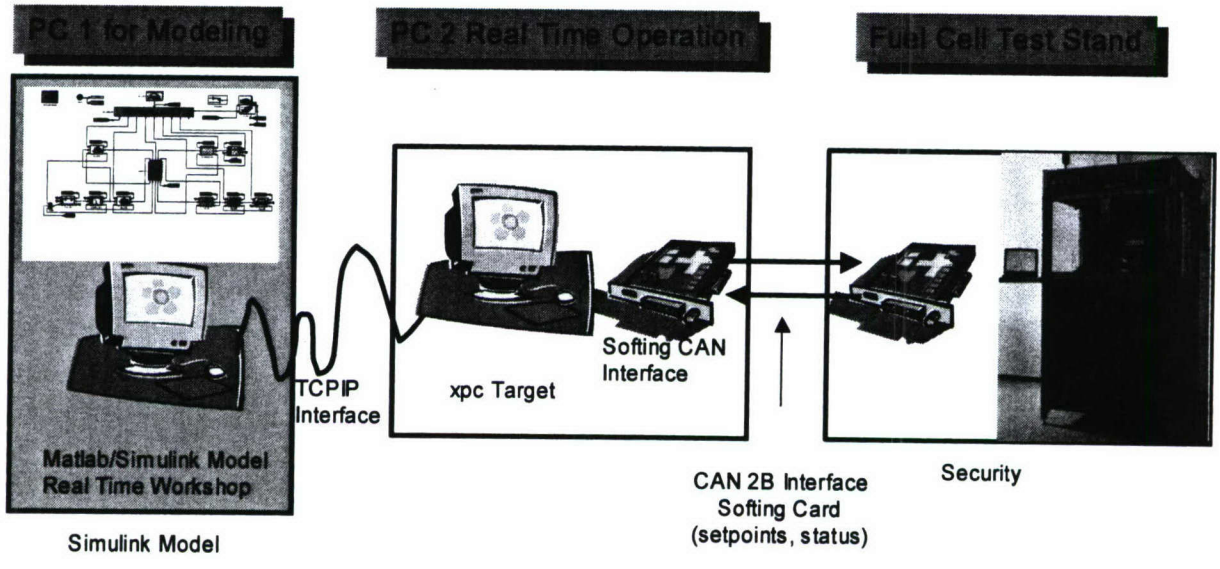

Figure 1: Sketch of the Overall HiL #1 System Setup

The evolution of this milestone included determining appropriate vendors for supplying fuel cell test stands or stations, establishing the specifications required for the particular vendor-supplied test station desired for HiL testing of fuel cells in this HiL #1 mode, purchasing the desired HiL test station from a vendor, conducting factory acceptance testing of the completed station (with a HNEI-supplied fuel cell and necessary support equipment) at the factory in Germany, shipping the station to the HFCTF in Hawaii, physically installing the delivered test station (plus the HNEI fuel cell and support equipment) at the HFCTF, conducting verification acceptance testing of the station after delivery, and initial testing of the complete system to determine actual test capabilities.

Actual functioning of the HiL #1 test system obviously requires more than the test stand or station itself. First, there must be a real fuel cell for testing in the test station. Acquisition of the fuel cell itself necessitated a process similar to that for the test station, including setting of specifications, identifying vendors, requesting and receiving quotations, and purchasing the fuel cell. Next, there must be a set of support equipment and supplies, including one computer unit for control of the test station (supplied with the station purchase) and another two computer units (PC1 – the Host unit, and PC2 – the Target unit) with: (1) simulation capabilities, and (2) real time operation capability plus a Controller Area Network (CAN) interface for rapid communication between the test station controller and simulations. Software elements of the overall system include the Front-End software for the test station itself plus software programs for the simulation and real time operation computers (Host and Target PCs). Finally, there must be facility support providing the gases, liquids, venting, and electrical requirements for operating the fuel cell.

Once installation was completed at the HFCTF, initial testing of the HiL #1 system produced a set of real-world results, providing the basis for the actual dynamic capabilities of this system at the HFCTF. These real-world results may show some variations from the original specifications for the tester established by HNEI, but they do give concrete indications for the actual capabilities and limitations of the overall system. These capabilities and limitations form the basis for determining the range of fuel cell system applications which can be examined faithfully by the HiL #1 system with the goal of assisting in rapid prototyping of such applications. Furthermore, and perhaps more importantly, the results obtained from operation of the HiL #1 system will provide invaluable inputs for designing the next generation HiL #2 system, which is planned to have improved capabilities.

2. Vendor Evaluation

HNEI employed a consultant (Karl-Heinz Hauer, PhD, of xcellvision, Wolfsburg, Germany) to assist in the vendor evaluation process. Dr. Hauer conducted an extensive search for suitable companies currently producing fuel cell test equipment and, specifically, fuel cell test stands or test stations. The goal was to identify vendors manufacturing sophisticated equipment that had the potential for adaptation to dynamic HiL test operations, or were, at least, the state-of-the-art at this time.

Initially, Dr. Hauer conducted a market survey to identify a group of vendors manufacturing test equipment potentially appropriate for this project. He then developed a set of preliminary performance specifications (including dynamic requirements) for fuel cell stations in various electric power ranges (12 kW, 4 kW, and below 1 kW). The vendors identified were each sent these specifications to obtain preliminary quotations for providing the fuel cell stations described.
The quotations received were valuable in at least three ways. First, they helped to narrow the list of vendors down to those considered most viable for delivering the desired test station. Next, they contributed useful information regarding the current state-of-the-art regarding the capability for providing selected dynamic parameters of interest for the HiL program. Finally, the quotations enabled HNEI to work towards refining the

specifications to be established for the fuel cell test station planned for the HiL #1 system.

Background material concerning the HiL #1 system, preliminary test station specifications, and the market survey described above are all contained in Dr. Hauer's Report A to HNEI (attached as Appendix I). In particular, the market survey efforts and results are presented in Section 7 of that Report.

3. HiL #1 Specifications

Following the conclusion of the vendor evaluation work, the final specifications for the fuel cell test station to be used in the HiL #1 system were developed. As mentioned above, the quotations received during the vendor evaluation process were very valuable for helping to determine the required dynamic capabilities for the desired test station. In addition, the dynamic demands imposed by operation of a fuel cell in a passenger vehicle were also carefully considered, since such dynamics could be expressed using the fuel cell vehicle simulation model to be employed as part of HiL #1.

One important feature was designation of the actual electric power level for the desired HiL #1 test station. This element was developed in conjunction with establishment of the specific HNEI fuel cell to be used for testing in this test station. Early discussions with fuel cell experts led to the decision to use a 100 square centimeter (sq cm) fuel cell as the test device to be employed by the HiL #1 test station. Such a fuel cell would be capable of yielding about 100 W of electric power, at least based on fueling with hydrogen and oxygen. The specifications began, therefore, with the requirement for a 100 W fuel cell tester or test station. Associated with this were the range of required specifications for the load bank, gases, pressures, humidification, and temperature control, together with dynamic capabilities.

The specifications included the ability to have two operational modes, either with or without the CAN interface being active. The first operation mode is basically operation as an independent tester. In this operation mode the CAN interface is inactive and all adjustments, security and the test protocol are handled with the graphical user interface of the tester. Under this mode, standard static testing of a fuel cell can be carried out. The second mode is HiL operation. In this mode the CAN interface is active and the set points (e.g., for current and flows) are provided by an external simulation model, being transmitted via the CAN interface to the tester. This arrangement allows for dynamic testing of a fuel cell within the test station.

For purposes of specifying the various dynamic characteristics of responses by the tester (pressure increases and decreases, fuel flow increases and decreases, changes in humidity, etc.), primary consideration was given to the dynamics associated with operation of a fuel cell powered vehicle. In previous work (at the University of California at Davis) directed by Dr. Robert M. Moore of HNEI, a simulation model had been developed that is called FCVSim (fuel cell vehicle simulation). This simulation incorporates the use of various driving cycles to provide different dynamic conditions for simulated operation of the vehicle and the resultant dynamic demands placed on the fuel cell system within the simulation. FCVSim was used as the dynamic software model to link with the 100 sq cm fuel cell being tested within the HiL #1 system during functional

testing or factory acceptance testing (FAT) of the test station after construction. The actual dynamic specifications used in the Request for Quotations sent out to vendors took into account the information gained from vendors earlier as well as the dynamics generated by the FCVSim.

Finally, the overall specifications included features covering the Front-End software, AC impedance measurement, protection, and safety standards. Support and warranty specifications were also delineated to cover the FAT at the factory and subsequent testing at the HFCTF.

4. Purchasing Process

After finalizing all specifications for the desired fuel cell test station, a Request for Quotations (RFQ) was prepared incorporating these specifications and this was sent out to the three vendors identified during the earlier vendor evaluation. These vendors were FuelCon Systems Inc., Greenlight Power Technologies, Inc., and Fideris Inc. A copy of this RFQ, which includes a delineation of the final specifications, is included as Appendix II to this report.

One of the specifications in the RFQ was that the Front-End software of the test station shall be based on LabVIEW™. This was done so that the test station software would be compatible with the testing and data analysis software used throughout all other equipment of HNEI's HFCTF. Fideris asked us to change this specification regarding the LabVIEW™ software, but we indicated that this was a necessary part of our overall program. Fideris was, therefore, unable to meet our specifications and did not submit a quotation.

We did receive quotations from FuelCon and Greenlight Power. The FuelCon quotation was $21,666 less than the Greenlight Power quotation, so the FuelCon quotation was, therefore, selected as the winner. The purchase order for the fuel cell test station was sent to FuelCon in June 2005.

In a similar manner, quotations were also requested for the 100 sq cm fuel cell needed for testing within the fuel cell test station. This effort resulted in the purchase of a Lynntech fuel cell that was initially evaluated at the HFCTF and then shipped to Germany to be used during the FAT of the test station there. Subsequently, this same fuel cell was shipped back to the HFCTF to be used for the final FAT in Hawaii, as well as for subsequent testing purposes.

5. Factory Acceptance Testing (FAT)

FuelCon completed construction of the test station at their factory in Germany late in October 2005. The FAT was conducted at the factory in November 2005, with representatives from HNEI in attendance and doing most of the testing. As a result of the meeting with FuelCon representatives at that time, along with the actual FAT results, some specification deficiencies (pressure response and software source code release) were noted. In compensation for these deficiencies, FuelCon provided an additional exit temperature control package; rapid service response for one year, including software modifications via remote software; and LabVIEW™ VI subroutines (Virtual Instruments) to remotely access setpoints and measurement data. Following the tests in Germany, an

FAT Report was prepared by Dr. Hauer, presenting some test results, the deficiencies and associated compensation, a listing and description of the various tests planned for the FAT, a flow diagram of the 100 sq cm fuel cell taken from HNEI to Germany for use in the FAT, figures presenting performance curves for the 100 sq cm fuel cell taken prior to the FAT, and a list of all items shipped to FuelCon from HNEI for use during the FAT. This report is attached as Appendix III.

Following the FAT in Germany, the test station was shipped to Hawaii and was received at the HFCTF in December 2005. The test station was installed at the HFCTF during December 2005 and January 2006. This installation included connection with the electrical system, gas feed supplies, deionized water supply (for humidification), cooling water supply, and exhaust ventilation system of the HFCTF. In addition, the HNEI 100 sq cm fuel cell (returned from its use in Germany) was installed in the tester. Finally, the compensatory additional exit temperature control package was received from Germany late in January 2006 and was subsequently installed into the tester. The FAT at the HNEI HFCTF was conducted during January and February 2006.

6. FAT Details

The overall FAT to be conducted at the factory, as delineated in Appendix III, was planned to consist of four separate sections for evaluation of different elements of the HiL #1 system. First, there was a set of diagnostic tests conducted on the 100 cm^2 Lynntech fuel cell used within the test station. Next was the standard set of tests specified and to be conducted by FuelCon to verify proper basic functioning of their test station. In addition to the tests identified by FuelCon, HNEI had a set of specification tests to be conducted by HNEI for checking the AC impedance measurement system and the transient performance of the test station in accordance with the specifications in the RFQ (see Appendix II). The fourth section included a series of tests that were to be conducted (again, by HNEI) to check operation of the FuelCon test stand in the HiL operation mode, using a fuel cell vehicle simulation program in real time via an xPC Target and CAN interface.

The FAT conducted at the HFCTF in Hawaii consisted of all four of the sections outlined above, except that the FuelCon standard set of tests (second section of tests) were conducted by HNEI. Another exception was that whereas the third section of tests were specified in Appendix III to be conducted using an external LabVIEW™ program via CAN (and this was done for the FAT in Germany), for the Hawaii FAT, this section was done using the Host and Target PCs via CAN (except for the load response time test and external data acquisition monitoring with high sampling rate).

6.1 Fuel Cell Diagnostic Tests

The Lynntech fuel cell was initially received by HNEI at the HFCTF and conditioning tests were conducted. Following this, a beginning set of polarization (VI) and power curves were obtained, using a GLP fuel cell test stand at the HFCTF. This fuel cell was then shipped to Germany for use during the FAT of the fuel cell test station there, and subsequently shipped back to the HFCTF for the FAT in Hawaii. VI curves for this fuel cell were also obtained during the FAT at both places (in Germany the VI curve was actually obtained just prior to the FAT). VI curves and corresponding power curves for

these three sets of diagnostic tests are presented on Figure 2. Subsequent to the FAT in Hawaii, a hydrogen crossover test was conducted with the Lynntech fuel cell. Results of this test are given on Figure 3. From this crossover test it can be concluded that the hydrogen crossover limiting current and current density at 0.3 volts are 0.018 amps and 0.18 mA/cm^2, respectively.

6.2 FuelCon Standard Functioning Tests

These tests included manual operation of the fuel cell test station as well as automatic testing using the test stand PC software features. In the manual mode, basic functioning of the purge system was tested, and, using a current ramp, tests were conducted of the electronic load. Software scripts were then used to test individual elements of the test station, including the humidifier, mass flow controller, mass flow meters, temperature controller, and basic purging. All of the manual and automatic tests were carried out with successful results.

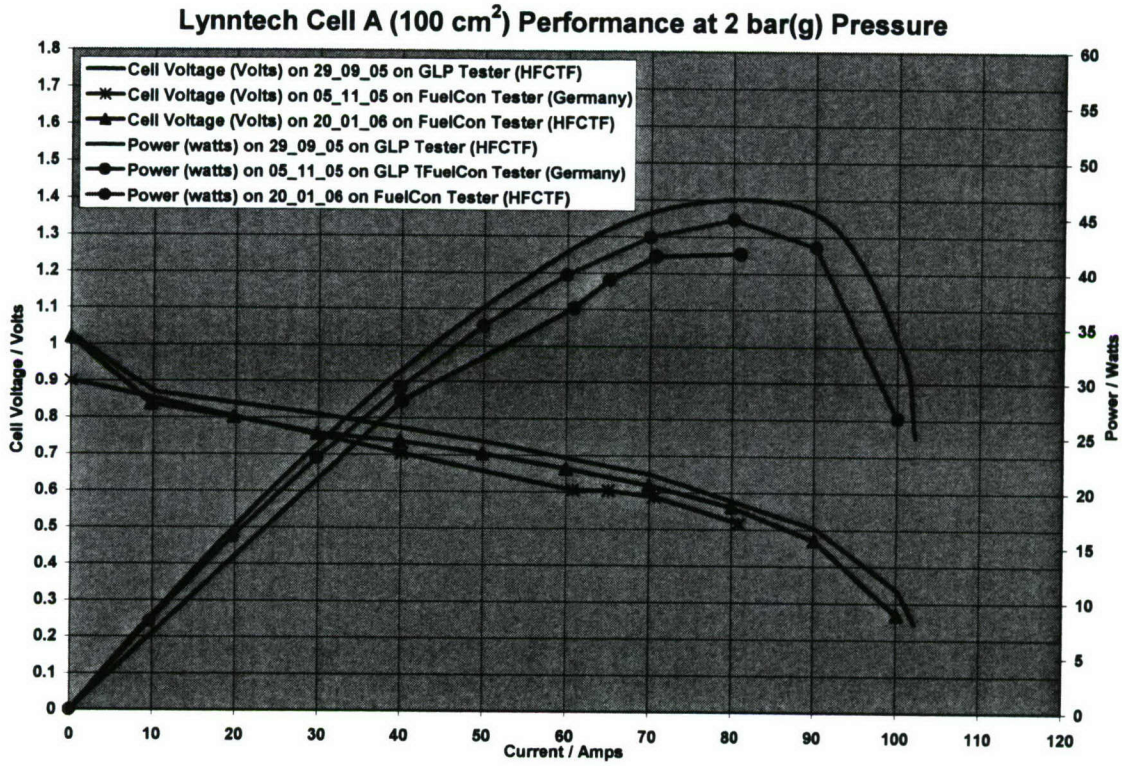

Figure 2: HNEI 100 cm^2 PEMFC Polarization (VI) and Power Curves

6.3 HNEI Specification Tests for Transient Performance

This section of tests consisted of three separate planned subsections. First there was a test to verify communication between the FuelCon tester CAN interface and either the Target unit PC with the Softing CAN card or the LabVIEW™ PC with the CAN card, depending on which of the tests in the second subsection were being conducted and where the tests were done. This communication was required before any of the tests in

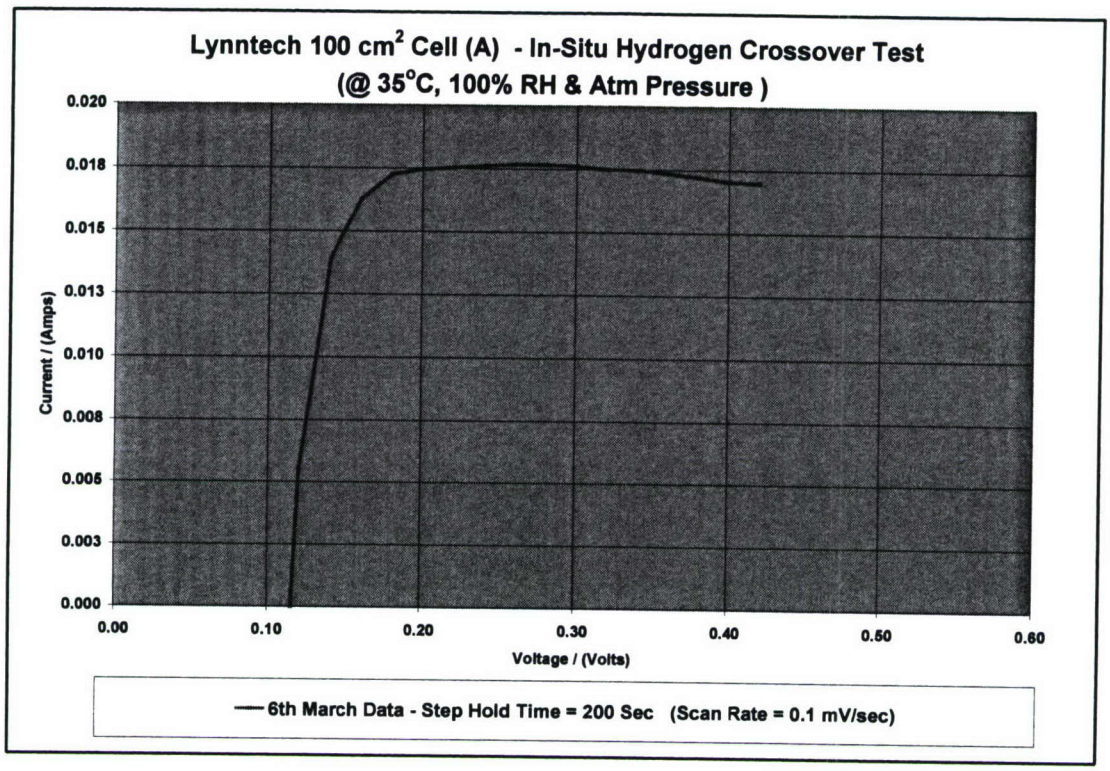

Figure 3: Hydrogen Crossover Test for Lynntech Fuel Cell

the second subsection could be conducted. Actually, although most of the second subsection of tests were then conducted via this Host/Target unit PC system (in Hawaii only), some tests were done using a laptop diagnostic LabVIEW™ PC. During use of the LabVIEW™ PC, communication with the FuelCon CAN interface was established via the LabVIEW™ PC's CAN Card. The LabVIEW™ PC was used for all transient tests in Germany, but only for the electronic load transients at the HFCTF.

The second subsection of tests was conducted using various Host/Target or LabVIEW™ PC software scripts (depending on which PC system was used), primarily to check the transient performance of the FuelCon tester. Performance was checked for the electronic load response (functionality only, in Germany; full testing in Hawaii), mass flow controller and mass flow meters, pressure swing, and humidification (see basic results in Figures 4 to 7). Figure 4 shows time delays for receiving various current level setpoints, with higher setpoints giving shorter delays. Further details on transient testing are given under the HiL tests. In addition to the above transient tests, this subsection involved doing AC impedance measurements at 10 amps (only conducted in Hawaii) for the HNEI fuel cell (see results in Figure 8), and using an external LabVIEW™ data acquisition system (the diagnostic LabVIEW™ PC) with high sampling rate to constantly monitor the FuelCon tester measurements of voltage, current, and pressure. In this way, we were able to verify that the FuelCon test station measurements were correct.

The third subsection consisted of a planned set of miscellaneous tests making use of a Matlab/LabVIEW™ interface for vehicle simulation testing, to be conducted according to requirements. In Germany, this testing was limited to performance of the FUDS cycle

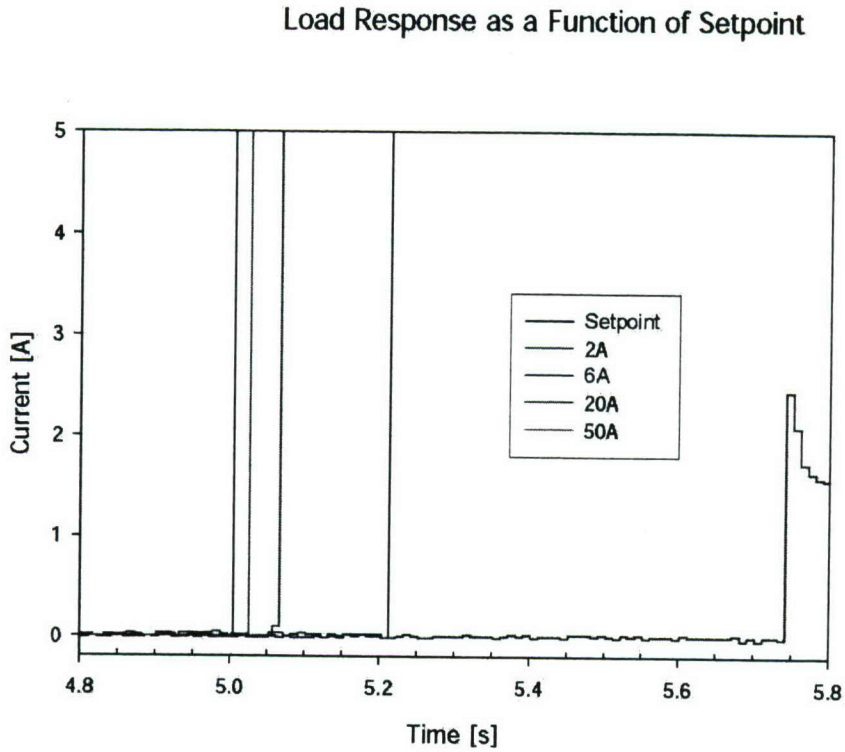

Figure 4: Electronic Load Setpoint Test

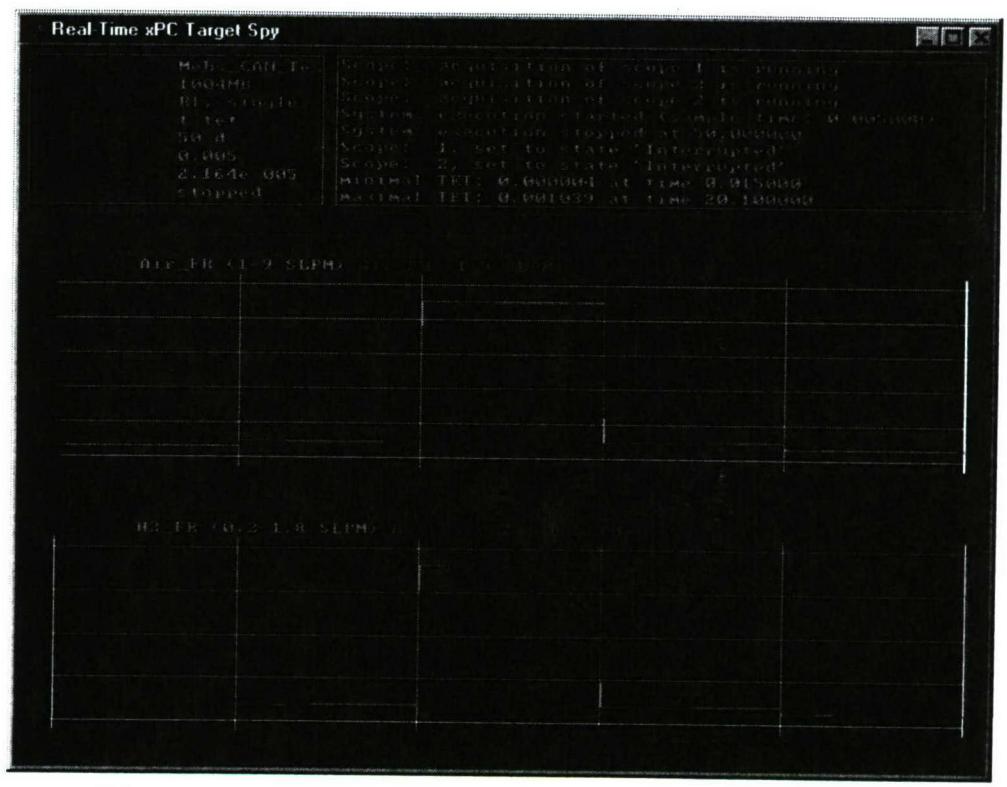

Figure 5: Mass Flow Controller Transient Response Test Using Air (Target PC Screen)

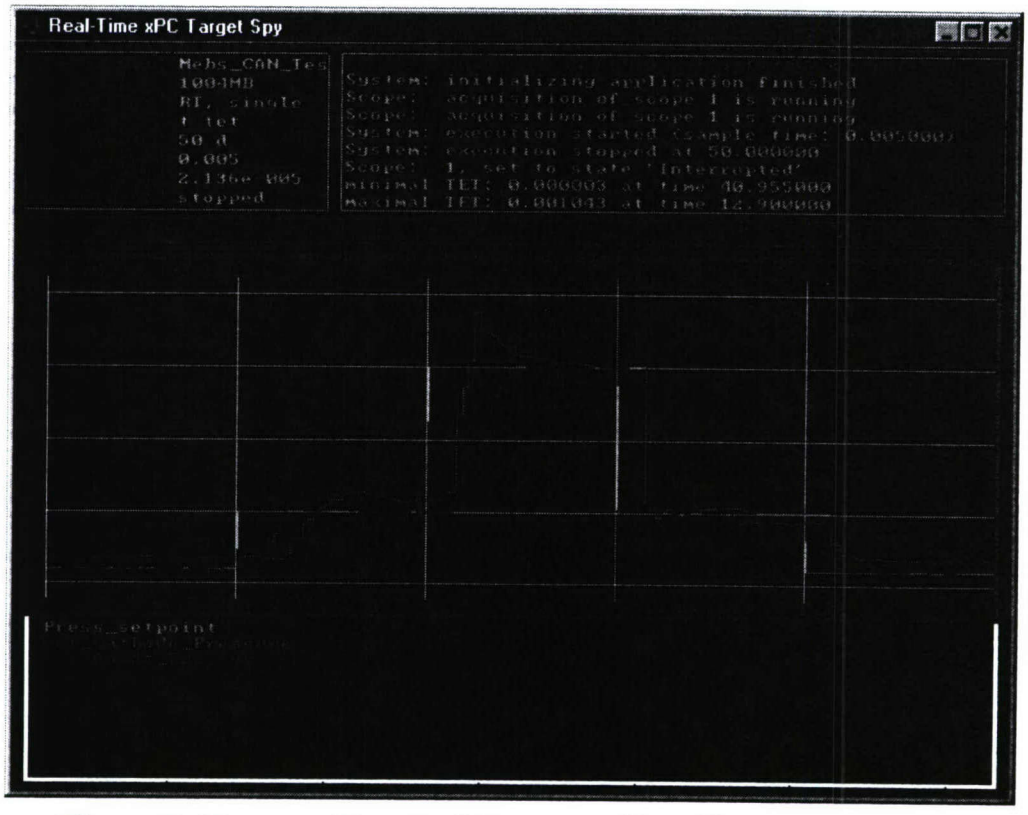

Figure 6: Pressure Transient Response Test (Target PC Screen)

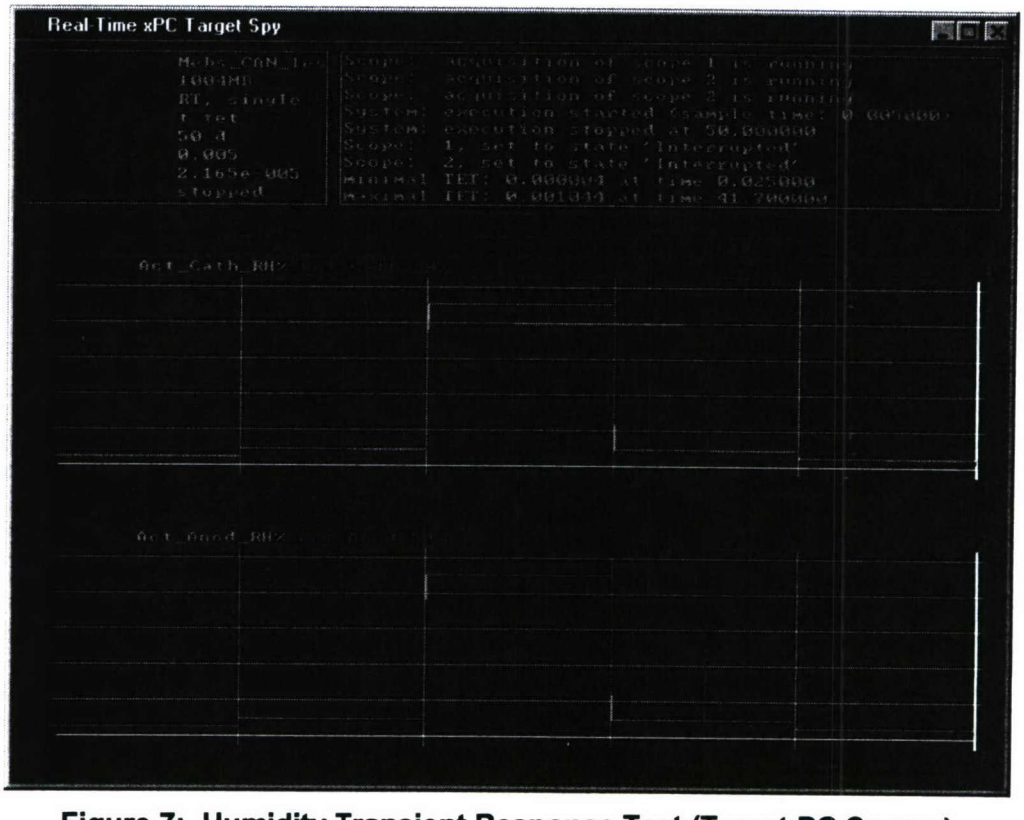

Figure 7: Humidity Transient Response Test (Target PC Screen)

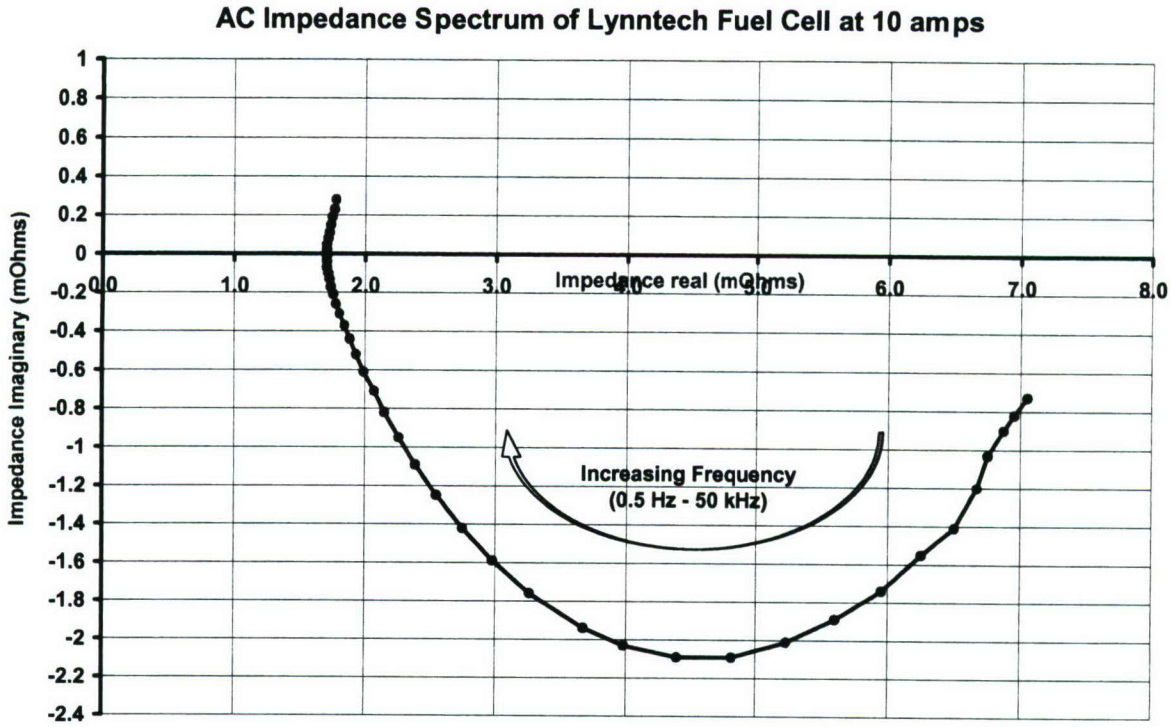

Figure 8: AC Impedance Spectrum of the HNEI Fuel Cell at 10 amps

only, for the first 100 seconds of the cycle. The test was terminated due to low cell voltage. Further tests were to be carried out in the event of failure of the simulation testing using the Host/Target unit system software. Since the Matlab/Simulink software via the Host/Target system was successful in conducting the simulation tests in Germany and Hawaii, additional tests using the LabVIEW™ PC interface were not required.

6.4 HiL Real Time Simulation Tests

The purpose of this series of tests was to verify successful operation of HiL concept through use of the previously-developed FCVSim fuel cell vehicle simulation model (within the Host unit) via xPC Target with a CAN interface (within the Target unit). The initial test verified communication between the Target unit CAN Softing Card and the FuelCon test station CAN interface.

Once the above communication was verified and established, a specific set of tests were conducted to prove functioning of the HiL concept. These tests included the following:

- Checking the ability to send and receive values of all data packages,
- Integrating the FuelCon tester with the simulation program,
- Checking the default configuration for stability during operation of the FUDS and UDDS drive cycles (and later, of the Extra Urban Drive Cycle),
- Stabilizing the simulation model (HiL configuration), if necessary, and
- Changing some model parameters (e.g., vehicle mass, aerodynamic drag, tire friction) on the fly to check the impact of such parameter changes.

During the testing in Germany, extensive time was required to achieve the initial communication between the test station and the Target PC. Although the tests in Germany were all basically successful, there were two features requiring modifications that were not tested in Germany, due to time constraints there. These modifications were made in Hawaii and all of the above tests were successfully conducted at the HFCTF. The modifications included 1) operation of the fuel cell at higher stoichiometric ratios to permit complete testing of a selected drive cycle, and 2) adjustments to driver parameters within the FCVSim simulation to achieve greater stability in the HiL configuration.

Figure 9 shows the overall arrangement of the HiL #1 system in operation at the HFCTF. The basic FuelCon test station with the HNEI fuel cell installed is on the right (operator reaching into the opened door). The two laptop PCs (with associated lit monitors) on the left end of the table are the diagnostic LabVIEW™ unit on the left (monitoring the CAN communications) and the Host unit (Matlab/Simulink plus Real Time Workshop and the simulation program) on the right. The dark monitor, directly behind the LabVIEW™ unit, operates from the Target PC (with xPC Target and the Softing CAN card) which is located on the floor beneath the table. The Target CAN card connects directly to the FuelCon test station PC via a CAN/Ethernet converter. These Host/Target PCs are the ones displayed graphically in Figure 1. The other two lit monitors on the table are displays from the FuelCon test station PC (the dark PC directly to the right of the right-hand lit monitor, and containing the FuelWork operating software). In front of one monitor is a keyboard connected to the FuelCon PC for directly running scripts to operate the test station and fuel cell.

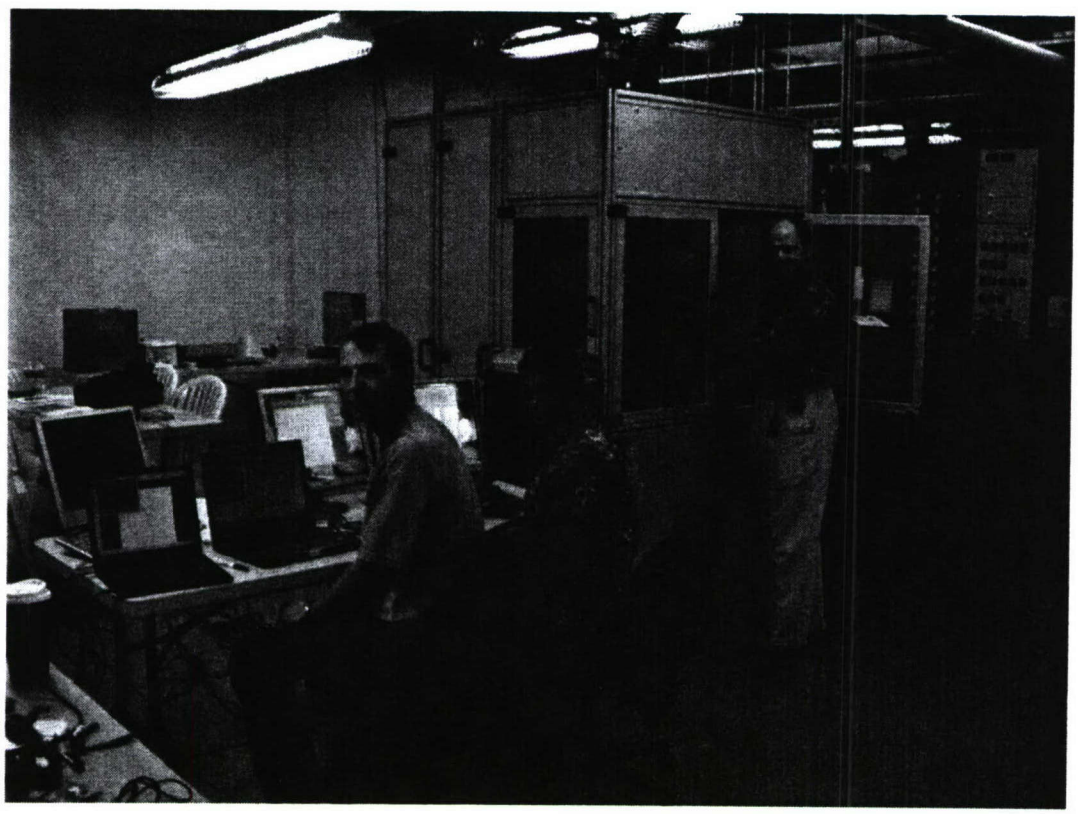

Figure 9: HiL#1 System Installed at the Hawaii Fuel Cell Test Facility

The primary driving cycle used for running the FCVSim simulation program in Hawaii during the various portions of the HiL simulation tests was the Extra Urban Drive Cycle (EUDC). The basic form of this cycle is shown in Figure 10, which is a shot taken from the Host PC.

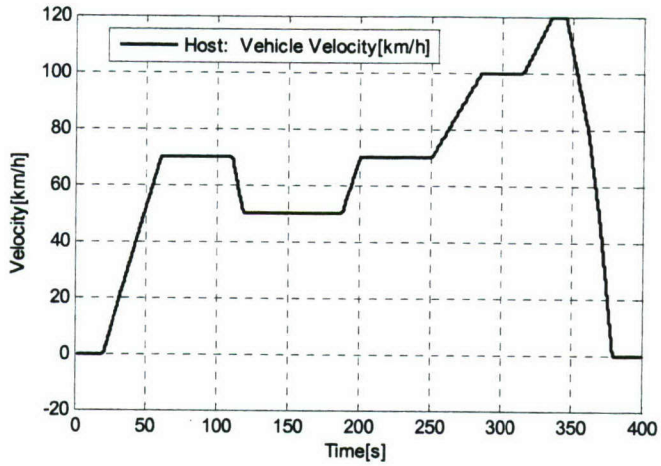

Figure 10: Extra Urban Drive Cycle (EUDC) from the Host PC Screen

This same drive cycle and the resultant vehicle velocities generated within FCVSim are shown on Figure 11. The exact coincidence of vehicle velocity with the driving cycle is easily seen. This velocity profile is then transformed into the demand (setpoint profile) transmitted via the CAN Interface to the FuelCon PC, resulting in the levels of gases and liquids supplied to the Lynntech fuel cell.

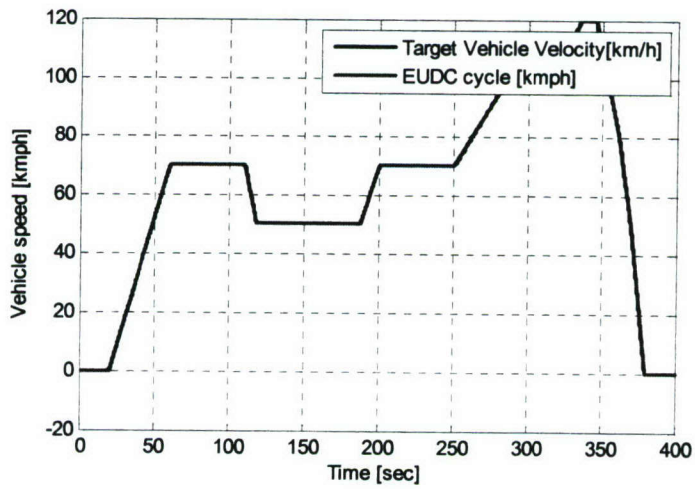

Figure 11: EUDC and Vehicle Velocity from the Target PC Screen

Figures 12 to 15 present plots of the setpoints and actual values for the fuel cell stack current, mass flow at the anode, mass flow at the cathode, and absolute pressure at the anode. Since the fuel cell used here has an area of 100 sq cm and the vehicle simulation assumes a full size of 360 sq cm, the displayed current values were scaled up by a ratio of 360/100.

For a closer analysis of the transient involved for fuel cell current, Figure 16 displays a portion of the data from Figure 12, as expanded for the interval from 40 to 85 seconds. Now, the response time of 3 to 4 seconds from the setpoint time to the time that the actual value reaches the setpoint value can be seen. This long response time could be caused by the data transfer rate, the slow serial data interface of the electronic load, or the CAN interface itself. The slow serial data interface is a hardware item that FuelCon elected to include in its tester design (although more rapid options are available). Figure 17 shows the results of optimizing the CAN data transfer rate, whereby the response time was reduced to 1 to 2 seconds, and the setpoint oscillations just before 350 seconds are greatly reduced. The matter of the CAN interface itself (CAN protocol and data transfer via the CAN interface) will also be addressed further on.

Figure 13, which presents plots of setpoints and actual data for mass flow of fuel at the anode, deserves more discussion. During the initial tests involving fuel flow, there was a problem in being able to complete the simulation test. Early in the drive cycle used for the simulation, there is a sharp ramp upwards in the current demanded (or vehicle speed required), and this followed directly after a short period of operation at a very low current value (essential an idling condition of the vehicle). In order to meet this demand, the fuel

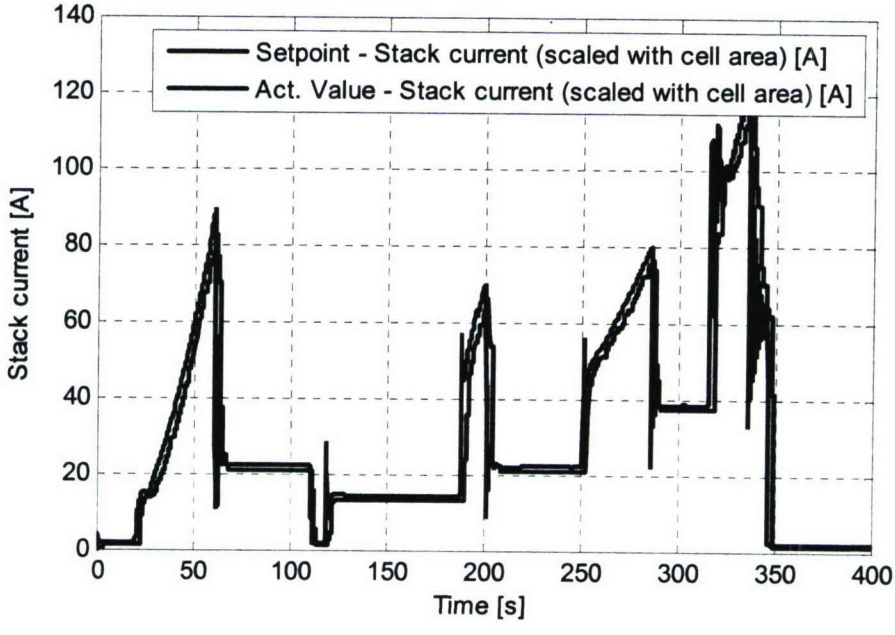

Figure 12: Fuel Cell Stack Current Setpoints and Actual Values

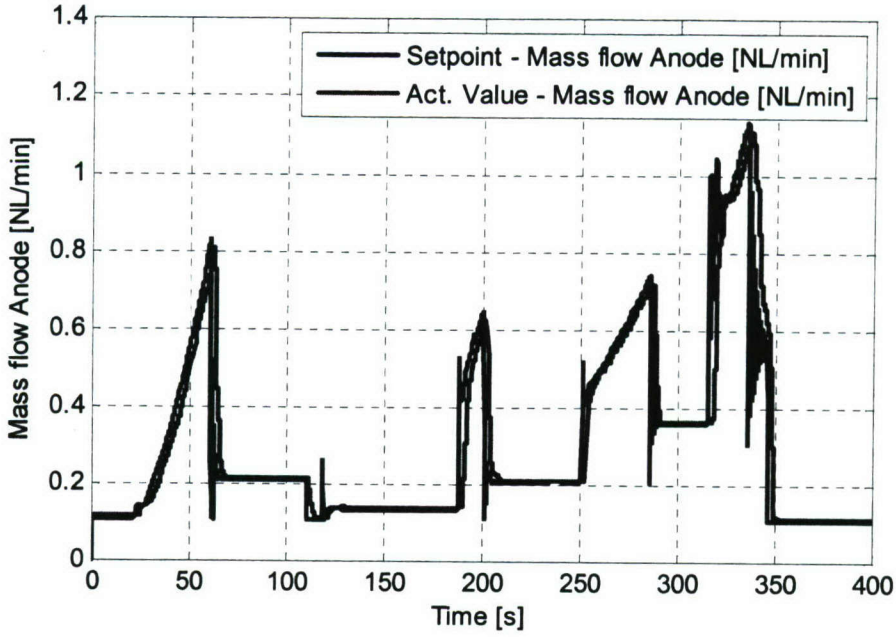

Figure 13: Anode Mass Flow Setpoints and Actual Values

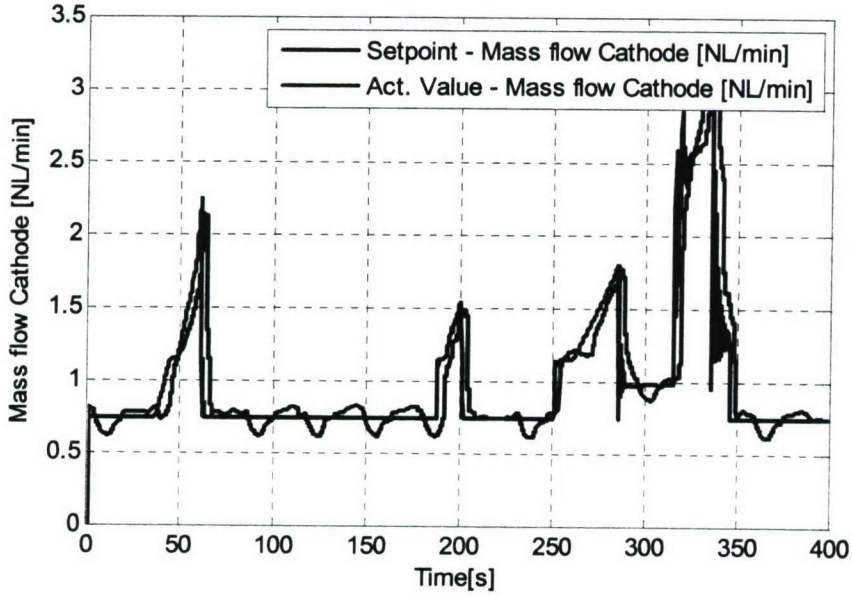

Figure 14: Cathode Mass Flow Setpoints and Actual Values

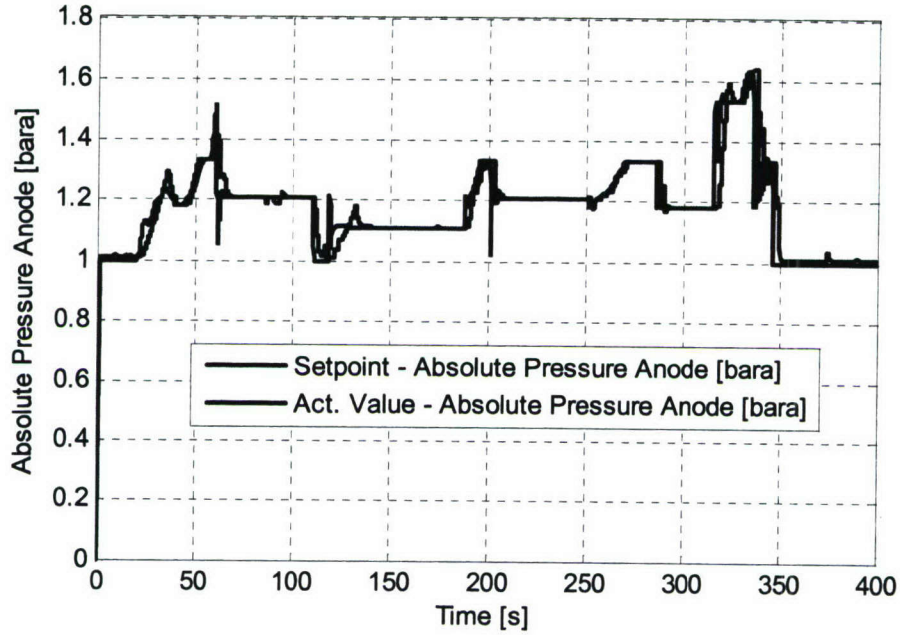

Figure 15: Anode Pressure Setpoints and Actual Values

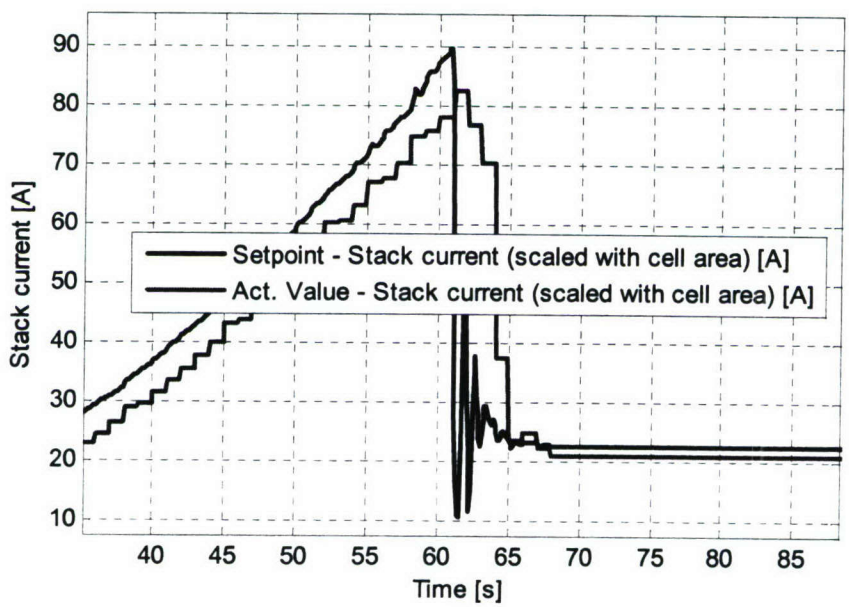

Figure 16: Expanded Time Segment from Figure 12 for Fuel Cell Current

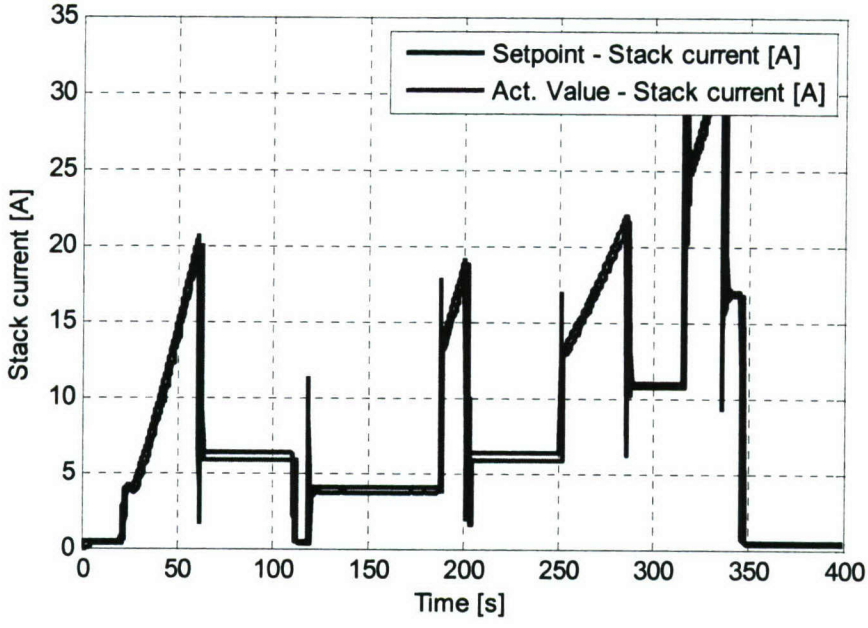

Figure 17: Current Setpoints and Actual Data after Optimizing Data Transfer Rates

flow rate would have to increase sharply from a very low idling value to a very high value. Unfortunately, the FuelCon tester was unable to provide the required fuel flow increase for this situation, and the result was excessively low cell voltage and termination of the test. In order to complete this test, it was necessary to artificially operate the system at a fuel flow rate much higher than needed for normal idling. In this way, the tester was then able to provide the fuel flow needed for the upramp, and the test could run without interruption. Under this condition, the fuel flow rate was much too large for good fuel economy of the overall vehicle being simulated.

Figure 18 presents an expanded time segment from 10 to 90 seconds, taken from Figure 15, showing setpoints and actual data for absolute pressure. Once more, the response times for the actual data to reach the setpoint values can be easily seen. Response times of more than 5 seconds can be noted on this figure, as well as some significant overshooting of the actual values above the pressure setpoints.

The dramatic effect of changing CAN data transfer rates is seen in Figure 19, for a simulation load response test, plotting current. The top two up-ramps of setpoints and actual values are for a data transfer rate of 300 ms. For these curves, the response time is on the order of 2 seconds. In an attempt to reduce response time by increasing the data transfer rate to 100 ms, the lower set of curves resulted, wherein the setpoints displayed wide oscillations and data values were reduced.

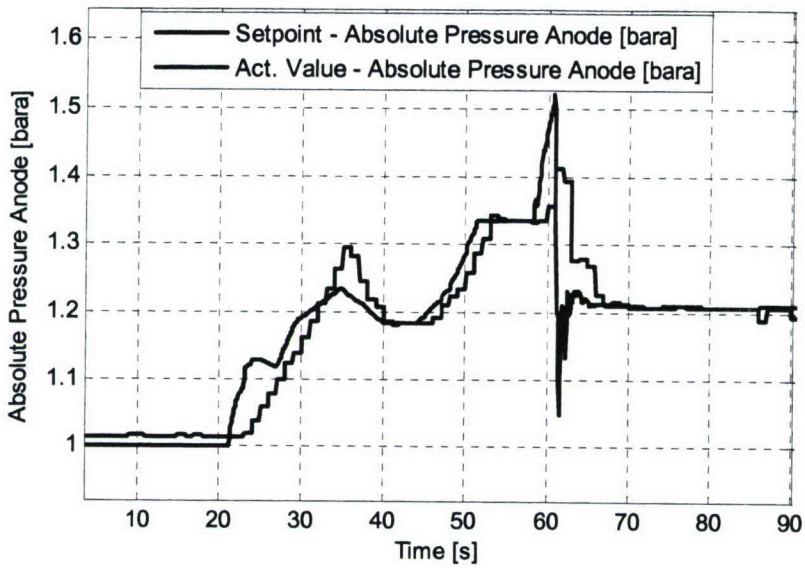

Figure 18: Expanded Time Segment from Figure 15 for Absolute Pressure at the Anode

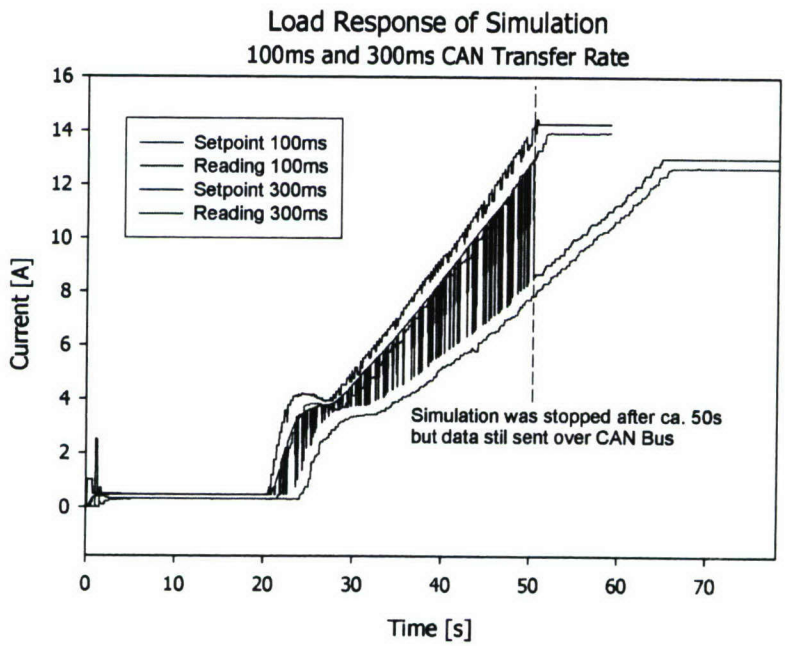

Figure 19: Electronic Load Response Test Results with Different CAN Data Transfer Rates

Figure 20 shows another set of ramp tests for the electronic load, via the CAN interface, with a sharp required increase in cell current near the beginning of each test. CAN data transfer rates of 100, 300, and 1,000 ms were used for these tests. The lower portion of this figure expands the time period (1.5 to 4.5 seconds) of the current up-ramp and the response times for each of the transfer rates can be seen clearly there. The response times for 100 and 300 ms CAN data transfer rates are both about 1 second. For 1,000 ms, the response time is about 2 seconds.

To determine the effect of the CAN protocol and data transfer on these response times, similar ramp tests for the electronic load were run using a direct connection to the FuelCon PC (bypassing the CAN interface) via the LabVIEW™ PC. Figure 21 presents the results of these tests using normal data transfer rates of 50, 100, 300 and 500 ms. The response times for the 50, 100 and 300 ms transfer rates were all about 1 second. So, the response times as well as the general characteristics of the load stayed nearly unchanged compared with sending the setpoints via the CAN interface. With the elimination of the CAN protocol and data transfer as being the cause of the long response times for the current data, it must be concluded that these response times are due to the data transfer rate, with some contribution by the slow serial data interface of the electronic load. Another feature seen on Figure 21 is the 800 ms for the raise time. Once the data began after the response time of 800 ms for this 50 ms setpoint test, the actual data took an additional 800 ms to rise up to within 90% of the setpoint value. An examination of all the tests on Figures 20 and 21 reveals that the rise times for the various setpoints are all somewhat less than 1 second.

A careful examination of Figure 20 during the period (12 to 18 seconds) of the current down-ramp reveals peculiarities in the setpoint values for the tests using the 100 and 300 ms data transfer rates. In order to study this phenomenon more closely and to determine the cause of these peculiarities, another set of ramp tests for the electronic load was conducted, all using the 100 ms data transfer rate. These tests involved setpoints being sent by the Target PC and being received in three different manners within the overall HiL #1 system and are displayed on Figure 22.

All data shown was monitored by LabVIEW™ CAN via laptop. In the first case, data was also received by FuelWork. In the second case, data was only received by the FuelCon CAN monitor, with FuelWork not involved. In the final case, data was only received by the LabVIEW™ CAN monitor and no FuelCon solftware was involved. The lower portion of the figure is an expansion of the time period of 12 to 20 seconds, during the down-ramp section of these tests. Especially in the expanded time section of this figure, the strange perturbations of the setpoint values are easily seen. These only occur for the case where the setpoints are received by the FuelWork software, so the data corruption must be happening within FuelWork.

Figure 23 presents an overview of the results of a final set of load response tests that were conducted using the 50 amp setpoint current that gave the lowest delay time, as seen on Figure 4. Figure 24 shows a time expansion for a portion of Figure 23. For these tests, a wide variety of measurement techniques were used to determine the times for receiving the current values from the electronic load. Response times for receiving the actual data readings coming back from the tester were also recorded for three of these locations.

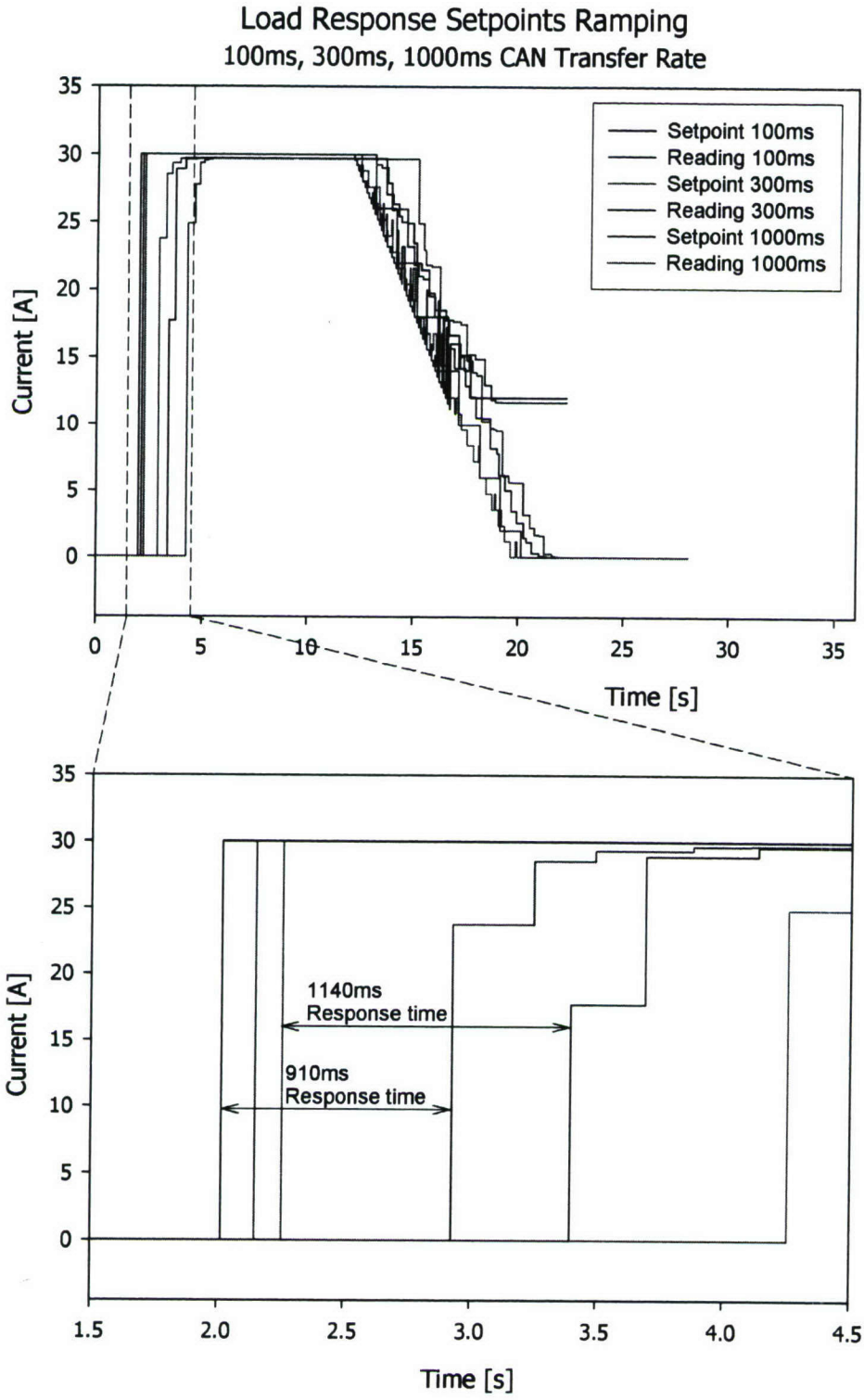

Figure 20: Electronic Load Ramp Test Using the CAN Interface

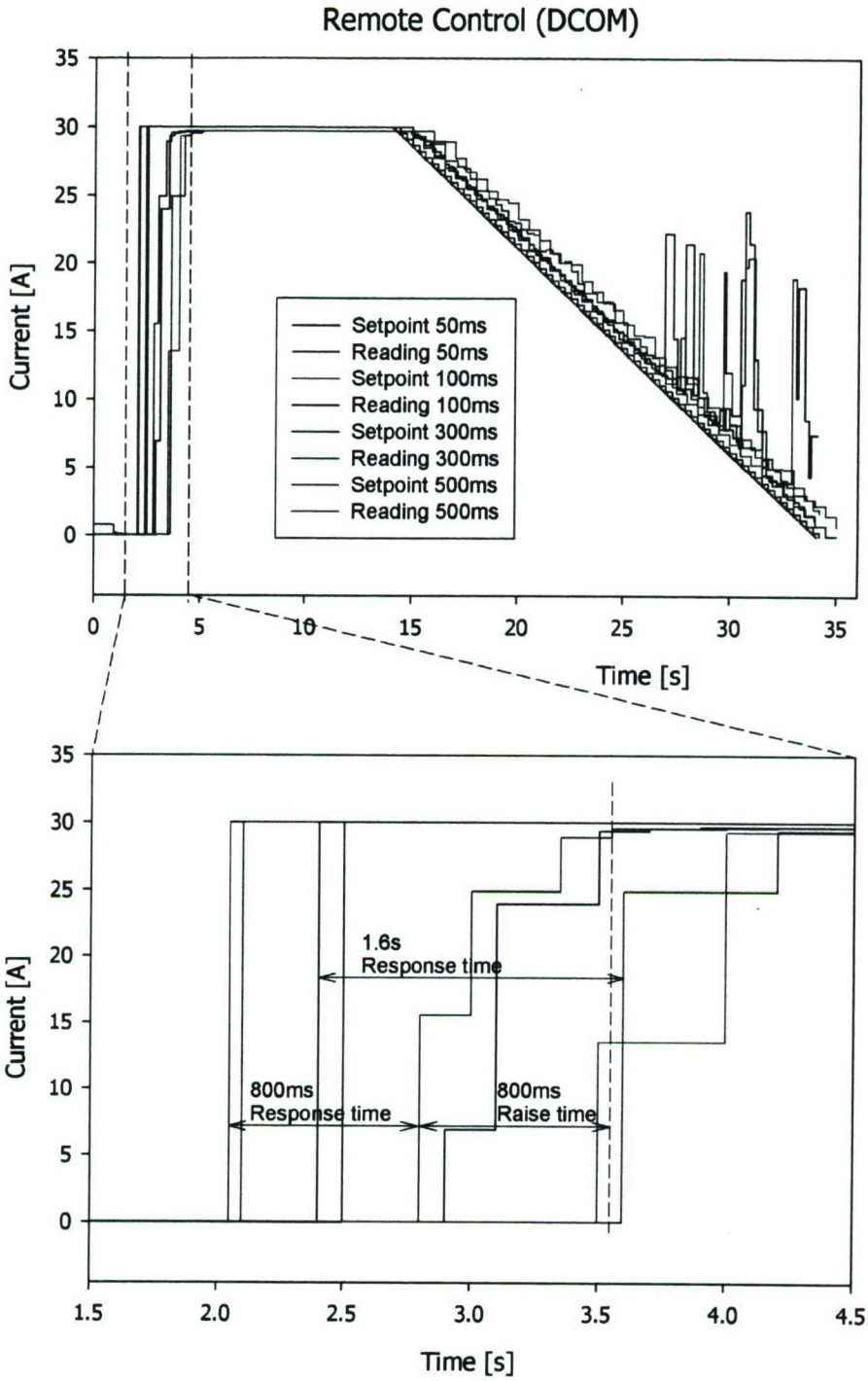

Figure 21: Electronic Load Ramp Test with Fuel Cell Direct Connection (No CAN Interface)

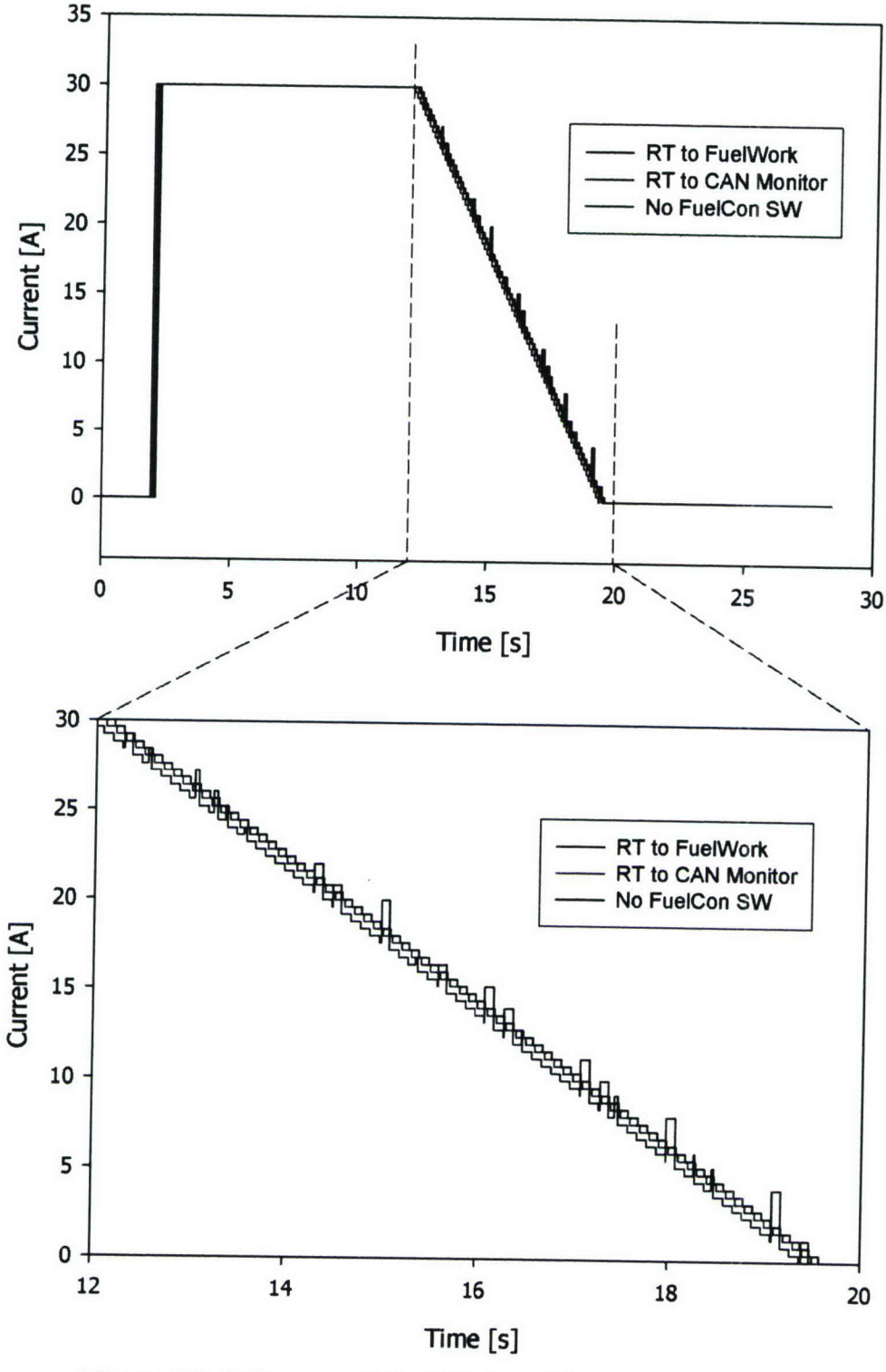

Figure 22: Influence of FuelWork on Measured Setpoints

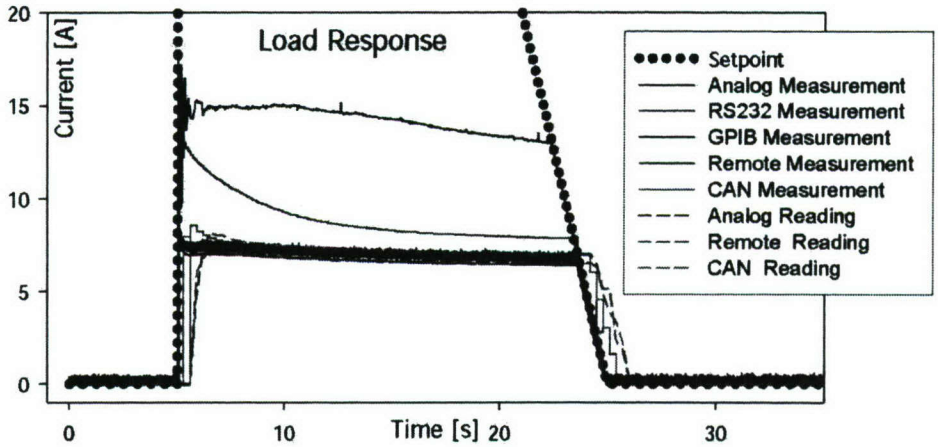

Figure 23: Various Electronic Load Measurements and Readings

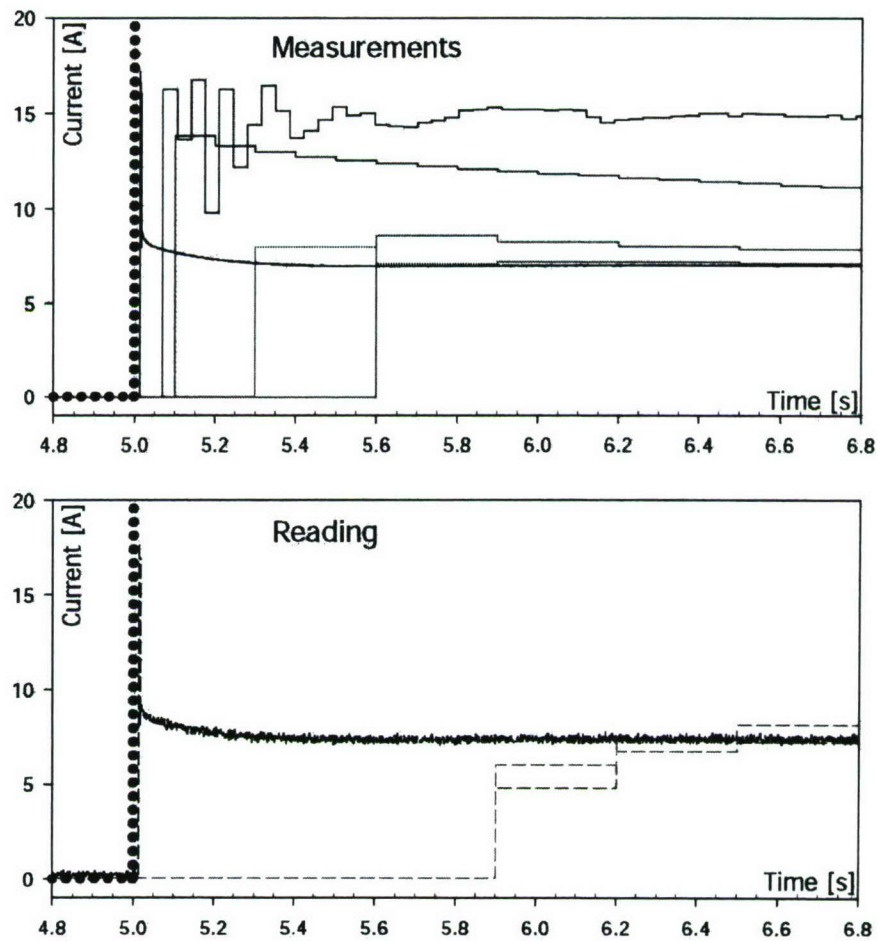

Figure 24: Measurements and Reading Values for Electronic Load Tests (time expansion from Figure 23)

The analog measurements were made directly at the electronic load, bypassing the rest of the FuelCon tester system. The RS232 measurements were done at the slow serial data interface located on the electronic load (see discussions relating to Figure 16). The GPIB measurements were carried out at the GPIB port, also on the electronic load, a faster data interface of the electronic load, but a hardware option that FuelCon elected not to incorporate for the electronic load. The remote measurements used another connection to the FuelCon PC, but one that bypasses the CAN interface. The CAN measurements were made directly to the CAN interface of the FuelCon tester.

As indicated earlier, Figure 24 presents two expanded time segments from Figure 23, for the period 4.8 to 6.8 seconds. The upper segment is for the various measurements of current generated at the electronic load by the setpoint values. The lower segment shows the actual current data readings as received back from the FuelCon tester.

The delays times for the various measurement techniques are as follow: analog – about 15 ms; GPIB – about 70 ms; RS232 – about 100 ms; CAN – 300 ms; and remote – 600 ms. The response time for noting the data readings coming from the tester is insignificant for the analog method. For the CAN and remote methods, the response times are 600 and 300 ms, respectively.

7. Software

Several sets of software are used within the overall HiL #1 system. The simulation elements operate using Matlab, Simulink and Real Time Workshop from Mathworks, Inc. and Microsoft Visual C++ .NET compiler in the Host PC. The desired simulation model or program is also used within the Host PC. The Target PC uses Mathworks, Inc. xPC Target and a Softing CAN-AC2-PCI Interface card. The FuelCon tester uses an operational software called FuelWork (which is a National Instruments LabVIEW™-based software system). Data management, data archiving and external LabVIEW™ executables (add-ons) are all operated on the FuelCon PC which uses LabVIEW™. HNEI's diagnostic LabVIEW™ PC uses LabVIEW™ plus a National Instruments CAN Interface card as well as Matlab.

8. Capabilities

The overall HiL #1 system has a wide spectrum of capabilities. In a general way, the fuel cell test station is capable of 24-hour automatic, unattended operation, and can accommodate a single- fuel cell. Such operation can be carried out in two different operational modes, either operating as an independent tester (with the CAN interface inactive) or in HiL operation (with an active HiL interface).

The test stand has a closed test cabin and an integrated ventilation system with LEL hydrogen detectors to safeguard the operators and facility. It includes direct-injection humidification technology plus electronic flow control, temperature and pressure control, nitrogen purge and electronic load management. The control software permits operation of the fuel cell on hydrogen and either with air or oxygen. The test station can operate in a power range of 0 to 200 W. The maximum anode and cathode flow ranges are 0-2 slpm (standard liters per minute) and 0 to 10 slpm, respectively. The maximum inlet gas temperature for both the anode and cathode is 150°C, and the relative humidity range is

from dry to 100% at 90°C. The back pressure control range is 1.1 to 5.0 bar(a). An optional feature of the test stand is an AC impedance measurement system (see Figure 8 for a result of using this system). This analytical tool provides full impedance spectroscopy in a wide frequency range for cell characterization and performance analysis.

One mode of operation for the test station is as an independent fuel cell tester. In this case, it would basically be working as a static test stand. Operation is controlled from the keyboard and monitor system of the FuelCon control PC. Various scripts could be run using this arrangement, some of which could be approximations of dynamic testing for a fuel cell. Such operation would be very limited, however, and for true dynamic testing with full simulations, HiL operation would be required.

The more important method of operation is, of course, in the HiL mode. In this configuration, complete simulations can be utilized, including, for example, use of the FCVSim fuel cell vehicle simulation model mentioned earlier, allowing operation of the fuel cell in a great variety of ways, including all the dynamism of the various drive cycles that have been formulated.

9. Limitations

The HiL #1 system does have a number of limitations in its capabilities. Some of these limitations relate specifically to failure of the FuelCon tester to meet certain of the specifications included in the RFQ. In the quotation provided by FuelCon, it was indicated that the tester to be supplied would "fully meet all your requirements." Unfortunately, this has proven not to be correct for several features. Not only was there a failure of the test station to meet some physical specifications (especially for transients), but the manufacturer also did not comply with our specification of providing the uncompiled control software (FuelWork).

The specifications for transient characteristics were not met for the performance of the pressure swing and humidification. For the gas flow, performance came close to the target, but was slightly off. Inability to meet the RFQ specifications for pressure swing is related somewhat to the physical design of the tester, especially the resultant void volume within the tester requiring rapid pressure changes.

Two major problems experienced with the FuelCon tester were: 1) oscillations and data corruption for setpoint values at data transfer rates as slow as 100 ms, and 2) the long response times between the setpoint time and the time for the actual data readings coming from the tester. The analyses in the text (with the corresponding figures presented) are primarily for current setpoints since they are most easily investigated, but all setpoints showed these problems. The difficulty with setpoint data corruption at the 100 ms transfer rate meant that test operations were required to be run at slower transfer rates, on the order of 300 ms. Furthermore, the test results presented in Figure 22 point out the fact that this data corruption is caused by the FuelWork software, so the tester must be operated at transfer rates slower than 100 ms to avoid the dynamic data corruption. This fact of required operation at slow data transfer rates carries with it the corresponding penalty of having long response times for the actual data to reach setpoint values.

Several contributions to the time penalties in obtaining actual data readings have been identified for the HiL #1 system. The first arena is that of the time delays experienced from the time that load current setpoints are sent directly to the electronic load to the time that corresponding actual currents are sent out from the electronic load. Data obtained for these time delays are displayed on Figure 4. As the values of the current setpoint are reduced, the delay times increase, with time delays varying from about 15 ms for 50 amps to 750 ms for 2 amps.

For the special case of using the 50 amp current setpoint (yielding the lowest time delay of 15 ms, as discussed above), additional measurements were made to identify the time delays for the current signal to reach other areas within the HiL #1 system (see Figure 24 and the associated discussions). One primary result here is the delay of 300 ms before the current setpoint is received by FuelWork via the CAN system and sent to the load. Finally, there is an additional 600 ms of delay before the actual data reading is detected, coming back from the measurement system through FuelWork. Obviously, due to the increasing delay times associated with decreasing current setpoints (as see in Figure 4), operation at currents below 50 amps will yield greater time delays for receipt of actual data than just discussed.

Furthermore, since the use of slower data transfer rates also results in slower response times, the fact that the FuelWork software is requiring much slower than desired data transfer rates (to avoid data corruption and/or oscillation) has adverse effects on how soon actual data can be received during dynamic test operations. Another feature regarding response of the actual data can be seen on Figures 20 and 24. The concern is the ability for the actual current data to quickly rise to the current setpoint. On both of these figures, it can be seen that the actual data points do not rise up to the setpoint in one step, but require several steps before the setpoint is reached. This feature, therefore, also results in additional time required for data to follow setpoint instructions, and evidently is another result of the FuelWork software.

The kinds of delay times identified above are factors that contributed to the fact that certain types of drive cycles (e.g., the FUDS and UDDS cycles) could not be completely used for testing within the HiL #1 system, since the inability to keep up with the dynamic requirements resulted in system shutdown. This means that only less demanding drive cycles can be used for test operations with HiL #1.

10. Limitation Summary

In summary, the HiL #1 system has limitations regarding control features, electronic communications, data flow, and lack of ability to modify features of the FuelCon tester FuelWork software.

One basic feature of HiL #1 is the long chain of controllers employed during system operation. The pathway includes the simulation within the Host PC, the Target PC, the CAN interface, the FuelCon PC with FuelWork, the actual FuelCon tester controller, and finally, the fuel cell being tested. Furthermore, this pathway includes the flow of setpoints towards the electronic load/fuel and actual data returning.

Another control feature presenting problems is the use of off-the-shelf, stand-alone pressure and flow controllers within the FuelCon tester. This control strategy, designed

and built into the tester by FuelCon, contributed to the inability to achieve the rapid transients of pressure and flow required for good HiL operations, especially where vehicle simulation calls for stringent drive cycles.

A final control issue is that the tester controller does have the ability to adjust PID (proportional-integral-derivative) parameters (as adapted by the RS232 slow serial data interface) to be optimum for a particular operating condition, but such settings remain fixed during any test session. As operating conditions change during a single test, no parameter changes can be made "on-the-fly" and parameters are optimum for only a portion of the test.

The electronic load of the FuelCon tester is set via the RS232 communication bus (the slow serial data interface). As seen on Figure 24, the time delay for setpoints to be detected at this interface is about 100 ms. The time delay to the CAN interface is on the order of 300 ms.

Ideally, data flow during any dynamic fuel cell test would utilize the highest possible data transfer rate. Due to the oscillations and data corruption obtained at a data transfer rate even as slow as 100 ms (see Figures 19 and 22), it became necessary to operate at the slower rate of 300 ms. This unsatisfactory operating method is caused by the data input/output passing through the Microsoft Windows-based FuelCon PC (with its FuelWork operating software). The result is the resultant indeterminate data, especially as seen in Figure 22.

Whereas HNEI had specified the requirement for the uncompiled development version of the tester operating software (FuelWork), FuelCon was unable to fulfill this specification. This has meant that HNEI personnel have not been able to write any adjustment codes for the software, in order to optimize operation of the tester for HNEI purposes, especially to help achieve better transient performance. Another element was the graphical user interface (GUI) portion of the software. The arrangement of GUI components and window-sizing capability were both fixed items. It was not possible to change any of the software code for these features and the embedding of add-ons was also not possible.

APPENDIX I

Dr. Hauer's Report A to HNEI

Report A for
Hawaii Natural Energy Institute (HNEI)

xcellvision
Karl-Heinz Hauer
kh.hauer@xcellvision.com
www.xcellvision.com

Table of Content

1. Introduction

This documents describes the minimum system requirements for a short stack (up to 20 cells) fuel cell test system. One key requirement of the system is that it is suitable for Hardware in the Loop (HIL) and Rapid Prototyping (RP) testing.
HIL in this context means that an existing fuel cell system is linked to a dynamic software model. The purpose is to evaluate the characteristics of the fuel cell system in a specific application, e.g. passenger vehicle, ship, airplane stationary power station prior to the integration of the system. Among others, key parameters of interest are performance degrading, lifetime, efficiency and the development of control patterns for optimal operation of the fuel cell in specific applications.
Medium term the test equipment should also be used for Rapid Prototyping (RP). RP

means: The control software developed in the simulation model is directly compiled and

downloaded into the controller hardware of the actual application.

For choosing the hardware and software industry standards are chosen whenever possible to minimize risk and for compatibility with a broad group of customers.

2. System overview

The tester should include flow controllers for anode (H_2, N_2, CO_2) and cathode (air, oxygen, N_2) gases, a humidification unit, a cooling system, an electronic load, a controls system and a CAN interface for the dynamic transmission of setpoints (current, flows ...) and status.
The tester should be able to work as "stand alone" tester. In this operation mode the CAN interface is inactive and all adjustments, security and the test protocol are handled with the internal controller of the tester.
The second operation mode is the "Hardware in the Loop" (HiL) operation. In this mode the setpoints (e.g. for current and flows) are provided from an external simulation model and dynamically transmitted (10 msec) via CAN interface to the tester. At the same time the tester provides the status of the test device (voltage, temperature, ...) to the simulation. The simulation model takes these values as actual values and generates a new set of setpoints. In the HiL mode the security of the tester should still be active. The tester should be self protecting and also protect the test object whenever possible. Especially internal limits are of higher priority than external setpoints received via CAN Bus.

2.1 Hardware

Main hardware components are:

- an electronic load
- humidification unit
- gas conditioning unit (reformate)
- a cooling system (temperature conditioning system)
- a controller with CAN interface

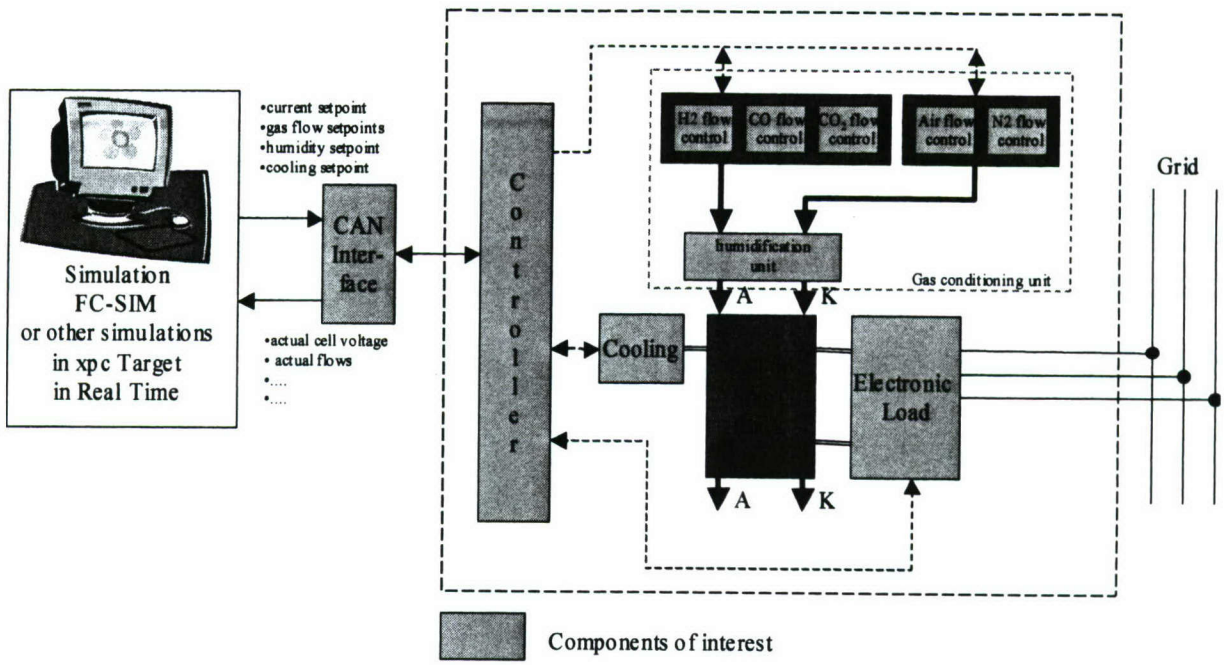

Figure 1: System overview

2.2 Software

The setpoints for all key parameters shall be internally derived. In this mode the test stand could operate in a stand alone mode without any HIL features.
For the HIL capabilities the tester should read all setpoints or a subset of setpoints (load, gases, cooling) from the CAN interface. The testers internal security levels for the tester itself and the test object are still active. In addition in HIL mode all relevant measurement data (temperatures, voltage, gas flows ...) are transmitted via CAN interface from the tester to the simulation model. Both (setpoints and actual measurement values) interact with the real time simulation. The simulation model shall read the actual measurement results and derive based on this results the actual setpoints for the tester. The setpoints are then send via the CAN interface to the tester. This procedure requires a real time simulation environment. The setup of this environment is outlined in chapter 5.

3. Requirements test stand (Specification sheet) for 12 kW Tester

Requirement	Range [Units]	Resolution (accuracy)	Comments
Electric load bank			
Voltage range	0 .. 100 [V]	0.1% FS	
Cell voltage	0 ..2 [V]	0.1%	16 channels minimum
Current range	0.. 600 [A]	0.1A (0.25 % FS)	Full size cells [600cm²]
Power range	0 .. 12 kW		
Gases			
Mixture of gases and flow controllers	Internal	Internal	Allows for the simulation of operation with reformate
Cathode	+ Air + Nitrogen + Oxygen		
Cathode flow control	0.. 0.30 [mol/sec] or 400 [NL/min]	2 NL/min (200:1 downturn)	see discussion below
Cathode pressure control	1.. 3 [bar]	100 [mbar] (3% FS)	
Cathode humidification	0 ..100 % relative humidity at 20-90°C		
Anode	Anode feed in + CO_2 + CO ? + H_2 +N_2		
Anode flow control	0 .. 0.062 [mol/sec] or 85 [NL/min]	0.4 [NL/min] (200:1 downturn)	see discussion below
Anode pressure control	1.. 3 [bar]	100 mbar (3% FS)	
Anode humidification	0 ..100 % relative humidity at 20-90°C		
Transient Characteristics			
Electric response times	< 0.001 sec from 0 to full load and back		
Gases	< 1 sec from 5% to 90% flow		

Protection			
Self protecting on different levels	level 1 -> information if limit is exceeded level 2 -> protection of the test device (cell) level 3 -> protection test stand		
Cooling			
Medium	Deionised water		
Temperature range	+20°C to 95°C	±1°C	
Cooling water flow	1 to 40L/min,	±1% flow meter range	
Cooling capacity	15 kW		
Interfaces			
Data interfaces	CAN interface	update sequence 10 [msec]	All relevant data packages should be updated very 10 [msec]
Electric interfaces	National grid standard	3-phase 220V/60Hz	
Gas interfaces	?		
Standards	TBD		
Safety	All safety standards of the US are applicable		The tester will be operated in a fuel cell laboratory environment in Hawaii
General requirements			
	Stand alone operation required (overnight)		
	Control of tester via CAN interface (HiL)		For HiL feature
	water recycling for humidification?	Yes?	

Table 1: System requirements

Note:
The specification describes minimum requirements. In case that single requirements are below the specification it should be noted in the quotation.

[1]Formula for the calculation of air flow requirement

$$q[mol/\sec] = \frac{\lambda[1] \cdot n_{cell}[1]}{F[As \cdot mol^{-1}] \cdot q_i[1] \cdot k_{O2}[1]} \cdot I_{cell}[A]$$

with

F= Faraday constant : F = 96400[As/mol]
n= cell number : n = 1.. 20
λ=stoic ratio: λ = 1..3
qi=charge per mol: qi = 4
k_{O2}=Oxygen fraction: k_{O2} = 0.21 if operated with air and k_{O2} = 1.0 if operated with Oxygen
I= cell current: I = 0..600 [A]

The design point for the flow is set to n=20, λ=2, I=600A, qi=4 and k_{O2}=0.21 (air). With this the flow requirement is 0.30 mol/sec (equivalent to 400 Norm Litre per minute).

The flow should be controllable down to 1/200 of this design point. Therefore the resolution requirement is 0.0015 mol/sec (equivalent to 2 Norm Litre / minute).

[2]Formula for the calculation of anode flow requirement

$$q[mol/\sec] = \frac{\lambda[1] \cdot n_{cell}[1]}{F[As \cdot mol^{-1}] \cdot q_i[1] \cdot k_{H2}[1]} \cdot I_{cell}[A]$$

with

F= Faraday constant : F = 96400[As/mol]
n= cell number : n = 1.. 20
λ=stoic ratio: λ = 1.05 (utilisation of 0.95)
qi=charge per mol: qi = 2
k_{H2}=Hydrogen fraction: k_{H2} = 1 if operated with pure hydrogen
I= cell current: I = 0..600 [A]

The design point for the flow is set to n=20, λ=1.05, I=600A, qi=2 and k_{H2}=1 (pure H_2). With this the flow requirement is 0.062 mol/sec (equivalent to 84 Norm Litre per minute).

The flow should be controllable down to 1/200 of this design point. Therefore the resolution requirement is 0.00030 mol/sec (equivalent to 0.4 Norm Litre / minute).

4. Requirements test stand (Specification sheet) for 1 kW Tester

Requirement	Range [Units]	Resolution (accuracy)	Comments
Electric load bank			
Voltage range	0 .. 10 [V]	0.1% FS	
Cell voltage	0 ..1 [V]	0.1%	4 channels minimum
Current range	0.. 100 [A]	0.1A (0.25 % FS)	Smaller cells and short stacks
Power range	0 .. 1 kW		approximately
Gases			
Mixture of gases and flow controllers	Internal	Internal	Allows for the simulation of operation with reformate
Cathode	+ Air + Nitrogen (purge) + Oxygen		2 gaslines total a.) Air + Oxygen b.) Nitrogen
Cathode flow control	0.. 0.015 [mol/sec] or 20 [NL/min]	0.4 NL/min (50:1 downturn)	see discussion below
Cathode pressure control	1.. 4 [bar]	100 [mbar] (3% FS)	absolute pressure
Cathode humidification	0 ..100 % relative humidity at 20-90°C		
Anode	Anode feed in + H_2 + N_2		2 gaslines total
Anode flow control	0 .. 0.0075 [mol/sec] or 10 [NL/min]	0.2 [NL/min] (50:1 downturn)	see discussion below
Anode pressure control	1.. 4 [bar]	100 mbar (3% FS)	absolute pressure
Anode humidification	0 ..100 % relative humidity at 20-90°C		
Transient Characteristics			
Electric response times	< 0.1 sec from 0 to full load and back		
Gases	< 1 sec from 5% to 90% flow		
Protection			

Self protecting on different levels	level 1 -> information if limit is exceeded level 2 -> protection of the test device (cell) level 3 -> protection test stand		
Cooling			
Medium	Deionised water		
Cooling water temperature	+20°C to 95°C	±0.5°C	
Cooling water flow	0.1 to 2L/min,	±5% flow meter range	
Cooling capacity	1 kW		
Interfaces			
Data	CAN interface	update sequence 100 [msec]	All relevant data packages should be updated very 100 [msec]
Electric Interfaces	National grid standard	3-phase 220V/60Hz	
Gas interfaces	TBD		
Standards			
Safety	All safety standards of the US are applicable		The tester will be operated in a fuel cell laboratory environment in Hawaii
General requirements			
	Stand alone operation required (overnight)		
	Control of tester via CAN interface (HiL)		For HiL feature
	water recycling for humidification?	Yes	

Table 2: System requirements

Note:
The specification describes minimum requirements. In case that single requirements are below the specification it should be noted in the quotation.

[1]Formula for the calculation of air flow requirement

$$q[mol/\sec] = \frac{\lambda[1] \cdot n_{cell}[1]}{F[As \cdot mol^{-1}] \cdot q_i[1] \cdot k_{O2}[1]} \cdot I_{cell}[A]$$

with

F= Faraday constant : F = 96400[As/mol]
n= cell number : n = 1.. 10
λ=stoic ratio: λ = 1..3
qi= charge per Mole-coolly: qi = 4
k_{O2}=Oxygen fraction: k_{O2} = 0.21 if operated with air and k_{O2} = 1.0 if operated with Oxygen
I= cell current: I = 0..100 [A]

The design point for the flow is set to n=5, λ=2, I=100A, qi=4 and k_{O2}=0.21 (air). With this the flow requirement is 0.0123 mol/sec (equivalent to 16.6 Norm Litre per min).

The flow should be controllable down to 1/50 of this design point. Therefore the resolution requirement is 0.33 Norm Litre / minute.

[2]Formula for the calculation of anode flow requirement

$$q[mol/\sec] = \frac{\lambda[1] \cdot n_{cell}[1]}{F[As \cdot mol^{-1}] \cdot q_i[1] \cdot k_{H2}[1]} \cdot I_{cell}[A]$$

with

F= Faraday constant : F = 96400[As/mol]
n= cell number : n = 1.. 20
λ=stoic ratio: λ = 1.05 (utilisation of 0.95)
qi=charge per mol: qi = 2
k_{H2}=Hydrogen fraction: k_{H2} = 1 if operated with pure hydrogen
I= cell current: I = 0..100 [A]

The design point for the flow is set to n=5, λ=1.05, I=100A, qi=2 and k_{H2}=1 (pure H_2). With this the flow requirement is 0.00272 mol/sec (equivalent to 3.7 Norm Litre per minute).

The flow should be controllable down to 1/50 of this design point. Therefore the resolution requirement is 0.07 Norm Litre / minute.

5. Real time HIL-Simulation

Key requirements for the HIL environment and the HIL Simulation are:

- Use of standard software for the simulation as well as for the real time capabilities
- Use of Standard interfaces
- Transparent design of the overall system
- Minimum risk

Based on these key requirements the following hardware software configuration is

proposed. Other configurations are possible but had not been investigated yet.

Simulation
The simulation software has to be written in Matlab/Simulink from Mathworks

Corporation. Matlab/Simulink represents a worldwide standard for dynamic simulation.

Real time capabilities
For running the simulation in real time (essential for HIL) Mathworks provides an add on (Real Time Workshop) which generates real time C-Code that could be transferred to a real time target (older PC or microcontroller based system). In addition Mathworks provides as a second add on the software xPC, which allows running the C-Code from the real time workshop on a normal PC. Both, simulation and real time PC are linked over a TCPIP interface.

Data Interface to test stand
The test stand and the real time PC (xPC) interface via a CAN 2B databus. The necessary drivers are included in the real time workshop (Softing CAN Card required).
There is no direct linage between the simulation PC and the test stand. However some parameters embedded in the C-Code could be changed via the TCPIP interface while the HIL system is active. Through this debugging and optimisation of the software is possible.
The CAN data interface is also a standard Industry interface. Standard tools for monitoring the CAN traffic are available.

Security
The external (remote) control of the test stand via the CAN data bus in the HIL mode does not release the test stand from security functions. The protection of the test stand itself and the test object (fuel cell) are in responsibility of the test stand.

Prices:

Software	List price single user (commercial license)	Comment
Matlab	$1900,-	Mathworks inc.
Simulink	$2800,-	Mathworks inc
Real Time Workshop	$7500,-	Mathworks inc
xPC Target	$4000,-	Mathworks inc
Softing CAN Interface Card	ca. $800,-	CAN-AC1-PC; http://www.hitex.co.uk/shop/
Microsoft Visiual C Professional Version	ca. $800,-	
Total	$17800,-	plus VAT

Table 3: Software Development Environment. Note: The prices listed are only approximate. European versions are generally more expensive. The HiL tools are not included in the tester quotations.

Summary (HiL)

The configuration above meets the basic requirements listed. The fact that both the simulation environment (Matlab/Simulink) as well as the real time software (Real Time Workshop, xPC target) comes from one supplier eases the setup and configuration of the system. The CAN interface to the test stand represents an industry wide standard with all its advantages (available tools for debugging and data monitoring/tracking). The Simulink platform allows the run of different simulation software, e.g. FCV-SIM, PSAT (after adaptation).

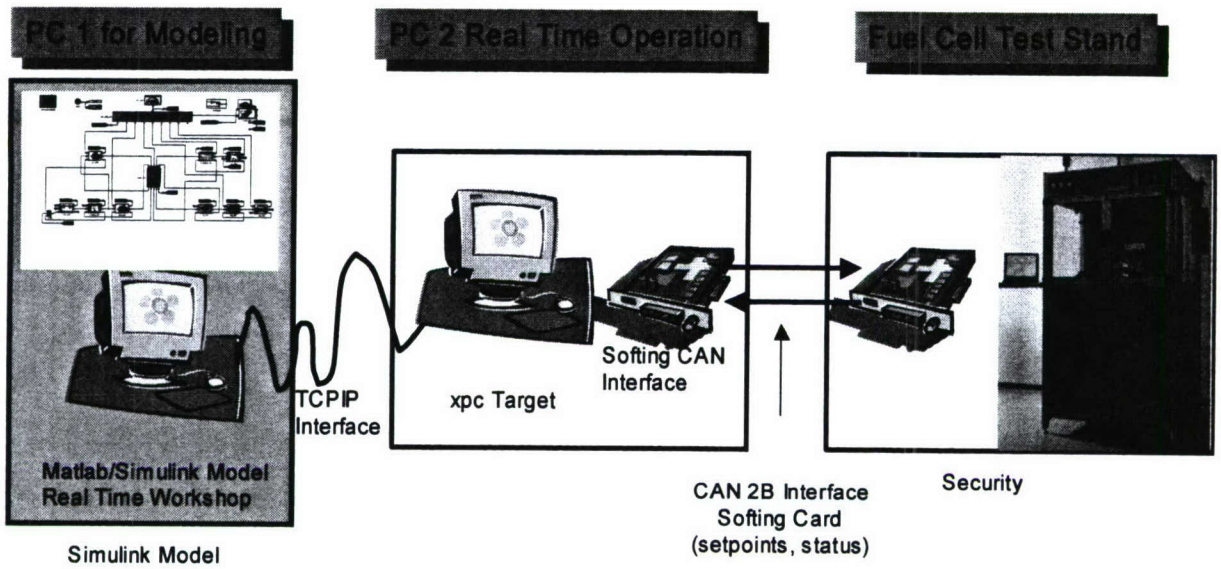

Figure 2: Sketch HIL Setup

6. Rapid Prototyping

Rapid prototyping is the transfer of in Simulink in the simulation developed control algorithms directly in the hardware controller box. The setup of the HIL environment supports this strategy. Only the target needs to be changed from xPC to the target hardware in the controller box (e.g. mpc 555 or other). Since it is not clear at the moment which target hardware will be used (this depends on the project and the customer) it is not certain that Mathworks supports the target system.

7. Market Survey

This chapter provides a comparison between the quotations of the fuel cell testers supplied by the companies in Table 4. The testers for a power range of 1kW and lower had only been quoted (and requested) by Greenlight Power and Fuel Con. All companies had been open in the discussion of technical issues. They also delivered the for the evaluation necessary information in time.

Company	FuelCon	Lynntech (Fideris)	Greenlight Power	Chino Works America Inc.
Contact information	FuelCon Mr. Bode Steinfeldstraße 3 39179 Barleben Germany	FIDERIS Abigail Smith Sales Manager Fideris Inc. 3900 State Hwy. 6, South, College Station, Texas 77845	ENKAT Dr.-Ing. Bernd Pitschak Managing Director A DIVISION OF HYDROGENICS CORPORATION Luggendelle 19 D-45894 Gelsenkirchen	CHINO Katsunori (Daniel) Terui 32-8 Kumano-Cho, Itabashi-Ku, Tokyo 173-8632 Tel : +81-3-3956-2171 Fax : +81-3-3956-0915

	http://www.fuelcon.de/en/index.html	979-694-5255 Phone, 979-694-5271 Fax abby.smith@fideris.com, http://www.fideris.com/DesktopDefault.aspx?tabid=2593	Germany FON: +49.209.933.122.11 FAX: +49.209.933.122.18 www.hydrogenics.com	E-mail : terui@chino.co.jp URL : http://www.chino.co.jp http://www.chinoamerica.com/products/systems/fcevaluation.html

Table 4: Overview Contacted Suppliers

Overall fuel cell testers for 3 different power ranges had been requested. The power ranges are:

- 12 kW electric power,
- 4 kW electric power
- below 1 kW electric power

Table 5 lists the quotations requested from the suppliers. Even though all suppliers got the same specification sheets the quotations are still not directly comparable. For example are the current and voltage ranges of each tester different. Other differences are in quoted the accuracy of sensors and actuators. However, in a bulk the quotations are comparable within a power range. Major differences are in the CAN interface required for the realisation of HiL. While GLP and FuelCon are well prepared for this kind of requirement Fideris and Chino had not been ready to offer this feature directly from the shelf.

	Power Range			
Supplier	**12 kW tester**	**4 kW tester**	**1 kW tester**	**Date/ Version**
FuelCon		Evaluator C600 2400 W cell and short stack tester **$172,200,-**[1]		March 7th 2004
Greenlight Power (GLP)			E-Series 1.5 kWmax cell and short stack tester **$107,700,-**	March 17th 2004
GLP		G300-Series 4 kW cell and short stack tester **$160,100,-**		March 17th 2004
GLP	G500-Series 12 kW stack tester **$ 230,400**			Mai 2004
GLP			G50 – Series 0.8 kWmax cell and short stack tester **$ 64,000,-**	Mai 2004
Fideris	12 kW stacktester **$ 223,023,-**			September 13th 2004
Chino	12 kW stacktester **$ 291,000,-**			September, 27th 2004
FuelCon			C100 400Wcont Tester **$121,100,-**[1]	October, 27th 2004
FuelCon			C050 400Wcont tester **$ 75,600,-**[1]	October, 27th 2004

Table 5: Quotations

For a better evaluation of the prices of the testers in the 1 kW range please pay attention to the comments in Table 6. The table compares and lists the main features of the 1kW test stands from GLP and FuelCon. From the appearance the with open cabin equipped G50 (GLP) and the C050 (FuelCon) testers are comparable as well the closed cabin testers E-series (GLP) and the C100 (FuelCon). Closed cabin testers have the advantage of a higher level of security and also of shielding the test objects from environmental impacts (temperature fluctuations, moved air).

Supplier	Product Name	Comments
GLP	G50 (Figure 3)	Medium size single cells and short stacks 0..150A; 0..50V; 800Wel, Anode: 1 mass flow controller 0.2 ..10NLPM, Nitrogen purge Cathode: 1 mass flow controller 0.4..20NLPM, Nitrogen purge 0..5 NLPM (rotameter)

[1] For the better comparison the quoted 16% has not been included (maybe not due)

		CAN interface included: no Coolant: adjustable (rotameter) Humidification: 100%RH up to 90°C Mechanics: Open cabin
GLP	E-Series (Figure 4)	Full size single cells and short stacks 0..500A; 150mV..20V; 1.5kWel, Anode: 1 mass flow controller 0..15NLPM, Nitrogen purge 10NLPM Cathode: 1 mass flow controller 0..50NLPM, Nitrogen purge 10NLPM CAN interface included: yes Coolant: adjustable flow Humidification: 100%RH up to 80°C Mechanics: Closed cabin
FuelCon	C050 (Figure 5)	Medium size single cells and short stacks 0..100A; 300mV..10V; 400Wel, Anode: 1 mass flow controller 0.2 ..10NLPM Cathode: 1 mass flow controller 0.4..20NLPM, Nitrogen purge CAN interface included: yes Coolant: adjustable flow 0.1..2lpm; 10°C above ambient temperature .. 130°C Humidification: yes for anode and cathode, (Bubbler) Mechanics: Open cabin
FuelCon	C100 (Figure 6)	Medium size single cells and short stacks 0..100A; 300mV..10V; 400Wel, Anode: 1 mass flow controller 0.2 ..10NLPM Cathode: 1 mass flow controller 0.4..20NLPM, Nitrogen purge CAN interface included: yes Coolant: adjustable flow 0.1..2lpm; 10°C above ambient temperature .. 130°C Humidification: 100%RH up to 90°C (Dynamic direct injection) Mechanics: Open Cabin

Table 6: More detailed information about the testers in the 1 kW range

Comments:

- The cost listed above is always without the reformate option.
- Applied cconversion factor Dollar – Euro:1.2$ / €; Yen – Dollar 110Yen/Dollar
- GLP also includes the commissioning cost and training on site (5 days). Travel and hotel cost are not included.
- FuelCon includes only training at the plant (up to 3 days) in Canada or Germany
- Shipment cost from plant to HNEI are neither included by GLP nor by FuelCon
- The hardware in the loop setup is included in the FuelCon quotation. In the GLP quotation a CAN interface is included.
- Both suppliers require the preparation of the site (piping, ...)
- All test stands could be operated as stand alone test equipment and immediately utilized until the HIL option is ready for use

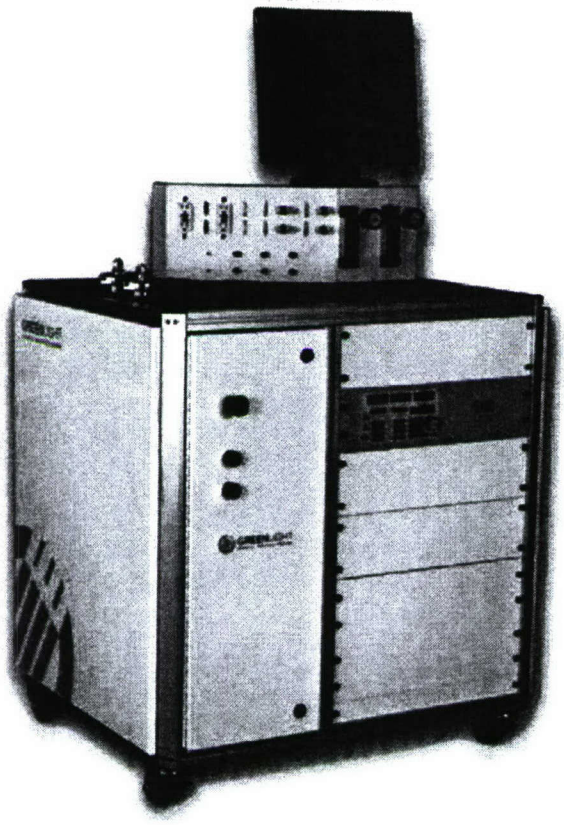

Figure 3: GLP tester G50

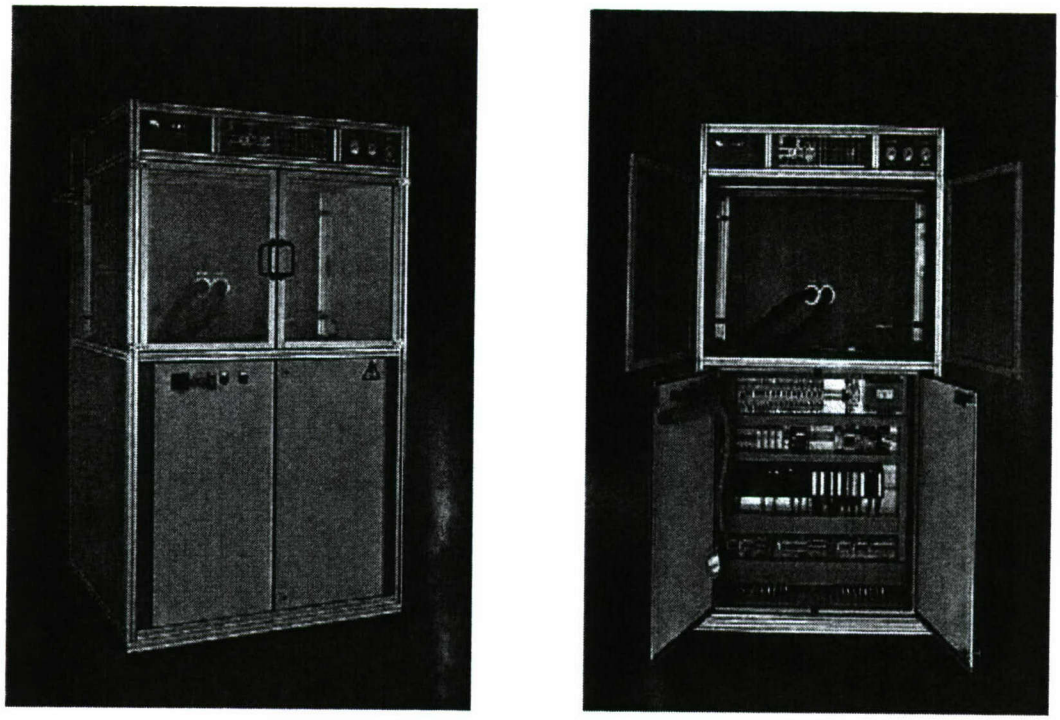

Figure 4: GLP tester E-300

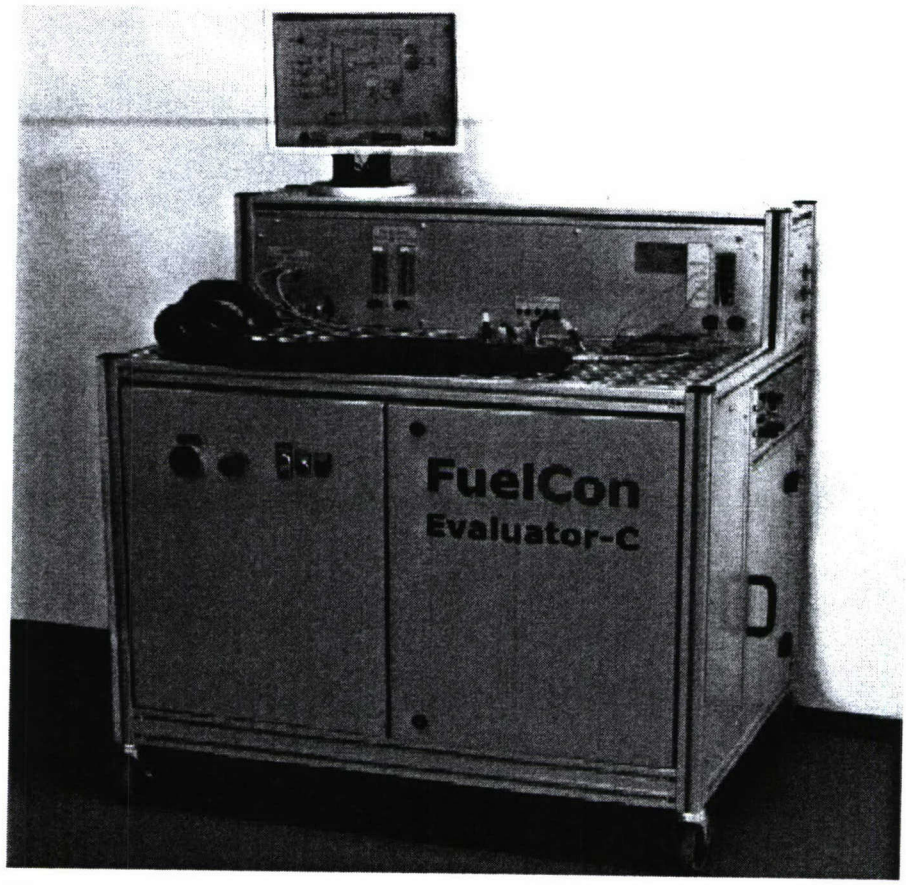

Figure 5: FuelCon tester C050

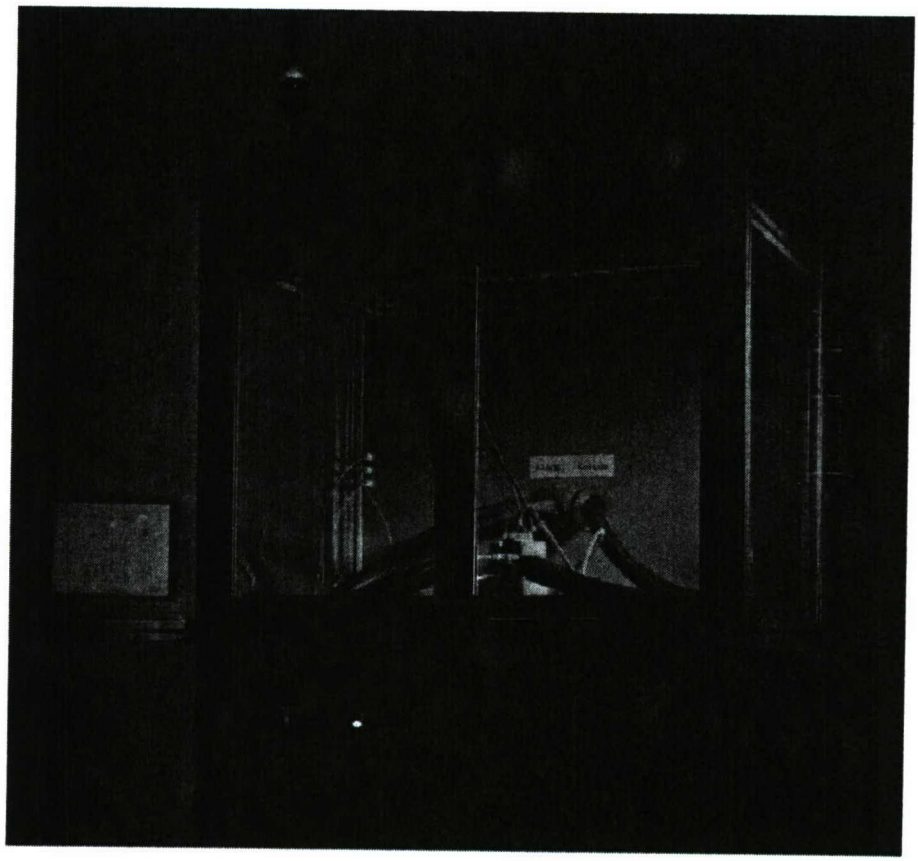

Figure 6: Fuelcon Tester C100

8. Summary and Conclusions

In total 9 quotations of four different suppliers for fuel cell testers had been compared in the document. The testers are for the 12 kW range, the 4 kW range and the 1 kW and lower range. The main focus has been put on the testers with an electrical power range of 1 kW or lower. For the request of the quotations a spec sheet with the minimum specifications had been developed which served as basis for the quotations. Besides the required process technology (gas supply, humidification, cooling) and the electrical load the issue of a CAN interface for the communication with external simulations (Hardware in the Loop, HiL) played an important role. While the process technology was very familiar with the companies the HiL feature was new though not totally new and of high interest for them. FuelCon and GLP provided a CAN interface though with only 100msec update intervals (for a maximum of 15 values). Although this seems slow and limited it may be more than enough for the implementation of HiL features given that slower messages (1sec intervals) could be transmitted without limitations in numbers (FuelCon). Also fuel Con offers already testers with HiL feature in the 80..150 kW range (see FuelCon webpage).

The direct comparison of the quotations of the G50 and C050 tester shows that the quoted price for the FuelCon product is about 18% higher than for the GLP product. The same trend could be observed for the E-300 tester from GLP and the C100 from FuelCon. The quoted FuelCon price is about 13 % higher than the price of the comparable GLP product.

9. Appendix

Revision date	Initiated by	Subject

Table 7: Table of Revisions

APPENDIX II

Request for Quotation for the HiL #1 Test Station

April 21, 2005
Request for Quotation
Fuel Cell Tester
Hawaii Natural Energy Institute
University of Hawaii

The Hawaii Natural Energy Institute (HNEI) at the University of Hawaii at Manoa issues the following request for quotation (RFQ) for a 100 W fuel cell tester. The issuance of this RFQ does not represent a commitment by HNEI to purchase any equipment offered in response to this RFQ. HNEI reserves the right to modify the terms of this RFQ and reissue the RFQ.

The system will be used for testing fuel cells in two operational modes, i.e., with or without the CAN interface being active. The CAN interface will be used for Hardware-in-Loop (HiL) operation. Technical aspects and HiL requirements for the tester are described in Sections 1 and 2, following this discussion of overall requirements.

The quotation should include the availability of the system stated as time to delivery after the order is received and this may be considered in the selection process. The vendor must permit system checkout by HNEI representatives (including test of the HiL feature) at the vendor's manufacturing facility. The price of the system should be quoted F.O.B. HNEI's Hawaii Fuel Cell Test Facility (HFCTF) in Honolulu, Hawaii (zip code 96813), presuming shipment by air, including costs for operator training (and assistance with system checkout including test of the HiL feature) at the HFCTF, and including all applicable taxes. The location of the vendor's manufacturing facility for this tester shall be specified. Educational discounts are encouraged and should be clearly identified.

Responding companies should provide evidence that they have previously sold systems similar to the proposed system. Responding companies are encouraged to provide names of three organizations that currently own similar systems. Submitting more than one quotation per vendor is not prohibited.

Questions should be directed to Robert M. Moore via email only (rmmoore@hawaii.edu) and include the subject line "*Your Company Name* – Fuel Cell Tester". Responses (quotations) to this RFQ are due on May 6, 2005 by 5 pm Hawaii Standard Time. If no suitable quotation is received by this date, the closing date will be extended another week to May 13, 2005 at 5 pm Hawaii Standard Time. Responses (quotations) should be emailed and contact information is provided below.

Robert M. Moore
Director of Fuel Cell Research
rmmoore@hawaii.edu
University of Hawaii at Manoa
Hawaii Natural Energy Institute
1680 East-West Rd., POST 109
Honolulu, HI 96822

Fax: (808) 956-2336

1. Technical aspects

The following list describes the minimum requirements for a $100W_{el}$ tester. The tester will be operated with air or oxygen on the cathode side. The anode will be fuelled with pure hydrogen; however, the tester shall provide the option of expansion to operation with reformate.

Requirement	Range [Units]	Accuracy	Comments
Electric load bank			
Voltage range	0.150 .. 10 [V].	+/- 0.2% of reading and +/- 0.05% FS (full scale).	Total voltage.
Cell voltage	0 ..1 [V].	+/- 0.2% of reading and +/- 0.05% FS (full scale).	Cell voltage monitoring: 4 channels minimum.
Current range	0 .. 200 [A].	0.1 [A] (0.25% reading and +/-0.05 FS).	For cells and short stacks with active cross sectional area of ca. 100 cm^2.
Power range	0 .. 200 W.		
Gases			
Mixture of gases and flow controllers	Internal.	Internal.	Expandable towards reformate operation.
Cathode	+ Air, + Oxygen, + Nitrogen (purge).		2 gas lines total: a.) Air + Oxygen, b.) Nitrogen.
Cathode flow control	0 .. 0.0074 [mol/sec] or 0 .. 10 [slpm].	50:1 downturn (+/- 0.5% rate and +/- 0.1% FS in range of 5%-100%; and +/- 1% rate and +/- 0.2% FS in range of 2%-5%).	
Cathode pressure control	1 .. 4 [bar].	+/- 1.5% rate and +/- 0.5% FS.	Absolute pressure.
Cathode humidification	0 .. 100% relative humidity at 20-90°C.	2% reading.	Injection system.
Anode	Anode feed in + Hydrogen, + Nitrogen.		2 gas lines total.
Anode flow control	0 .. 0.0015 [mol/sec] or 0 .. 2 [slpm].	50:1 downturn (+/- 0.5% rate and +/- 0.1% FS in range of 5%-100%; and +/- 1% rate and +/- 0.2% FS in range of 2%-5%).	

Anode pressure control	1 .. 4 [bar].	+/- 1.5% rate and +/- 0.5% FS.	Absolute pressure.
Anode humidification	0 .. 100% relative humidity at 20-90°C.	2% reading.	Injection system.
Transient Characteristics			
Electric response times	Current step < 1 msec from 10% load to 90% load[2]; current step < 1 msec from 90% load to 10% load.	See Figure 7: T_1 = 1 msec, T_2 = 1 msec, static tolerances for t > T_1 + T_2.	Electronic load only.
Gas flow	< 1 sec from 10% to 90% flow[3] at 2 bar absolute and constant RH = 90%. < 1 sec from 90% to 10% flow at 2 bar absolute and constant RH = 90%.	See Figure 7: T_1 = 1 sec, T_2 = 1 sec, static tolerances for t > T_1 + T_2.	RH below 100% is to avoid condensation.
Pressure swing	< 1 sec from 1.5 bar absolute to 2.5 bar absolute at constant RH = 90% and constant gas flow (1.8 slpm anode and 9 slpm cathode). < 1 sec from 2.5 bar to 1.5 bar absolute pressure at constant RH = 90% and constant gas flow (1.8 slpm anode and 9 slpm cathode).	See Figure 7: Upward swing: T_1= 1 sec, T_2 = 1 sec, static tolerances for t > T_1 + T_2. Downward swing: T_1 = 1 sec, T_2 = 3 sec, static tolerances for t > T_1 + T_2.	Note: differential pressure from anode to cathode shall not exceed 0.1 bar at any time during the pressure swing. Total open volume of the test object (cell) is 10cm^3 on the anode and 20 cm^3 on the cathode.
Humidification	< 5 sec from 10% to 90% RH at 2 bar absolute and constant gas flow (1.8 slpm anode and 9 slpm cathode). < 5 sec from 90% to 10% RH at 2 bar absolute and constant gas flow (1.8 slpm anode and 9 slpm cathode).	See Figure 7: T_1 = 1 sec, T_2 = 4 sec, static tolerances for t > T_1 + T_2.	
Protection			
Self protecting on different levels	Level 1: in the event that any limit is exceeded.		Level 1 has the highest priority.

[2] 100% is equivalent to 100 A.

[3] Specified is a percentage of the maximal anode hydrogen and cathode air flow (anode: 2 slpm; cathode: 10 slpm).

	level 2: protection of the test device (cell). level 3: protection of the test stand.		
Temperature Management (cooling + heating)			
Medium	Deionised water.		Ambient pressure.
Cooling water temperature	+20°C to 95°C.	±1°C.	Set point room range / Minimum temperature 20 - 30°C / 10°C 30 - 40°C / 20°C 40 - 95°C / 25°C
Cooling water flow	0.1 to 2 L/min.	±2% reading.	
Cooling and heating capacity	500 W.		
Hoses	Heated hoses required.		
Electric heating	2 – Outputs, 250 W each. 2 - thermo elements, NiCrNi.		One output and one input for both the anode and cathode.
Interfaces			
Data	CAN interface.	Update sequence 100 [msec].	All relevant data packages should be updated every 100 [msec].
Electric interfaces	National grid standard.	3-phase, 208 V, 60 cycles, 15 kW.	
Gas interfaces	Gas inlet and outlet plus cooling inlet and outlet – Swagelok ½".		
Safety standards	All applicable safety standards of the US need to be considered.		The tester will be operated in a fuel cell laboratory environment in Hawaii.
General requirements			
Software	Operational software shall be based on LabVIEW™. Uncompiled development version of the software is required. Subroutines which contain vendor's core knowledge shall be protected. Documentation of the original software shall be included.		
Special arrangements	Discretion agreements and software warranty waiver may apply as arranged upon vendor's request.		
Support and warranty	Detailed checkout at factory by HNEI representative and functional test upon arrival at Hawaii (with original software) shall be covered by hardware and software warranty. Software support thereafter shall be included for one year but may be limited to the original runtime version. Hardware warranty thereafter shall be included for one year but may be limited to material break down and evident manufacturing failure.		

Automation	24-hour automated, unattended operation ability required.
Housing	Encapsulated test chamber for the fuel cell.
AC Impedance Measurement	The AC impedance measurement system shall be integrated into the tester and have the following specifications: Impedance range: 0.01 mOhm to 1,000 Ohm Frequency range: 0.01 Hz to 10 kHz Frequency accuracy: +/- 1% DC voltage maximum: 10 V DC current maximum: 150 A Load Mode: constant current, constant voltage, constant power Phase angle accuracy: +/- 0.5° Impedance accuracy: +/- 1%

Table 1: System requirements

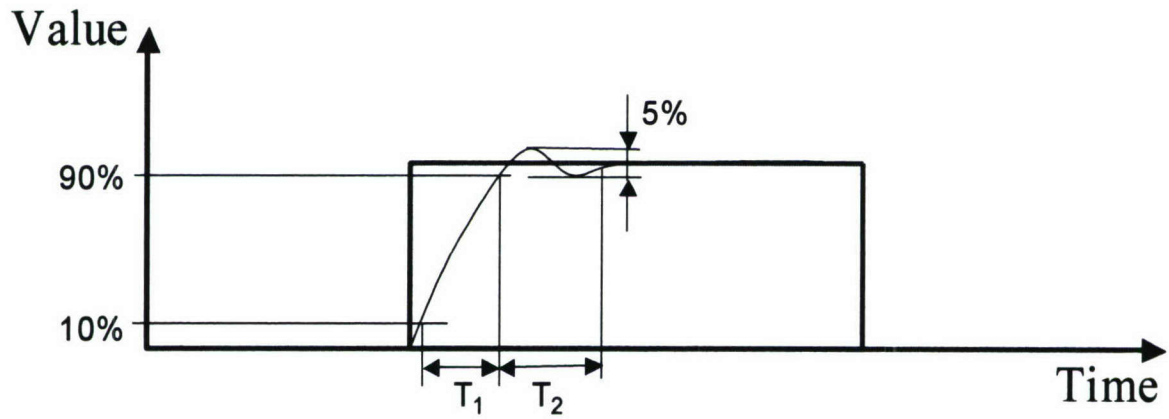

Figure 7: Ramp up or ramp down time (T_1) and settling time (T_2)

2. HiL requirements

The tester should provide two 24-hour automatic, unattended operational modes, as described below.

The first operation mode is the operation as an independent tester. In this operation mode the CAN interface is inactive and all adjustments, security and the test protocol are handled with the internal controller of the tester.

The second operation mode is the "Hardware-in-Loop" (HiL) operation (see Figure 2). In this mode the set points (e.g., for current and flows) are provided by an external simulation model and dynamically transmitted (100 msec) via CAN interface to the tester. At the same time, the tester provides the status of the test device (voltage, temperature, ...) to the simulation. The simulation model takes these values as actual values and generates a new set of set points. In the HiL mode, the security levels of the tester should still be active. The tester should be self-protecting and also protect the test object whenever possible. The internal limits are of especially higher priority than the external set points received via the CAN Bus.

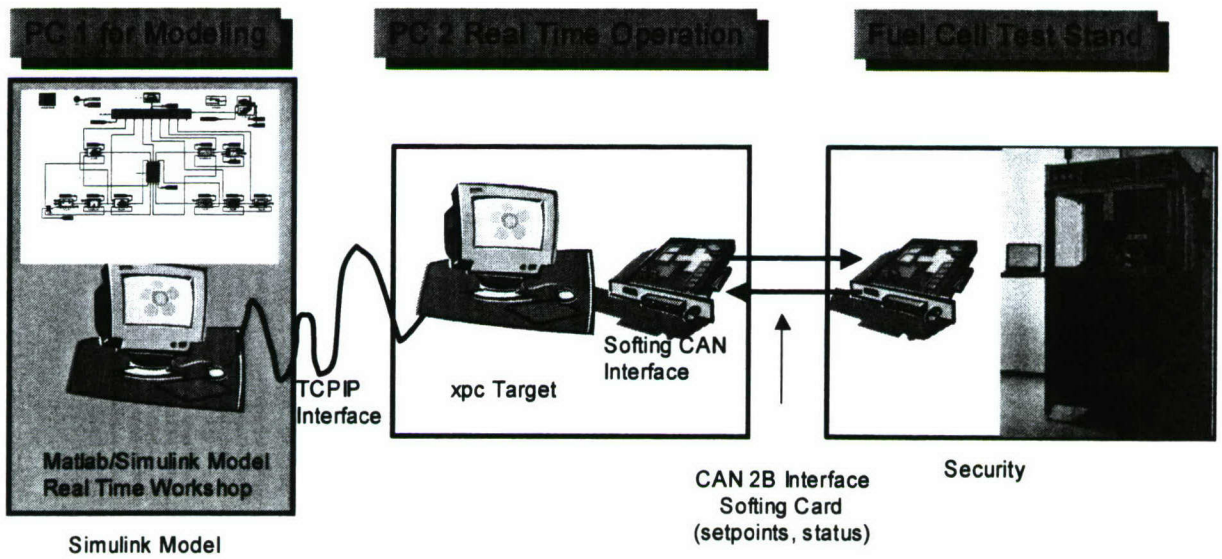

Figure 8: Sketch of the HiL Setup

APPENDIX III

Dr. Hauer's Factory Acceptance Test (FAT) Report

Fuel Cell Tester Factory Acceptance Test (FAT) Report

by

Karl-Heinz Hauer

January 2006

Fuel Cell Stack Tester FAT

Date: 11/14/2005 – 11/15/2005

Participants
Karl-Heinz Hauer (xcellvision)
Günter Randolf (HNEI)
Mr. Buhro (FuelCon)
Mr. Heinze (FuelCon)
Mr. Berlin ; part time (FuelCon)
Mr. Benecke ; part time (FuelCon)
Mr. Bode ; part time (FuelCon)

Location: FuelCon AG, Steinfeldstrasse 3, Barleben, 39179 Magdeburg – Germany

Summary:
The Factory acceptance test has been to general satisfaction. The tester worked problem free with the exception that the dynamic requirements could not be fully met. The general impression of the tester and software was very good and had been accepted (**attachment 1**). Because of time constraints only some of the requirements in the specification sheet (**attachment 4**) had been performed. The control via CAN interface worked after some initial communication problems between tester and real time PC.

Dynamic Requirements:
Because of the failure on FuelCon's side meeting the dynamic requirements completely the agreement in **attachment 3** had been made between HNEI and FuelCon.

Attachments

Signature sheet

FBF-016-00 **FuelCon**

protocol of the FAT

#	1	
Project No.:	4200137	
Date:	2005-11-14	2005-11-15
Participants:	Günter Randolf	Hawaii Natural Energy Institute
	Karl Heinz Hauer	XCELLVISION
	Mr. Buhro, Eckhard	FuelCon AG
	Mr. Heinze, Daniel	FuelCon AG
Customer No.:	D017406	
Customer:	Hawaii Natural Energy Institute	

Customer Information

- supplyer no.:
- your order no.: Z732450
- your sign:
- project: Evaluator C100, direct injection

Station specifications

Transient measured, Pressure not 100% Accuracy could not be verified, Calibration sheets attached

- Flow, software, current and voltage meet accuracy requirements.
- Training for soft- and hardware was executed
- CAN-communication was successful
- printed manuals for hard- and software and Documentation-CD-ROM transfered

note:
Software for Pressure Regulator and Flow Controller required
Self regulated Heatpipe (2 x 1,5 m) required

- Remaining issues
Open Source Software as requested in RFQ

Signature Customer
Günter Randolf, Hawaii

Signature Contractor
Eckhard Buhro, FuelCon AG

Figure 9: Signature sheet page 1/1

Initial summary report by Email

This initial email report has been written by Günter Randolf in discussion with Karl-Heinz Hauer on the evening of November 15th

1. The pressure swing:
From my experience with other industrial test stands (for combustion engines), tuning hardware controllers via an external laptop and a separate, manufacturer provided software is state of the art. Since usually this is done infrequently, it is OK. If the pressure controller is tuned to the specific conditions (e.g. from 1,5 to 2 bar step) the PID parameter can be optimize to result in good response time and little overshooting. For other conditions (e.g. from 1,0 to 1,5 bar step) other parameters might be better. If we run a simulation, we have to decide which pressure steps are most important for us since the parameters can not be changed fast enough on-the-fly, neither with external software nor if they would implement something. Hardware controllers are simple not designed for such a treatment. And that is why I want to avoid them in HiL3 ... . FC is already on the right way as they have no HW controllers for temperature.
-----> My conclusion is that there is nothing better available on the market (yet).

2. Open source:
After all discussions with Berlin, Benecke and Buhro, I think that the Bode (why do all start with "B"?) had a wrong understanding of what the software guys are talking about. Benecke and Berlin are promoting a set of VIs which enables the user to read and write Tags (Values of every channel) with an external program (e.g. to avoid the CAN and have excess to more data than usually). They provide this VIs to "special users" like VW who also have special requirements. Those VIs are open source, but have nothing to do with "FuelWork", they are just a tool of communication. No critical alternation like changing the front panel (moving or creating buttons, changing labels, ...) as well as careful modification of the code cannot be done, so it is not what we originally had in mind. However, no other company (e.g. GLP) would share their source either, this is usually a companies core knowledge and holy.
As Bodes promise was (in my understanding) based on a misinterpretation, we could either let him pay for his mistake or find some agreement, which I basically would prefer. In order to keep face and not let them fob us off easily we may threaten them with rejection and insist on hardware improvement, e.g. two integrated and controlled auxiliary heaters.
------> Off course, I would prefer the software, but if they are not going to release it, it may be better to get the test stand (which is a good test stand anyway) than to sue and have nothing to work with for the next half year. And if we force them to give us source, we do not really know what we will get. Maybe it is not going to work well for whatever reason and we have than no way to complain. We simply can never proof that what we get is really THE source code of FuelWork.

3. Checkout paper:
FC prepared a checkout paper, I put some remarks on (e.g. things we did not validate, the unresolved software issue, ...) and signed the remaining (what we could check and approve). I will send you a copy as soon as I have access to a scanner.

Please let me know about your opinion, we should contact FC soon because Buhro has mentioned a scheduled shipment next Wednesday.

Nice greetings, Guenter

Agreement between FuelCon regarding dynamic requirements

FuelCon

FuelCon Systems Inc.
3250 East Mall
Vancouver, BC, Canada V6T 1W5

Tel: 604-696-1290
Fax: 604-472-1712
Website: www.fuelcon.com
Reference No: D017406

November 30, 2005

Mr. Milton Staackmann
University of Hawaii at Manoa
Hawaii Natural Energy Institute
Holmes Hall 246, 2540 Dole Street
Honolulu, HI
96822

Dear Milton,

Re: Completing project 4200137 (Fuel Cell Tester)

As I understand, from the discussions between Drs Hauer and Benecke, that the outstanding issues related to this equipment has been resolved. Specifically, as compensation for our inability to meet the few specification deficiencies (pressure response and software source code release), FuelCon will provide the following:

1) An exit temperature control for anode and cathode (temperature regulated and controlled by Fuel-works).
2) Rapid service response for a 1 year period including software modifications via remote software maintenance.
3) Labview VI's for changing internal tags (variables).

As you know, the equipment was shipped last week and is scheduled to arrive in Los Angeles on December 2, 2005. Ms. Kuhne of our German office will forward the details concerning the follow on shipment from Los Angeles to Honolulu once they become available.

With the completion of the FAT and the shipment of the equipment, I now attach the final invoice and software license agreement.

Finally, we appreciate your willingness to be referenced in a press release and will forward a draft for your approval based on the wording that you provided.

If you have any questions or concerns, please let me know.

Kind regards,

Blair Heffelfinger

Attach:
FCS-0030 D017406 4100191 (final).pdf
D017406-1 70186 FuelWorklicense.pdf

Attachment FACTORY ACCEPTANCE TESTS (FATs) OF THE FuelCon PEMFC TESTER

The following tests will be performed using a 100 cm^2 PEMFC provided by HNEI, University of Hawaii for the FATs of a PEMFC Dynamic Tester at FuelCon® AG, Magdeburg-Barleben, Germany. Phase I of the FAT will be signed off at FuelCon.

FAT phase II will be re-testing with the same fuel cell and the same testing procedure at the Hawaii Fuel Cell Test Facility in Honolulu, Hawaii to ensure no damaged occurred during shipping.

A successful completion of the FAT requires passing phase I and phase II. The signed document for the completed FAT will be sent back to FuelCon.

1. HNEI 100 cm^2 PEMFC Diagnostic Tests:

The 100 cm^2 PEMFC will be shipped form HNEI, Hawaii to FuelCon® AG, Germany and on arrive at FuelCon the following diagnostic tests will be performed to check the integrity of the PEMFC prior to using it for the FATs:

I. Hydrogen crossover test (in-situ Method) or any other crossover test available at FuelCon.
Not performed in Germany

II. H_2/Air polarization curve at 206.84 kPag (2 barg)
Performed in Germany (at least to a degree showing that taking a polarization curve is in principle possible) --> This was enough for the FAT purpose.

The figures at the end of the documents are for reference propose and can be used to compare results from FuelCon tester in Germany.

Figure 1 shows the PEMFC test hardware flow diagram which can assist in connecting the fuel cell to the tester.

Figures 2 & 3 shows the polarization curves at 2 barg and hydrogen crossover test results respectively. These test results were performed when the 100 cm2 PEMFC was received (27^{th} September 2005) at HNEI and just before shipping the cell to Germany.

Table 1 shows the list of items including the 100 cm^2 PEMFC which were shipped to FuelCon for the checkout process.

2. **FuelCon Standard FAT which will include the following tests:**

I. Manual mode test using current-ramp

- Electronic Load Test
  Principle functionality tested

Not tested with respect to dynamics, accuracy, noise (these tests require a significant effort in terms of hardware and probably several days time)

- Purge-Function Test

Tested and OK (principle functionality only)

II. Scripts tests

- Humidifier Test
  Tested and in principle OK. However we relied on the indicators displayed by Fuelwork since we did not have own instrumentation for humidification
- Mass Flow Controller (MFC) & Mass Flow Meters Test
  Basic functionality tested but not compared with independent instrumentation --> OK
- Temperature Test
  Basic functionality tested --> OK
- Purge Function Test
  Basic functionality tested --> OK

3. **HNEI Specification Tests (using an external LabVIEW™ program via CAN)**

The aim of this specification test is to check the transient performance of the tester as specified in the RFQ (**Use RFQ sent to FuelCon as reference for accuracy**).

The LabVIEW™ test program shall run similar scripts as previously run with FuelWorks (FuelCon software). However, some additional properties will be monitored with an external DAQ system.

I. CAN network communication test

- To check the communication between the laptop with LabVIEW™/CAN Card and the FuelCon tester CAN interface.
  Successful after 2 hours experimental work since the parameters were not 100% clear. Stable communication.

II. LabVIEW™ scripts tests

- Electronic Load Response Time Test
  (<**1 msec** from 10% to 90% load and <**1 msec** from 90% to 10% load)
  A current transducer shall additionally monitor the current with high sample rate.

Not executed in Germany. Basic functionality of electronic load was OK.

- Mass Flow Controller (MFC) & Mass Flow Meters Test
  (<**1 sec** from 10% to 90% of max. flow at 2 bar(a) and constant RH= 90% and <**1 sec** from 90% to 10% of max. flow at 2 bar(a) and constant RH= 90%)

Executed and close to target but slightly off.

- Pressure Swing Test
  (<**1 sec** from 1.5 bar(a) to 2.5 bar(a) at constant RH=90% & constant gas flow (1.8 slpm anode & 9 slpm cathode) and <**1 sec** from 2.5 bar(a) to 1.5 bar(a) at constant RH=90% & gas flow)
  A pressure transducer shall additionally monitor the pressure on the air side with high sample rate.

Executed but off Target

- Humidification Test
  (<**5 sec** from 10% to 90% RH at 2 bar(a) and constant gas flow (1.8 slpm anode & 9 slpm cathode) and <**5 sec** from 90% to 10% RH at 2 bar(a) and constant gas flow)

In principle executed but no reference / benchmark available . Dynamics off target.

- AC Impedance Measurement Test
  To test the capability of the AC impedance measurement system, a frequency response spectrum of the HNEI fuel cell should be measured at discrete frequencies (5 points/decade) between 1Hz and 10 kHz (inclusive)
  In principle executed but proper wiring was not possible without cell modification --> FAT result : OK

- External DAQ

Cell voltage, current and cathode air pressure will constantly be monitored via an external DAQ system with high sample rate

OK – most of the time the monitoring of the external values was problem fee. At other times the monitoring failed because of timing problems and the very quick and basic setup.

III. Miscellaneous tests

- Matlab/LabVIEW™ Vehicle Simulation Test

Additional tests using the vehicle simulation in Matlab/LabVIEW™ interface may be considered on site according to requirements.

Performed but only with the FUDS cycle for the first 100 sec. Termination of the tester due to low cell voltage. All functionality could be in principle proven during the FAT. However due to the complexity of the system only a small fraction of possible states (tester and simulation) had been tried.

4. Hardware in Loop (HiL) Real Time Simulation Test (Using DHFC vehicle Simulation developed in Matlab/Simulink)

The aim of this test is to check the real time HiL concept using DHFC vehicle simulation in real time via xPC target and CAN Network.

I. CAN network communication test

- To check the communication between the xPC Target system (Host and Target PCs)/CAN Card and the FuelCon tester CAN interface.
  Tested successful.

II. Real time HiL simulation test

- Establish communication via CAN interface according to the CAN Specification. Successful
- Check send and receive values of all data packages Successful
- Integrate the stack tester within the simulation (checkbox activate HiL) Successful
- Check default configuration for stability (Drive cycles FUDS and UDDS) Successful but termination of tester because of low cell voltage -->Y Fix in Honolulu: Operate with higher stoic ratios.
- If necessary try to stabilize the model (HiL configuration)
  Initial tests in Germany showed reasonable stability --> Stability improvements had been implemented in Honolulu (Driver parameters)
- Change some parameters on the fly for checking the impact of parameter

changes (vehicle mass, aerodynamic drag, tire friction).
Successful but sometime the model run into the woods (meaning it did not came back into normal mode) after entering a totally unreasonable parameter e.g. friction coefficient of 100 instead of 0.01.

Figure 1: HNEI PEMFC Flow Diagram

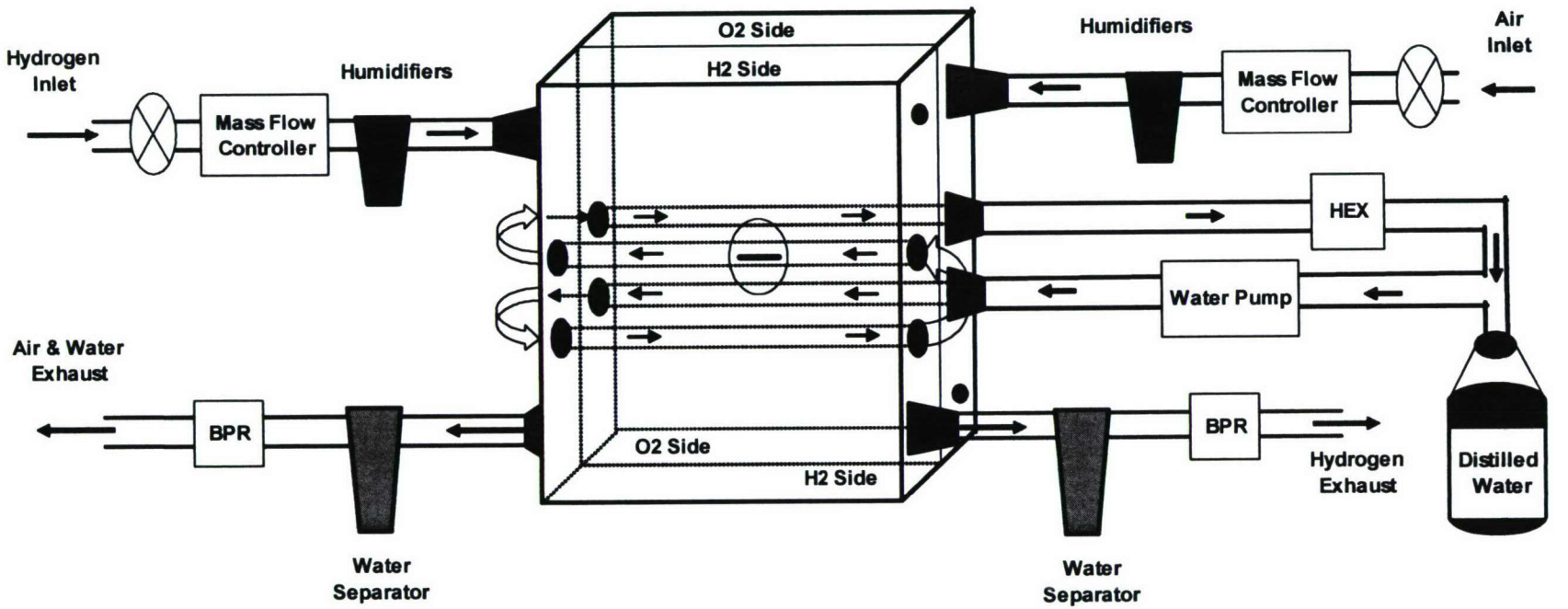

Figure 2: HNEI 100 cm^2 PEMFC Polarization Curves at Different Pressures

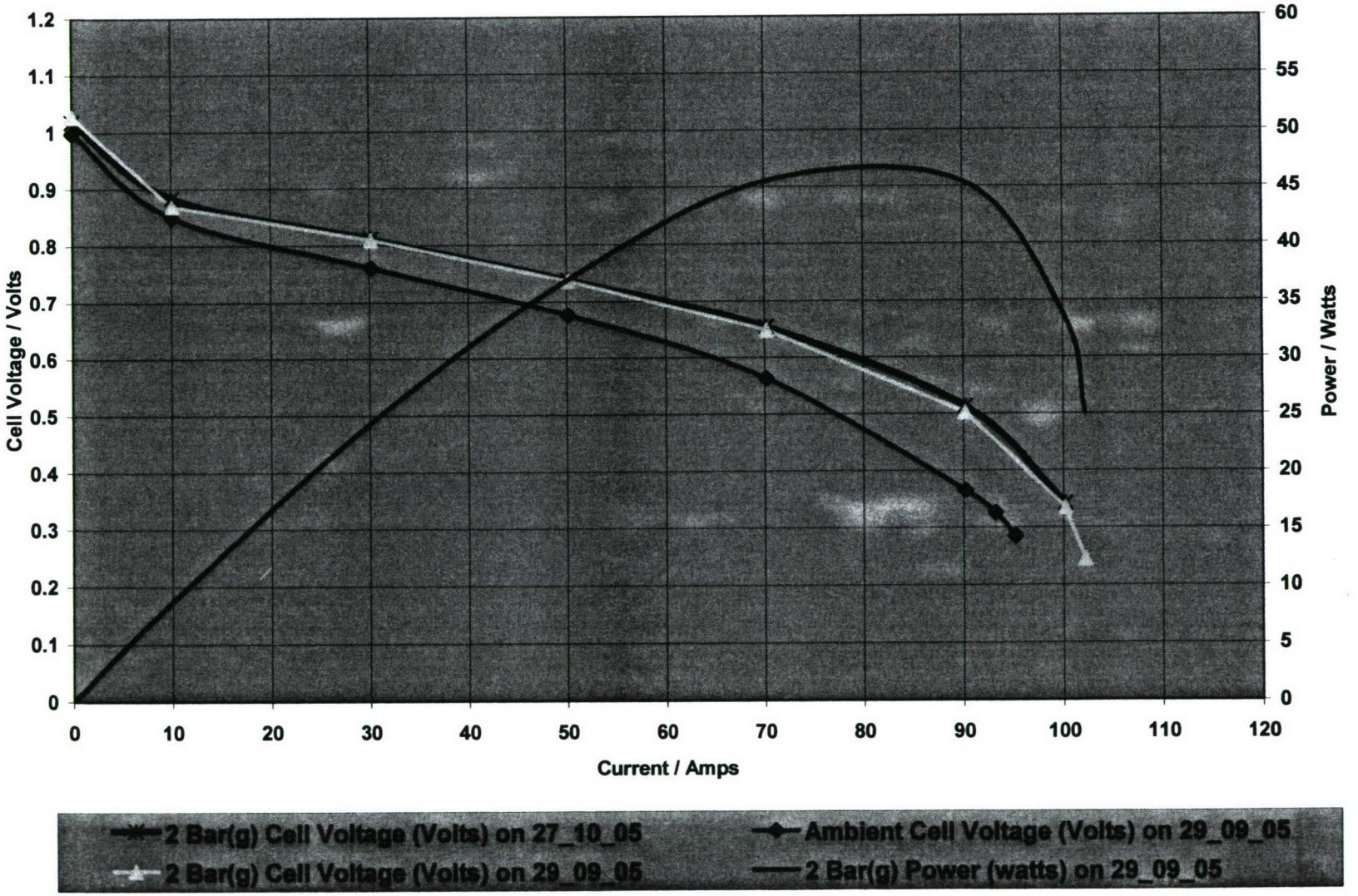

Figure 3: HNEI 100 cm^2 PEMFC Hydrogen Cross-Over Test Performance

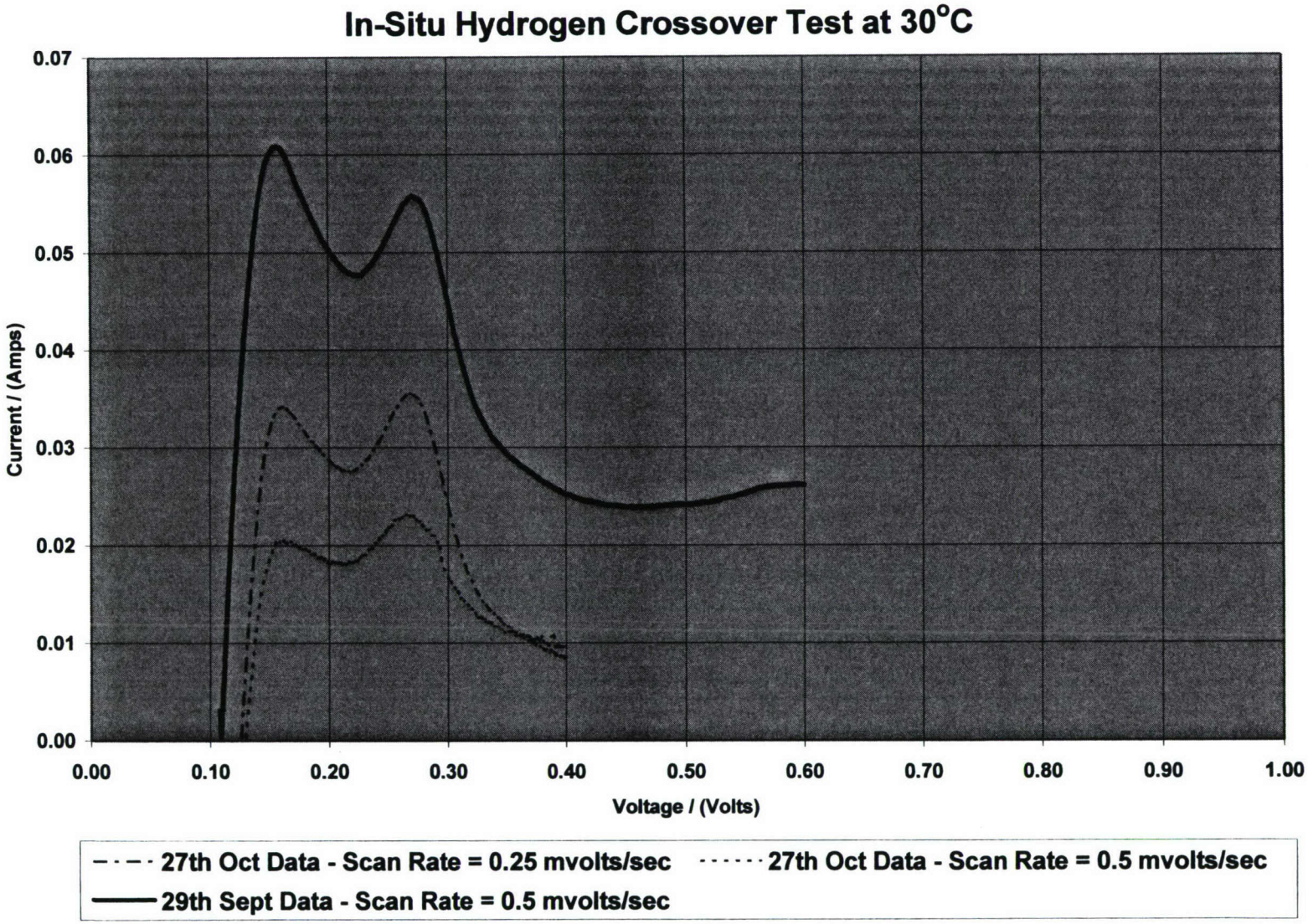

Table 1: List of items shipped to FuelCon for the checkout process

Item	Brand / Type
Measurement Notebook PC	IBM 380ED
PCMCIA Extension Module	IBM
2 Power Supplies	IBM
2nd Battery	IBM
Modular Signal Conditioning Unit NI SCC1234 With 20 SCC Modules	National Instruments
Data Cable	
Power Cable	
4 BNC Signal Cables	
BNC Connection Adapters 3 sets each: BNC Male - BNC Male BNC Female - BNC Female BNC Male - 4mm Banana Male BNC Female – 4mm Banana Female BNC – T	
Current Transducer Clamp	Fluke i1010
Pressure Transducer plus Swagelock connections	Keller PR21S, 2.5 BAR rel.
1 x 100 cm2 HNEI 100 cm^2 PEMFC	
2 x K-type thermocouples with male connectors	
4 x ¼' SS Swagelock connectors and 1 set of nuts and ferrule (10 pieces)	
1 x Extech Hydro-Thermometer clock instrument	

APPENDIX B

GEN 0
Fuel Cell Energy/Power System Simulation for an Unmanned Underwater Vehicle

Report
June 2006

Dr. Mebs Virji
Associate Specialist

1.0 INTRODUCTION

UUVs (Unmanned Underwater Vehicles) are mainly powered by either primary or secondary battery power systems. The concept of a Fuel Cell Energy/Power System (FCEPS) is currently being evaluated to increase specific energy and energy density of the FCEPS system for longer UUV mission durations. The use of an FCEPS as an electrical power source for UUVs is currently in the research and development phase, but has been demonstrated in a developmental Japanese UUV -- the "URASHIMA."

Research at the Hawaii Natural Energy Institute (HNEI) is focused on assessing available Polymer Electrolyte Membrane Fuel Cell (PEMFC) systems operating on hydrogen and oxygen for their energy (fuel and oxidant storage system) and on the development of a UUV simulation tool (UUVSim) to be used in the evaluation of the performance of an FCEPS UUV for dynamic mission profiles.

This report will introduce the GEN 0* FCEPS design concepts being evaluated for UUVs and will focus on the development of a GEN 0 PEM FCEPS model for use with UUVSim. The PEM FCEPS model is developed and simulated in the Matlab/Simulink environment either under a dynamic duty cycle (current or power demand) or under a UUV mission profile (vehicle speed, propeller speed, motor speed or torque, etc.) in conjunction with UUVSim. The choice of compressed Hydrogen and Oxygen (0.19 kWh/kg and 0.21 kWh/L) in tanks as a storage option for the initial design concept for PEM FCEPS was due to its similar specific energy and energy density in comparison with a rechargeable battery energy/power system (RBEPS - 0.17 kWh/kg and 0.19 kWh/L)[1]. However, future designs of the UUVSim (i.e., GEN 1, 2) may use different fuel and oxidant storage options for the PEM FCEPS which will be practical and have higher specific energy and energy density.

The report will also present results of simulation of the PEM FCEPS under a dynamic duty cycle of the "URASHIMA" UUV [2].

---

* GEN O is intended to designate a preliminary or 'strawman' level of design conception, not intended for actual deployment, but useful for initial considerations.

2.0 GEN 0 FCEP SYSTEM

Figure 1 shows the schematic representation of a GEN 0 PEM FCEP system as the power source for a UUV. Within Figure 1, MFC stands for mass flow controller.

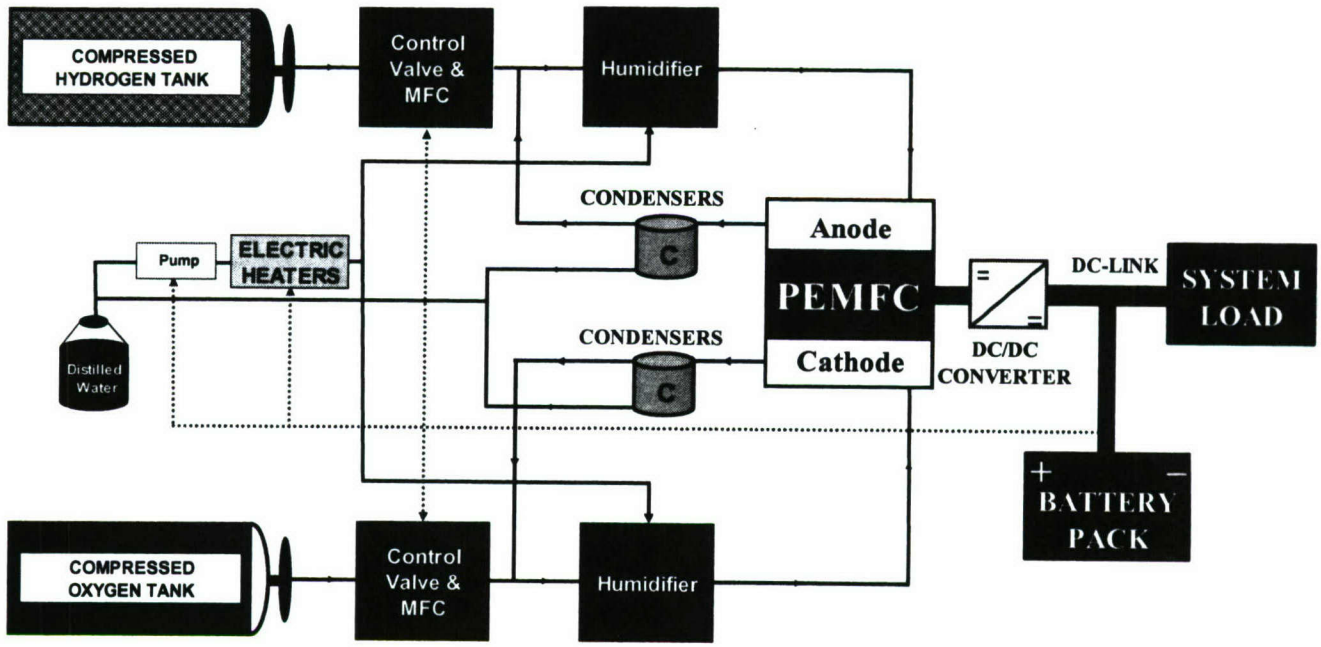

Figure 1: Schematic Representation of the GEN 0 FCEP System

The main components of the system include a PEMFC stack and its associated control electronics, electrical drive train, fuel and oxidant supply chain and water storage and supply for both humidification and cooling processes. The anode and cathode supply consists of respective compressed storage tanks, pressure regulator, mass flow controllers (MFCs) and humidifiers. The anode and cathode exhaust gases are re-circulated after the water is condensed out in the condensers. The exhaust water is also pumped back to the storage tank to be reused. The aim of the complete system design is to maintain buoyancy close to neutral, i.e., close to the density of the sea water, when installed into the UUV. The current GEN 0 system is not a hybrid system and hence does not have a battery pack. However, the next phase of the model development of GEN 0 may include a battery pack as shown in Figure 1.

The next section will describe the modeling and specification of individual components of the system. The model of each component is generic in nature and hence the user has the option of choosing different types of components with

varying specifications, i.e., the user can chose different capacities and types of storage tanks or types or sizes of fuel cell stacks with different operating PEMFC characteristics.

3.0 MODELING AND SIMULATION OF THE FCEPS

In this section, the models of the individual components of the PEM FCEP system and the data used in development of these models in the Matlab/Simulink environment are described.

3.1 FCEPS Simulation Tool

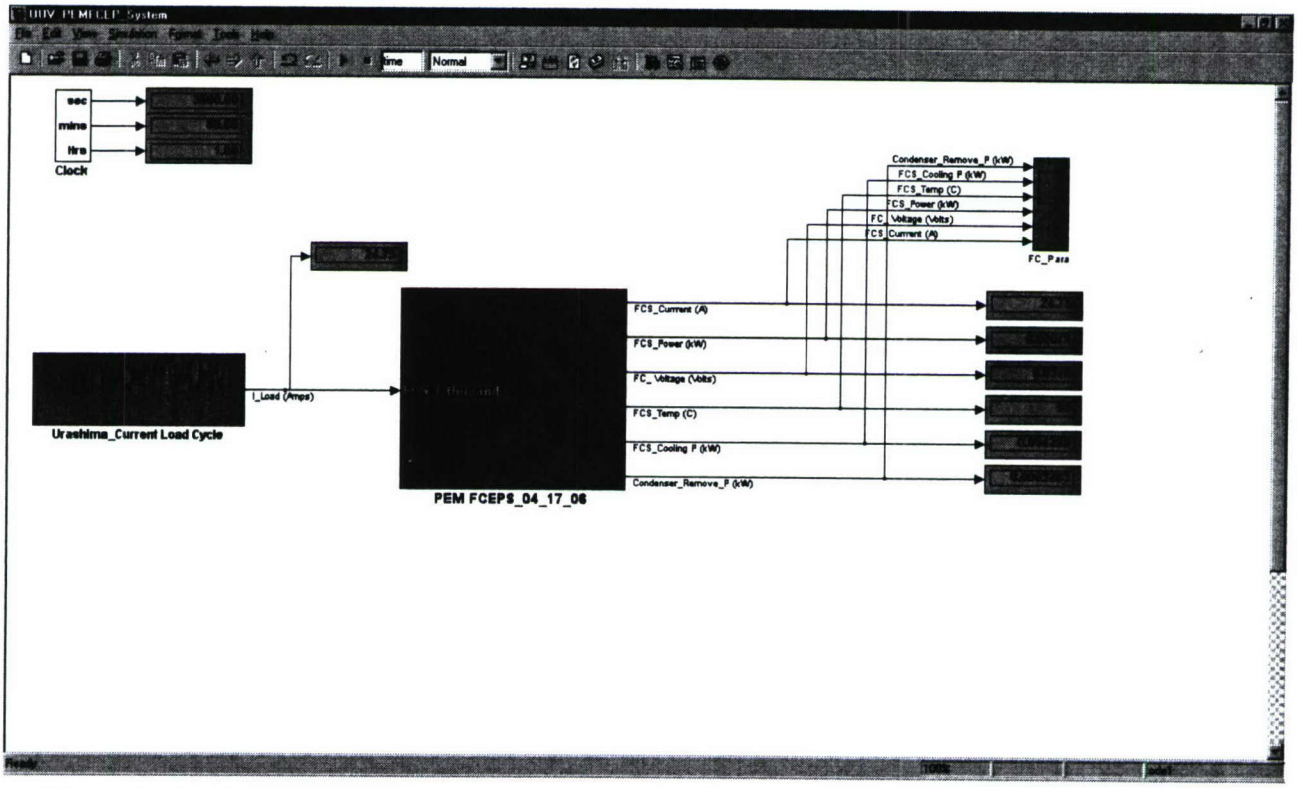

Figure 2: The PEM FCEP System simulation tool in the Matlab/Simulink Environment

Figure 2 shows the top level of the simulation tool for a PEM FCEPS in the Matlab and Simulink environment. The input to the PEM FCEPS simulation tool can be run with any duty cycle, but in this report the dynamic behavior of the PEM FCEPS is analyzed using a realistic "URASHIMA" UUV current load cycle[2].

3.2 FCEPS System

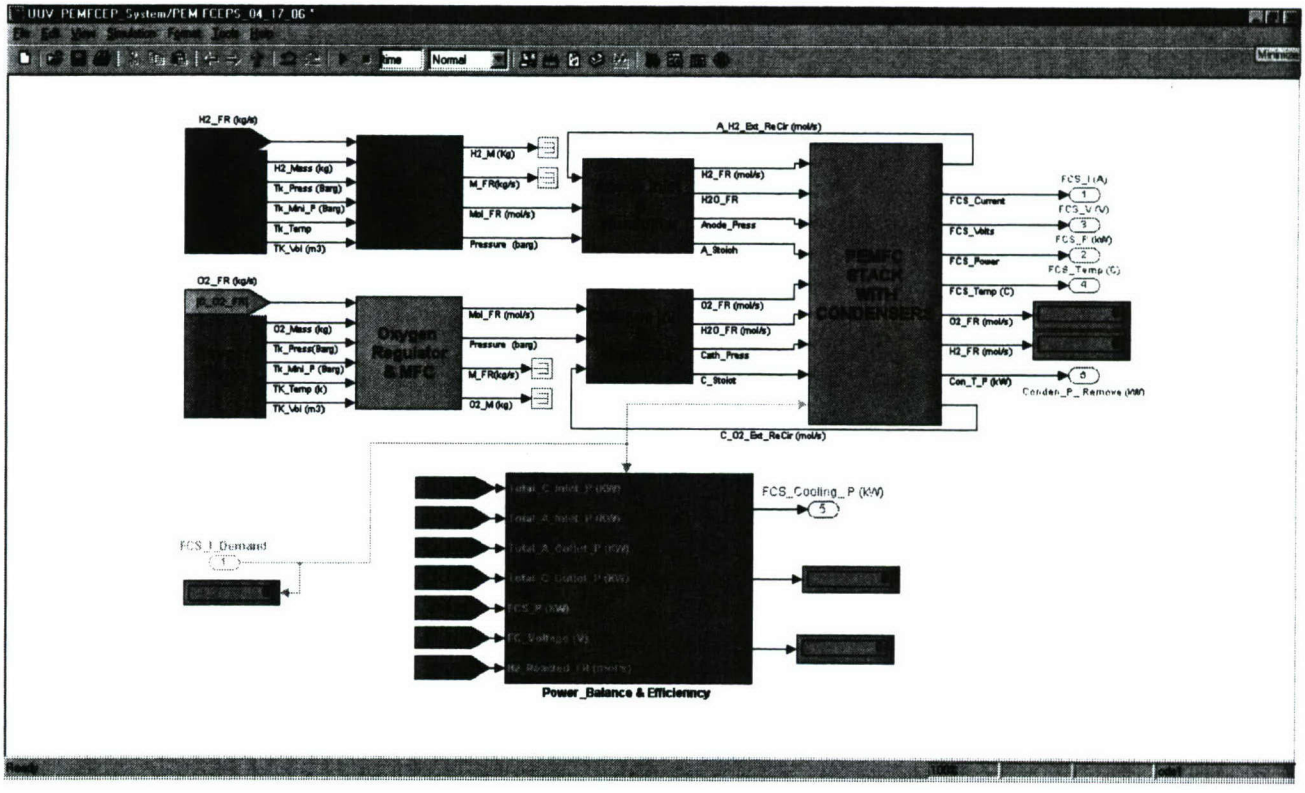

Figure 3: GEN 0 PEM FCEP System within the simulation tool

Figure 3 shows the representation of the GEN 0 PEM FCEP system as depicted in Figure 1 in the Matlab/Simulink environment. The GEN 0 PEM FCEP system in this environment consists of following blocks:

- *Hydrogen and Oxygen Tanks*
- *Pressure Regulator and MFC for Hydrogen and Oxygen*
- *Inlet & Humidifier for the Fuel Cell Anode and Cathode*
- *PEMFC Stack with Condensers*
- *Power Balance & Efficiency*

Each of these blocks has specific models related to that particular component and each of these blocks is masked to create a graphical user interface (GUI) to input the component's physical data and set point of the operating conditions. The *Power Balance & Efficiency block* is also included in the simulation tool to verify that PEMFC system calculations are correct, estimate the cooling power required by the PEMFC or stack, and indicate overall gross and net system efficiencies of the PEMFC or stack.

3.2.1 Hydrogen and Oxygen Tanks

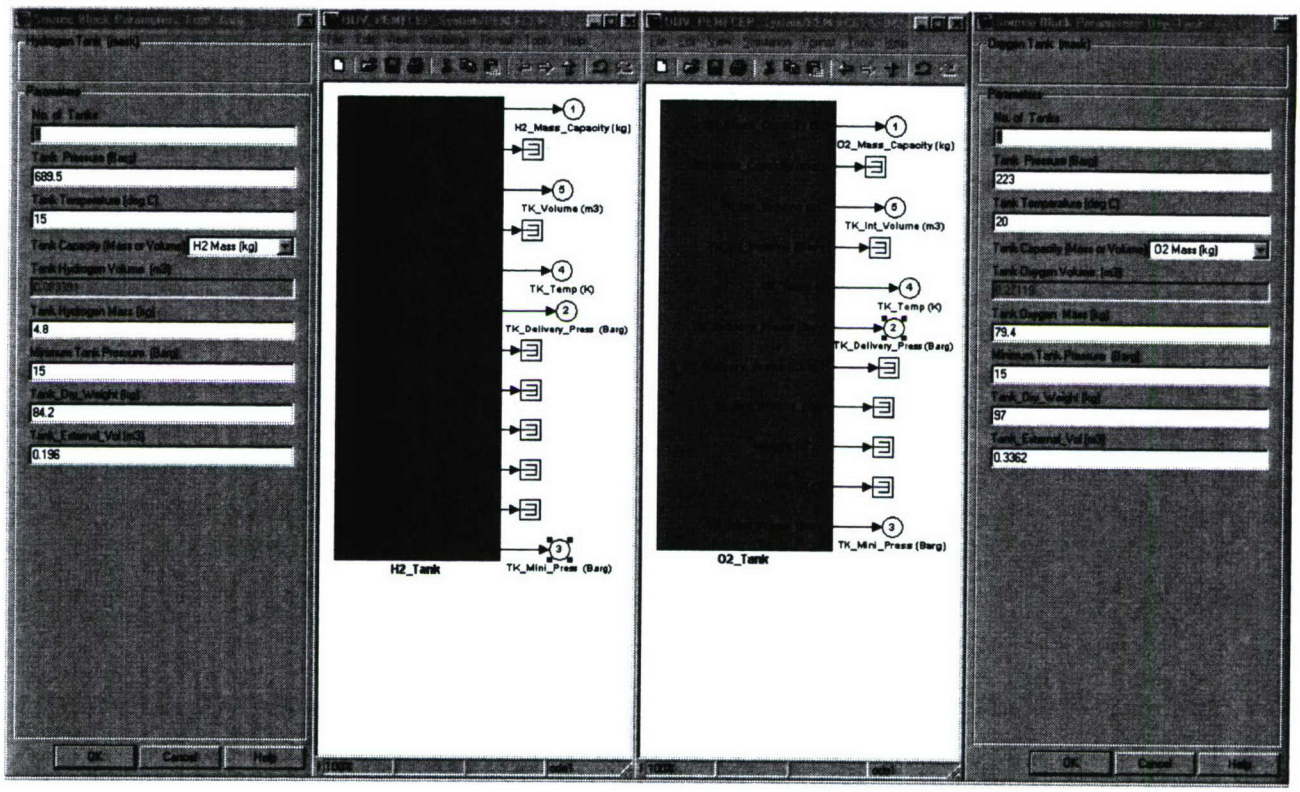

Figure 4: Hydrogen & Oxygen Tank GUI and block outputs

In the *Hydrogen and Oxygen Tank blocks* the user specifies particular hydrogen and oxygen tanks by inputting physical characteristic such as the pressure, temperature, external volume and weight (dry) for each tank and also selects the number of tanks to be used in the simulation. The user can either input the volume or the mass of the gas in the tank from manufacturing data and the masked GUI automatically calculates either the volume or mass of the gas in each tank depending on what information is provided. Each block uses the Beattie-Bridgeman equation rather than the Ideal gas law to calculate the mass or volume for a given pressure and temperature[1]. Figure 4 shows the GUI for the hydrogen and oxygen tanks.

3.2.2 Pressure Regulator and MFC for the Hydrogen and Oxygen

Figure 5 shows the masked GUI for the H_2 and O_2 Regulator and MFC blocks. From this GUI the user can specify the gas delivery pressure for the anode and cathode of the PEMFC and switch on/off the supply. The block also checks the capacity and pressure of gas in the tanks, and if the tanks are empty or have reached the minimum delivery pressure, the simulation is automatically stopped.

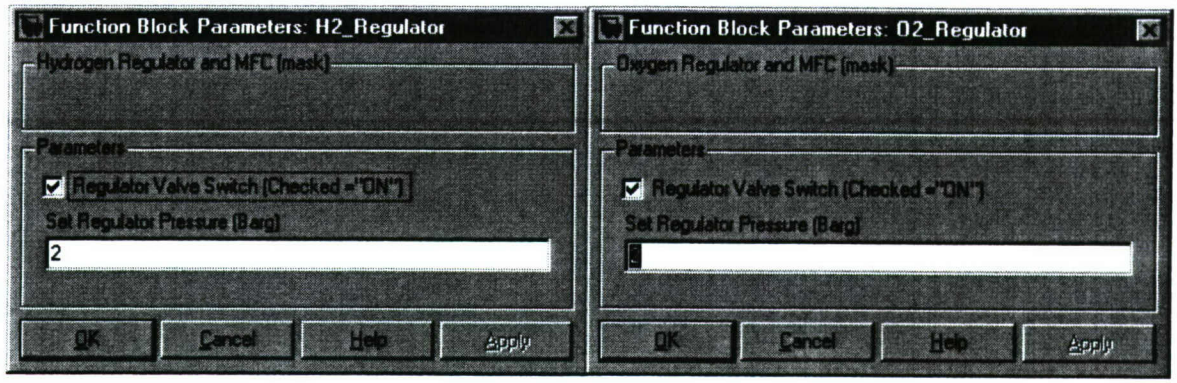

Figure 5: H_2 & O_2 Regulator and MFC GUI

3.2.3 Inlet & Humidifier for the Fuel Cell Anode and Cathode

The Anode and Cathode inlet operating conditions are set via the GUI shown in Figure 6. The GUI for these blocks allows the user to input the set point of the anode and cathode operating temperature, stoichiometry and relative humidity. The GUI also has a check box which allows an option of running either or both of the anode and cathode inlets dry. The relative humidity model uses inlet temperature and pressure, gas flow and relative humidity set point values to calculate the amount of water to be inject into the humidifier to achieve the desired relative humidities of the anode and cathode inlet flows. At present there is no thermal model to determine the temperature of the gas flow, but a transfer function with a time constant of one minute is used to account for the thermal mass and capacity of the flow and inlet pipe.

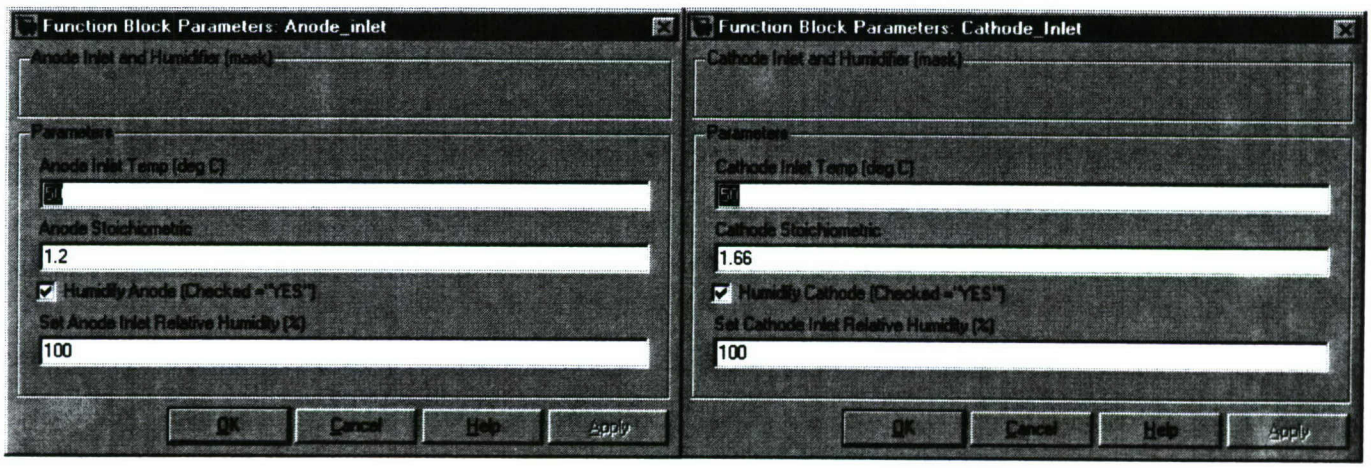

Figure 6: Anode and Cathode Inlet GUI

3.2.4 PEMFC Stack with Condensers

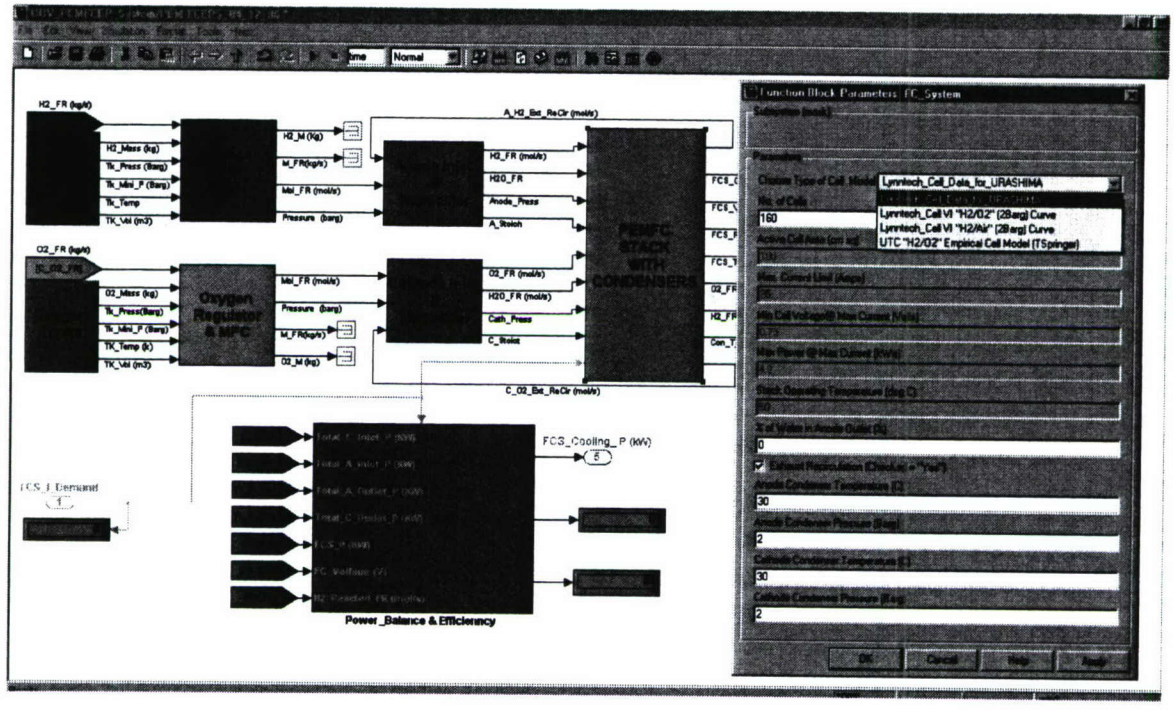

Figure 7 : PEMFC Stack & Condenser GUI

Figure 7 shows the masked GUI of the *PEMFC Stack with Condensers* block. Through this GUI the operating conditions of the PEMFC and anode and cathode condensers are set, and also the type of cell model or operational characteristic (i.e., VI curve) of a particular PEMFC is chosen. When a particular fuel cell characteristic is chosen the model automatically loads the physical characteristic of the cell or stack and also calculates the maximum power of the cell or stack at its maximum allowable current and corresponding minimum cell voltage, hence limiting the operation of the cell to this power. At present the fuel cell model has the choice of a (1) 100 cm^2 Lynntech PEMFC with VI curves at different operating pressures and media (H_2/O_2 & H_2/Air), or (2) a 400 cm^2 UTC PEMFC empirical cell model. Figures 8 and 9 show how fuel cell models are implemented in the Matlab/Simulink simulation tool. The PEMFC model also has an option of recalculating the anode and cathode exhausts which can be used if it's a H_2/O_2 PEMFC system using high pressure tanks to store the gases. This PEMFC system model also includes condensers to remove most of the water from the exhaust gases. The operating conditions of the anode and cathode condensers can also be inputted via the masked GUI (Figure 7). The condenser model uses these values to calculate the amount of water which is condensed in these condensers. The cooling cycle of the condenser's heat exchanger is not included the model.

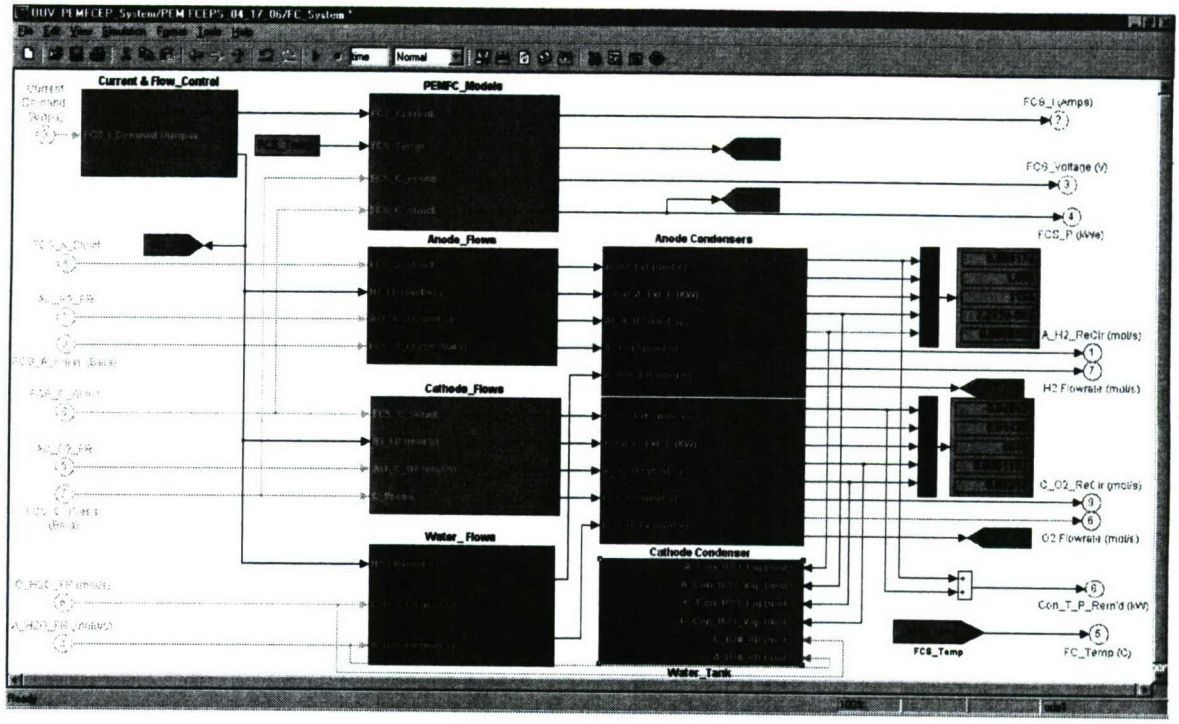

Figure 8: PEMFC System & Condensers model implementation in the simulation tool

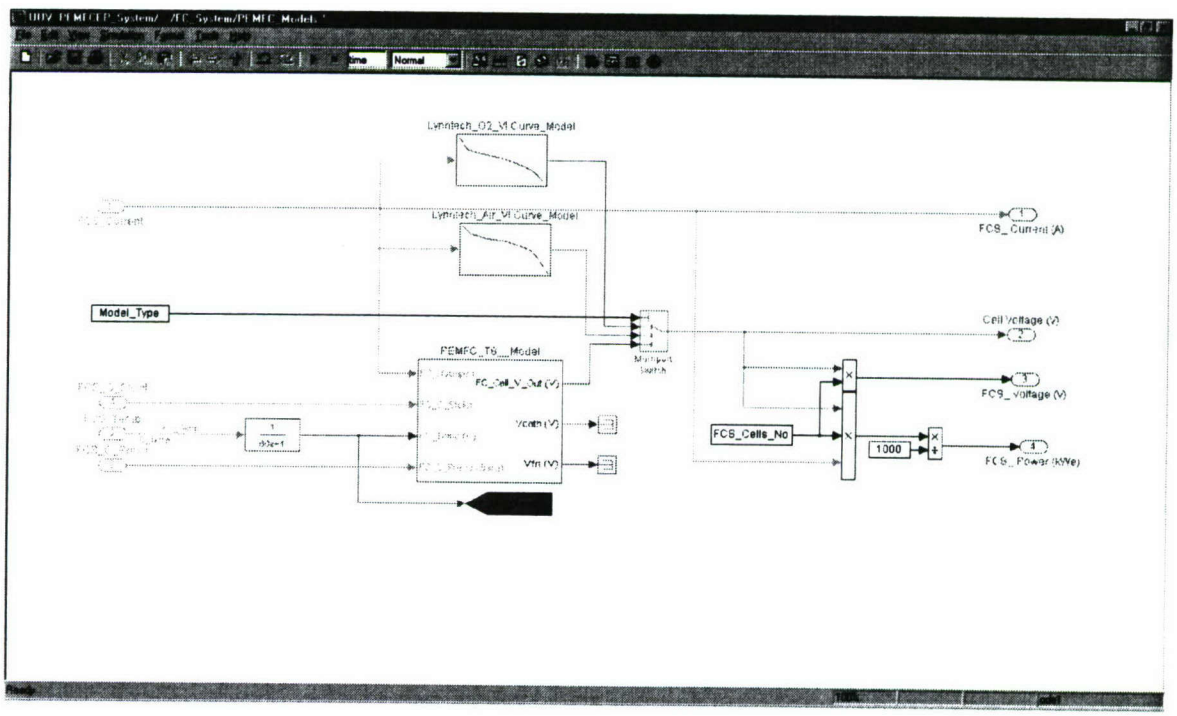

Figure 9: Implementation of PEMFC models in the simulation tool

4.0 GEN 0 FCEP SYSTEM SIMULATION SETUP

To evaluate the performance of the GEN 0 FCEP system simulation, the simulation was setup to operate similar to the "URASHIMA" PEMFC system[2]. Figure 10 shows the schematic and characteristics of the "URASHIMA" PEMFC system.

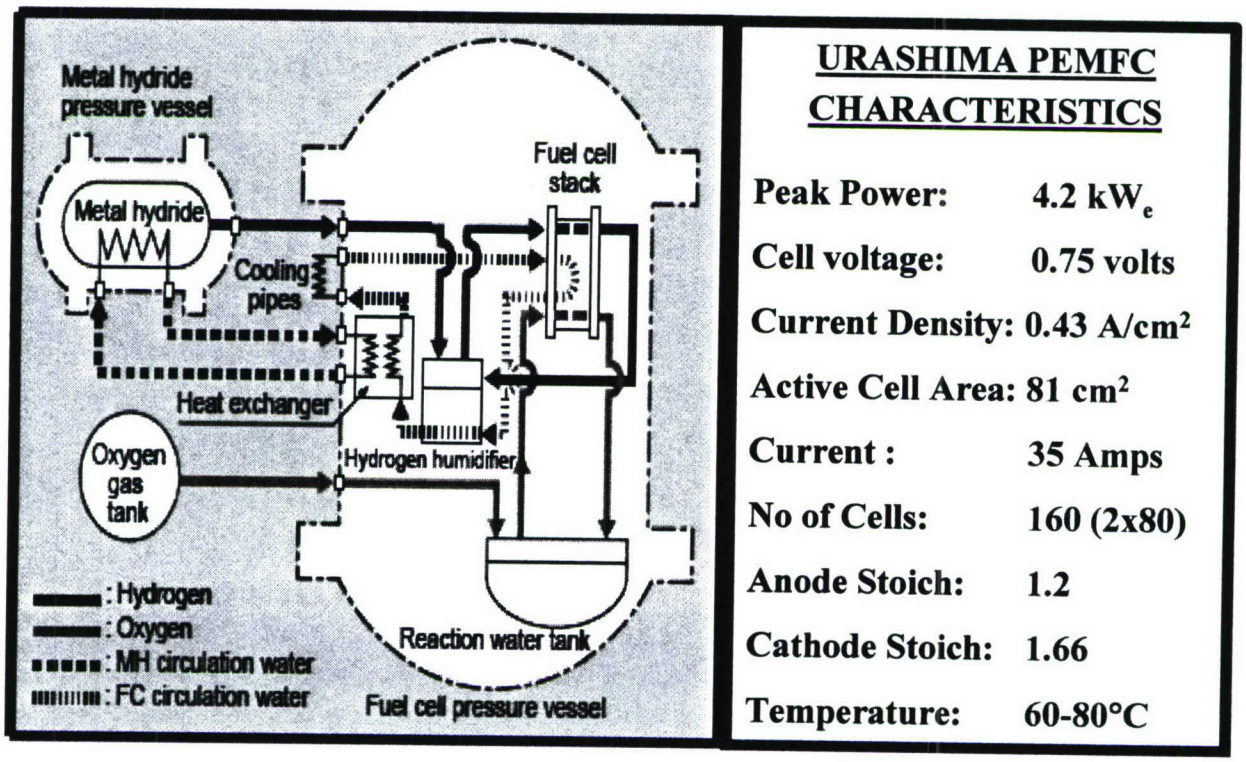

Figure 10 : Schematic and characteristics of the "URASHIMA" PEMFCS

Compared to the "URASHIMA" PEMFC system, the GEN 0 FCEP system uses hydrogen tanks instead of metal hydride pressure vessels to store hydrogen and condensers to collect the water. The other major difference is the use of a 100 cm^2 Lynntech PEM fuel. However, this fuel cell is sized up to a stack to produce a maximum power of 4.2 kW_e (2 × 80 cells) at a temperature of 60°C and at an average cell voltage of 0.75 volts, corresponding to a thermal efficiency of 60% (LHV of H_2). Figure 11 shows the GUI of the GEN 0 PEM FCEPS setup for the "URASHIMA" PEMFC system. The main components of the GEN 0 PEM FCEPS and their operating conditions are summarized as following:

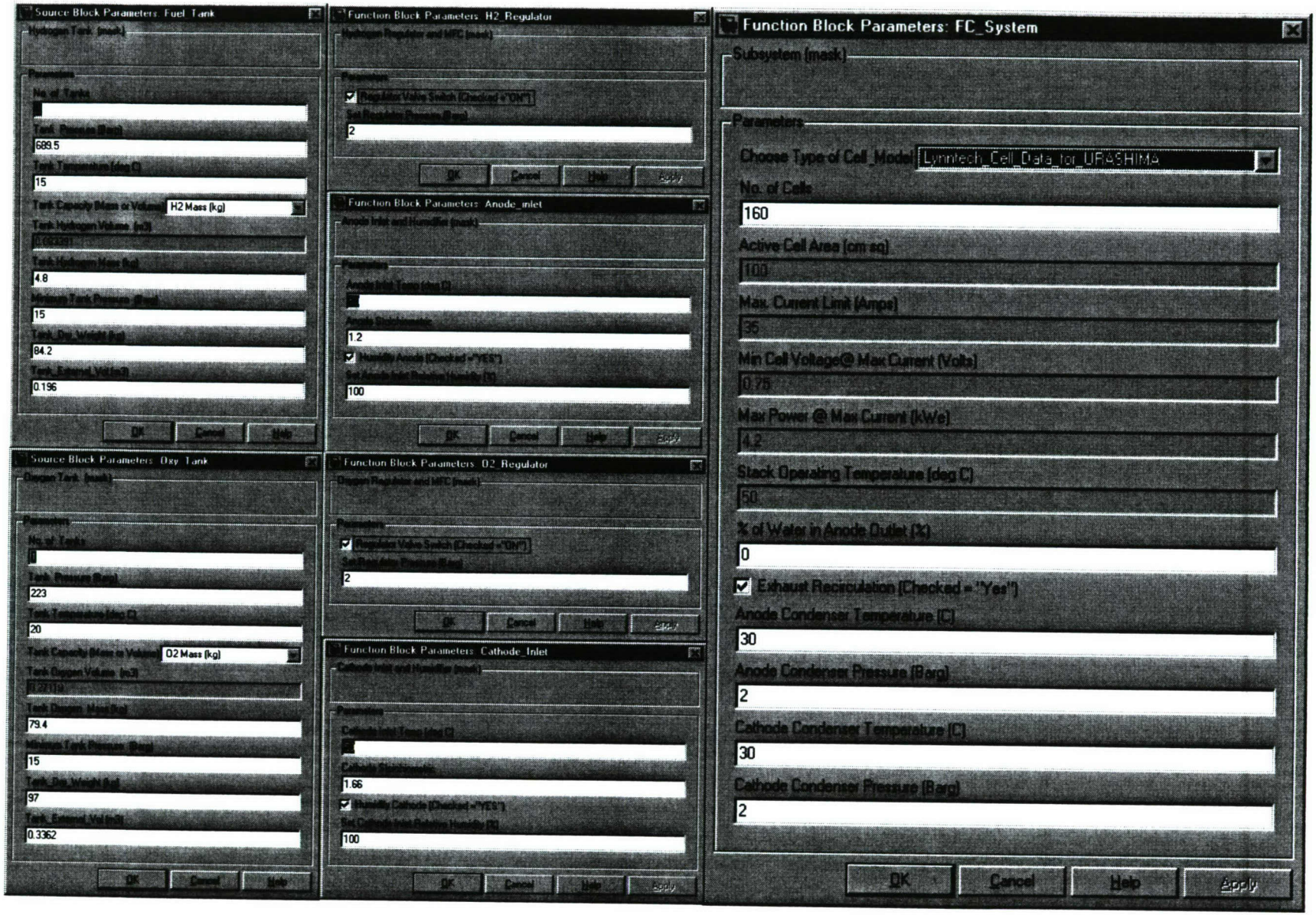

Figure 11: GEN 0 PEM FCEPS Simulation Setup

Hydrogen Tank:	Name	= Lincoln Composites TuffShell 118L
	Tank Pressure	= 10,000 psi =68.95 MPa =689.5 bars
	H_2 Volume	= 118.40 liters = 0.1184 m^3
	H_2 Mass	= 4.8 kg (6.8 kg by the ideal gas law)
	Tank Dry Mass	= 84.20 kg
	Tank Ext. Vol.	= 195.67 liters = 0.19567 m^3
	Tank Temp.	=15°C
Oxygen Tank:	Name	= Dynetek V260TDG233GM
	Tank Pressure	= 3240 psi = 22.339 MPa =223.39 bars
	O_2 Volume	= 258 liters = 0.258 m^3
	O_2 Mass	= 79.4 kg (75.67 kg by the ideal gas law)
	Tank Dry Mass	= 97 kg
	Tank Ext. Vol.	= 336.2 liters = 0.3362 m^3
	Tank Temp.	= 20°C
Anode:	Pressure	= 2 Bar(g) = 3 Bar(a)
	Temperature	= 50°C
	Stoichiometry	= 1.2
	Relative Humidity	= 100%
Cathode:	Pressure	= 2 Bar(g) = 3 Bar(a)
	Temperature	= 50°C
	Stoichiometry	= 1.66
	Relative Humidity	= 100%
PEMFC Stack:	Name	= Lynntech PEMFC
	Active Area	= 100 cm^2
	No. of Cells	= 160 = 2 × 80 cell stack
	Max. Current	= 35 amps
	Cell Voltage	= 0.75 volts/cell @ Max. Current
	Max. Power	= 4.2 KW_e
Condensers:	Name	= Anode & Cathode
	Pressure	= 2 Bar(g) = 3 Bar(a)
	Temperature	= 30°C

The performance of the GEN 0 PEM FCEPS simulation setup for the "URASHIMA" PEMFC system was determined by using a realistic dynamic duty cycle of "URASHIMA" UUV[2]. This duty cycle (shown in Figure 12) is a five-hour current load cycle which was used to study the behavior of the "URASHIMA" fuel cell system and represents an average load consumption of the UUV during the 43-hour long-distance sea trial.

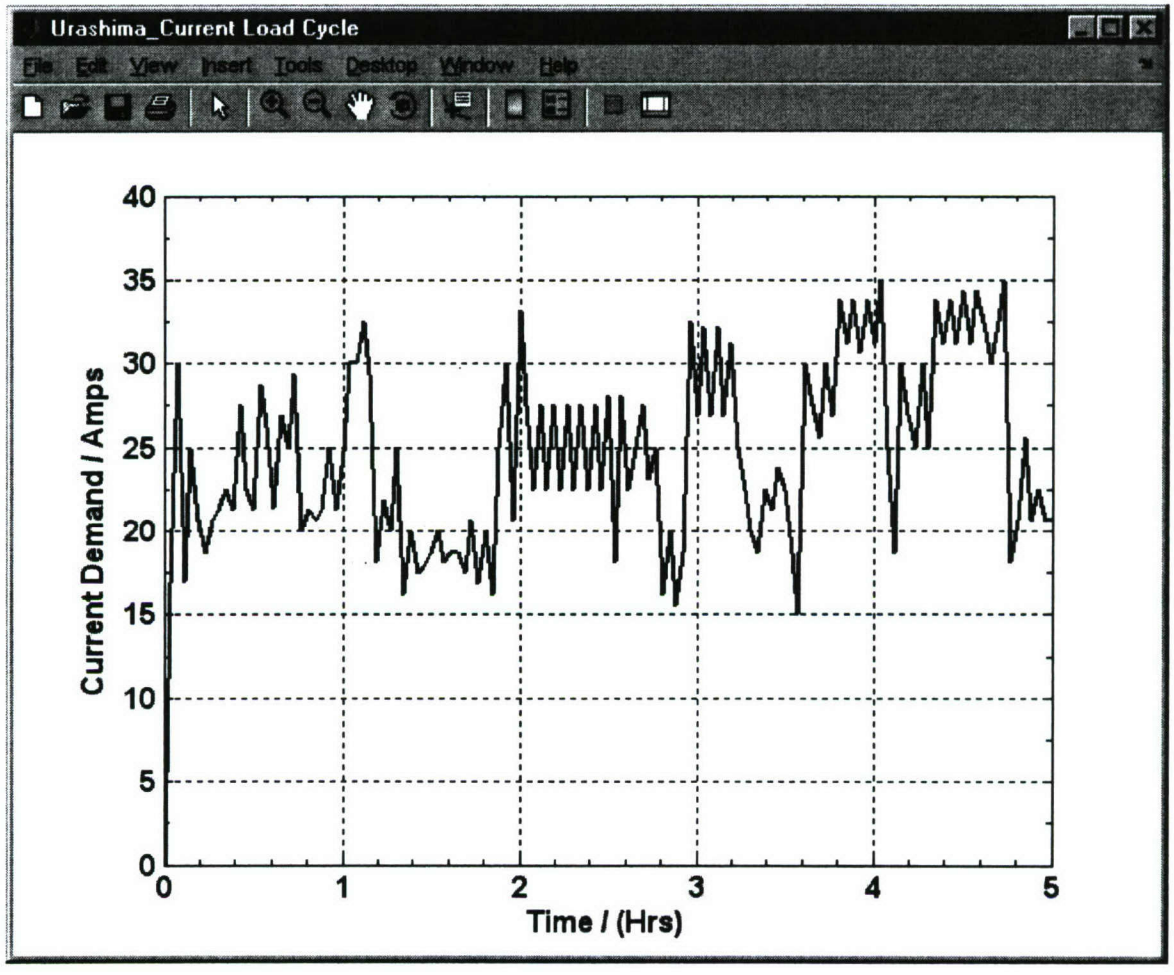

Figure 12: Dynamic Duty Cycle of "URASHIMA" UUV used to run the simulation (see Figure 2 for implementation of the duty cycle in the simulation)

5.0 RESULTS

The results of the simulation of the GEN 0 PEM FCEPS under a dynamic duty cycle of the "URASHIMA" UUV are presented in Figures 13-18. Each figure shows data for the first minute (60 seconds) of the simulation time and for the full five-hour (18,000 seconds) duty cycle. The figures show the performance of either the main system component or/and the gas stream properties such as flowrate, temperature, relative humidity, time constants etc.

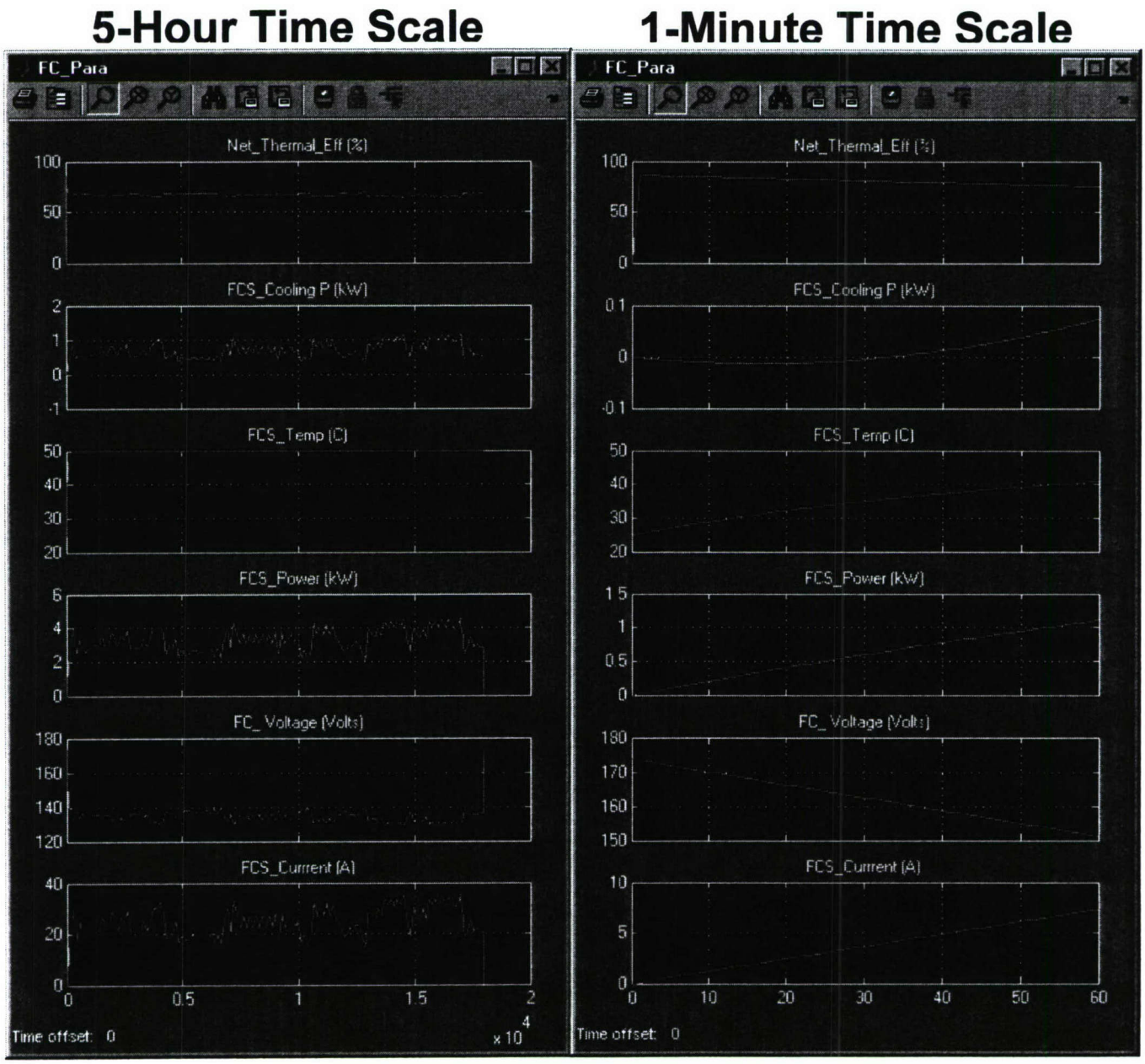

Figure 13: PEMFC performance under a dynamic UUV duty cycle

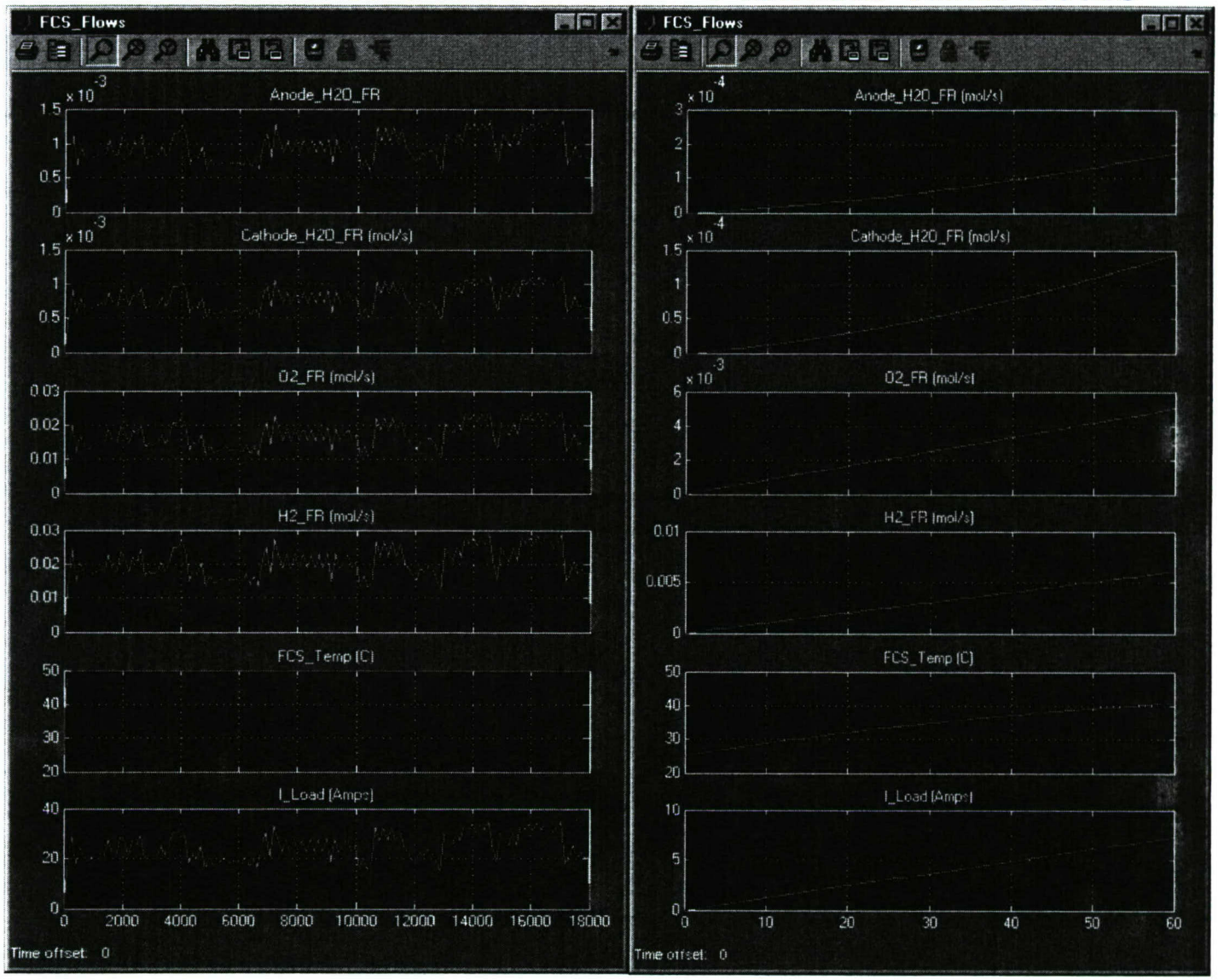

Figure 14: Anode and Cathode flowrates under a dynamic UUV duty cycle

Figure 15: Anode and Cathode relative humidities under a dynamic UUV duty cycle

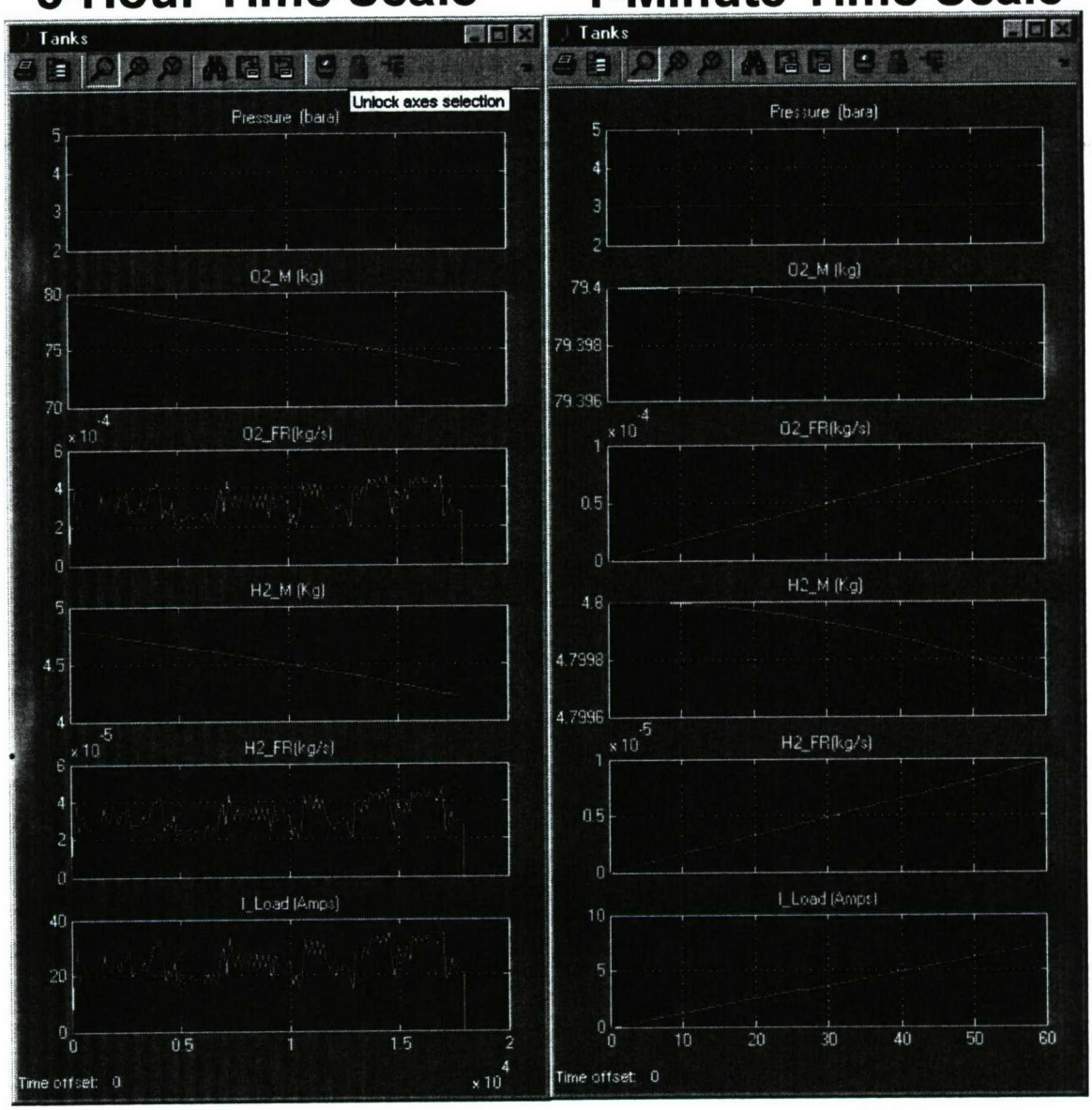

Figure 16: H_2 and O_2 tanks mass and flowrates under a dynamic UUV duty cycle

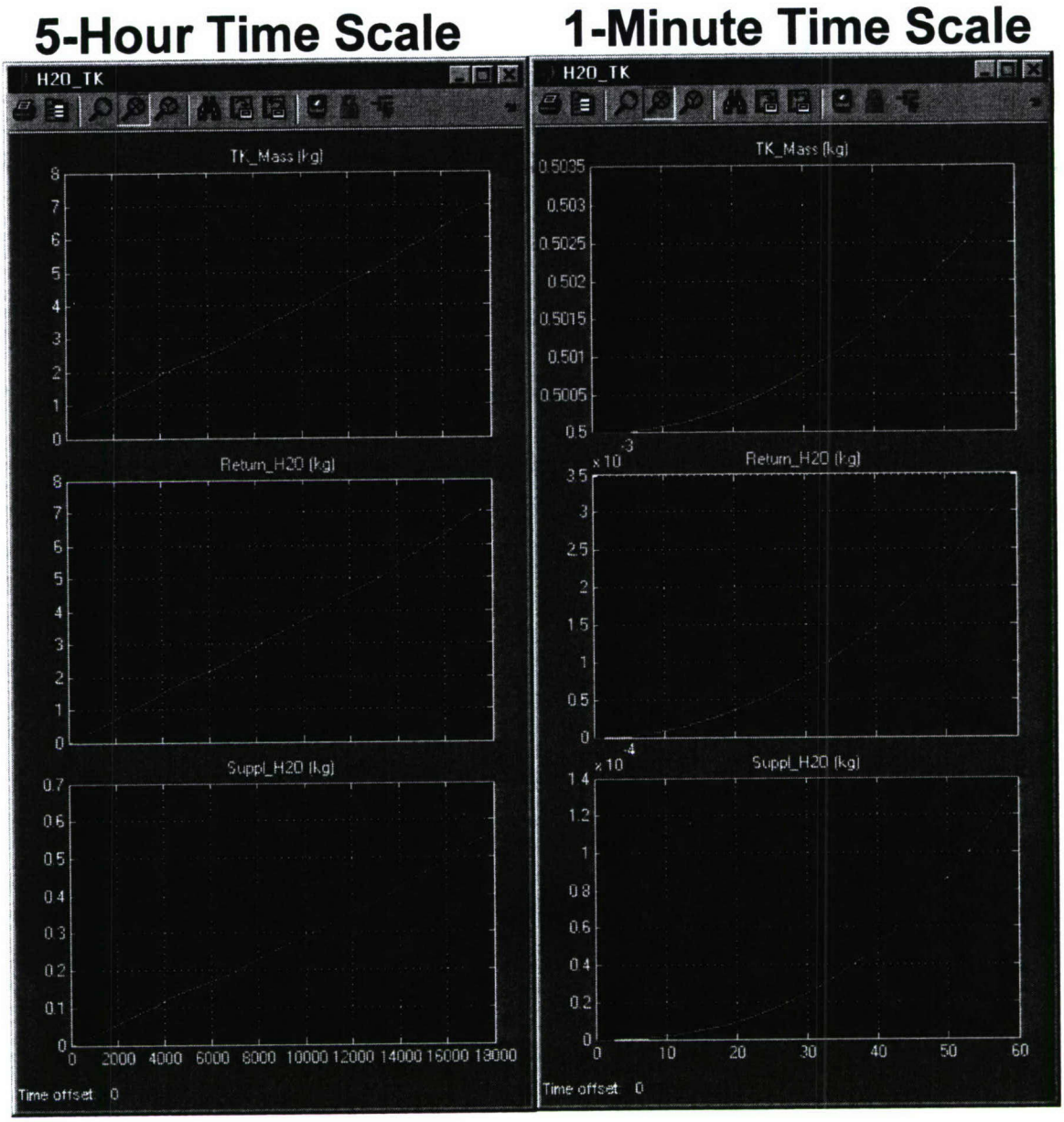

Figure 17: Water tank mass and flowrates under a dynamic UUV duty cycle

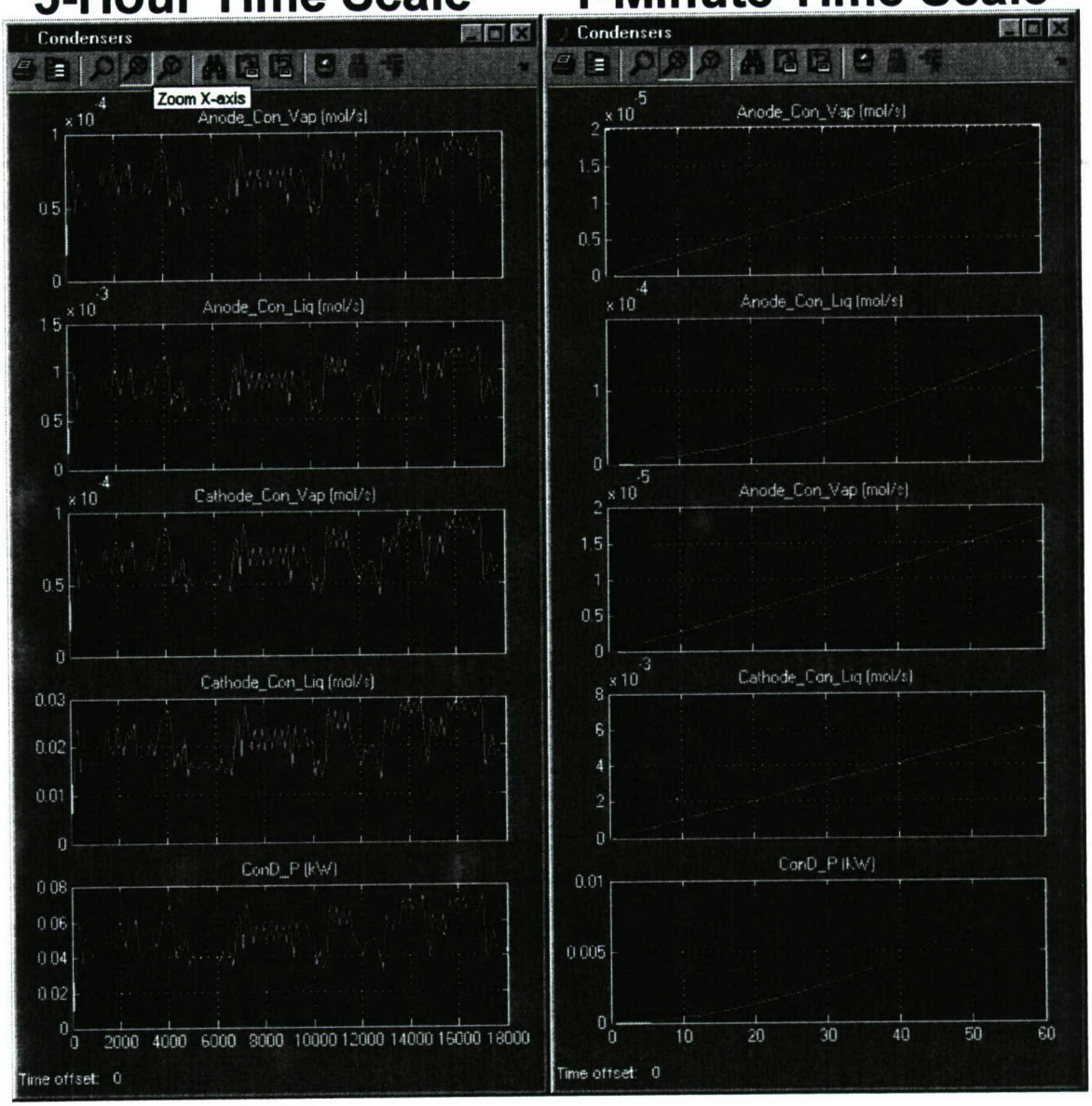

Figure 18: Condenser performance under a dynamic UUV duty cycle

6.0 CONCLUSIONS

The design concept of GEN 0 PEM FCEPS is introduced and the development of the GEN 0 PEM FCEPS model for use with UUVSim in the Matlab/Simulink environment is addressed. The GEN 0 PEM FCEP system simulation is setup to operate similar to the "URASHIMA" PEMFC system and the performance results of this simulation setup under a realistic dynamic duty cycle of "URASHIMA" UUV are presented.

The results from the simulation (Fig 13-18) of the FCEPS under a realistic dynamic duty cycle verify that the models in the GEN 0 PEM FCEPS simulation are predicting the transient and steady state performance of the individual components and the system overall accurately.

7.0 REFERENCES

1. **Davies, K. L. et al. UUV FCEPS Technology Assessment and Design Process, http://www.hnei.hawaii.edu/UUV_FCEPS_ReportRev3.pdf , January 2006.**

2. **Maeda, T. et al. Development of Fuel Cell AUV "URASHIMA" Mitsubishi Heavy Industries, Ltd. Technical Review, Vol. 41 No.6, Dec 2004.**

APPENDIX C

UUV FCEPS
Technology Assessment
and
Design Process

Report
October 2006

"UUV FCEPS Technology Assessment and Design Process"

Kevin L. Davies[1] and Robert M. Moore
Hawaii Natural Energy Institute (HNEI), School of Ocean and Earth Science and Technology (SOEST)
University of Hawaii at Manoa

Executive Summary

The primary goal of this technology assessment is to provide an initial evaluation and technology screening for the application of a Fuel Cell Energy/Power System (FCEPS) to the propulsion of an Unmanned Underwater Vehicle (UUV). The impetus for this technology assessment is the expectation that an FCEPS has the potential to significantly increase the energy storage in an UUV, when compared to other refuelable Air-Independent Propulsion (AIP) energy/power systems, e.g., such as those based on rechargeable ("secondary") batteries. If increased energy availability is feasible, the FCEPS will enable greater mission duration (range) and/or higher performance capabilities within a given mission. A secondary goal of this report is to propose a design process for an FCEPS within the UUV application.

This executive summary is an overview of the findings in the attached main report body ("UUV FCEPS Technology Assessment and Design Process") which provides a complete technology assessment and design process report on available UUV FCEPS technology, design methodology, and concepts. The report is limited to the Polymer Electrolyte Membrane (PEM) Fuel Cell (FC) operating on hydrogen and oxygen.

The Fuel Cell System (FCS) within the FCEPS is the systematic combination of the fuel cell stack and its supporting valves, manifolds, and other components, hybrid/auxiliary battery or other energy storage, electric conversion devices (DC/DC converter, inverter, etc.), and, optionally, a fuel processing system (reformer). The Storage System (SS) is defined as the onboard stored fuel, oxidant, and product water. The overall FCEPS is the combination of the FCS, SS, ballast or floats, and overhead structure, insulation, etc. – as required for the UUV application and mission profiles.

In this report, the FCEPS is compared to two benchmark metrics for refuelable AIP energy/power systems, as applied to UUV propulsion. These benchmark metrics are:

1. A "Threshold" energy density value
2. An energy density value for a Rechargeable Battery Energy/Power System (RBEPS) based on the use of Li-Ion (or Li-Poly) rechargeable batteries.

A 60" LD MRUUV is used as the nominal application for the FCEPS technology assessment provided in this report. The U.S. Navy has set Threshold and Objective energy storage requirements for the 60" LD MRUUV. The Threshold requirement is used as the primary benchmark for this assessment. To provide additional context for the assessment, the energy density value for a RBEPS is used as a secondary benchmark for this assessment. This RBEPS metric is based on the use of Li-Ion (or Li-Poly)

---

[1] kdavies@hawaii.edu

rechargeable batteries in a RBEPS designed for the 60" UUV application – i.e., with the density (buoyancy) set by the U.S. Navy for the 60" LD MRUUV.

The FCEPS design concept presented in this report uses a holistic approach in combining alternative hydrogen and oxygen storage, and fuel cell system, options to provide the highest specific energy (SE) and energy density (ED) within the UUV constraints – including the FCEPS mass, volume, and required power. Using this method, some surprising combinations appear as the theoretical "winners" – when used in an FCEPS with the BZM 34 (Siemens) fuel cell system. Of course, a complete prototype design and application simulation would have to be carried out using each of the alternative fuel cell system and H2-O2 storage combinations to determine the SE and ED values for each FCEPS design concept with a high degree of precision. However, the screening methodology used in this assessment is quantitatively useful in reducing the number of different storage and fuel cell system combinations which will eventually need to be evaluated in this more resource intensive fashion.

Keeping in mind this disclaimer regarding precision, the technology assessment presented in the main body of this report leads to the conclusion that a combination of the 60% lithium hydride slurry system (Safe Hydrogen, LLC) with CAN 33 chlorate candles (Molecular Products) provides the best energy storage option – with SE and ED for the 60" UUV application at 0.44 kWh/kg and 0.48 kWh/L, respectively. In contrast, an FCEPS using a very conservative H2-O2 storage combination of compressed hydrogen and compressed oxygen provides less than half of these values – with SE and ED at 0.19 kWh/kg and 0.21 kWh/L, respectively. These bounding values of SE and ED for an FCEPS provide a range of options that can be compared with the Threshold and RBEPS values of SE and ED at 0.29 kWh/kg and 0.25 kWh/L, and 0.17 kWh/kg and 0.19 kWh/L, respectively, in order to provide perspective for the FCEPS options.

Overall, the FCEPS SE and ED range noted above (for the best and the very conservative H2-O2 storage options, with the BZW fuel cell system) compares extremely favorably with the Navy Threshold and the RBEPS benchmark metrics for energy storage. Based on these SE and ED values for the FCEPS, this initial technology assessment supports the expectation that an FCEPS has the potential to significantly increase the energy storage in a UUV, when compared to other refuelable Air-Independent Propulsion (AIP) energy/power systems, and, in addition, indicates a high probability that an FCEPS can achieve the Threshold value for energy storage of the 60" LD MRUUV.

However, to balance this very positive conclusion, it is also clear that there is no reasonable near-term expectation of achieving the Objective energy storage value set by the Navy (SE and ED at 3.18 kWh/kg 2.20 kWh/L) using any of the FCEPS technologies assessed in this report. Achieving the Objective energy storage metric will require a breakthrough in either H2-O2 storage technology or in enabling an FCS which can convert high energy liquid fuels within the constraints of an AIP designed for the UUV application.

One final caveat on the SE and ED values for the best combination of H2-O2 storage considered here (the 60% lithium hydride slurry plus CAN 33 chlorate candle H2-O2 system) is that this option can perhaps be most fairly compared to a primary battery based EPS rather than a RBEPS – unless these storage media can be implemented as truly a "refuelable" technology. But, even using this combination, the Objective energy storage value set by the Navy for the 60" LD MRUUV is not attainable.

Contents

Figures

Tables

Revision History

January 3, 2006: Initial Draft

October 27 2006: Final Report:

Section and Page	Change
Page 55 (Fuel Cell System)	Updated Figure 21 to include Navy requirements
Correction of Energy Density of Ideal 100% hydrogen peroxide:	
• Page 48 (Table 7)	Energy density of "Ideal hydrogen peroxide (H_2O_2)" changed from 4.74 kWh/L to 5.53 kWh/L
• Page 48 (Table 7)	Reference for "Ideal hydrogen peroxide (H_2O_2)" changed
• Page 75-79 (Appendix B: Storage System Options)	Energy Density of Storage System options involving "Ideal hydrogen peroxide (H_2O_2)" (symbol 5) updated
• Page 45 (Figure 16), Page 52 (Figure 18), Page 53 (Figure 19)	Updated to reflect new Energy Density
Correction of typographical errors:	
• Page 2 (Executive Summary)	Fixed typographical error
• Page 16 (Hydrogenics 5 kW for NASA)	Fixed typographical error
• Page 32 (Rechargeable Battery Energy/Power System (RBEPS))	Corrected spelling of Lithium Thionyl Chloride
Page 49 (Compressed Oxygen)	Noted reactivity of compressed oxygen gas very high pressures
Page 50 (Chlorate Candles)	Noted that the output rate of chlorate candles is not controllable during operation

Introduction

In general, the interest for applying fuel cells to Unmanned Underwater Vehicles (UUVs) comes from the assumption that fuel cells have the potential to increase the energy storage in a given UUV as compared to other Air-Independent Propulsion systems such as batteries. This increased energy storage would enable greater mission durations and/or ranges.

This report will summarize the available fuel cell and hydrogen/oxygen storage technologies and their relevant previous applications. The report will then present methods of assessing the technology and designing high-level Fuel Cell Energy/Power System (FCEPS) concepts. The goal is to develop a foundation for designing a FCEPS for an UUV and prove or disprove the previous assumptions associated with the application in the process. Here, the assessment is limited to Polymer Electrolyte Membrane (PEM) Fuel Cells (FC) operating on hydrogen and oxygen.

Definitions

Below are definitions of terms and acronyms used in this report:

AIP	Air-Independent Propulsion
ASDS	Advanced SEAL Delivery System
AUV	Autonomous Underwater Vehicle
COTS	Commercial Off The Shelf
DOD	Depth Of Discharge
ED	Energy Density
FC	Fuel Cell
FCEPS	Fuel Cell Energy/Power System
FCS	Fuel Cell System
FMEA	Failure Modes and Effect Analysis
H2/Air FC	Fuel Cell operating on hydrogen and air
H2/O2 FC	Fuel Cell operating on hydrogen and oxygen
LD	Large Displacement
LOX	Liquid Oxygen
MRUUV	Mission Reconfigurable Unmanned Underwater Vehicle
MTBF	Mean Time Between Failures
PD	Power Density
PEM	Polymer Electrolyte Membrane or Proton Exchange Membrane
RBEPS	Rechargeable Battery Energy/Power System
SE	Specific Energy
SP	Specific Power
SS	Storage System
UUV	Unmanned Underwater Vehicle

Figure 1 defines the FCS and FCEPS by showing and grouping the basic propulsion-related components of the UUV.

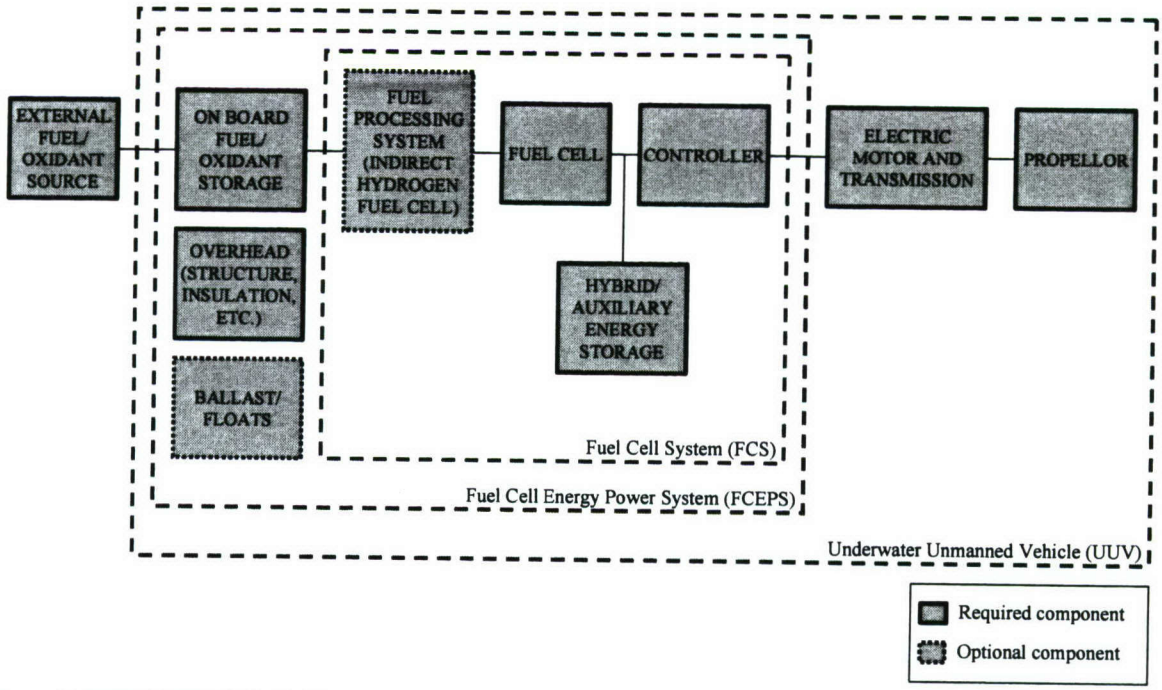

Figure 1: UUV FCEPS block diagram

Requirements and Environmental Conditions

There are a number of FCEPS requirements that must be balanced while meeting the constraints imposed by harsh environmental conditions.

General UUV

Below is a list of general requirements for the FCEPS design. Some requirements are interrelated, for instance physical dimensions, mass, and buoyancy.

1. Electrical (net energy available, maximum power, average power, nominal voltage, voltage response under transient loads, etc.)
2. Physical dimensions (diameter, length, volume)
3. Mass
4. Buoyancy (density at start of mission, density change throughout mission, center of mass, center of buoyancy)
5. Safety (FMEA risk levels, etc.)
6. Cost (unit cost and recurring cost)
7. Operation (fueling procedure, startup time, shutdown time, fueled and defueled shelf life)
8. Maintenance and repair (repair procedures and intervals; mean time between failures (MTBF); lifetime in terms of time, start/stop cycles, kWh; etc.)
9. Noise and vibration (maximum levels)

The environmental conditions include those below. The conditions are those as experienced by the FCEPS, not the UUV. For example, depending on the pressure hull arrangement of the UUV, the pressure experienced by the FCEPS may be different than that experienced by the UUV. The conditions must be considered not only during operation, but during transport and storage as well.

1. Operating pressure (minimum and maximum).
2. Temperature (minimum and maximum)

3. Orientation (pitch and roll)
4. Relative humidity
5. Corrosion
6. Vibration
7. Electromagnetic radiation

Navy 60" LD MRUUV

The 60" Large Displacement Mission Recoverable UUV (60" LD MRUUV) is used as the subject for the FCEPS assessment presented in this report. The U.S. Navy has set threshold and objective requirements for the 60" LD MRUUV. Since the objectives are more stringent than the thresholds (smaller in the case of physical dimensions, larger in the case of energy and power, etc.), they are used as the target requirements for the assessment presented in this paper. Table 1 and Table 2 list the threshold and objective requirements for the 60" LD MRUUV. The PD, SP, ED, and SE values in normal font style are the Draft Fuel Cell Propulsion System Requirements [Egan]. The PD, SP, ED, and SE values in parenthesized italics are based on a division of the energy and peak power values by the volume and mass requirements. For the purposes of this assessment, the objective Draft Fuel Cell Propulsion System Requirements are used as the FCEPS requirements for PD, SP, ED, and SE, even though these values do not equate to a consistent FCEPS density value.

The 60" LD MRUUV will be designed with a modular architecture so that certain components (including the energy Storage System) can be exchanged [Egan]. In order to maintain neutral overall vehicle buoyancy, any two components to be swapped must have equal density. The components may or may not have neutral buoyancy independent of the entire UUV, however. Note that the objective volume and mass values in Table 2 equate to a FCEPS density of 1.11 kg/L. This is used as the target FCEPS density to generate design concepts later, although it is higher than the standard of 1.0275 kg/L used for neutral buoyancy in submarine design [Burcher and Rydill, p. 38].

	Power 40 kW peak	**Energy** 1725 kWh
Volume 5663 L	**Power Density** 0.006 or *(0.007)* kW/L	**Energy Density** 0.247 or *(0.305)* kWh/L
Mass 7575 kg	**Specific Power** 0.009 or *(0.005)* kW/kg	**Specific Energy** 0.285 or *(0.228)* kWh/kg

Table 1: Navy LD MRUUV FCEPS threshold requirements [Egan, 18-19, 22]

	Power 70 kW peak	**Energy** 11,500 kWh
Volume 3681 L	**Power Density** 0.026 or *(0.019)* kW/L	**Energy Density** 3.178 or *(3.124)* kWh/L
Mass 4082 kg	**Specific Power** 0.018 or *(0.017)* kW/kg	**Specific Energy** 2.200 or *(2.817)* kWh/kg

Table 2: Navy LD MRUUV FCEPS objective requirements [Egan, 18-19, 22]

Although the outside diameter of the 60" LD MRUUV is 60 inches, the available diameter for the FCEPS is 55 inches, or 1.40 m. [2] Using the volume requirements in Table 1 and Table 2, the resulting FCEPS length is 3.69 m and 2.40 m for the threshold and objective requirements, respectively.

The UUV must be capable of being fueled and refueled onboard a ship or submarine. The UUV may be transported by air, truck, rail, or ship, which imposes environmental conditions that must be considered in addition to those imposed in the underwater environment[3].

The voltage output of the FCEPS must be between 100 and 400 VDC. The maximum fixed cost of the FCEPS is $10,000 per kWh of capacity. The maximum recurring cost is $100 per kWh used [Egan, 20].

The UUV is expected to experience a minimum temperature of -7 °C during transport and storage to a maximum of 54 °C while deployed on a submarine. The UUV will experience a minimum pressure of 10 kPa during transport by airplane and a maximum pressure during underwater operation[4]. Seawater pressure will increase by about 10 kPa per meter of seawater depth. However, the expected operating depth of the LD MRUUV is unknown, and it is also unknown whether the FCEPS will be installed inside an existing UUV pressure hull or be subjected to seawater pressure itself.

Previous H2/O2 PEM Fuel Cell Stacks, Systems, and Applications

Numerous H2/O2 PEM Fuel Cell stacks and systems have been designed or are in development for marine and space vehicular applications. Summaries of the relevant projects are below. Table 3 lists the power, mass, dimensions, voltage, current, pressure, efficiency, and other characteristics where available.

Helion 20 kW

The Helion fuel cell stack is water cooled and uses graphite polymer composite bipolar plates[5]. Additional information is listed in Table 3.

Lynntech Gen IV Flightweight 5 kW for Helios

The maximum operating pressure of the Lynntech fuel cell stack is 0.690 MPa, and the maximum anode-cathode pressure difference is 0.345 MPa [Velev, et al., p. 2]. The minimum and maximum operating temperatures are 40 and 60 °C, respectively [Velev, et al.]. The fuel cell stack is 54% efficient at 350 mA/cm^2 and 0.80 volts per cell average (70 A total current) and 48% efficient at 500 mA/cm^2 and 0.71 volts per cell average (100 A total current) [Garcia, et al., p. 5-6]. The polarization of the fuel cell stack is shown in Figure 2, where temperature of the fuel cell ranged from 20 °C and 60 °C depending on the load point and pressure was constant [Garcia, et al., p. 5]. Figure 2 shows the average cell voltage of the Lynntech fuel cell stack as a function of current density. Figure 3 shows the efficiency as a function of stack power. Additional information is listed in Table 3.

---

[2] Maria Medeiros, email communication, 21-Jul-2005

[3] "Table 3.2.5-1. BLQ-11 Environmental Conditions," received by email from Maria Medeiros, 21-Jul-2005

[4] "Table 3.2.5-1. BLQ-11 Environmental Conditions," received by email from Maria Medeiros, 21-Jul-2005

[5] press release, "AREVA develops the first French 20 kW fuel cell stack," http://www.areva.com/servlet/ContentServer?pagename=arevagroup_en%2FPressRelease%2FPressReleaseFullTemplate&cid=1095412362058, December 8, 2004

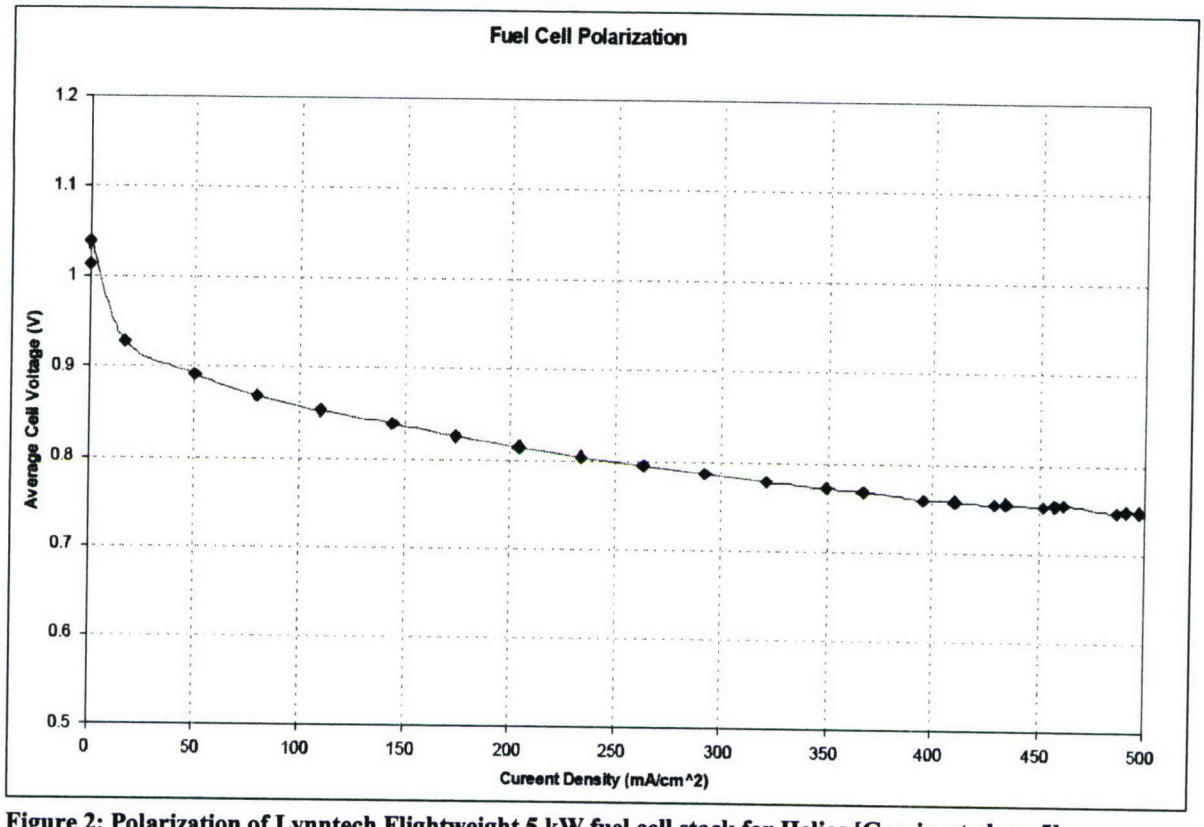

Figure 2: Polarization of Lynntech Flightweight 5 kW fuel cell stack for Helios [Garcia, et al., p. 5]

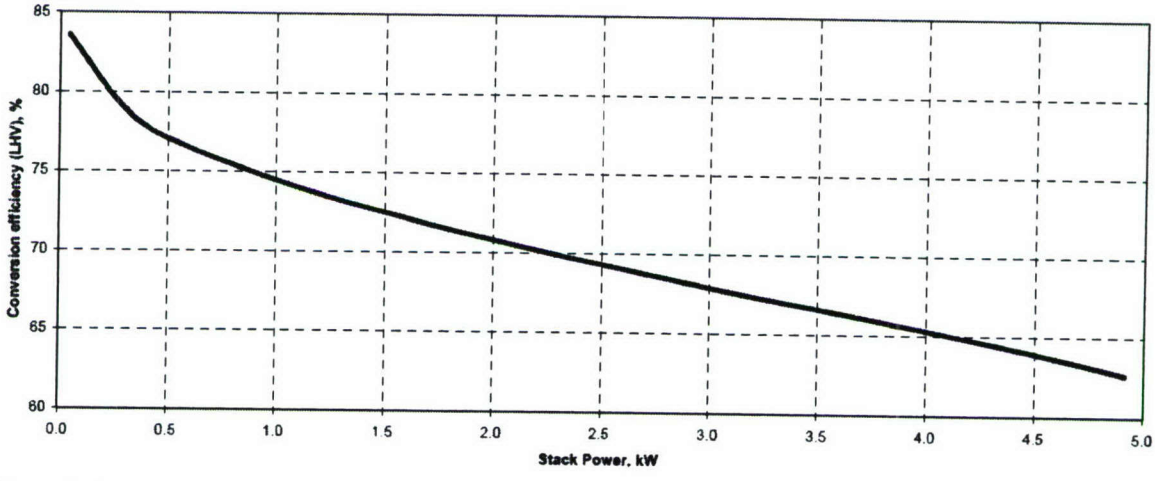

Figure 3: Efficiency of Lynntech Flightweight Gen IV fuel cell stack for Helios [Velev, et al., p. 4]

Helios was a solar/regenerative fuel cell powered airplane for high altitude operation [Bents, et al.] The Helios system used a separate electrolyzer and fuel cell in a closed cycle H2/O2 system. The system was designed at the NASA Glenn Research Center. Hydrogen and oxygen were both stored as compressed gas in composite tanks from Quantum Technology. In operation, the tanks are only charged to 190 psig and discharged to 90 psig, storing a net 21 kWh of hydrogen and oxygen[6].

[6] Based on hydrogen LHV and 317 moles H2 and 158 moles O2 as specified in [Garcia, p. 3]

Nedstack

Nedstack develops and utilizes composite bipolar plates (Conduplate-LT; Conduplate-MT-X; Conduplate HT-X) for their fuel cell stacks[7].

Nedstack A200 (5, 10, 20 kWe)

The Nedstack A200 is designed for both air and oxygen operation. The stack is liquid cooled, with operation between 0 and 80 °C. The stack lifetime is listed as greater than 5000 hours. The anode and cathode are capable of operating with reactants between 0 and 100% relative humidity [8, 9, 10]. Polarization graphs are shown in Figure 4. Additional information is listed in Table 3.

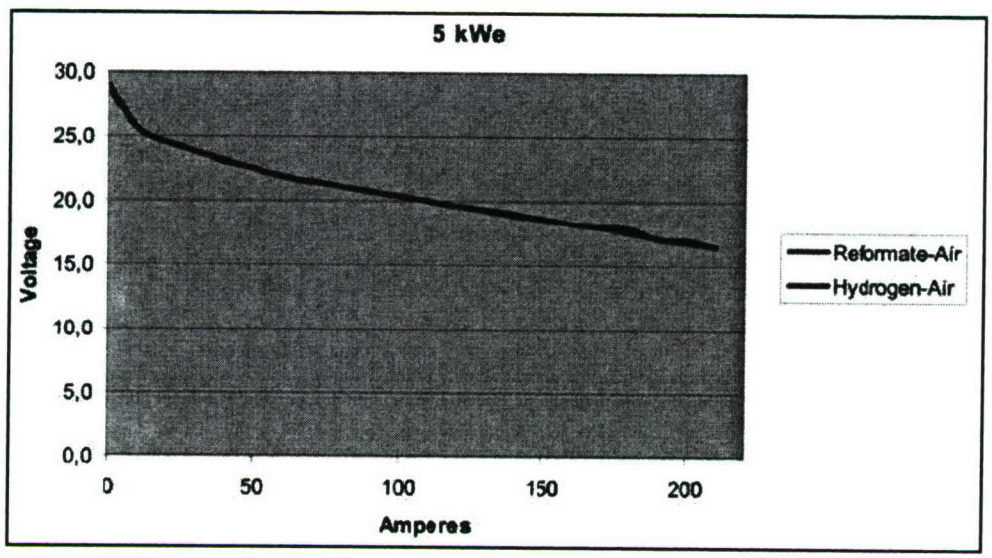

[7] http://www.nedstack.com/

[8] product literature, "PEM fuel cell stacks Nedstack 5 kWe – A200," http://www.nedstack.com/pdf/Nedstack_05-A200.pdf, April 2005

[9] product literature, "PEM fuel cell stacks Nedstack 10 kWe – A200," http://www.nedstack.com/pdf/Nedstack_10-A200.pdf, April 2005

[10] product literature, "PEM fuel cell stacks Nedstack 20 kWe – A200," http://www.nedstack.com/pdf/Nedstack_20-A200.pdf, April 2005

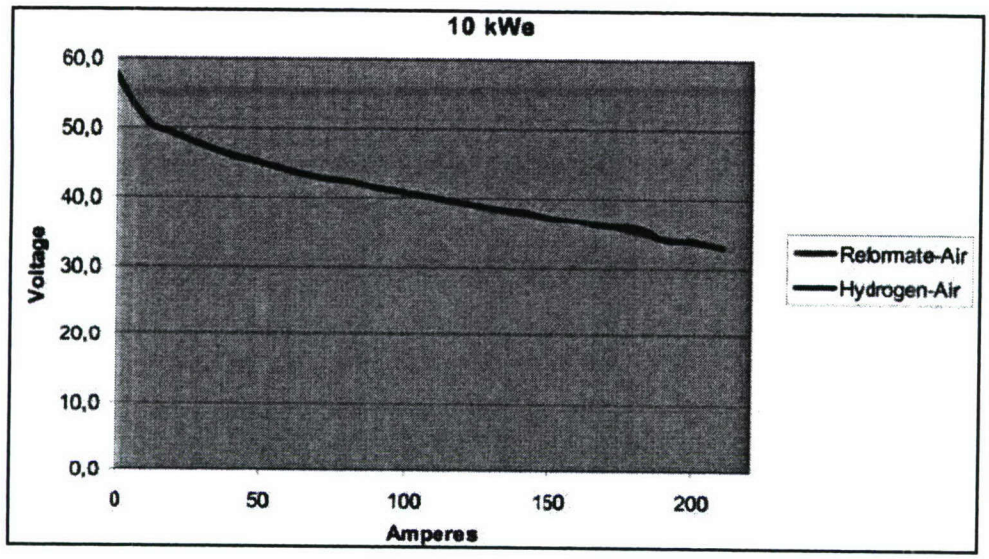

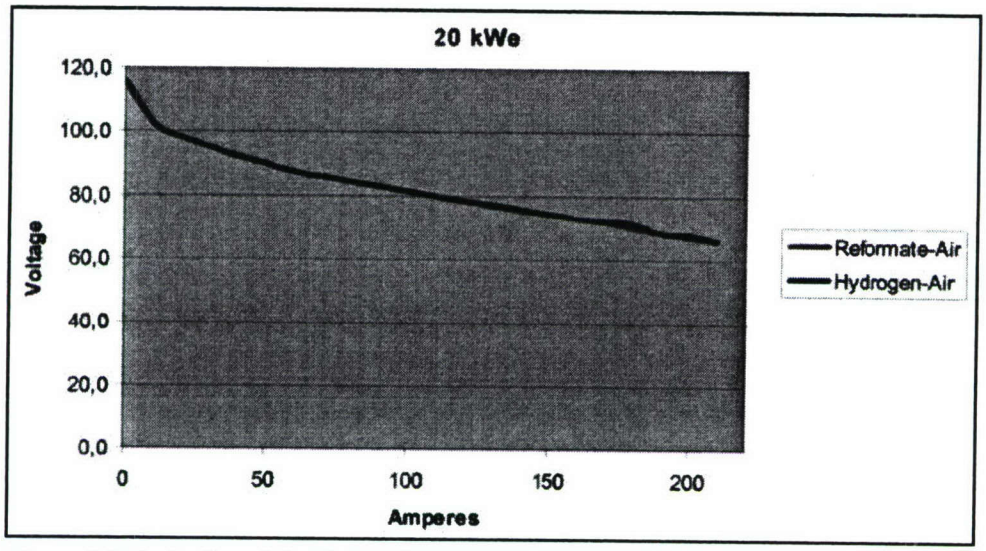

Figure 4: Polarization of the Nedstack A200 fuel cell stacks

Nedstack for Submarine

Nedstack is developing a 300 kW fuel cell for a European submarine [Baker and Jollie, p. 21]. The Nedstack website claims greater than 10,000 hour lifetime and 60% efficiency at atmospheric pressure and extremely high Specific Energy and Energy Density values as listed in Table 3[11].

Siemens

The Siemens BZM 34 and BZM 120 Fuel Cell Systems are based on technology originally developed by General Electric [Strasser, p. 1201]. The PEM is DuPont Nafion® 117 [Strasser, p. 1203], and the cell thickness is 2.2 mm [Hammerschmidt, 2003]. The fuel cells are water cooled [Hammerschmidt, 2003]. The reactants are humidified before introduction to the stack by water exchange through PEM material [Strasser, p. 1206]. The reactants are not recirculated, but are passed through four groupings of decreasing numbers of cells with water separation stages between each group. The voltage of the final

[11] http://www.nedstack.com/

grouping (a single cell) is used to control the reactant purging [Strasser, p. 1205]. The Siemens fuel cells offer quick start up and shutdown [Hammerschmidt and Lersch, p. 2] and respond to dynamic load changes within 100 ms [Strasser, p. 1207].

For safety reasons, the fuel cell stacks operate inside a pressure vessel which contains nitrogen gas at a pressure of 0.35 MPa [Strasser, p. 1206]. The mass specifications in Table 3 include the pressure vessel [Hammerschmidt, 2003]. The ambient pressure outside the pressure vessel is that of the submarine environment [Hammerschmidt, 2003].

The Siemens BZM 34 and BZM 120 have been or are being installed in at least 16 submarine applications[12]. Typically, eight of the modules are connected in series with one backup module available in each installation. Hydrogen is stored in a maintenance-free metal hydride tank which can be mounted between the outer hull and inner pressure hull. Oxygen is stored as a liquid in double-walled and vacuum-insulated tanks [Hauschildt and Hammerschmidt].

Siemens BZM 34

The BZM 34 has an efficiency of 69% at 6.8 kW (20% of the maximum continuous power rating)[13].

BZM 34 modules are being installed in Type 212 submarines ordered by Germany and Italy[14]. The power system also includes high-performance lead acid batteries and a diesel generator[15].

Siemens BZM 120

The BZM 120 has an efficiency of 68% at 24 kW (20% of the maximum continuous power rating)[16]. The BZM 120 module consists of two fuel cell stacks. Electrical and cooling water flows are parallel, and reactant flow is serial [Hammerschmidt and Lersch, p. 2]. Figure 5 shows the polarization of the BZM 120 before and after about 1000 hours of operation. The information in Table 3 refers to the system with both stacks together as one unit.

The BZM 120 is undergoing sea trials. It has been or will be installed in new German Type 212B submarines. It will be installed in Italian Type 212A submarines and retrofitted Greek and Portuguese Type 209 submarines. Each Type 214 submarine ordered by Greece and Korea will be powered by 2 BZM 120 modules [Baker and Jollie, p. 17-18]. The Type 214 power system also includes high-performance lead acid batteries and a diesel generator[17]. The oxygen tank is installed inside the pressure hull of the Type 214 submarine [Hauschildt and Hammerschmidt].

---

[12] "Fuel cell submarines offer underwater stealth," http://www.gizmag.com/go/3434/, November 7, 2004

[13] Siemens AG product literature, "SINAVYcis Application Potential," 2004, p. 5

[14] "Type 214" http://www.globalsecurity.org/military/world/europe/type-214.htm, accessed 12-Oct-2005

[15] "Fuel cell submarines offer underwater stealth," http://www.gizmag.com/go/3434/, November 7, 2004

[16] Siemens AG product literature, "SINAVYcis Application Potential," 2004, p. 5

[17] "Fuel cell submarines offer underwater stealth," http://www.gizmag.com/go/3434/, November 7, 2004

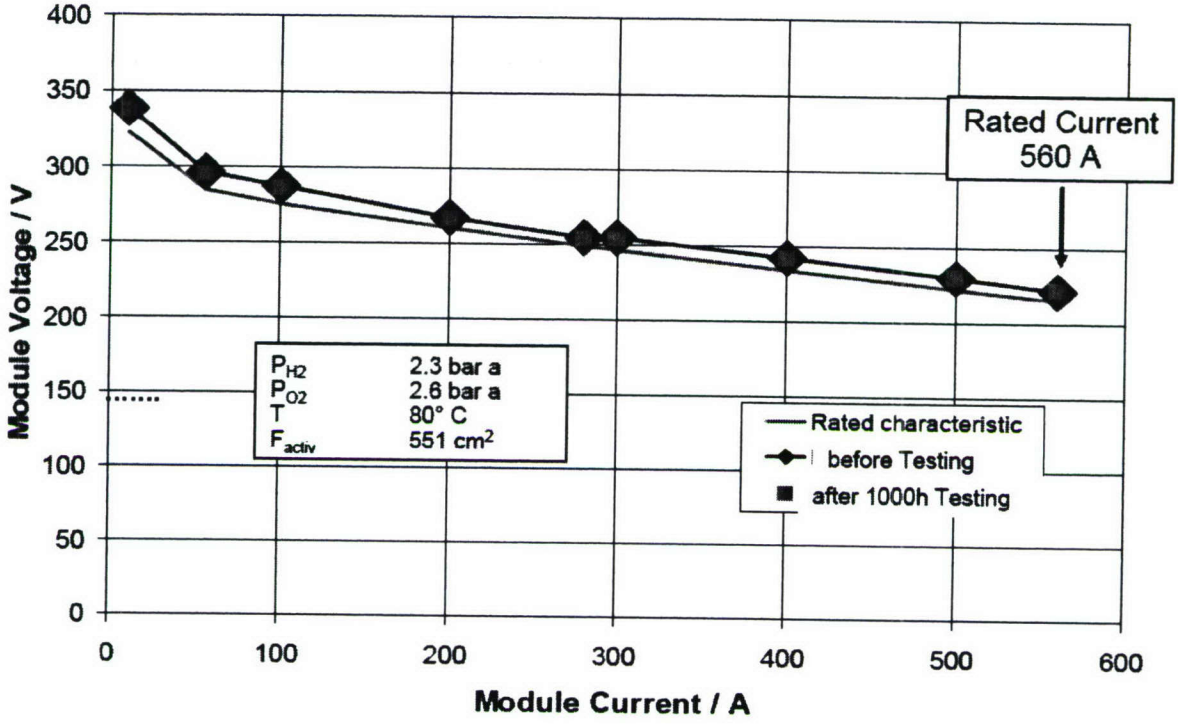

Figure 5: Polarization of Siemens BZM 120 (before and after ~ 1000 hr. operation) [Hammerschmidt, 2003]

ZSW

ZSW (Centre for Solar Energy & Hydrogen Research) in Germany has developed a series of fuel cell stacks and is developing a Fuel Cell System for DeepC, an underwater research vehicle. ZSW uses graphite composites for some bipolar plate designs and injection-molding for others[18].

ZSW BZ 100 (100, 250, 500, 1000W)

The ZSW BZ 100 series is designed for air or O2 cathode operation[19]. Figure 6 shows the polarization and power of the BZ 100 as a function of current loading. Additional information is listed in Table 3.

[18] product literature, "Electrochemical Hydrogen Technology (ECW) PEM-Fuel-Cells," http://www.zsw-bw.de/en/docs/products/pdfs/ECW_BZ_en.pdf, accessed 12-Oct-2005

[19] product literature, "Electrochemical Hydrogen Technology (ECW) PEM-Fuel-Cells," http://www.zsw-bw.de/en/docs/products/pdfs/ECW_BZ_en.pdf, accessed 12-Oct-2005

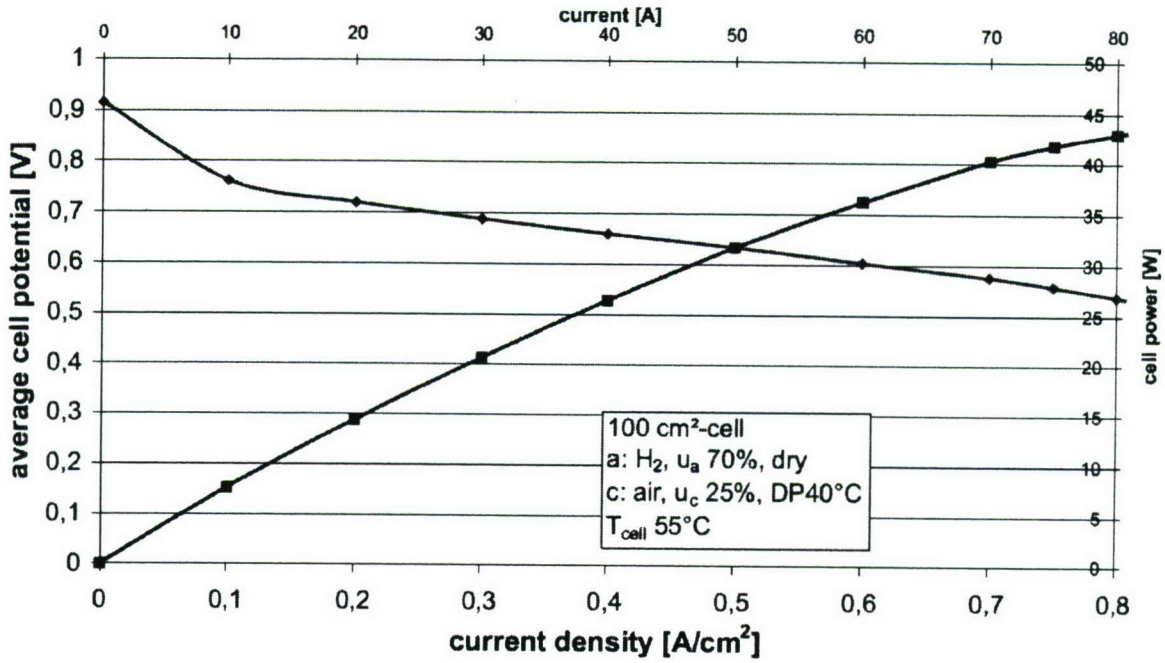

Figure 6: Polarization and power curves of ZSW BZ 100 fuel cell stack[20]

ZSW for DeepC

The DeepC AUV design is powered by two ZSW stacks, each capable of 1.8 kW net electrical power [Joerissen, et al., p. 1013-1014]. The reactants are recirculated with small diaphragm pumps and inert gases are purged [Joerissen, et al., p. 1013-1014]. The reactants are not humidified externally of the fuel cell stack [Hornfeld, p. 4]. The information listed in Table 3 refers to both fuel cell stacks as one unit.

The fuel cell stack, cooling equipment, storage tanks, and power distribution electronics will be installed inside the pressure hull of the vehicle [Geiger, 2002], [Joerissen, et al., p. 1013]. Hydrogen and oxygen will be compressed in composite tanks [Joerissen, et al., p. 1013].

Electrochem 1 kW for NASA

The Electrochem Fuel Cell System was developed and delivered to NASA for potential space applications. Reactants are recirculated passively with ejectors[21]. Additional information is listed in Table 3.

Honeywell 5.25 kW for NASA

The Honeywell (formerly AlliedSignal Aerospace) fuel cell stack was designed and developed in 1998 for testing for future NASA Reusable Launch Vehicle (RLV) applications. Testing of both short stacks and the full 5.25 kW stack was successful. The cells were hexagonally shaped [Perez-Davis, et al.]. No further information is available of the stack.

---

[20] product literature, "Electrochemical Hydrogen Technology (ECW) PEM-Fuel-Cells," http://www.zsw-bw.de/en/docs/products/pdfs/ECW_BZ_en.pdf, accessed 12-Oct-2005

[21] "Proton-Exchange-Membrane Fuel Cell Powerplants Developed and Tested for Exploration Missions," http://www.grc.nasa.gov/WWW/RT/2004/RP/RPC-hoberecht.html, accessed 12-Oct-2005

Hydrogenics 5 kW for NASA

Hydrogenics provided a 5 kW fuel cell stack to the NASA Glenn Research Center for testing as a part of the regenerative fuel cell effort. This is Hydrogenics' fuel H2/O2 PEM fuel cell[22]. Hydrogenics adapted it from a H2/air stack. NASA has not yet tested the stack[23]. No further information is available.

MHI for Urashima

The Mitsubishi Heavy Industries (MHI) Fuel Cell System includes two stacks electrically in series [Hyakudome, et al., p. 164]. The information listed in Table 3 refers to the entire system with both stacks. The anode flow is actively humidified and the cathode flow is humidified by passing the oxygen through the product water tank. Hydrogen and oxygen are both recirculated, but the system is closed in that all product water and impurities accumulate within the system. The stacks are water cooled [Maeda, et al., p. 3]. Figure 7 shows a block diagram of the system.

The Japan Marine Science and Technology Center (JAMSTEC) installed the MHI Fuel Cell System in its Urashima AUV. The entire Fuel Cell System, including the stack, heat exchanger, and reaction water tank, is mounted inside a titanium alloy pressure vessel having the dimensions listed in Table 3 [Maeda, et al., p. 3].

Hydrogen is stored in an AB5 rare earth alloy metal hydride in a pressure vessel at 0.95 to 1.05 MPa and between 20 and 60 °C. This pressure vessel is external to and separate from the Fuel Cell System pressure vessel [Maeda, et al., p. 3]. The metal hydride absorbs hydrogen at 0 °C and discharges hydrogen at 20 to 25 °C [Sawa, et al., p. 5]. JAMSTEC also studied a BCC type metal hydride, but ultimately chose the AB5 metal hydride based on its thermal characteristics [Sawa, et al., p. 5]. Oxygen is stored in a compressed oxygen tank at 14.7 MPa [Maeda, et al., p. 3]. The volume of the storage tank is 0.5 m^3 [24].

The Urashima FCEPS is hybridized using Li-Ion rechargeable batteries. Three cells are connected in parallel [Ishibashi, et al.]. The battery system has a nominal voltage of 130 V and a capacity of 30 Ah [Ishibashi, et al.], [Yamamoto, et al., p. 3]. The Specific Energy of the battery system is 0.15 kW/kg [Hyakudome, et al.].

Urashima was successfully sea-trialed with the MHI Fuel Cell System, but the group is now developing an updated version of the Fuel Cell System[25]. No further information is available on the new system.

---

22 press release, "NASA Buys Hydrogenics Light Weight Fuel Cell Stack To Test For Potential Uses In Space," 15-Nov-2004

23 David Bents (NASA Glenn Research Center), telephone conversation, 7-Oct-2005

24 Ikuo Yamamoto, conversation with Gwyn Griffiths, week of 26-Sep-2005

25 Ikuo Yamamoto, email communication, 22-Jun-2005

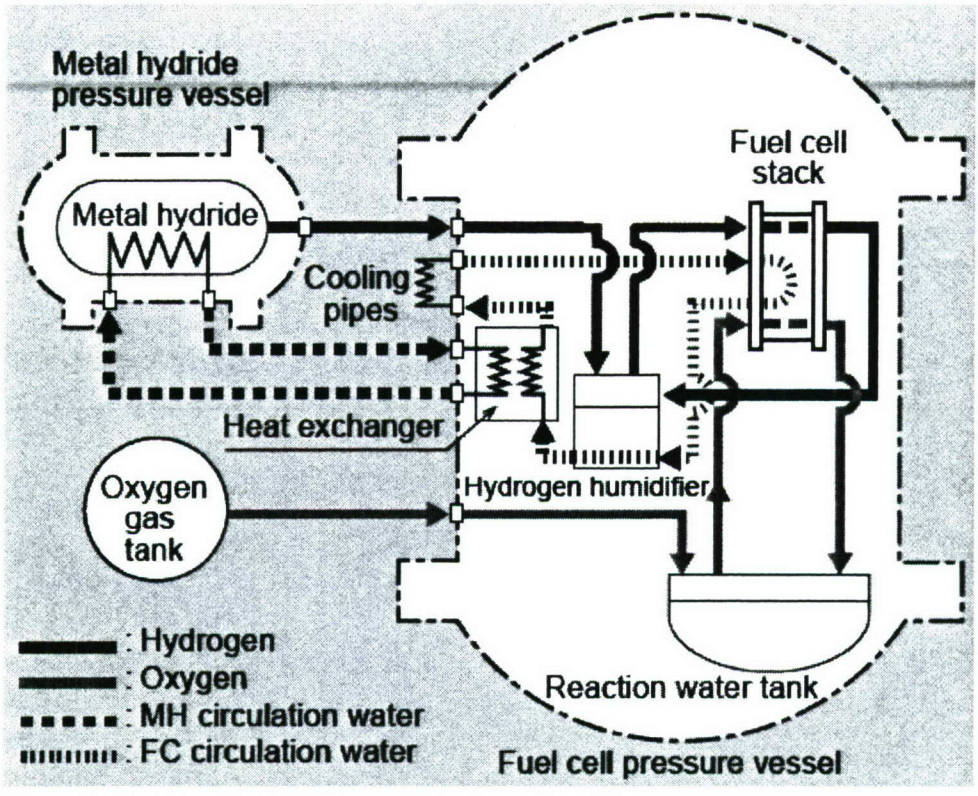

Figure 7: Urashima Fuel Cell System [Maeda, et al., p. 3]

Teledyne 7 kW for NASA

The Teledyne Fuel Cell System was delivered to NASA for potential space applications. The reactants are actively recirculated. The peak power to nominal power capability ratio is greater than 6:1. The system is designed to utilize cryogenic hydrogen and oxygen storage[26]. Additional information is listed in Table 3. The system has not been fully tested by NASA yet[27].

UTC for 44" UUV

International Fuel Cells (IFC), which is now UTC Fuel Cells, developed a Fuel Cell System for a 44 inch diameter UUV in the early 1990s [Rosenfeld]. A water circulation loop cooled the fuel cell and passively humidified the PEM through controlled-porosity graphite flow fields [DeRonck]. Water was collected internally to the power system and was periodically emptied to an external storage tank [DeRonck]. Reactants were not recirculated [Rosenfeld]. The system was orientation independent and was capable of withstanding 200 to 250 G shock [DeRonck]. The fuel cell had a polarization of 0.8 V/cell at 300 mA/cm^2 [Rosenfeld].

The full system was based on four 5 kW stacks, each of which could fit in a 21 inch diameter UUV. A 10 kW system (two stacks of 5 kW) was tested for 2000 hours including 1000 hours at full power [Rosenfeld]. The information in Table 3 references the entire system (four stacks), which are presumably connected in series.

---

[26] James Braun, telephone conversation, 1-Jul-2005

[27] "Proton-Exchange-Membrane Fuel Cell Powerplants Developed and Tested for Exploration Missions," http://www.grc.nasa.gov/WWW/RT/2004/RP/RPC-hoberecht.html, accessed 12-Oct-2005

Zongshen PEM Power Systems

Zongshen is designing 1 kW, 2 kW, and 5 kW H2/O2 Fuel Cell Systems for availability in 2006. Hydrogen flow is dead-ended and oxygen is purged. The stacks are water cooled[28]. No further information is available at this time.

Other Applications

Perry Technologies developed PC14, a two-person submarine in 1989 powered by a 3 kW Ballard fuel cell system [Baumert and Epp], [Geiger and Jollie, p. 29]. This was the first fuel cell powered submarine. Perry Technologies later became Energy Partners and was then bought by Teledyne [Geiger and Jollie, p. 29]. Presumably, the fuel cell technology and expertise is now owned by Teledyne and Ballard.

Ballard Power Systems was contracted by the Canadian Maritime Command from 1994 to 1998 to produce 50 kW and 250 kW Fuel Cell Systems for submarine use [Geiger and Jollie, p. 8]. No additional information is available on that project.

FMV (Försvarets Materielverk) in Sweden investigated PEM fuel cells for submarines in the 1990s, but the work was discontinued due to high projected cost of the fuel cells [Geiger and Jollie, p. 20].

Pennsylvania State University's Applied Research Laboratory and the US Army Research Laboratory's Energy Science and Power Systems Division investigated the use of a Fuel Cell System in the Seahorse UUV, which has a 38 inch diameter [Keeter]. A 400 W PEM Fuel Cell System was used as basis for projecting performance along with other potential power systems. Hydrogen was provided from onboard fuel processing. Oxygen was stored in lithium perchlorate (LiClO4). The Fuel Cell System was never operated in the Seahorse UUV. The conclusion was that Solid Oxide Fuel Cells are a better match given the limited volume available in UUVs; however, the reasoning has not been explained[29, 30].
Bertin Technologies is evaluating a 200 kW fuel cell for a French submarine, and is involved in developing components for that fuel cell [Baker and Jollie, p. 14], [31]. Bertin is also designing a 2 kW fuel cell stack for underwater vehicles, in partnership with ECA and Ifremer (French Research Institute for Exploitation of the Sea) [32]. No further information is available on those projects at this time.

Purdue University is simulating a 500 kW regenerative Fuel Cell System for a solar high altitude helium-filled aircraft. The project is funded by the US Air Force Research Laboratory[33]. No information is available on a fuel cell supplier for the project.

---

[28] http://www.zongshenpem.com/products/, accessed 12-Oct-2005

[29] http://www.engr.psu.edu/h2e/Pub/Peters/Peters_2.htm, accessed 11-Oct-2005

[30] Tom Hughes, email communication, 22-Jun-2005

[31] http://www.fuelcelltoday.com/FuelCellToday/IndustryDirectory/IndustryDirectoryExternal/IndustryDirectoryDisplayCompany/0,4591,2234,00.html, accessed 18-Oct-2005

[32] http://www.fuelcelltoday.com/FuelCellToday/IndustryDirectory/IndustryDirectoryExternal/IndustryDirectoryDisplayCompany/0,4591,2234,00.html, accessed 18-Oct-2005

[33] Press release, http://news.uns.purdue.edu/UNS/html4ever/2005/050321.Sullivan.airship.html, 21-March-2005

The Rubin Central Marine Design Bureau, a part of the Russian government, is developing a fuel cell for a Russian Amur 1650 class submarine [Geiger and Jollie, p. 29], [and 34]. The project is in the early stages and no information is available on the fuel cell at this time.

34

http://www.fuelcelltoday.com/FuelCellToday/IndustryDirectory/IndustryDirectoryExternal/IndustryDirectoryDisplayCompany/0,1664,2364,00.html, accessed 18-Oct-2005

Symbol	Description	Stack or System?	Specific Power (kW/kg)	Power Density (kW/L)	Maximum Continuous Power (kW)	Volume (L)	Mass (kg)	Diameter (m)	Height (m)	Width (m)	Length (m)	Active area (cm^2)	Number of cells	Rated voltage (V)	Minimum Operating Voltage (V)	Maximum Operating Voltage (V)	Cell Degradation Rate (μV/hr)	Rated Current (A)	Current density (A/cm^2)	Peak Power (kW)	Minimum Continuous Power (kW)	Operating temperature (°C)	Degree of Fuel Purity	Degree of Oxidant Purity	Anode Operating Pressure (MPa)	Cathode Operating Pressure (MPa)	Efficiency at Maximum Continuous Power	Maximum Efficiency
1	Helion 20 kW[35]	stack	0.125	0.182	20.00	110.0	160.0	N/A	0.690	0.470	0.335																	
2	Lynntech Gen IV Flightweight 5 kW for Helios[36, 37, 38]	stack	0.250	0.263	5.00	19.0	20.0	0.254	N/A	N/A	0.406	200	64			64					0.5	57.2	99.99 9%	99.99 9%	0.536			54% @ 70A
3	Nedstack 5 kWe-A200[39]	stack	0.357	0.505	5.00	9.9	14.0	N/A	0.180	0.250	0.220	200	30	18				278	1.39									
4	Nedstack 10 kWe-A200[40]	stack	0.357	0.419	10.00	23.9	28.0	N/A	0.180	0.250	0.530	200	60	36				278	1.39									
5	Nedstack 20 kWe-A200[41]	stack	0.357	0.473	20.00	42.3	56.0	N/A	0.180	0.250	0.940	200	120	72				278	1.39									

[35] press release, "AREVA develops the first French 20 kW fuel cell stack," http://www.areva.com/servlet/ContentServer?pagename=arevagroup_en%2FPressRelease%2FPressReleaseFullTemplate&cid=1095412362058, December 8, 2004

[36] [Velev, et al.]

[37] http://www.grc.nasa.gov/WWW/ERAST, accessed 12-Oct-2005

[38] [Garcia]

[39] product literature, "PEM fuel cell stacks Nedstack 5 kWe – A200," http://www.nedstack.com/pdf/Nedstack_05-A200.pdf, April 2005

[40] product literature, "PEM fuel cell stacks Nedstack 10 kWe – A200," http://www.nedstack.com/pdf/Nedstack_10-A200.pdf, April 2005

Symbol	Description	Stack or System?	Specific Power (kW/kg)	Power Density (kW/L)	Maximum Continuous Power (kW)	Volume (L)	Mass (kg)	Diameter (m)	Height (m)	Width (m)	Length (m)	Active area (cm^2)	Number of cells	Rated voltage (V)	Minimum Operating Voltage (V)	Maximum Operating Voltage (V)	Cell Degradation Rate (µV/hr)	Rated Current (A)	Current density (A/cm^2)	Peak Power (kW)	Minimum Continuous Power (kW)	Operating temperature (°C)	Degree of Fuel Purity	Degree of Oxidant Purity	Anode Operating Pressure (MPa)	Cathode Operating Pressure (MPa)	Efficiency at Maximum Continuous Power	Maximum Efficiency
6	Siemens BZM 34[42, 43]	FC system	0.052	0.102	34.00	334.1	650.0	N/A	0.480	0.480	1.450	1163	72	52.3	50	55	1.76	650	0.56	68		80			0.23	0.26	59%	75% @ 25A
7	Siemens BZM 120[44, 45, 46]	FC system	0.133	0.257	120.00	466.4	900.0	N/A	0.500	0.530	1.760	1163	320	215	208	243	1.76	560	0.48	240		80	99.99 %; no S or CO	99.5 %	0.23	0.26	56%	
8	ZSW BZ 100 100W[47]	stack	0.022	0.039	0.10	2.5	4.5	N/A	0.140	0.140	0.130	100		2.4				41.7	0.42			50 to 60			0.2	0.2		
9	ZSW BZ 100 250W[48]	stack	0.042	0.071	0.25	3.5	5.9	N/A	0.140	0.140	0.180	100		6				41.7	0.42			50 to 60			0.2	0.2		
10	ZSW BZ 100 500W[49]	stack	0.059	0.102	0.50	4.9	8.5	N/A	0.140	0.140	0.250	100		12				41.7	0.42			50 to 60			0.2	0.2		

[41] product literature, "PEM fuel cell stacks Nedstack 20 kWe – A200," http://www.nedstack.com/pdf/Nedstack_20-A200.pdf, April 2005

[42] Siemens AG product literature, "SINAVYcis Application Potential," 2004, p. 4-6

[43] [Strasser]

[44] Siemens AG product literature, "SINAVYcis Application Potential," 2004, p. 4-6

[45] [Hammerschmidt, 2003]

[46] [Hammerschmidt and Lersch]

[47] product literature, "Electrochemical Hydrogen Technology (ECW) PEM-Fuel-Cells," http://www.zsw-bw.de/en/docs/products/pdfs/ECW_BZ_en.pdf, accessed 12-Oct-2005

[48] product literature, "Electrochemical Hydrogen Technology (ECW) PEM-Fuel-Cells," http://www.zsw-bw.de/en/docs/products/pdfs/ECW_BZ_en.pdf, accessed 12-Oct-2005

[49] product literature, "Electrochemical Hydrogen Technology (ECW) PEM-Fuel-Cells," http://www.zsw-bw.de/en/docs/products/pdfs/ECW_BZ_en.pdf, accessed 12-Oct-2005

Symbol	Description	Stack or System?	Specific Power (kW/kg)	Power Density (kW/L)	Maximum Continuous Power (kW)	Volume (L)	Mass (kg)	Diameter (m)	Height (m)	Width (m)	Length (m)	Active area (cm^2)	Number of cells	Rated voltage (V)	Minimum Operating Voltage (V)	Maximum Operating Voltage (V)	Cell Degradation Rate (μV/hr)	Rated Current (A)	Current density (A/cm^2)	Peak Power (kW)	Minimum Continuous Power (kW)	Operating temperature (°C)	Degree of Fuel Purity	Degree of Oxidant Purity	Anode Operating Pressure (MPa)	Cathode Operating Pressure (MPa)	Efficiency at Maximum Continuous Power	Maximum Efficiency
11	ZSW BZ 100 1 kW[50]	stack	0.074	0.131	1.00	7.6	13.6	N/A	0.140	0.140	0.390	100		24				41.7	0.42			50 to 60			0.2	0.2		
-	Electrochem 1 kW for NASA[51]	FC system			1.00			N/A				232	45						0.11	6								
-	Honeywell 5.25 kW for NASA[52]	stack			5.25																							
-	Hydrogenics 5 kW for NASA[53]	stack			5.00																							
-	MHI for Urashima[54], [55], [56]	FC system		0.011	4.20	381.7		0.900	0.900	N/A	N/A			120				35			1.2	60 to 80						54%

[50] product literature, "Electrochemical Hydrogen Technology (ECW) PEM-Fuel-Cells," http://www.zsw-bw.de/en/docs/products/pdfs/ECW_BZ_en.pdf, accessed 12-Oct-2005

[51] "Proton-Exchange-Membrane Fuel Cell Powerplants Developed and Tested for Exploration Missions," http://www.grc.nasa.gov/WWW/RT/2004/RP/RPC-hoberecht.html, accessed 12-Oct-2005

[52] [Perez-Davis, et al.]

[53] press release, "NASA Buys Hydrogenics Light Weight Fuel Cell Stack To Test For Potential Uses In Space," 15-Nov-2004

[54] [Maeda, et al.]

[55] [Tsukioka]

[56] Tadahiro Hyakudome, email communication, 19-July-2005

Symbol	Description	Stack or System?	Specific Power (kW/kg)	Power Density (kW/L)	Maximum Continuous Power (kW)	Volume (L)	Mass (kg)	Diameter (m)	Height (m)	Width (m)	Length (m)	Active area (cm^2)	Number of cells	Rated voltage (V)	Minimum Operating Voltage (V)	Maximum Operating Voltage (V)	Cell Degradation Rate (μV/hr)	Rated Current (A)	Current density (A/cm^2)	Peak Power (kW)	Minimum Continuous Power (kW)	Operating temperature (°C)	Degree of Fuel Purity	Degree of Oxidant Purity	Anode Operating Pressure (MPa)	Cathode Operating Pressure (MPa)	Efficiency at Maximum Continuous Power	Maximum Efficiency
-	Nedstack for submarine[57], [58]	stack	1.000	1.000	300.00																							60%
-	Teledyne 7 kW for NASA[59]	FC system			5 as delivered; 7 under design			N/A				302	82	30					0.270	12								
-	UTC for 44" UUV[60], [61]	FC system			20.00								320	264			3				1.33	82.2			0.34	0.34	68%	
-	Zongshen PEM Power Systems[62]	FC system			5.00																							

[57] [Baker and Jollie]

[58] http://www.nedstack.com/, accessed 12-Oct-2005

[59] "Proton-Exchange-Membrane Fuel Cell Powerplants Developed and Tested for Exploration Missions," http://www.grc.nasa.gov/WWW/RT/2004/RP/RPC-hoberecht.html, accessed 12-Oct-2005

60 [DeRonck]

61 [Rosenfeld]

62 http://www.zongshenpem.com/products/, accessed 12-Oct-2005

Symbol		Stack or System?	Specific Power (kW/kg)	Power Density (kW/L)	Maximum Continuous Power (kW)	Volume (L)	Mass (kg)	Diameter (m)	Height (m)	Width (m)	Length (m)	Active area (cm^2)	Number of cells	Rated voltage (V)	Minimum Operating Voltage (V)	Maximum Operating Voltage (V)	Cell Degradation Rate (µV/hr)	Rated Current (A)	Current density (A/cm^2)	Peak Power (kW)	Minimum Continuous Power (kW)	Operating temperature (°C)	Degree of Fuel Purity	Degree of Oxidant Purity	Anode Operating Pressure (MPa)	Cathode Operating Pressure (MPa)	Power	Maximum Efficiency
-	ZSW for DeepC[63, 64, 65]	FC system			3.60							100	120		72			50	0.50									

Table 3: H2/O2 PEM Fuel Cell stacks and systems

63 [Joerissen, et al.]

64 [Geiger, 2002]

65 http://www.deepc-auv.de/deepc/englisch/e_home.html, accessed 20-Oct-2005

Design Tools and Methodology

Relationship of Specific Energy, Energy Density, and Buoyancy

Being that the most important attribute of the FCEPS is high energy storage, it is important to carefully consider effects of design tradeoffs on Specific Energy (SE) and Energy Density (ED).

Specific Energy is energy per unit mass:

$$SE = \frac{E}{m} \tag{1}$$

Energy Density is energy per unit volume:

$$ED = \frac{E}{V} \tag{2}$$

Both metrics refer to the same quantity of energy, and density is Energy Density divided by Specific Energy:

$$D = \frac{m}{V} = \frac{\mathrm{ED}}{\mathrm{SE}} \tag{3}$$

When ED is plotted as a function of SE on x-y axes, the slope from the x-y intercept to any point is the corresponding density at the point. Figure 8 shows this relationship. The dotted line represents the density of seawater, or about 1.03 kg/L. Any point above the line has negative buoyancy, or is denser than seawater. Any point below the line has positive buoyancy, or is less dense than seawater.

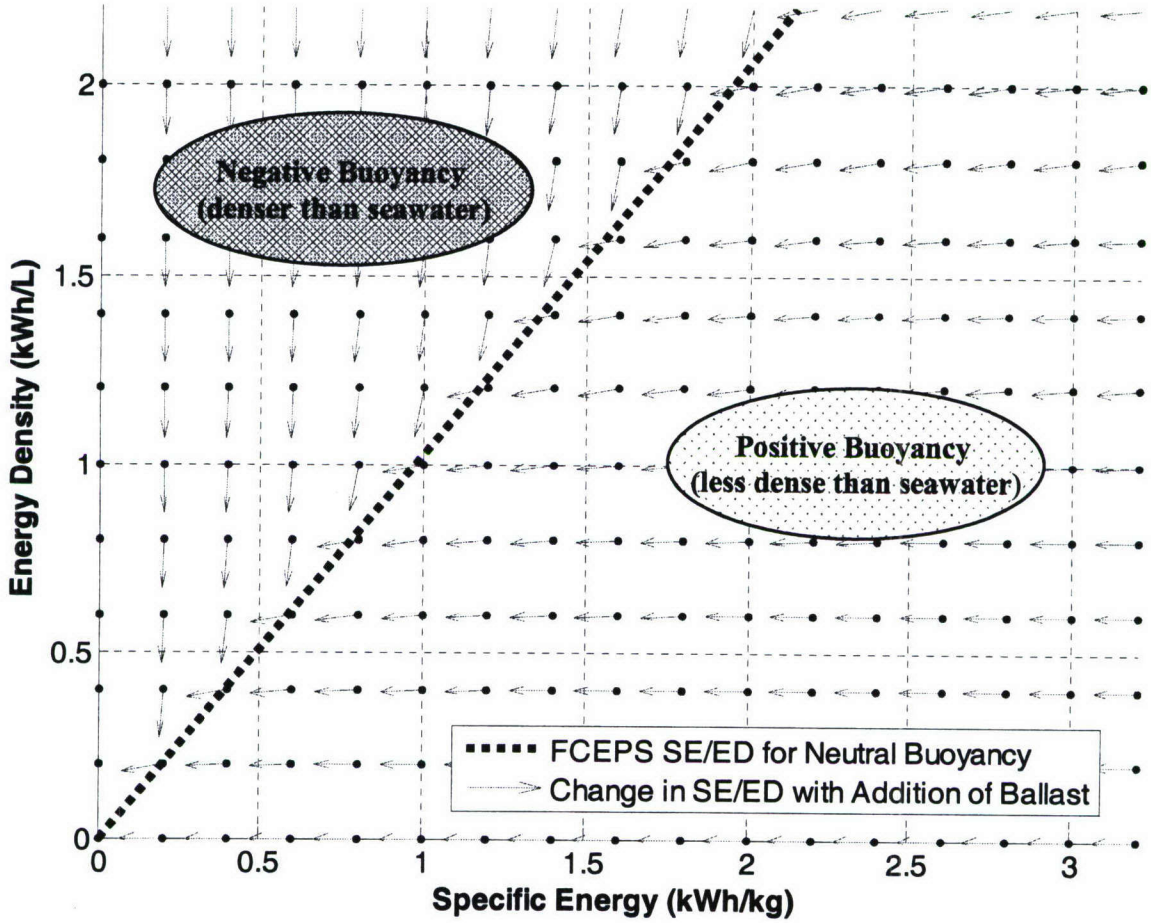

Figure 8: Specific Energy, Energy Density, and buoyancy

If a given FCEPS design did not have the required buoyancy as represented by the dotted line in Figure 8, then ballast or float material would have to be added to the design in order to meet the buoyancy requirement. Assuming the FCEPS mass and dimensions are limited, this ballast or float would displace mass and volume otherwise available for FCEPS components, particularly energy storage. In the case of negative buoyancy, floats would have to be added, occupying a large volume and a small mass. As a result, the entire FCEPS (including floats) would have considerably less Energy Density and slightly less Specific Energy. In the case of positive buoyancy, on the other hand, ballast would have to be added, occupying a large mass and a small volume. As a result, the entire FCEPS would have considerably less Specific Energy and slightly less Energy Density. This interaction is represented by the vectors in Figure 8. The vectors are based on a float density of 0.288 kg/L (corresponding to marine structural foam) and a weight density 8.93 kg/L (copper). These values are used throughout this assessment.

Particular energy storage options can be evaluated using graphs as in Figure 8. Versions of the Energy Density/Specific Energy graph have been used before for terrestrial applications where it is not important to draw conclusions about density. One graph is shown in Figure 9 [Pinkerton and Wicke].

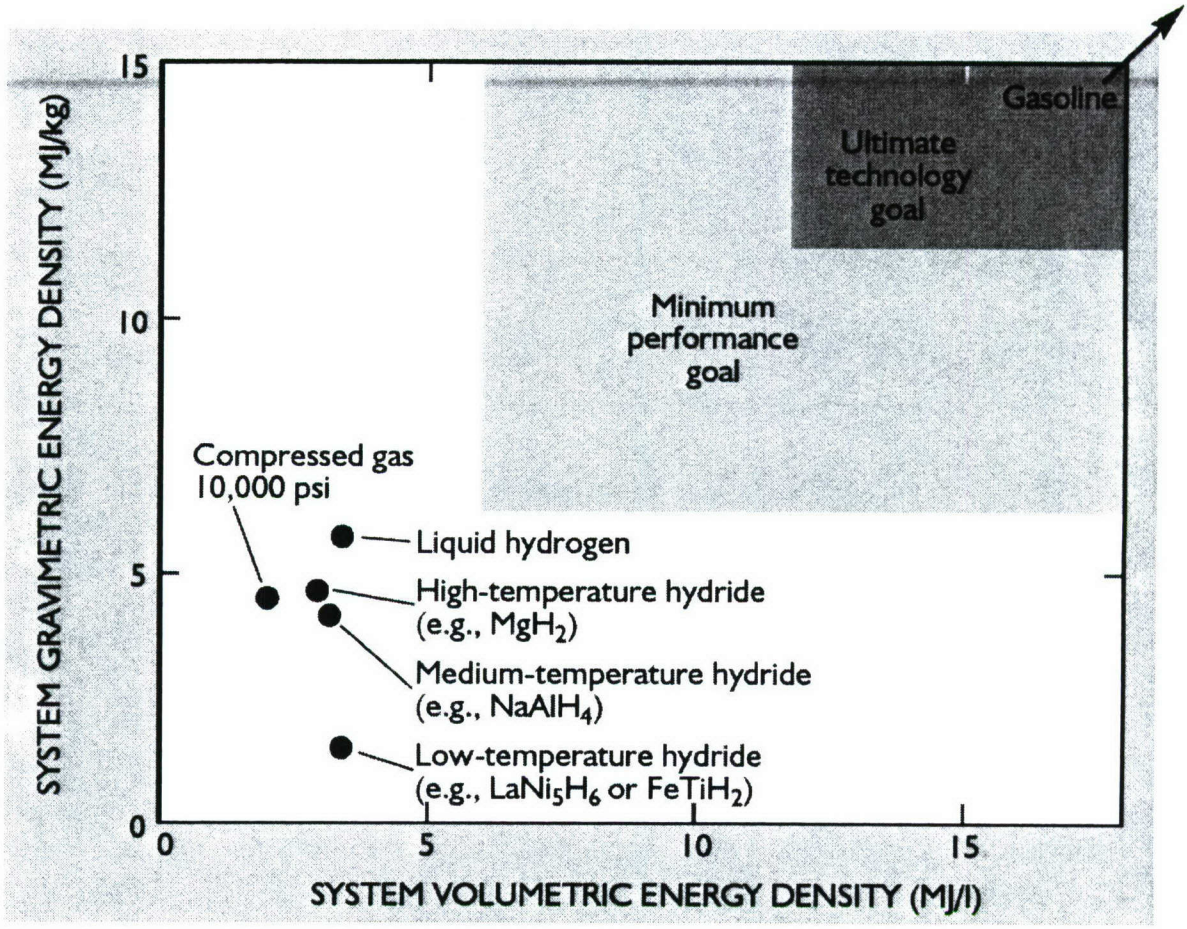

Figure 9: Gravimetric Energy Density as a function of Volumetric Energy Density for energy storage mediums [Pinkerton and Wicke]

Since the UUV FCEPS must provide AIP, oxygen must be carried onboard as well as hydrogen. Previously, oxygen storage has been evaluated in terms of weight (or mass efficiency):

$$\text{stored oxygen mass} \,/\, \text{oxidizer system mass}$$

and volumetric efficiency [Reader, et al., p. 884]:

$$\text{stored oxygen mass} \,/\, (\text{LOX density} \times \text{oxidizer system volume}).$$

Although the energy is considered to be stored in the hydrogen, the oxygen is an integral part of the energy system as well. Instead of using weight efficiency and volume efficiency, oxygen storage can be evaluated in terms of SE and ED based on the stoichiometric ratio of the fuel cell reaction.

Table 4 below summarizes the metrics for quantitatively expressing the effectiveness of hydrogen and oxygen storage in terms of volume and mass.

	Fuel	Oxidant
Volume	Energy Density (ED_{H2}) (kWh/L)	Energy Density at Stoichiometric Ratio (ED_{O2}) (kWh/L)
Mass	Specific Energy (SE_{H2}) (kWh/kg)	Specific Energy at Stoichiometric Ratio (SE_{O2}) (kWh/kg)

Table 4: Hydrogen and oxygen storage metrics

Using the metrics in Table 4, it becomes possible to calculate the overall Storage System (hydrogen + oxygen) Specific Energy and Energy Density:

$$SE_{SS} = \frac{SE_{H2} SE_{O2}}{SE_{H2} + SE_{O2}} \tag{4}$$

$$ED_{SS} = \frac{ED_{H2} ED_{O2}}{ED_{H2} + ED_{O2}} \tag{5}$$

If a product water storage tank is included in the Storage System, then the SE (energy produced divided by mass of product water and tank) and ED (energy produced divided by volume of product water tank) of the product water storage is included in the overall Storage System SE and ED calculations as shown below. The need for a water storage tank is discussed in the Product Water Storage section on page 50.

$$ED_{SS} = \frac{1}{\frac{1}{ED_{H2}} + \frac{1}{ED_{O2}} + \frac{1}{ED_{H2O}}} \tag{6}$$

$$SE_{SS} = \frac{1}{\frac{1}{SE_{H2}} + \frac{1}{SE_{O2}} + \frac{1}{SE_{H2O}}} \tag{7}$$

The derivation of the equations above is included in Appendix A under Storage Metrics.

Relationship of Specific Power, Power Density, and Buoyancy

Substituting Power for Energy, the same relationship between Specific Power (SP), Power Density (PD), and density exists as for SE, PE, and density as described above. This is a useful relationship for designing the FCS or choosing among FCS options.

Just as the overall Storage System SE and ED can be determined from the SE and ED of Storage System components (hydrogen storage, oxygen storage, and product water storage), the Specific Power (SP) and Power Density (PD) of the FCS can be determined from the SP and PD of the FCS components. The Specific Power is calculated as follows:

$$SP_{FCS} = \frac{1}{\frac{1}{SP_{Comp1}} + \frac{1}{SP_{Comp2}} + \ldots + \frac{1}{SP_{CompN}}} = \frac{1}{\sum_{n=1}^{N} \frac{1}{SP_{Compn}}} \tag{8}$$

The Power Density is calculated as follows:

$$PD_{FCS} = \frac{1}{\frac{1}{PD_{Comp1}} + \frac{1}{PD_{Comp2}} + \ldots + \frac{1}{PD_{CompN}}} = \frac{1}{\sum_{n=1}^{N} \frac{1}{PD_{Compn}}} \tag{9}$$

Impact of Efficiency on Net Energy

FCS Choice

Suppose that two Fuel Cell Systems (FCS0 and FCS1) are available that provide different energy conversion efficiencies (ε_{FCS1} and ε_{FCS0}), but have different volumes (V_{FCS1} and V_{FCS0}) and masses (m_{FCS1} and m_{FCS0}). If $\frac{\varepsilon_{FCS1}-\varepsilon_{FCS0}}{\varepsilon_{FCS1}} > \frac{m_{FCS1}-m_{FCS0}}{m_{SS0}}$ and $\frac{\varepsilon_{FCS1}-\varepsilon_{FCS0}}{\varepsilon_{FCS1}} > \frac{V_{FCS1}-V_{FCS0}}{V_{SS0}}$, then FCS1 will provide a net usable FCEPS energy benefit over FCS0. Here, m_{SS0} and V_{SS0} are the mass and volume of the Storage System in the FCEPS design with FCS0. The assumption is made that the Storage System SE and ED will not change with the selection of the new FCS. The derivation of this tradeoff is given in Appendix A under FCS Choice.

Additional FCS Components

Suppose a new component or system enhancement is available that will increase the efficiency of the FCEPS, but will add additional mass and volume. The overall FCEPS volume and mass cannot change with the addition of the new component because the FCEPS has fixed size and density. This means that the additional mass and volume introduced by the new component must be offset in a reduction of mass and volume from the Storage System, ballast, and floats. If $1-\frac{\varepsilon_{FCS\,0}}{\varepsilon_{FCS\,1}} > \frac{V_{New}}{V_{SS\,0}}\frac{(D_B - D_{New})}{(D_B - D_{SS})}$, then the new component or system enhancement will increase the net usable energy of the FCEPS. The variables are defined as follows:

V_{New}	Volume of new component
V_{SS0}	Initial volume of Storage System
D_{New}	Density of new component
D_{SS}	Density of Storage System
D_B	Density of ballast or floats
ε_{FCS0}	Initial FCS efficiency
ε_{FCS1}	FCS efficiency with new component

The statement is based on the following assumptions:
The Storage System Energy Density is the same with and without the new component.
The Storage System density is the same with and without the new component.
The ballast or float density is the same with and without the new component.
$D_{SS} \neq D_B$. If $D_{SS} = D_B$, then it would be more effective to increase the size of the Storage System and remove the ballast or floats anyway.

The derivation of this tradeoff is given in Appendix A under FCS Choice. Figure 10 shows this tradeoff graphically in terms of volume.

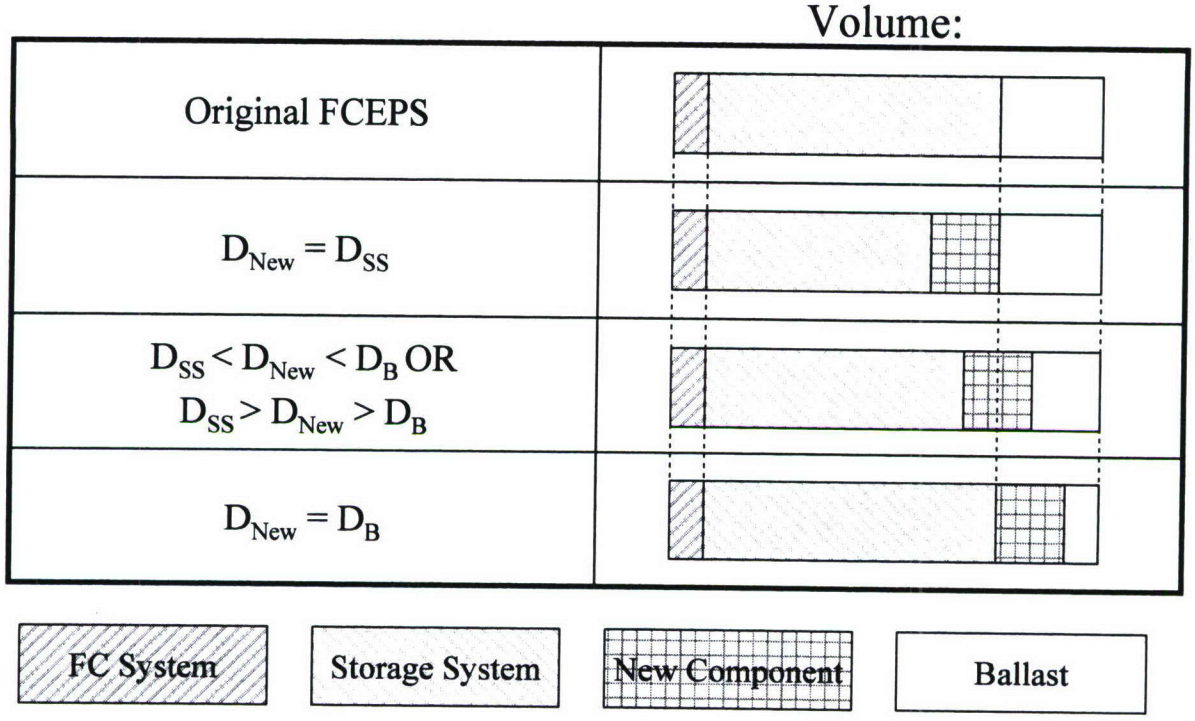

Figure 10: Effect of additional FCEPS component on Storage System volume

Concept Design Steps

The following steps provide a method for generating FCEPS design concepts which specify high-level system considerations such as reactant storage type and size, FCS choice, etc:

1. Determine m_O and V_O, the mass and volume of overhead FCEPS components (structure, insulation, etc.), based on thermal, pressure, and other requirements.
2. Choose the FCS option.
   a. Choose the FCS concept with the highest Specific Power and Power Density at seawater FCS density. This can be done graphically on a plot of SP and PD with contour lines overlaid as will be shown in Figure 21.
   b. Determine the volume and mass of the FCS at the required FCEPS Specific Power and Power Density levels.

$$V_{FCS} = \frac{\max\left(PD_{FCEPS\_REQ} V_{FCEPS},\ SP_{FCEPS\_REQ} m_{FCEPS}\right)}{PD_{FCS}} \tag{10}$$

$$m_{FCS} = V_{FCS} \cdot \frac{PD_{FCS}}{SP_{FCS}} \tag{11}$$

3. Determine the desired Storage System density based on the remaining volume and mass available in the FCEPS.

$$V_{SS\_Desired} = V_{FCEPS} - V_{FCS} - V_O \tag{12}$$

$$m_{SS\_Desired} = m_{FCEPS} - m_{FCS} - m_O \tag{13}$$

$$D_{SS\_Desired} = \frac{m_{SS\_Desired}}{V_{SS\_Desired}} \tag{14}$$

4. Choose the Storage System concept with the highest Specific Energy and Energy Density at the desired Storage System density. This can be done graphically on a plot of SE and ED with contour lines overlaid as will be shown in Figure 18, for example. It can also be done numerically using Equations 75 and 76 by comparing the adjusted Specific Energy values of each Storage System option once the required ballast or floats are included. Here, D_{SS} is the density of the Storage System without the ballast and floats. D_B is the density of the ballast (if $D_{SS} < D_{SS\_Desired}$) or floats (if $D_{SS} > D_{SS\_Desired}$). SE_{SS_B} and ED_{SS_B} are the net Specific Energy and Energy Density of the Storage System and ballast/floats required to bring the FCEPS to the desired density, $D_{SS\_Desired}$. . ED_{SS} is the Energy Density of the Storage System option (without ballast or floats included). These equations are derived and defined in Appendix A under Equivalent Specific Energy and Energy Density at Desired Density.

$$SE_{SS\_B} = \frac{ED_{SS}\left(1 - \frac{D_B}{D_{SS\_Desired}}\right)}{(D_{SS} - D_B)} \tag{75}$$

$$ED_{SS\_B} = SE_{SS\_B} D_{SS\_Desired} \tag{76}$$

5. Choose and size the ballast or floats.
   a. Choose ballast or floats based on whether positive or negative buoyancy is required to bring the FCEPS to neutral buoyancy.
      If $D_{SS} > D_{SS\_Desired}$ then floats must be added ($D_B < D_{SS}$).

      If $D_{SS} < D_{SS\_Desired}$ then ballast must be added ($D_B > D_{SS}$).

      If $D_{SS} = D_{SS\_Desired}$ then ballast and floats are not needed.
   b. Determine the volume and mass of the ballast or floats required to bring the FCEPS to neutral buoyancy. These equations are derived and defined in Appendix A under Ballast/Float Sizing.

$$V_B = \frac{m_{FCS} + m_O + D_{SS}(V_{FCEPS} - V_{FCS} - V_O) - m_{FCEPS}}{D_{SS} - D_B} \tag{81}$$

$$m_B = V_B D_B \tag{82}$$

6. Determine the net FCEPS Specific Energy and Energy Density given the volume and mass available for the Storage System and the FCS efficiency.

$$V_{SS} = V_{FCEPS} - V_{FCS} - V_O - V_B \tag{15}$$

$$m_{SS} = m_{FCEPS} - m_{FCS} - m_O - m_B \tag{16}$$

$$ED_{FCEPS} = \varepsilon_{FCS} \frac{ED_{SS} V_{SS}}{V_{FCEPS}} \tag{17}$$

$$SE_{FCEPS} = \varepsilon_{FCS} \frac{SE_{SS} m_{SS}}{m_{FCEPS}} \tag{18}$$

7. Iterate the FCS choice.
   a. If ballast or floats were required, then attempt to choose another FCS with a density (D_{FCS}) that eliminates or reduces the need for ballast/floats.
      i. Repeat 2.a, selecting the FCS with the highest Specific Power and Power Density at $D_{FCS\_Desired} = \frac{m_{FCEPS} - m_{SS} - m_O}{V_{FCEPS} - V_{SS} - V_O}$ instead of seawater density.
      ii. Repeat 2.b through 6 to evaluate the FCEPS with the new FCS.
   b. Attempt to choose alternative FCSs with densities (D_{FCS}) that complement the densities of each of the unselected SS options with both higher SE and ED than the selected SS option and associated ballast or floats.
      i. Repeat 2.a, selecting the FCS with the highest Specific Power and Power Density at $D_{FCS\_Desired} = \frac{m_{FCEPS} - m_{SSn} - m_O}{V_{FCEPS} - V_{SSn} - V_O}$ instead of seawater density.
      ii. Repeat 2.b through 6 to evaluate the FCEPS with the new FCS.
   c. If any unselected FCSs present a potential advantage due to higher operating efficiency than the selected FCS ($\frac{\varepsilon_{FCS1} - \varepsilon_{FCS0}}{\varepsilon_{FCS1}} > \frac{m_{FCS1} - m_{FCS0}}{m_{SS}}$ or $\frac{\varepsilon_{FCS1} - \varepsilon_{FCS0}}{\varepsilon_{FCS1}} > \frac{V_{FCS1} - V_{FCS0}}{V_{SS}}$), then for each:
      i. Select the new FCS in 2.a.
      ii. Repeat 2.b through 6 to evaluate the FCEPS with the new FCS.
8. Choose the FCEPS with the highest SE and ED from 7.a, 7.b, and 7.c7.c. Compare the Power and Energy capabilities of the conceptual FCEPS to the requirements.

Rechargeable Battery Energy/Power System (RBEPS)

In order to provide a fair benchmark for the FCEPS design concepts, an assessment of lithium based rechargeable batteries is included here. Lithium Ion (Li-Ion) and Lithium Ion Polymer (Li-Poly) batteries are chosen as a comparison because they are being heavily considered as alternatives to the Silver-Zinc (Ag-Zn) secondary and Lithium Thionyl Chloride (Li-$SOCL_2$) primary batteries currently used in UUVs [Egan]. Li-Ion and Li-Poly batteries are seen as preferable to Ag-Zn batteries due to their lower life-cycle cost [Gitzendanner et al.]. Lithium Ion (Li-Ion) and offer the highest ED of any COTS rechargeable battery technology, and have competitive SE to Ag-Zn batteries[66, and] [Gitzendanner et al.]. Primary battery systems such as Lithium Thionyl Chloride (Li-$SOCL_2$) are not considered here because of their high recurring cost as compared to a FCEPS.

[66] Yardney Technical Products, Inc. "Sec 10 Li-ion Battery Technology – Secondary Cells," 2003 Battery Technology Workshop

The density of a RBEPS must be considered just as the FCEPS. Typically, battery systems are denser than seawater, so floats or void space must be added at a loss to ED. In the design of a Li-Ion battery system for the Advanced SEAL Delivery System (ASDS), the cells filled the available volume and caused the battery to be overweight [Gitzendanner et al.].

The Li-Ion and Li-Poly cells considered in this assessment are small (much less than 1 kg), with the exception of the Guangzhou Markyn Battery and Valence Technology models. Multiple cells are used to fill the available volume and mass. It has been stated that larger Li-Ion cells have SE values up to 200 Wh/kg, but suppliers for such cells was not found [Gitzendanner et al.]. Regardless, the supporting system (thermal management and electrical interconnects) will decrease the overall SE and ED from the SE and ED values for any individual cells, and the supporting system is not considered here. The cell packaging is considered to be perfect (no unused space).

Some approximations and assumptions were made in order to make a first cut among the numerous battery models available. The stored energy was assumed to be the published nominal voltage (v) times the nominal capacity (Ah). Supplier specified energy storage values were not used because of the inconsistent methods of determining these values. Only the batteries with sufficient available data (nominal voltage, capacity, mass, dimensions, and discharge curves) were considered. Among the models of the same type (Li-Ion cylindrical, Li-Ion prismatic, or Li-Poly prismatic) from a single supplier, the batteries with significantly worse SE and ED at neutral buoyancy (1.03 kg/L) were excluded. Battery capacity data was taken from the published nominal capacity. The published capacity values were generally measured between C/5 and C/5.75 discharge rates, with the exception of the Guangzhou Markyn Battery models, which were measured at C/2 or C/2.4. This may have contributed to the slightly worse SE and ED values for the Guangzhou Markyn models. The batteries are listed in Table 5 and the SE and ED values are plotted in Figure 11. As shown by the graph, the density of Li-Ion and Li-Poly batteries is significantly greater than seawater density.

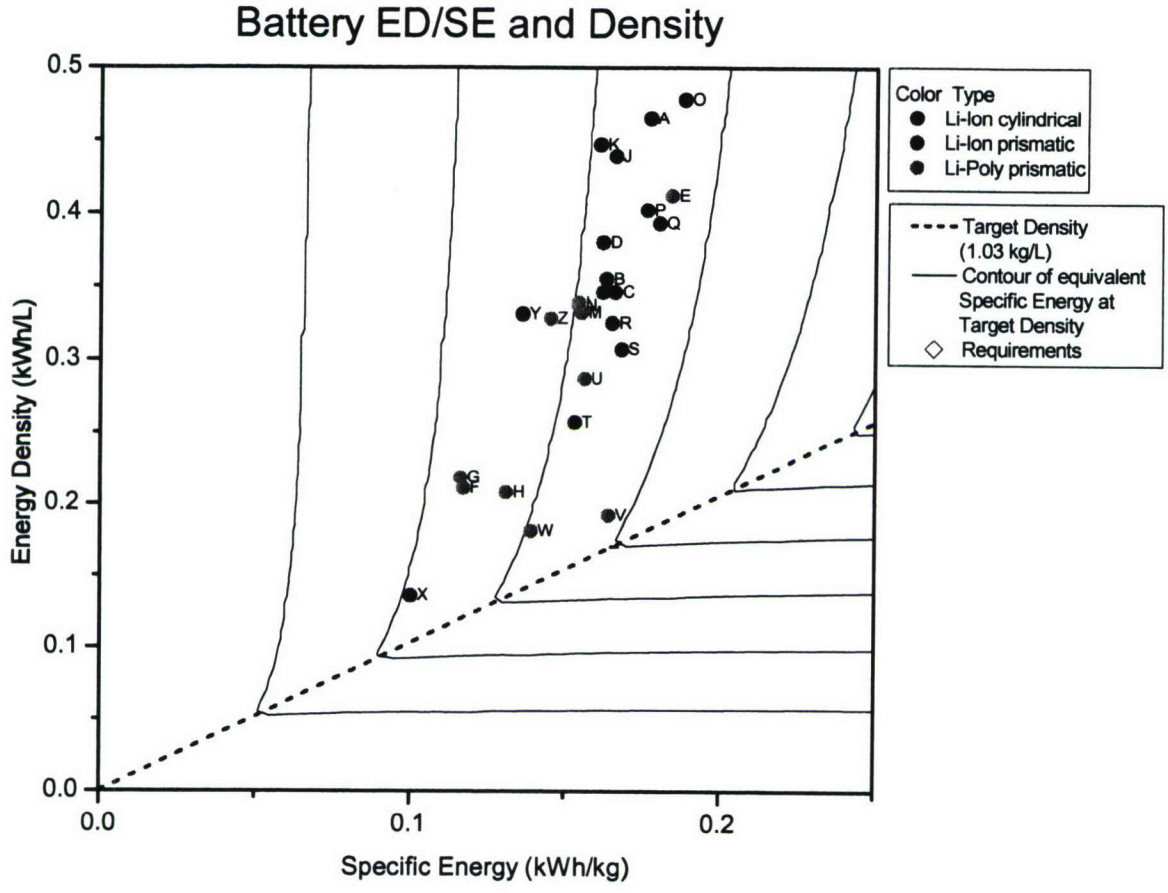

Figure 11: SE and ED of rechargeable lithium battery options

Sym-bol	Company & Model	SE (kWh/ kg)	ED (kWh/ L)	Type & Shape
A	EEMB LIR18650[67]	0.177	0.465	Li-Ion cylindrical
B	EEMB LIR053436A[68]	0.163	0.355	Li-Ion prismatic
C	EEMB LIR063048A[69]	0.166	0.346	Li-Ion prismatic
D	EEMB LIR103450A[70]	0.162	0.380	Li-Ion prismatic
E	EEMB LP383450[71]	0.184	0.412	Li-Poly prismatic
F	Guangzhou Markyn Battery PL10ICP11/106/58-3[72]	0.117	0.211	Li-Poly prismatic

[67] "Lithium ion Battery LIR18650 Brief Datasheet," http://eemb.com/PDF/LIR/LIR18650%20Brief.pdf, downloaded 15-Nov-2005

[68] "Lithium ion Battery LIR053436A Brief Datasheet," http://eemb.com/PDF/LIR/LIR053436A%20Brief.pdf, downloaded 16-Nov-2005

[69] "Lithium ion Battery LIR063048A Brief Datasheet," http://eemb.com/PDF/LIR/LIR063048A%20Brief.pdf, downloaded 16-Nov-2005

[70] "Lithium ion Battery LIR103450A Brief Datasheet," http://eemb.com/PDF/LIR/LIR103450A%20Brief.pdf, downloaded 16-Nov-2005

[71] "Lithium ion Polymer Battery LP383450 Brief Datasheet," http://eemb.com/PDF/Lp/Lp383450%20Brief.pdf, downloaded 16-Nov-2005

G	Guangzhou Markyn Battery PL10ICP08/106/58-3[73]	0.116	0.218	Li-Poly prismatic
H	Guangzhou Markyn Battery PL10ICP06/83/116-3[74]	0.131	0.208	Li-Poly prismatic
I	Huanyu Power Source HLP063040[75]	0.162	0.346	Li-Ion prismatic
J	Huanyu Power Source HLP053467[76]	0.166	0.439	Li-Ion prismatic
K	Huanyu Power Source HLC18650[77]	0.161	0.447	Li-Ion cylindrical
L	Huanyu Power Source HYPL-053759[78]	0.154	0.339	Li-Poly prismatic
M	Huanyu Power Source HYPL-395370[79]	0.155	0.332	Li-Poly prismatic
N	Huanyu Power Source HYPL-383562[80]	0.154	0.337	Li-Poly prismatic
O	Panasonic CGR18650D[81]	0.188	0.478	Li-Ion cylindrical
P	Panasonic CGA5234361[82]	0.176	0.402	Li-Ion prismatic
Q	Panasonic CGA103450A[83]	0.180	0.393	Li-Ion prismatic
R	Saft MP 176065[84]	0.165	0.325	Li-Ion prismatic
S	Ultralife Batteries UBP543048/PCM[85]	0.168	0.307	Li-Ion prismatic
T	Ultralife Batteries UBP463048/PCM[86]	0.153	0.257	Li-Ion prismatic
U	Ultralife Batteries UBC425085[87]	0.156	0.287	Li-Poly prismatic
V	Ultralife Batteries UBC641730[88]	0.164	0.192	Li-Poly prismatic

[72] "PL10ICP11/106/58-3 Data Sheet," http://www.gmbattery.com/production/dl/cpNew/PL10ICP11-106_58_3.pdf, downloaded 30-Nov-2005

[73] "PL10ICP08/106/58-3 Data Sheet," http://www.gmbattery.com/production/dl/cpNew/PL10ICP08-106-58-3.pdf, downloaded 30-Nov-2005

[74] "PLC10ICP06/83/116-3 Data Sheet," http://www.gmbattery.com/production/dl/cpNew/PL10ICP06_83_116-3.pdf, downloaded 15-Nov-2005

[75] "Huanyu Battery Specifications HLP063040," http://www.huanyubattery.com/load/HLP063040.pdf, downloaded 16-Nov-2005

[76] " Huanyu Battery Specifications HLP053467," http://www.huanyubattery.com/load/HLP053467.pdf, downloaded 16-Nov-2005

[77] " Huanyu Battery Specifications HLC18650," http://www.huanyubattery.com/load/HLC18650.pdf, downloaded 16-Nov-2005

[78] " Huanyu Battery Specifications HYPL-053759," http://www.huanyubattery.com/load/HYPL-053759.pdf, downloaded 16-Nov-2005

[79] " Huanyu Battery Specifications HYPL-395370," http://www.huanyubattery.com/load/HYPL-395370.pdf, downloaded 16-Nov-2005

[80] " Huanyu Battery Specifications HYPL-383562," http://www.huanyubattery.com/load/HYPL-383562.pdf, downloaded 16-Nov-2005

[81] "Lithium Ion Batteries: Individual Data Sheet CGR18650D," http://www.panasonic.com/industrial/battery/oem/images/pdf/Panasonic_LiIon_CGR18650D.pdf, June 2005

[82] "Lithium Ion Batteries: Individual Data Sheet CGA523436," http://www.panasonic.com/industrial/battery/oem/images/pdf/Panasonic_LiIon_CGA523436.pdf, November 2003

[83] "Lithium Ion Batteries: Individual Data Sheet CGA103450A," http://www.panasonic.com/industrial/battery/oem/images/pdf/Panasonic_LiIon_CGA103450A.pdf, November 2003

[84] "Rechargeable lithium-ion battery MP 176065," Doc. No 54037-2-0305, http://www.saftamerica.com/120-Techno/20-10_produit.asp?paramtechnolien=20-10_lithium_system.asp&paramtechno=Lithium+systems&Intitule_Produit=MP, downloaded 18-Nov-2005

[85] "UBP543048/PCM Technical Datasheet," http://www.ultralifebatteries.com/documents/techsheets/UBI-5092_UBP543048.pdf, UBI-5092 REV F, 25-Jul-2005

[86] "UBP463048/PCM Technical Datasheet," http://www.ultralifebatteries.com/documents/techsheets/UBI-5105_UBP463048.pdf, UBI-5105 REV E, 25-Jul-2005

[87] "UBC425085 Technical Datasheet," http://www.ultralifebatteries.com/documents/techsheets/UBI-5127_UBC425085.pdf, UBI-5127 REV C, 25-Jul-2005

W	Ultralife Batteries UBC422030[89]	0.139	0.181	Li-Poly prismatic
X	Valence Technology U27-FN130[90]	0.100	0.136	Li-Ion prismatic
Y	Wuhan Lixing (Torch) Power Sources LIR17335[91]	0.136	0.331	Li-Ion cylindrical
Z	YOKU Energy Technology Limited 653135[92]	0.145	0.328	Li-Poly prismatic

Table 5: Lithium rechargeable battery options

Using the approximated SE and ED values described above, the batteries with the best ED at required density values over the range of 0.3 kg/L to 3.5 kg/L were chosen. The Ultralife Batteries model UBC641730 battery (symbol V) has the highest ED at required densities below approximately 1.20 kg/L, and the Panasonic model CGR18650D battery (symbol O) has the highest ED at required densities above that value.

These two battery models, Ultralife Batteries UBC641730 and Panasonic CGR18650D, were more closely evaluated. It was important to consider the energy available from the batteries at the required discharge rate, as heat losses increase as the discharge rate increases. The manufacturer discharge curves graphs were numerically integrated to verify the energy storage at the appropriate discharge rate. In order to fairly compare the RBEPS to the FCEPS using the Siemens BZM 34 FCS, a continuous power demand of 34 kW was considered. This power demand was divided by the number of cells in the RBEPS concept at each required density value. The resulting cell power was divided by the discharge cutoff voltage for the battery model of interest, giving a discharge current value. In all but the RBEPS concepts for required densities of 0.3 to 0.6 kg/L, the discharge rate was smaller than that of the lowest published discharge curve, and the lowest published discharge curve was used. The most appropriate discharge curve graph was numerically integrated to find the final energy value for comparison to the FCEPS. Note that if data was available for lower discharge rates, it would yield slightly higher energy values for the RBEPS.

One notable characteristic of Li-Ion and Li-Poly batteries is capacity fade over the life of the battery. As the battery ages, the electrical storage capacity decreases. This is usually expressed in terms of % fade per charge/discharge cycle. Figure 12 shows the capacity fade of the Ultralife Batteries model UBC641730, which is fairly typical. Capacity fade is shown as 80% at 500 cycles, and specified as > 300 cycles to 80% at the C/5 charge/discharge rate[93]. Full charge/discharge cycles have a more significant impact on capacity fade than partial charge/discharge cycles, and battery suppliers sometimes quote the cycle life with 80% Depth Of Discharge (DOD), rather than 100% DOD[94], [95], [96]. However, the usage profile of a UUV RBEPS would likely require nearly full charge/discharge cycles.

---

[88] "UBC641730 Technical Datasheet," http://www.ultralifebatteries.com/documents/techsheets/UBI-5113_UBC641730.pdf, UBI-5113 REV C, July 25, 2005

[89] "UBC422030 Technical Datasheet," http://www.ultralifebatteries.com/documents/techsheets/UBI-5116_UBC422030.pdf, UBI-5116 REV C, 25-Jul-2005

[90] "UCharge Family Datasheet," http://www.valence-tech.com/pdffiles/U-Charge_Datasheet.pdf, v.0.98, downloaded 30-Nov-2005

[91] http://www.lisun.com/2/asppd/Product6.htm, accessed 30-Nov-2005

[92] http://www.yokuenergy.com/doce/products.asp, accessed 30-Nov-2005

[93] "UBC641730 Technical Datasheet," http://www.ultralifebatteries.com/datasheet.php?ID=UBC005, July 25, 2005

[94] Isidor Buchmann, "How to prolong lithium-based batteries," http://www.batteryuniversity.com/parttwo-34.htm, 2005

[95] "Saphion Rechargeable Lithium Ion Battery IFR18650e," http://www.valence-tech.com/ucharge.asp, downloaded 15-Nov-2005

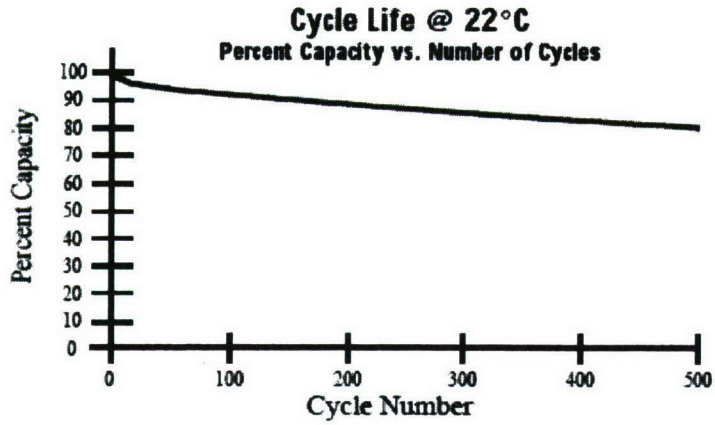

Figure 12: Capacity fade of Ultralife UBC641730[97]

Li-Poly cells can operate at up to 60 MPa with 90% of the rated capacity as at atmospheric pressure [Rutherford]. This corresponds to a depth of about 5940 m at a seawater density of 1.03 kg/L. This may be desirable in a RBEPS design; however, the Li-Poly cells must be maintained at a suitable operating temperature [Rutherford].

Fuel Cell Energy/Power System (FCEPS)

Storage System

Hydrogen Storage

This UUV FCEPS assessment considers four types of hydrogen storage: compressed, liquid, metal hydride, and chemical hydride. There are other hydrogen storage approaches that are currently excluded. Liquid hydrocarbon fuels have not been included yet because of the high complexity and overhead mass and volume associated with fuel reformation to condition the fuel for use with PEM fuel cells. Carbon nanostructures have not yet been demonstrated on a practical scale [Pinkerton and Wicke, p. 24]. Glass microspheres have also been mentioned, but no complete systems seem to be available[98].

The LHV of hydrogen is 33.32 kWh/kg. This sets an upper bound on the SE of hydrogen storage, which is the mass of the hydrogen itself without any tank mass or mass of other chemical elements.

Figure 13 and Figure 14 plot a set of hydrogen storage options on the SE and ED graph discussed in the Relationship of Specific Energy, Energy Density, and Buoyancy section. On the graphs, ideal options are those which do not take into account the full storage system, for instance, the theoretical density of hydrogen gas at 700 atm. Complete system options include the storage tank and supporting equipment. Table 6 lists the hydrogen storage options that have been included on the graphs.

---

[96] "UCharge Family Datasheet," http://www.valence-tech.com/pdffiles/U-Charge_Datasheet.pdf, v.0.98, downloaded 30-Nov-2005

[97] "UBC641730 Technical Datasheet," http://www.ultralifebatteries.com/datasheet.php?ID=UBC005, July 25, 2005

[98] http://www.fuelcellstore.com/information/hydrogen_storage.html, accessed 25-Oct-2005

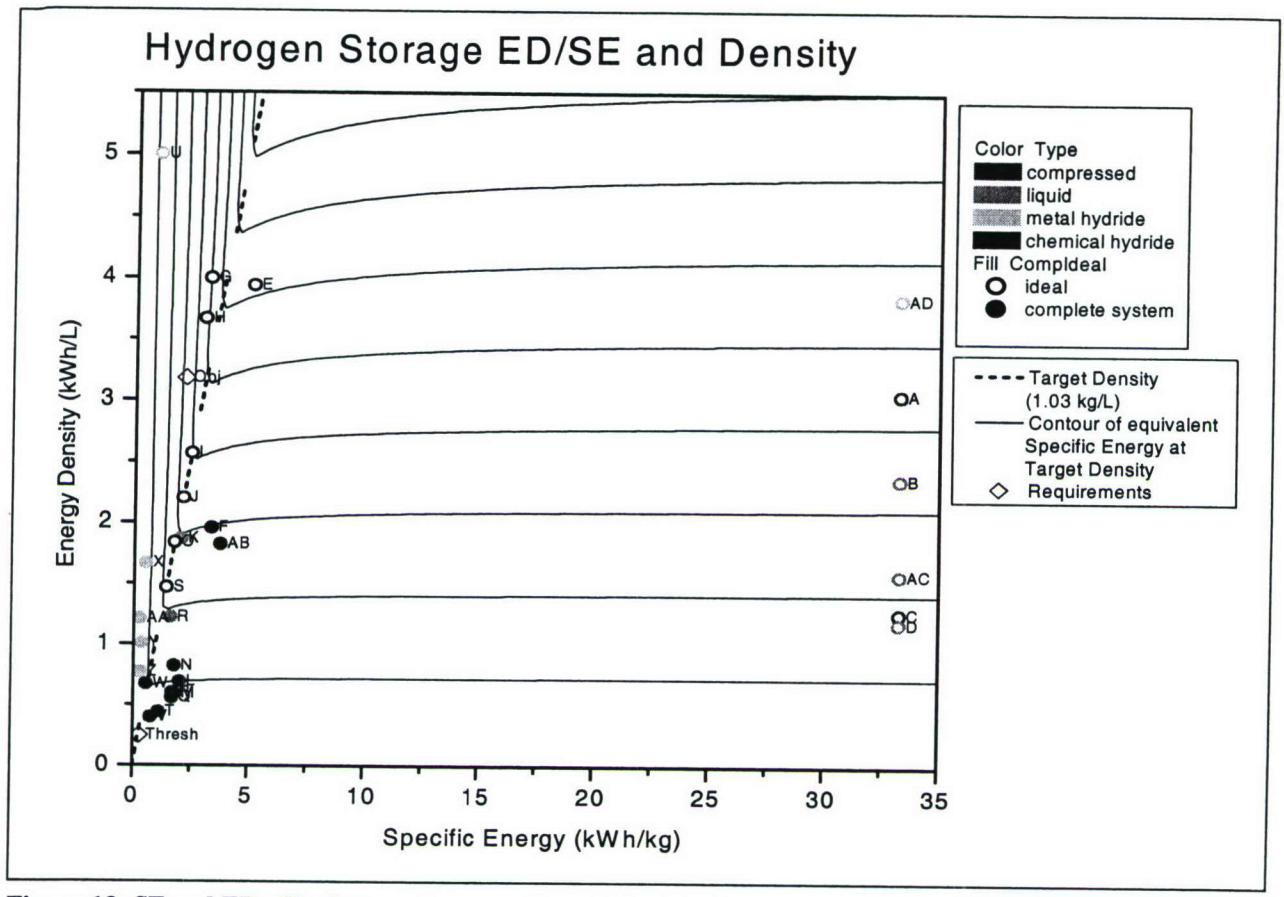

Figure 13: SE and ED of hydrogen storage options (all options)

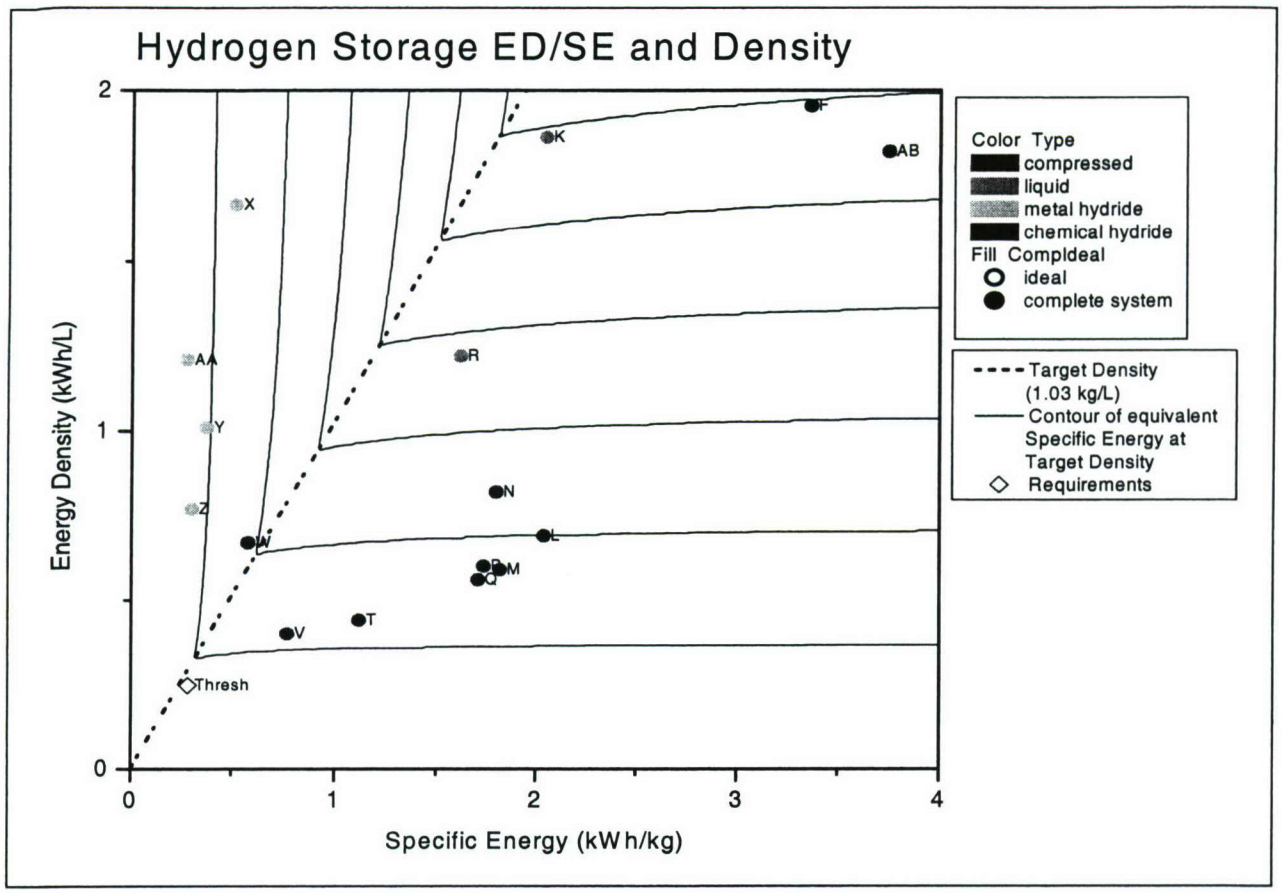

Figure 14: SE and ED of hydrogen storage options (complete systems only)

Symbol	Description	Specific Energy (kWh/kg)	Energy Density (kWh/L)	Type
A	Ideal 700 atm H2 at LOX temp[99]	33.32	3.05	Compressed
B	Ideal liquid H2[100]	33.32	2.36	Liquid
C	Ideal 700 atm H2[101]	33.32	1.26	Compressed
D	Ideal mass Linde[102]	33.32	1.18	Liquid
E	Ideal lithium hydride (60%) slurry[103]	5.10	3.94	chemical hydride
F	Safe Hydrogen lithium hydride (60%) slurry system[104]	3.36	1.95	chemical hydride
G	Ideal Ca metal ammine[105]	3.23	4.00	chemical hydride
H	Ideal Mg metal ammine[106]	3.03	3.67	chemical hydride
I	Ideal sodium borohydride (by wt: 35% NaBH_4; 3% NaOH; 62% H_2O)[107]	2.50	2.57	chemical hydride
J	Ideal sodium borohydride (by wt: 30% NaBH_4; 3% NaOH; 67% H_2O)[108]	2.13	2.20	chemical hydride
K	Magna Steyr Liquid H2[109]	2.05	1.86	Liquid
L	TUFFSHELL 539L[110]	2.04	0.69	Compressed
M	Dynetek V174[111]	1.82	0.59	Compressed
N	TUFFSHELL 118L[112]	1.80	0.82	Compressed

[99] based on the Beattie-Bridgeman equation and constants presented in *Physical Chemistry* [Castellan, p. 46-48]

[100] Based on liquid H2 density [Züttel, p. 25]

[101] based on the Beattie-Bridgeman equation and constants presented in *Physical Chemistry* [Castellan, p. 46-48]

[102] "Liquid Hydrogen Storage," http://www.euweb.de/fuel-cell-bus/storage.htm, accessed 24-Jun-2005

[103] [McClaine, p 11]

[104] [McClaine, p 11]

[105] [Christensena, et al.]

[106] [Christensena, et al.]

[107] "Millennium Cell Hydrogen on Demand Fact Sheet," www.millenniumcell.com, 2/03 R, downloaded 26-Jul-2005

[108] "Millennium Cell Hydrogen on Demand Fact Sheet," www.millenniumcell.com, 2/03 R, downloaded 26-Jul-2005

[109] http://www.magnasteyr.com/frames.php?seite=http%3A//www.magnasteyr.com/automobilentwicklung/1342_ENG_HTML.asp, accessed Jun-2005

[110] "TUFFSHELL H2 Fuel Tanks Product Information," http://www.lincolncomposites.com/media/Tuffshell%20h2%20facts.pdf, downloaded 20-Jun-2005

[111] "DyneCell® Lightweight Fuel Storage Systems," http://www.dynetek.com/pdf/350.pdf, February 2004

[112] "TUFFSHELL H2 Fuel Tanks Product Information," http://www.lincolncomposites.com/media/Tuffshell%20h2%20facts.pdf, downloaded 20-Jun-2005

O	Ideal sodium borohydride (by wt: 25% NaBH_4; 3% NaOH; 72% H_2O) [113]	1.77	1.83	chemical hydride
P	Dynetek W205 [114]	1.74	0.60	Compressed
Q	SCI ALT909 [115]	1.71	0.56	Compressed
R	GM HydroGen3 liquid [116]	1.62	1.22	Liquid
S	Ideal sodium borohydride (by wt: 20% NaBH_4; 3% NaOH; 77% H_2O) [117]	1.43	1.47	chemical hydride
T	SCI ALT898 [118]	1.12	0.44	compressed
U	Ideal Mg_2FeH_6 (Type A_2B) and Al(BH_4)_3 [119]	0.97	5.00	metal hydride
V	Faber Industrie 20 MPa [120]	0.77	0.40	compressed
W	Faber Industrie 45 MPa [121]	0.58	0.67	compressed
X	Ovonic Onboard Solid H2 [122]	0.52	1.67	metal hydride
Y	HCI SOLID-H BL-750: Alloy H [123]	0.38	1.01	metal hydride
Z	Hydrocell HC-MH1200 [124]	0.30	0.77	metal hydride
AA	H Bank HB-SG02-0500-N [125]	0.28	1.21	metal hydride
AB	TUFFSHELL 118L at LOX temp [126], [127]	3.75	1.82	compressed
AC	Ideal NASA spherical liquid H2 [128]	33.32	1.57	liquid

[113] "Millennium Cell Hydrogen on Demand Fact Sheet," www.millenniumcell.com, 2/03 R, downloaded 26-Jul-2005

[114] "DyneCell® Lightweight Fuel Storage Systems," http://www.dynetek.com/pdf/350.pdf, February 2004

[115] http://www.scicomposites.com/alternative_fuel_cylinders.html, accessed 2-Dec-2005

[116] " Technical Data of HyrdoGen3 liquid," http://www.gmeurope.com/marathon/downloads/factsheets/factsheet_hydrogen3_liquid.pdf, downloaded 2-Dec-2005

[117] "Millennium Cell Hydrogen on Demand Fact Sheet," www.millenniumcell.com, 2/03 R, downloaded 26-Jul-2005

[118] http://www.scicomposites.com/alternative_fuel_cylinders.html, accessed 2-Dec-2005

[119] [Züttel, p. 31]

[120] "Faber Cylinders Dbase & Drawings," http://www.faber-italy.com/light/fullver.htm, accessed 2-Dec-2005

[121] "Faber Cylinders Dbase & Drawings," http://www.faber-italy.com/light/fullver.htm, accessed 2-Dec-2005

[122] [Young, Rosa C.]

[123] "BL-750 Metal Hydride," http://www.fuelcellstore.com/cgi-bin/fuelweb/view=Item/cat=17/product=133, accessed 2-Dec-2005

[124] "HC-MH1200: A portable, low pressure metal hydride hydrogen storage," http://www.hydrocell.fi/en/pdf/HC-MH1200_brochure.pdf, downloaded 24-Jun-2005

[125] http://www.hbank.com.tw/eg/pr2_07.htm, accessed 2-Dec-2005

[126] "TUFFSHELL H2 Fuel Tanks Product Information," http://www.lincolncomposites.com/media/Tuffshell%20h2%20facts.pdf, downloaded 20-Jun-2005

[127] Based on the Beattie-Bridgeman equation and constants presented in *Physical Chemistry* [Castellan, p. 46-48]

[128] [Moran, et al.]

AD	Ideal LaNi_5 (AB_5)[129], [130]	0.47	3.83	metal hydride

Table 6: Hydrogen storage options

[129] [Pettersson]

[130] [Züttel, p. 31]

Compressed Hydrogen

The density of compressed hydrogen deviates from the ideal gas equation very significantly at high pressures. At 10,000 psi, storage is only about two-thirds of what the ideal gas law predicts [Pinkerton and Wicke]. Figure 15 shows the Energy Density of compressed hydrogen gas as a function of pressure at room temperature (20 °C) and 87 K (slightly below the liquid oxygen boiling point). The Beattie-Bridgeman equation and constants are presented in *Physical Chemistry* [Castellan, p. 46-48].

The values shown in Figure 15 are for the volume of the hydrogen itself, neglecting the volume occupied by the walls of the storage tank and any impurities. At higher pressures, tank wall thickness will generally need to increase, which lessens the Energy Density advantage of higher pressures. However, the Energy Density advantage of higher pressures still exists. Product data for composite hydrogen tanks indicates that higher pressure (10,000 psi as opposed to 5,000 psi) tanks have higher Energy Density, but lower Specific Energy[131].

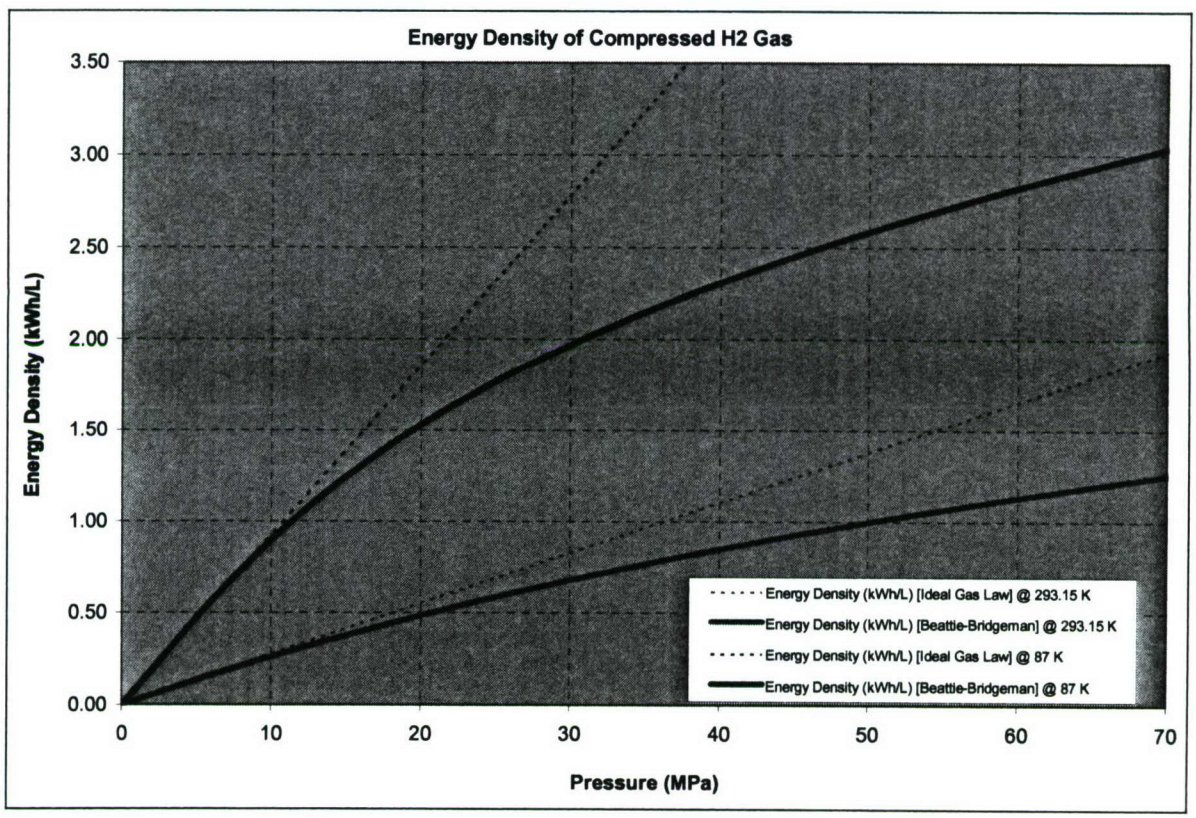

Figure 15: Energy Density of compressed hydrogen gas as a function of pressure

The maximum pressure of commercial off the shelf (COTS) compressed hydrogen tanks is 10,000 psi (68.9 MPa). The overall density of compressed hydrogen systems is typically less than water, as shown by the fact that the systems are generally below the dotted lines in Figure 13 and Figure 14.

[131] "TUFFSHELL® H2 Fuel Tanks Product Information," Lincoln Composites, Inc., www.lincolncomposites.com, accessed 24-Oct-2005

There is also the possibility of storing hydrogen as a cryogenically compressed gas [Powers]. Although the specifications are not available on a complete system design for this temperature at this time, Figure 15 shows that there is a considerable advantage to cryo-compressed hydrogen storage. At liquid oxygen temperature (87 K) and 700 atm, the theoretical or ideal ED is 3.05 kWh/L as opposed to 1.26 kWh/L at 20 °C.

Liquid Hydrogen

The boiling point of hydrogen is 20.26 K [Young, Hugh D., ch. 15]. This presents considerable, but not necessarily insurmountable, complications for the UUV FCEPS application. Thermal management would have to be carefully considered given the heat generated by the fuel cell and present in seawater, all in close proximity. Evaporation is an issue, but if the base evaporation rate is lower than the consumption rate of hydrogen based on the power requirements of the UUV, then vaporized hydrogen gas can be utilized rather than wasted.

Liquid hydrogen has a density of 0.0708 kg/L [Züttel, p. 25]. This sets a maximum theoretical ED of 2.36 kWh/L. Liquid hydrogen is much less dense than water, and typically, liquid hydrogen tanks have a density slightly less than water as well. This is shown by the graphs in Figure 13 and Figure 14.

Metal Hydride

Metal hydride storage systems typically have high ED, but low SE as evidenced by Figure 13 and Figure 14. These systems have a fairly high level of technical maturity, but require thermal management to attain the proper temperatures for absorption and desorption of hydrogen. The temperatures depend on the type of metal hydride used.

Chemical Hydride

Chemical hydrides typically have densities similar to water, as shown in Figure 13 and Figure 14. Chemical hydride systems such as those based on lithium hydride promise relatively high SE and ED [McClaine, et al.]. However, in general chemical hydride systems are at a low level of technical maturity as compared to metal hydrides. Hydrogen is often stored in slurry that must be pumped and held in a separate tank or tank partition after hydrogen is removed[132].

Oxygen Storage

There are several classifications of oxygen storage, including compressed, liquid, and chemical. For the purposes of this assessment, chlorate candles are treated as a separate classification. Even though chlorate candles rely on a chemical reaction to release oxygen, chlorate candles are readily available in COTS systems, while other chemical types of oxygen storage require some level of development and integration in order to produce a complete Storage System.

The equivalent Specific Energy and Energy Density of oxygen storage options at the stoichiometric ratio is slightly better than those for hydrogen. Nonetheless, oxygen storage is an important consideration as well.

[132] Millennium Cell, "Hydrogen on Demand Fact Sheet," www.millenniumcell.com, 2/03 R

There is an upper bound on the SE of oxygen storage based on the mass of the oxygen itself without any tank mass or mass of other chemical elements. This can be calculated as follows:

$$SE_{O2} = 0.24183 \frac{\text{MJ}}{\text{mol H}_2} \cdot \frac{1\,\text{mol H}_2}{1\,\text{mol O}} \cdot \frac{1}{16.00\,\text{g O/mol O}} \cdot \frac{1000\,\text{g}}{1\,\text{kg}} \cdot \frac{1\,\text{kWh}}{3.6\,\text{MJ}} = 4.20 \frac{\text{kWh}}{\text{kg O}}$$

Figure 16 plots a set of oxygen storage options, which are listed in Table 7.

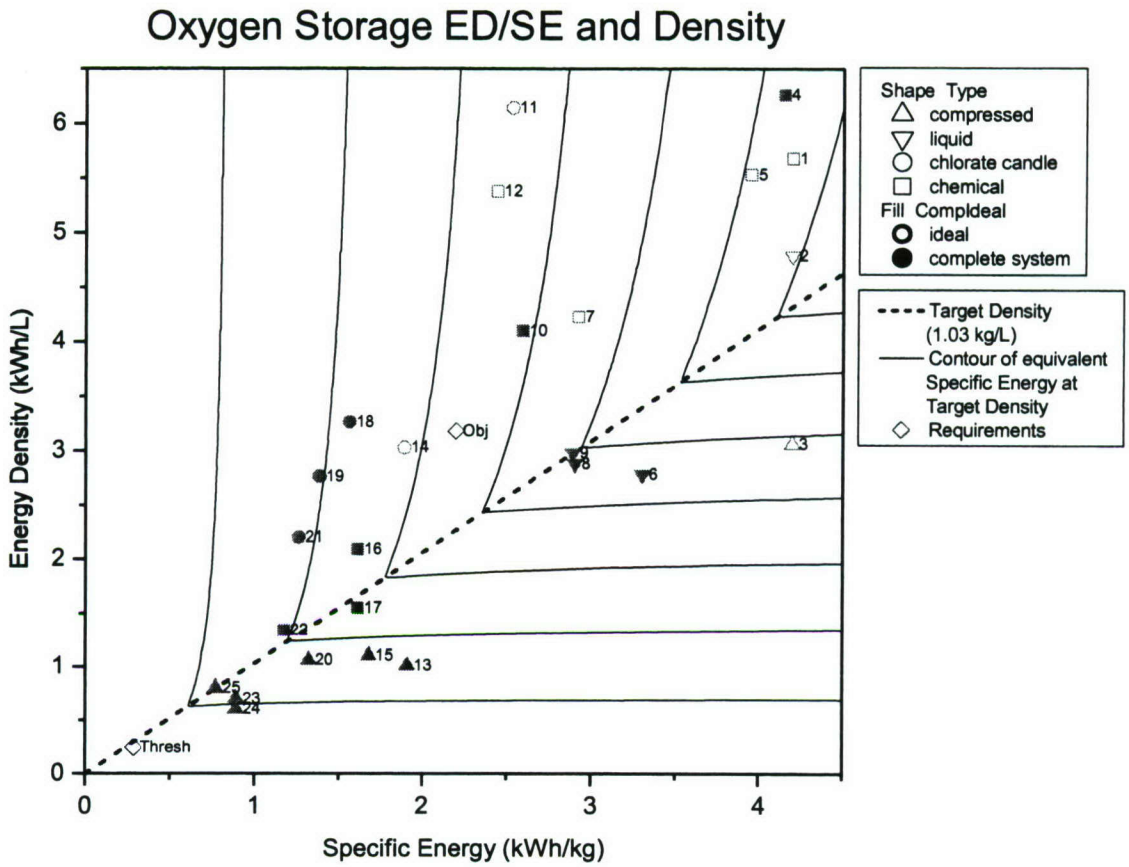

Figure 16: SE and ED of oxygen storage options

Symbol	Description		Specific Energy (kWh/kg)	Energy Density (kWh/L)	Type
1	Ideal liquid ozone (O_3)[133]		4.20	5.68	chemical
2	Ideal LOX[134]		4.20	4.79	liquid
3	Ideal 700 atm O_2[135]		4.20	3.05	compressed
4	Liquid ozone (O_3) system (Directed Technologies study)[136]		4.15	6.26	chemical
5	Ideal hydrogen peroxide (H_2O_2)[137]		3.95	5.53	chemical
6	Sierra Lobo Advanced LOX system[138], [139], [140]		3.30	2.78	liquid
7	Ideal nitrogen tetroxide (N_2O_4)[141]		2.92	4.23	chemical
8	Andonian Cryogenics LOX-425-V[142]		2.90	2.88	liquid
9	Andonian Cryogenics LOX-240-V[143]		2.89	2.98	liquid
10	Nitrogen tetroxide (N_2O_4) system (Directed Technologies study)[144]		2.59	4.10	chemical
11	Ideal lithium perchlorate (LiClO_4)[145], [146]		2.53	6.14	chlorate candle

[133] Based on "Gas Data," http://www.airliquide.com/en/business/products/gases/gasdata/index.asp?GasID=137, accessed 2-Dec-2005

[134] Based on "Oxygen (O2) Properties and Uses," http://www.uigi.com/oxygen.html, accessed 2-Dec-2005

[135] Based on the Beattie-Bridgeman equation and constants presented in *Physical Chemistry* [Castellan, p. 46-48]

[136] [James, p 10]

[137] Based on "Hydrogen peroxide," http://en.wikipedia.org/wiki/Hydrogen_peroxide, accessed 29-Sept-2005

[138] [Griffiths]

[139] [Griffiths, et al.]

[140] "Fuel Cell Reactant Storage Systems," http://www.sierralobo.com/technology/storage.shtml, accessed 13-Jul-2005

[141] "Dinitrogen tetroxide," http://www.answers.com/topic/nitrogen-tetroxide, accessed 2-Dec-2005

[142] http://www.andoniancryogenics.com/Van_Tanks/van_tanks.html, accessed 2-Dec-2005

[143] http://www.andoniancryogenics.com/Van_Tanks/van_tanks.html, accessed 2-Dec-2005

[144] [James, p 10]

[145] Based on "Safety (MSDS) data for lithium perchlorate, anhydrous," http://physchem.ox.ac.uk/MSDS/LI/lithium_perchlorate_anhydrous.html, accessed 2-Dec-2005

12	Ideal sodium superoxide (NaO_2)[147]		2.44	5.38	chemical
13	Dynetek V260TDG233G5N[148]		1.91	1.01	compressed
14	Ideal sodium chlorate (NaClO_3)[149]		1.89	3.03	chlorate candle
15	SCI 604[150]		1.68	1.09	compressed
16	Hydrogen peroxide (90% H_2O_2) system (Directed Technologies study)[151]		1.61	2.09	chemical
17	Sodium superoxide (NaO_2) system (Directed Technologies study) [152]		1.61	1.55	chemical
18	Molecular Products CAN 33[153]		1.56	3.26	chlorate candle
19	Chlorate candle system (Directed Technologies study) [154]		1.38	2.76	chlorate candle
20	SCI 295S[155]		1.31	1.06	compressed
21	Molecular Products SCOG 26[156]		1.26	2.20	chlorate candle
22	Hydrogen peroxide (66% H_2O_2) system (Directed Technologies study) [157]		1.17	1.34	chemical
23	Luxfer M265[158]		0.89	0.70	compressed

[146] Based on "Lithium perchlorate," http://www.chemexper.com/chemicals/supplier/cas/7791-03-9.html, accessed 2-Dec-2005

[147] Based on http://www.webelements.com/webelements/compounds/text/Na/Na1O2-12034127.html, accessed 2-Dec-2005

[148] email communication from Dynetek Industries, Ltd., 28-Jun-2005

[149] Based on http://www.kerr-mcgee.com/businesses/chemicals/chemprods/bus_ch_sodiumchlorate.htm, accessed July, 2005

[150] "SCBA," http://www.scicomposites.com/scba.html, accessed 2-Dec-2005

[151] [James, p 10]

[152] [James, p 10]

[153] "Chlorate Candle 33 Specifications," http://www.molecularproducts.co.uk/v2/products/candle_33/specs.htm, accessed 2-Dec-2005

[154] [James, p 10]

[155] "SCBA," http://www.scicomposites.com/scba.html, accessed 2-Dec-2005

[156] "Chlorate Candle SCOG 26 Specifications," http://www.molecularproducts.co.uk/v2/products/candle_scog_26/specs.htm, accessed 2-Dec-2005

[157] [James, p 10]

[158] [Griffiths, et al.]

24	Mesa Specialty Gases & Equipment A030-HP Aluminum[159]		0.89	0.60	compressed
25	Mesa Specialty Gases & Equipment 049-HP Steel[160]		0.77	0.80	compressed

Table 7: Oxygen storage options

[159] http://www.mesagas.com/CylinderSpecifications.htm, accessed 2-Dec-2005

[160] http://www.mesagas.com/CylinderSpecifications.htm, accessed 2-Dec-2005

Compressed Oxygen

Compressed oxygen gas density does not deviate from the ideal gas law as significantly as hydrogen at the feasible storage pressures at room temperature. As with hydrogen, however, increasing pressure still brings diminishing returns. At 10,000 psi, the oxygen density is 79% of that predicted by the ideal gas law[161]. Figure 17 shows the Energy Density at the stoichiometric ratio for oxygen as a function of pressure at room temperature (20 °C). The Beattie-Bridgeman equation and constants are presented in *Physical Chemistry* [Castellan, p. 46-48]. These values are for pure oxygen, neglecting the volume occupied by the walls of the storage tank. At higher pressures, tank wall thickness will generally need to increase, which lessens the Energy Density advantage of higher pressures. Also, gaseous oxygen is very reactive at high pressures, and this poses a potential safety concern and constraints on the tank design [Reader, et al., p. 885].

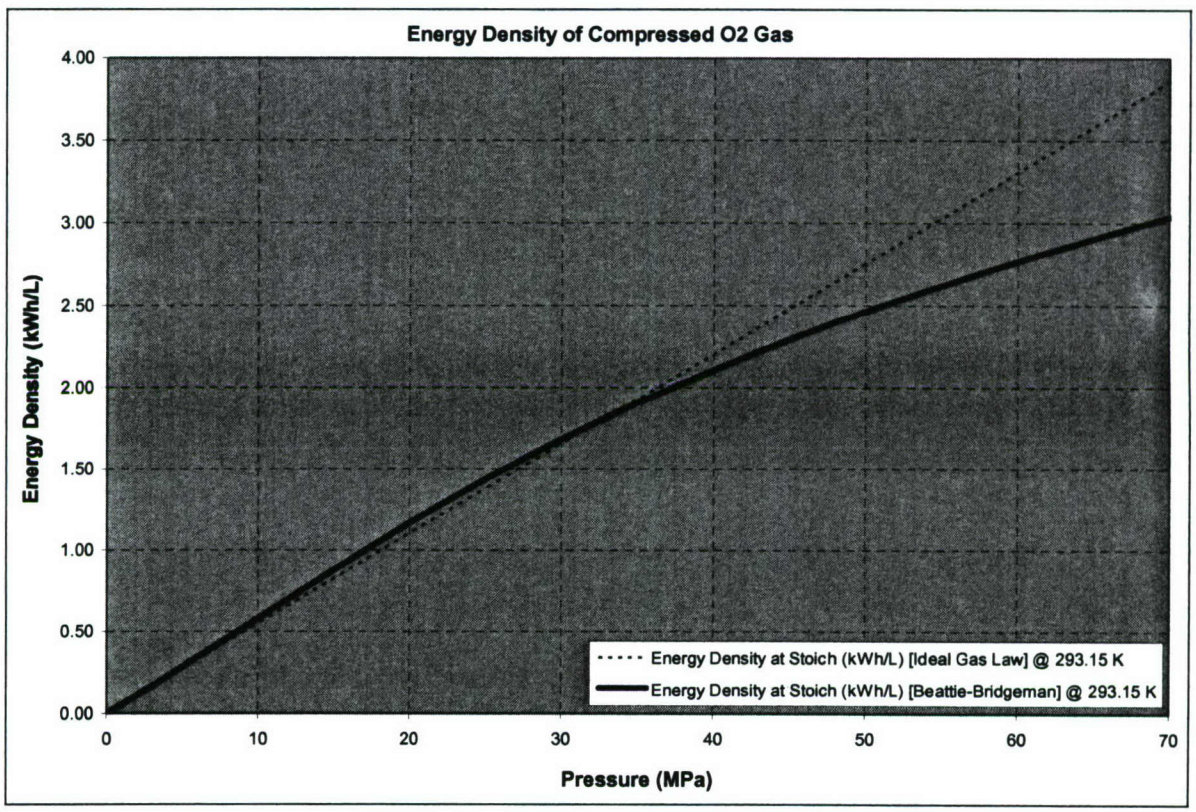

Figure 17: Energy Density of compressed oxygen gas as a function of pressure

Fewer lightweight compressed tanks are available for oxygen storage than for hydrogen. This is most likely due to the fact that the demand for hydrogen tanks is for automobile applications, whereas the demand for oxygen tanks comes from medical and SCUBA applications. Presumably, hydrogen tanks could be adapted for oxygen storage.

[161] based on the Beattie-Bridgemann equation [Castellan, p. 46-48]

Liquid Oxygen

The boiling point of oxygen is 90.18 K [Young, Hugh D., ch. 15]. This is warmer than the hydrogen boiling point, but still imposes difficulties. Sierra Lobo, Inc. has designed a complete liquid oxygen storage system for a 21" diameter UUV [Haberbusch].

Chlorate Candles

Once started, a chlorate candle continues producing oxygen until depleted. Chlorate candles are currently used in submarine and emergency applications[162], and [Reader, et al., p. 884]. Chlorate candles are very stable and can produce oxygen under pressure. However, the rate of oxygen output of a given chlorate candle is not adjustable during operation, and the reaction is not extinguishable once started. The output rate of the chlorate candle may be higher than required by the fuel cell, so the oxygen delivery system should be designed to buffer the oxygen. Sodium chlorate is most commonly used in chlorate candles, but lithium perchlorate is also used. [Reader, et al., p. 884-886]

Other Chemical Oxygen Storage

Oxygen can also be stored in other chemical compounds such as hydrogen peroxide, nitrogen tetroxide, and sodium superoxide. These systems must be designed and managed properly for safety considerations.

Product Water Storage

Assuming that the volume of the UUV does not change throughout the mission, the mass cannot change either due to the constant buoyancy requirement. As a result, fuel cell product water cannot be exhausted to the environment surrounding the UUV. For the purposes of this assessment, it has been assumed that product water must be stored in a tank separate from the hydrogen and oxygen storage tanks. Certain Storage System options such as chemical hydride slurries may present the opportunity to store product water within the reactant tank as the hydrogen is utilized, but this will be the exception rather than the rule.

The hydrogen LHV is used as the basis of energy content in the FCEPS assessment. The mass of water produced is:

$$SE_{H2O} = \frac{0.242\,\text{MJ}}{\text{mol}\,H_2} \cdot \frac{1\,\text{mol}\,H_2}{1\,\text{mol}\,H_2O} \cdot \frac{1}{18.015\,\text{g}\,H_2O/\text{mol}\,H_2O} \cdot \frac{1000\,\text{g}}{1\,\text{kg}} \cdot \frac{1\,\text{kWh}}{3.600\,\text{MJ}} = 3.73\frac{\text{kWh}}{\text{kg}\,H_2O}$$

The volume of water produced is:

$$ED_{H2O} = 3.73\frac{\text{kWh}}{\text{kg}\,H_2O} \cdot \frac{1\,\text{kg}\,H_2O}{1\,\text{L}\,H_2O} = 3.73\frac{\text{kWh}}{\text{L}\,H_2O}$$

The value of 3.73 kWh/L can be entered into Equation 6 for calculating the overall system Energy Density:

$$ED_{SStorage} = \frac{1}{\frac{1}{ED_{H2}} + \frac{1}{ED_{O2}} + \frac{1}{ED_{H2O}}} = \frac{1}{\frac{1}{ED_{H2}} + \frac{1}{ED_{O2}} + \frac{1}{3.73\,\text{kWh/L}}}$$

[162] "Joint Fleet Maintenance Manual Volume II, Integrated Fleet Maintenance List of Effective Pages", COMFLTFORCOMINST 4790.3 REV A CH-2, http://www.submepp.navy.mil/Jfmm/index.htm, p. II-I-3M-2

Product water storage may affect the hydrogen storage and oxygen storage choices due to the change in storage system density.

The mass of the product water will not affect the overall Storage System Specific Energy because of mass conservation. As mass leaves the storage tanks, it will enter the fuel cell and later the water storage tank. It is assumed that the dry mass of the water storage tank is negligible. A lightweight expandable bladder may suffice. However, the design must be carefully considered so that the FCEPS center of mass does not shift significantly during the mission.

Integrated Storage System

The overall Storage System Energy Density will be asymptotic to 3.73 kWh/L. Even if the hydrogen and oxygen could be stored in zero volume, the product water must still be stored:

$$ED_{SS} = \lim_{ED_{H2}\to\infty,\, ED_{O2}\to\infty} \left(\frac{1}{\frac{1}{ED_{H2}} + \frac{1}{ED_{O2}} + \frac{1}{3.73\,\frac{\text{kWh}}{\text{L}}}} \right) = 3.73\,\frac{\text{kWh}}{\text{L}}$$

Any realistic values of ED_{H2} and ED_{O2} will reduce this overall Storage System Energy Density even further.

An upper bound exists on overall Storage System Specific Energy as well. This is the mass of the hydrogen and oxygen divided by the energy stored, which is the same as the SE of the product water storage calculated above.

$$SE_{SS} = SE_{H2O} = 3.73\frac{\text{kWh}}{\text{kg}}$$

Another way to derive the upper bound of the Storage System SE is by entering the upper bounds of SE_{H2} and SE_{O2} discussed above into Equation 4:

$$SE_{SS} = \frac{SE_{H2}SE_{O2}}{SE_{H2} + SE_{O2}} = \frac{33.32\frac{\text{kWh}}{\text{kg}} \cdot 4.20\frac{\text{kWh}}{\text{kg}}}{33.32\frac{\text{kWh}}{\text{kg}} + 4.20\frac{\text{kWh}}{\text{kg}}} = 3.73\frac{\text{kWh}}{\text{kg}}$$

Figure 18 below plots the SE and ED of all the combinations of the hydrogen storage and oxygen storage options discussed above, assuming product water storage does not require extra volume. Figure 19 plots all of the combinations with product water storage volume included, but assuming that the product water tank has negligible mass and wall volume. The data plots retain the same SE values, but have reduced ED values. Figure 20 is the same as Figure 19, but filters out all storage combinations which include ideal hydrogen and/or oxygen storage options (options which neglect the impact of tank and supporting system mass and volume).

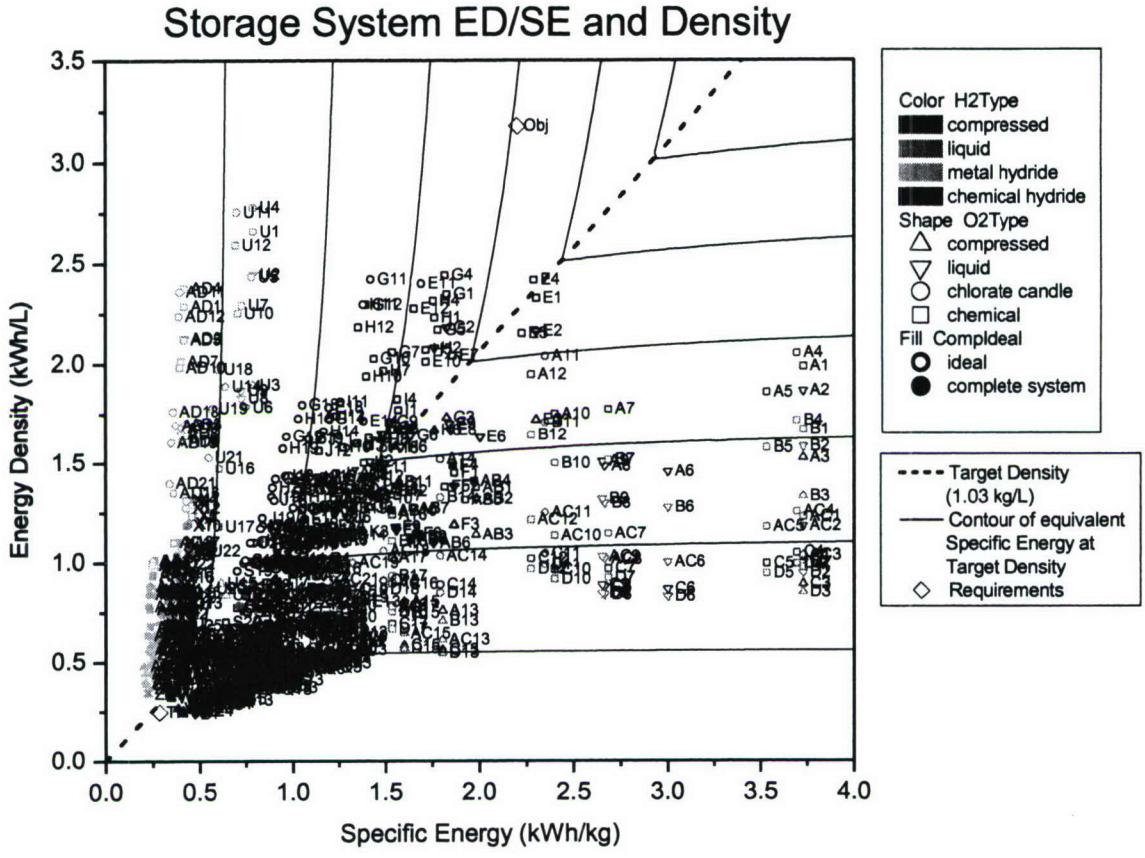

Figure 18: SE and ED of Storage System options (all options, neglecting product water storage)

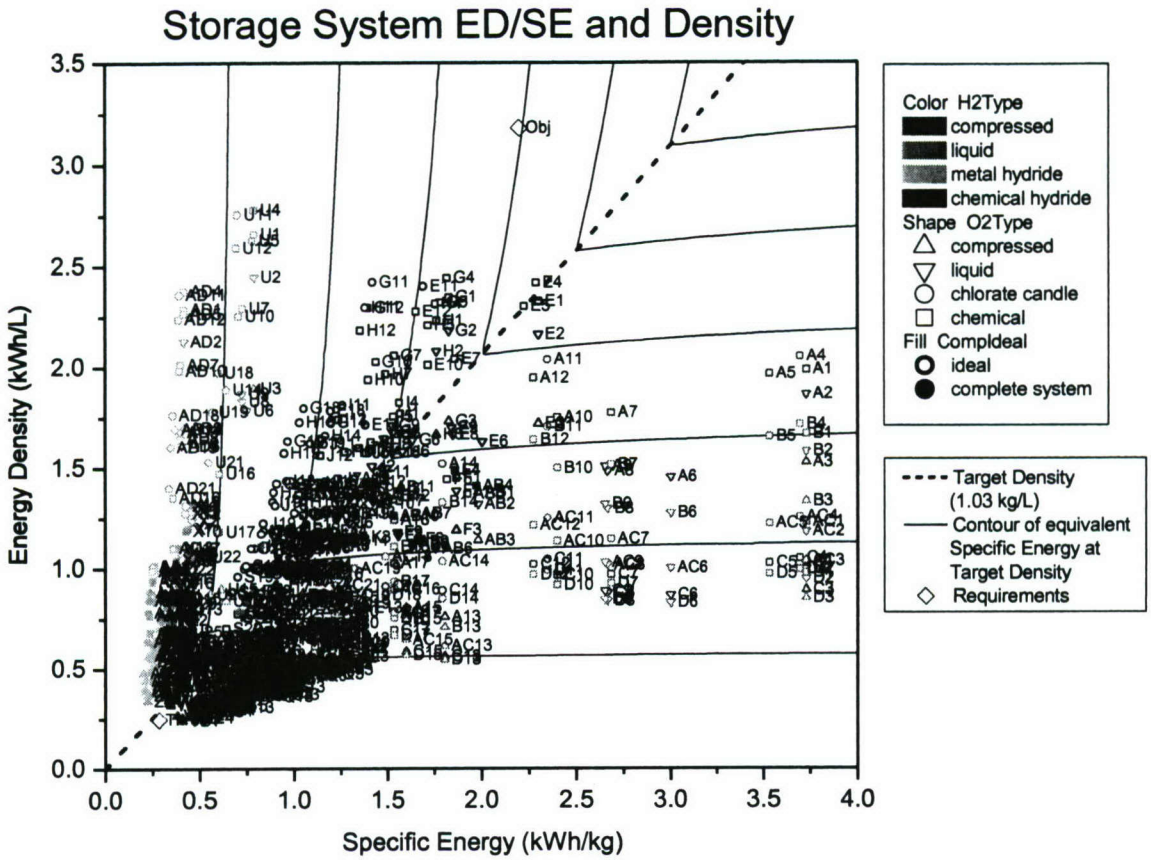

Figure 19: SE and ED of Storage System options (all options, with product water storage)

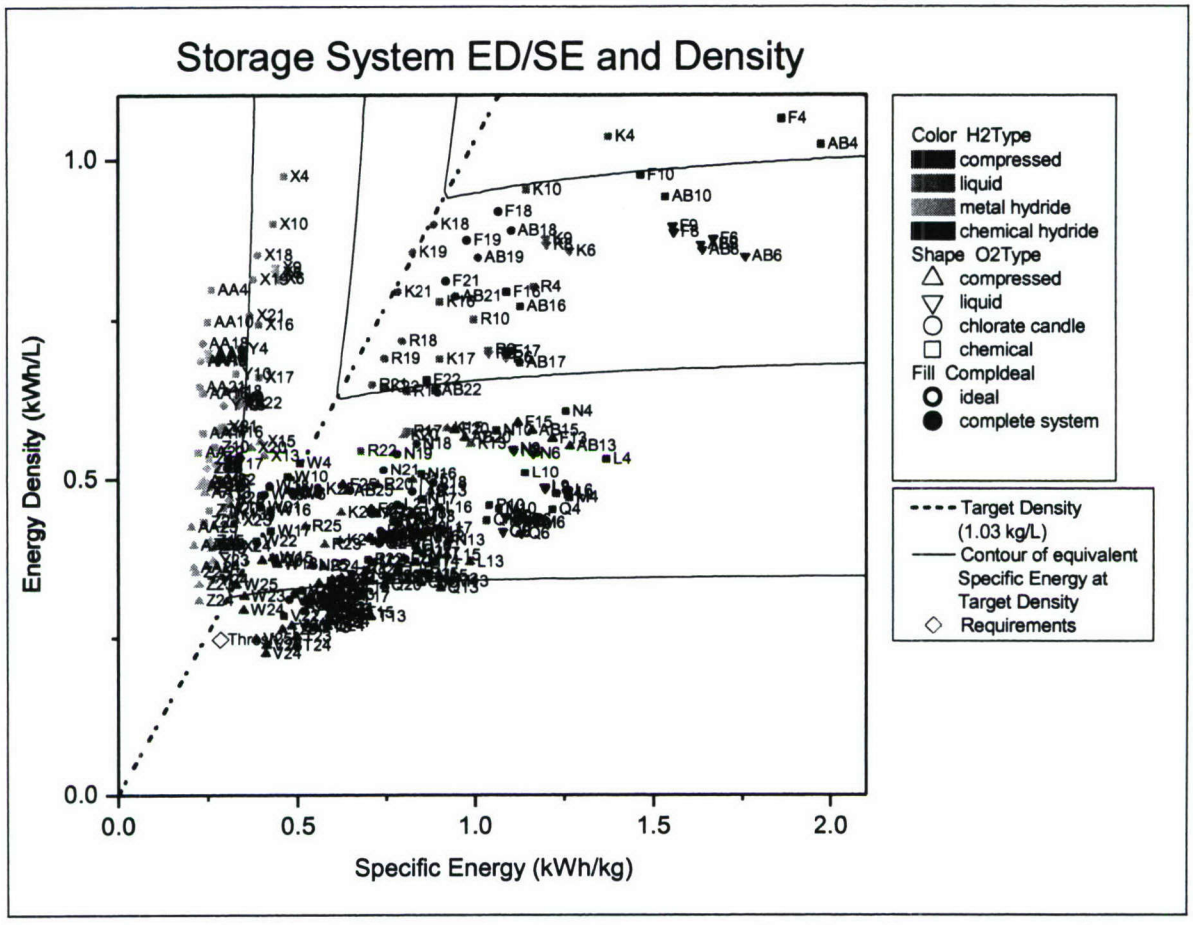

Figure 20: SE and ED of Storage System options (complete systems only, with product water storage)

Fuel Cell System

Due to the AIP constraint of the UUV application, it is desirable to operate the FC on H2/O2 rather than H2/Air. A H2/O2 FC will be capable of higher current densities and thus have higher Power Density. The impurities of the H2/O2 storage will be the only inert gases to build up in the FC stack, which is a very small fraction of the stored H2/O2 as compared to the nitrogen and other gases present in air. This presents the possibility to purge inert gases less frequently if at all, saving energy and system complexity. In addition, H2/O2 storage will almost certainly have higher SE and ED values than H2/Air storage.

In the UUV application, high cathode, anode, and ambient pressures are available due to the pressure at the operating depth and depending on the method of H2/O2 storage. This presents the possibility to operate the fuel cell stack at a higher Power Density and efficiency. The situation is in contrast to land applications, where cathode pressure is generally produced by a compressor which introduces parasitic electrical losses to the system. However, there are tradeoffs that must be considered. There will be higher reactant cross-over through the PEM at the higher hydrogen and oxygen partial pressures, which introduces another energy loss of its own. This Fuel Cell System tradeoff has not been evaluated at this point in the project.

Cold seawater is available for cooling of the UUV FCEPS. Heat will be much easier to remove than in a terrestrial application—perhaps too easy. The thermal management of the system must be carefully

considered, especially if cryogenic hydrogen and/or oxygen storage is used. This Fuel Cell System tradeoff has not been evaluated at this point in the project.

Figure 21 is a graph showing the Specific Power and Power Density values of the fuel cell stacks and systems discussed above in the Previous H2/O2 PEM Fuel Cell Stacks, Systems, and Applications section. The list of fuel cell stacks and systems and their corresponding symbols is included in Table 3.

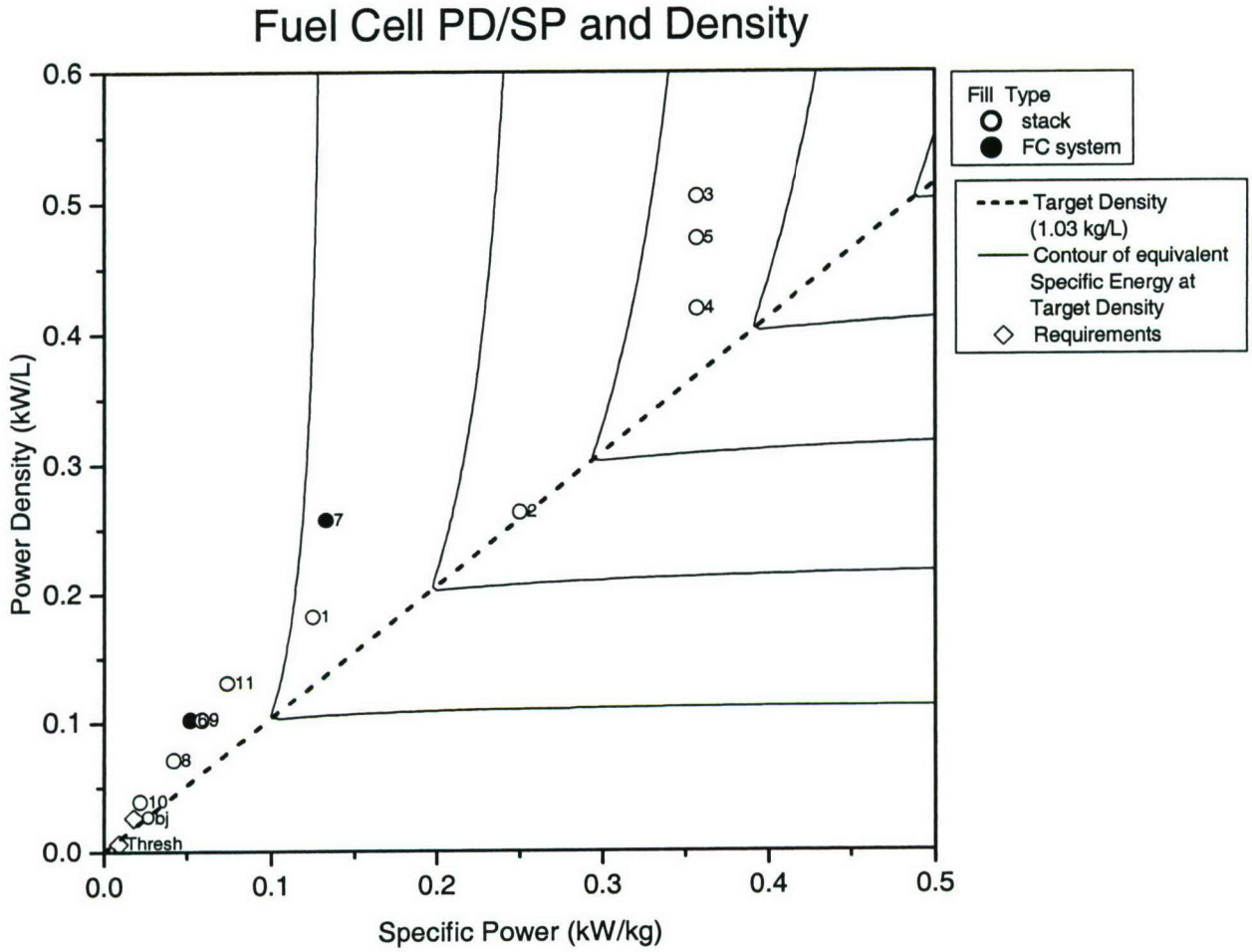

Figure 21: SP and PD of Fuel Cell stacks and systems

Depending on the power demand profile of the UUV, it may be advantageous to design the FCEPS as a hybrid system. This would reduce the peak power demand on the FCS, allowing a reduction in FCS mass and volume. A hybrid power system could be designed based on batteries (Li-Ion, NiMH, etc.), ultracapacitors, flywheel(s), or other means. Batteries and ultracapacitors would offer low development effort and could be integrated into unused FCEPS space since they are modular. Depending on the density of the FCEPS components, batteries could be used instead of ballast to achieve the desired FCEPS density (batteries are generally denser than water). Flywheels might present other opportunities, such as potential integration with UUV guidance systems.

FCEPS Integration and Supporting Technology

Several opportunities may exist within the UUV FCEPS for integration of components and systems. This integration may enhance the FCEPS design beyond what might be expected when assessing its individual

FCEPS Integration and Supporting Technology

Several opportunities may exist within the UUV FCEPS for integration of components and systems. This integration may enhance the FCEPS design beyond what might be expected when assessing its individual components. The hydrogen and oxygen storage could be thermally integrated with the Fuel Cell System, providing advantages depending on the choice of storage system options. As discussed earlier, it may be an advantage to operate the fuel cell stack at higher pressures offered by compressed and other H2/O2 storage options. Additionally, integration of the product water and reactant storage might be possible. Some FCEPS components might be better suited to operate at seawater pressure rather than the atmospheric pressure inside a pressure vessel. Components should be grouped accordingly.
The FCEPS concept design process presented above is suitable for a first pass at choosing among Storage System and Fuel Cell System options to maximize net energy storage. However, there may be other technologies which would enhance the FCEPS, but have not been included into the concept design framework yet. These technologies require further assessment to determine their feasibility and benefit to the FCEPS design.

One of these FCEPS enhancing technologies is thermoelectric modules. Thermoelectrics are capable of pumping heat using electricity or generating electricity from a temperature difference. This might be useful for cooling the fuel cell stack while at the same time generating a small amount of electric power from the temperature difference between the seawater and the fuel cell stack. In FCEPS designs with cryogenic hydrogen and/or oxygen storage, it might be practical to generate additional electric power, vaporize and preheat the reactants, and cool the fuel cell. Thermoelectric technology could enable precise control of Fuel Cell System and Storage System temperatures during operation, or prevent freezing of the fuel cell stack during UUV transport. It may be possible to include thermoelectric technology in the FCEPS with a small impact on mass and volume since they are fairly thin and modular. The inclusion of thermoelectrics would require further investigation and would increase the development effort compared to traditional means of thermal management such as heat exchangers.

Electric turbines might also enhance the FCEPS design. A turbine could utilize the pressure energy stored in compressed Storage Systems to complement the fuel cell power output. Again, this would require further investigation and would increase the development effort.

Superconductors might enhance the FCEPS and UUV design as well. If cryogenic hydrogen and/or oxygen are used, superconductors might be practical for reducing the power loss associated with electrical components (DC/DC converters, solenoids, motors, motor controllers) and wires within the FCS and the entire UUV. Once again, this would require further investigation and would increase the FCEPS and UUV development effort.

FCEPS Design Concepts

This initial assessment has been done under the assumption that there is no overhead volume and mass. At this point, the information is not available to determine the other overhead volume and mass contributions such as insulation, structure, and pressure vessel(s). As mentioned above, the FCEPS volume and mass is 3681 L and 4082 kg based on the Navy 60" LD MRUUV objectives, resulting in a density of 1.11 kg/L [Egan, p. 22]. Note that the FCS volume and mass are a small portion of the total FCEPS volume and mass (9.1% by volume and 15.9% by mass for the BZM 34 FCS option) [Baumert and Epp].

Storage options from the Directed Technologies study [James] have been excluded from the ternary graphs in Figure 22 and Figure 23. Table 8 shows the 15 FCEPS design concepts with the highest net energy storage, as well as:

- Symbol 6K6: Sierra Lobo Advanced LOX system with the most optimal liquid H2 storage (Magna Steyr Liquid H2)
- Symbol 6X6: The most optimal Storage System using metal hydride hydrogen storage and excluding any of the storage options from the Directed Technologies study (Ovonic Onboard Solid H2 and Sierra Lobo Advanced LOX system)
- Symbol 6N15: The most optimal compressed hydrogen and compressed oxygen Storage System (TUFFSHELL 118L, SCI 604)

The FCEPS options are sorted in order of descending net energy storage. Symbols for the FCEPS options are a concatenation of the Fuel Cell System, hydrogen storage, and oxygen storage, respectively. As a comparison, the best RBEPS at the required density of 1.11 kg/L uses the Ultralife Batteries model UBC641730 Li-Poly prismatic cell, and gives a SE of 0.168 kWh/kg and an ED 0.186 kWh/L.

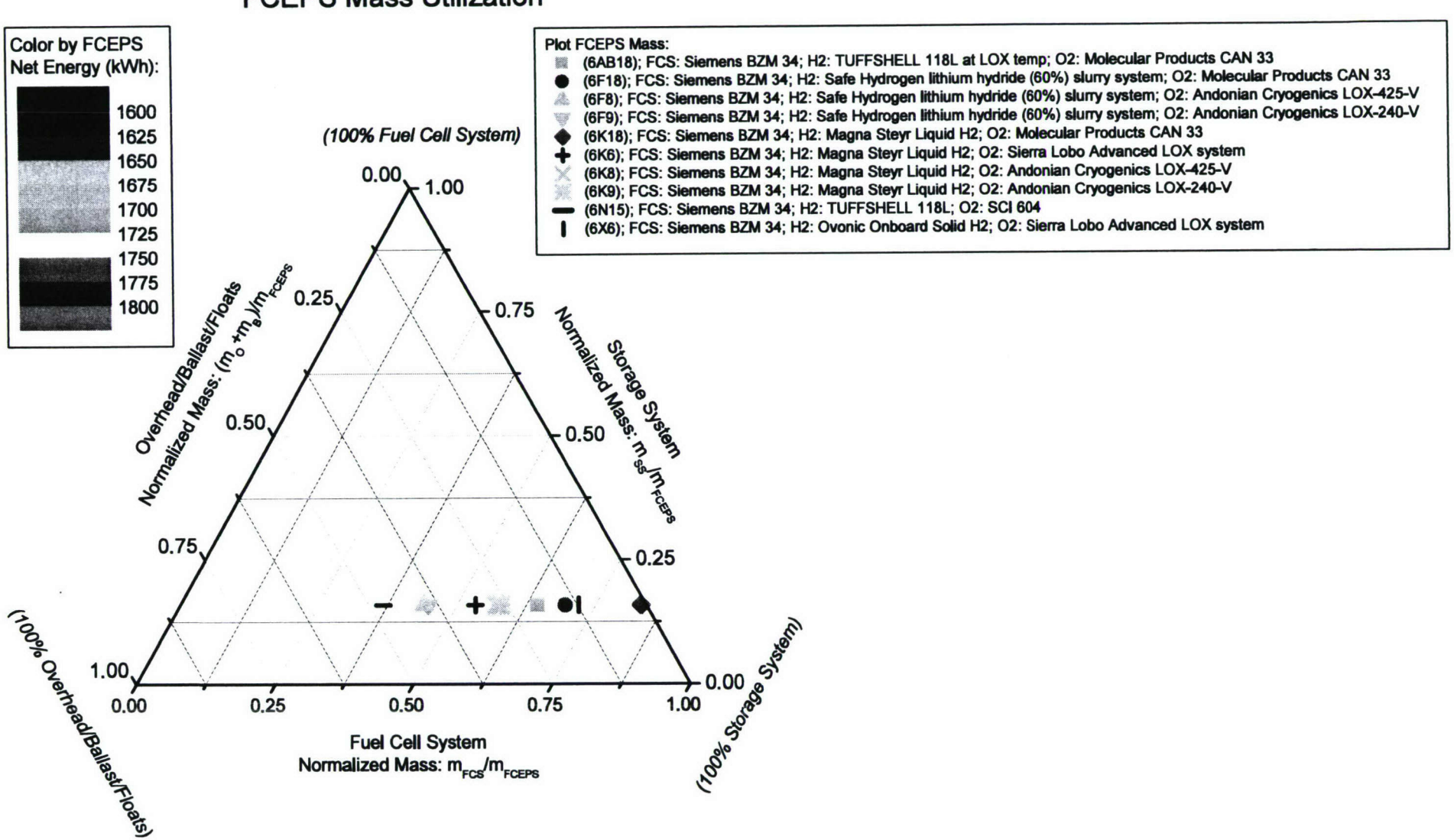

Figure 22: Utilization of available mass for selected FCEPS concepts

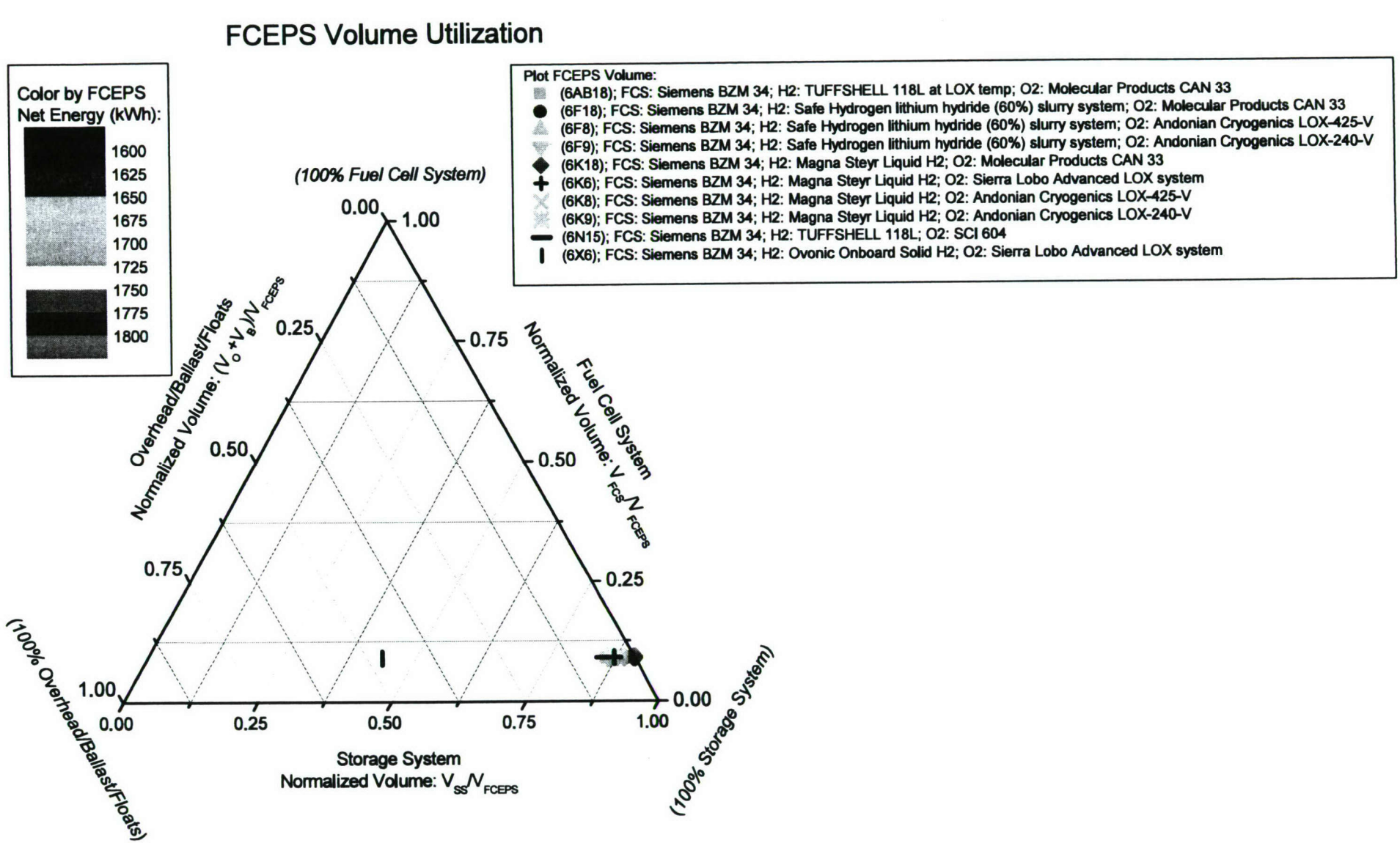

Figure 23: Utilization of available volume for selected FCEPS concepts

Sym-bol	Design Description	SS Volume (L)	FCS Volume (L)	Overhead / Ballast/ Float Volume (L)	SS Mass (kg)	FCS Mass (kg)	Overhead / Ballast/ Float Mass (kg)	Net Energy (kWh)	SE (kWhe/ kg)	ED (kWhe/ L)
6F4	FCS: Siemens BZM 34 H2: Safe Hydrogen lithium hydride (60%) slurry system O2: Liquid ozone (O_3) system (Directed Technologies study)	3166	334	181	1812	650	1620	1987	0.487	0.540
6K4	FCS: Siemens BZM 34 H2: Magna Steyr Liquid H2 O2: Liquid ozone (O_3) system (Directed Technologies study)	3236	334	111	2444	650	988	1979	0.485	0.538
6AB4	FCS: Siemens BZM 34 H2: TUFFSHELL 118L at LOX temp O2: Liquid ozone (O_3) system (Directed Technologies study)	3146	334	202	1632	650	1800	1900	0.465	0.516
6F10	FCS: Siemens BZM 34 H2: Safe Hydrogen lithium hydride (60%) slurry system O2: Nitrogen tetroxide (N_2O_4) system (Directed Technologies study)	3202	334	145	2139	650	1293	1846	0.452	0.501
6K10	FCS: Siemens BZM 34 H2: Magna Steyr Liquid H2 O2: Nitrogen tetroxide (N_2O_4) system (Directed Technologies study)	3268	334	79	2725	650	707	1838	0.450	0.499
6F18	FCS: Siemens BZM 34 H2: Safe Hydrogen lithium hydride (60%) slurry system O2: Molecular Products CAN 33	3280	334	67	2835	650	597	1781	0.436	0.484
6K18	FCS: Siemens BZM 34 H2: Magna Steyr Liquid H2 O2: Molecular Products CAN 33	3343	334	4	3397	650	35	1774	0.434	0.482
6AB10	FCS: Siemens BZM 34 H2: TUFFSHELL 118L at LOX temp O2: Nitrogen tetroxide (N_2O_4) system (Directed Technologies study)	3182	334	165	1958	650	1474	1770	0.433	0.481

6AB18	FCS: Siemens BZM 34 H2: TUFFSHELL 118L at LOX temp O2: Molecular Products CAN 33	3258	334	90	2632	650	800	1710	0.419	0.465
6F19	FCS: Siemens BZM 34 H2: Safe Hydrogen lithium hydride (60%) slurry system O2: Chlorate candle system (Directed Technologies study)	3293	334	54	2949	650	484	1701	0.417	0.462
6F9	FCS: Siemens BZM 34 H2: Safe Hydrogen lithium hydride (60%) slurry system O2: Andonian Cryogenics LOX-240-V	3168	334	180	1829	650	1603	1676	0.411	0.455
6K9	FCS: Siemens BZM 34; H2: Magna Steyr Liquid H2 O2: Andonian Cryogenics LOX-240-V	3227	334	120	2362	650	1070	1670	0.409	0.454
6K19	FCS: Siemens BZM 34 H2: Magna Steyr Liquid H2 O2: Chlorate candle system (Directed Technologies study)	3285	334	62	3414	650	18	1660	0.407	0.451
6F8	FCS: Siemens BZM 34 H2: Safe Hydrogen lithium hydride (60%) slurry system O2: Andonian Cryogenics LOX-425-V	3165	334	182	1804	650	1628	1657	0.406	0.450
6K8	FCS: Siemens BZM 34 H2: Magna Steyr Liquid H2 O2: Andonian Cryogenics LOX-425-V	3224	334	123	2331	650	1101	1651	0.404	0.449
6K6	FCS: Siemens BZM 34 H2: Magna Steyr Liquid H2 O2: Sierra Lobo Advanced LOX system	3206	334	141	2177	650	1256	1623	0.398	0.441
6X6	FCS: Siemens BZM 34 H2: Ovonic Onboard Solid H2 O2: Sierra Lobo Advanced LOX system	1613	334	1734	2933	650	499	775	0.190	0.210
6N15	FCS: Siemens BZM 34 H2: TUFFSHELL 118L O2: SCI 604	3131	334	217	1498	650	1934	769	0.188	0.209

Table 8: FCEPS design concepts

Comparison of FCEPS and RBEPS

A particular UUV design may be optimal with an energy/power system that has a density higher or lower than seawater density or that required by the 60" LD MRUUV. In order to see the effect of required energy/power system density on the FCEPS and RBEPS designs, a range of required densities from 0.3 kg/L to 3.5 kg/L is additionally considered.

The FCEPS and RBEPS design concepts are compared in terms of ED at the required density. At each required density in the set, the FCEPS design steps above were followed (assuming zero overhead mass and volume). Only the confirmed data for complete storage systems was used, and the Directed Technology data was excluded. Likewise, the best battery option was chosen at each required density, and ballast or floats were added as necessary within the RBEPS. The results are shown in Figure 24 and Figure 25. In Figure 24, the SE and ED of the FCEPS and RBEPS concepts are scatter-plotted. In Figure 25, the SE and ED are plotted separately as a function of required density. The range of 1.03 to 1.11 kg/L (seawater density to 60" LD MRUUV required density) is highlighted with a hashed pattern. In both figures, the FCEPS and RBEPS concepts are labeled with the symbol of the corresponding design (FCS, H2 storage, and O2 storage, or battery). As was seen in Figure 11, Li-Ion and Li-Poly cells have a density significantly greater than seawater. As a result, RBEPS designs become more desirable at higher required densities.

Unfortunately, it is difficult to compare the life expectancy and the lifetime capacity fade of a FCEPS to a RBEPS. Fuel cell lifetime and degradation is largely dependent on the FCS design and the operating conditions, and little or no information has been published on the Siemens BZM 34 with respect to this. The lifetime performance of the FCEPS would have to be carefully considered later in the design process.

It is also difficult to draw any general comparisons of refueling between the FCEPS and the RBEPS. The refueling/recharging operation will vary greatly on the particular RBEPS or FCEPS design. The batteries in some RBEPSs, the Ag-Zn batteries of the U.S. Navy MK30 target for example, must be removed from the UUV for recharging and conditioning[163]. Others, for example the Li-Ion batteries of the REMUS AUV, can be recharged internally[164]. The FCEPS may or may not be capable of internal refueling depending on the hydrogen and oxygen storage options.

[163] Leighton Otoman, "MK 30 MOD 1 MOBILE USW TARGET" presentation, Pacific Missile Range Facility, Kauai, Hawaii, 27-Oct-2005

[164] "REMUS Autonomous Underwater Vehicle" brochure, http://www.hydroidinc.com/remus_brochure.pdf, downloaded 30-Nov-2005

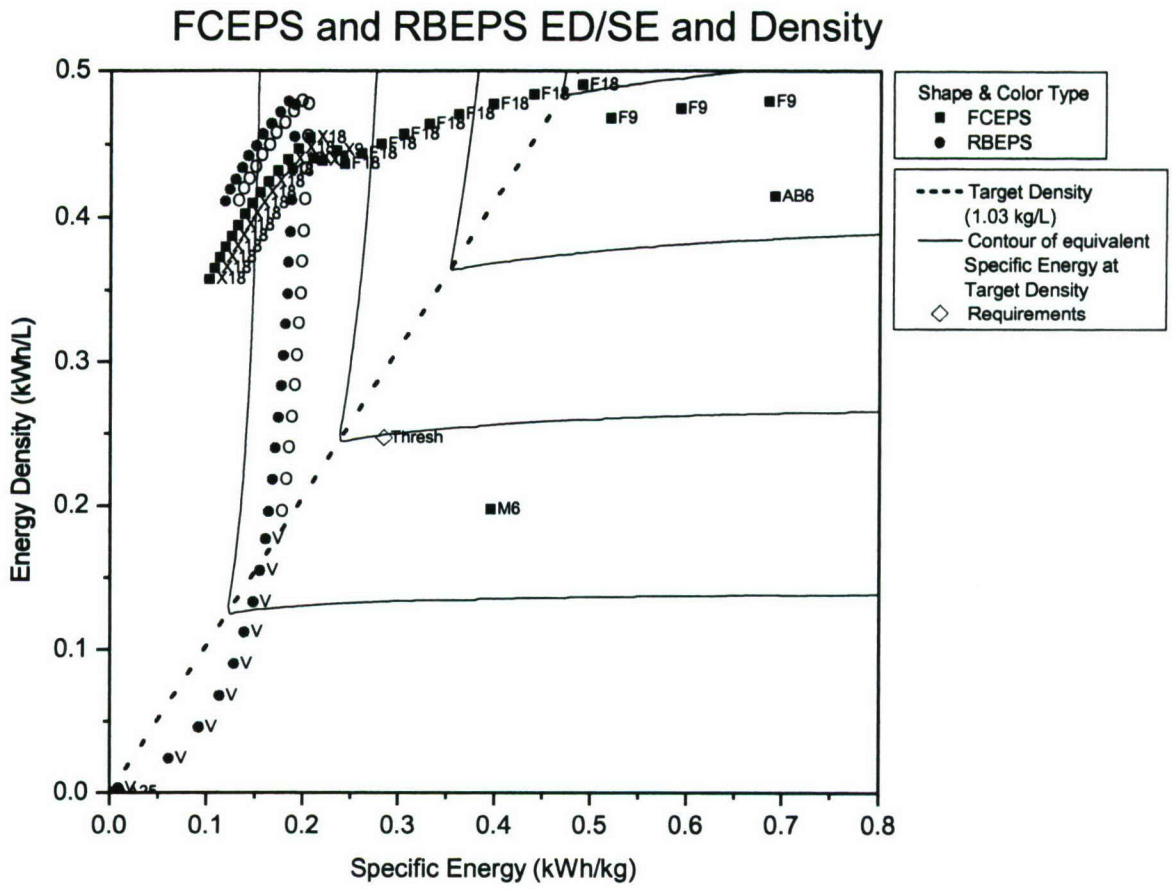

Figure 24: SE and ED of FCEPS and RBEPS at various required densities

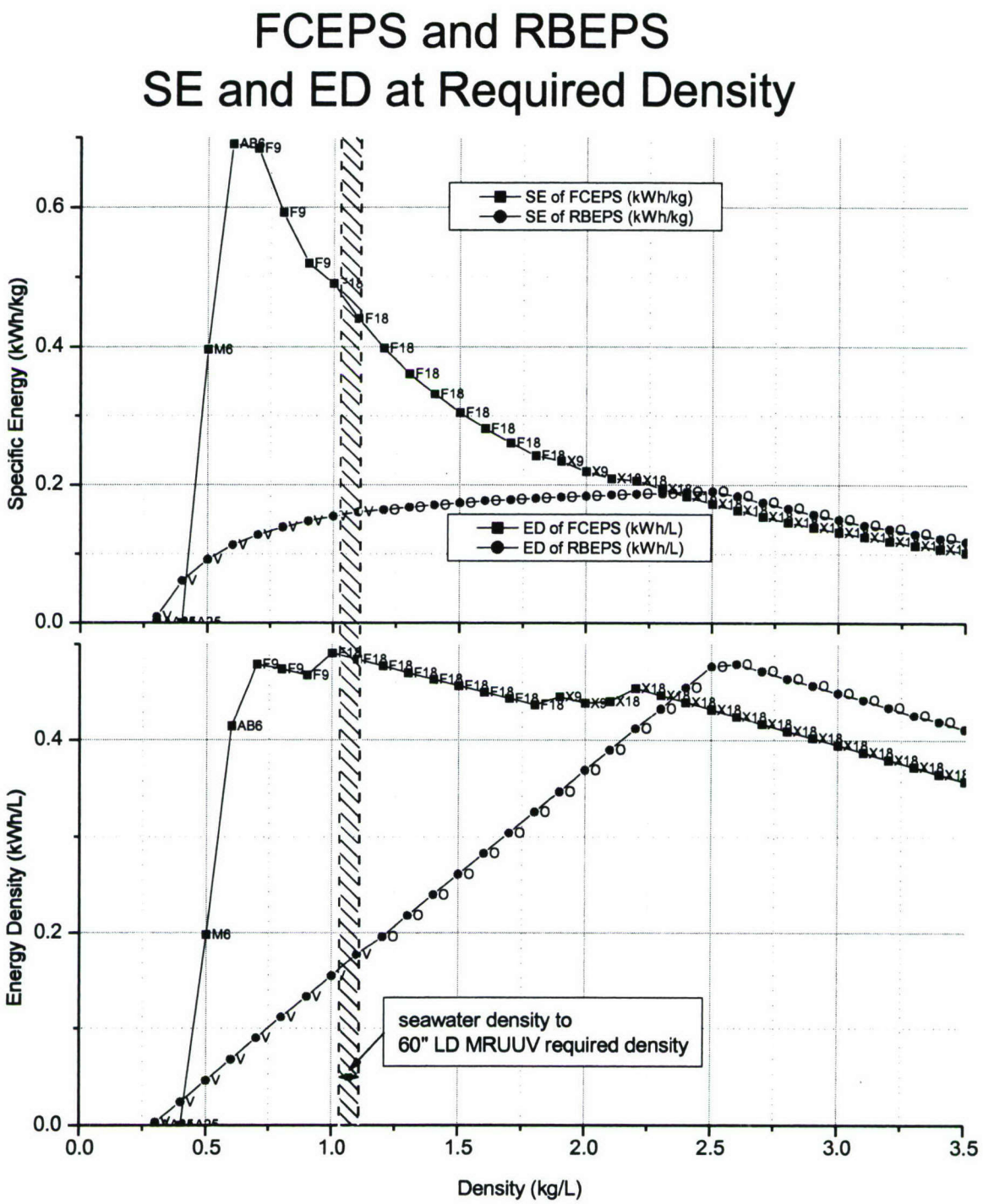

Figure 25: SE and ED of FCEPS and RBEPS as a function of required density

Conclusions

An UUV Fuel Cell Energy/Power System is a highly integrated system with many design tradeoffs. However, the UUV application offers unique possibilities for FCEPS design and fuel cell technology. Some simple analytical tools can help guide FCEPS design. As has been shown, the relationships of

Specific Energy, Energy Density, Specific Power, Power Density, and density are important keys to optimizing the FCEPS design.

The FCEPS design concept method presented in this report gives a holistic approach to choosing the hydrogen and oxygen storage and fuel cell options to provide the highest Specific Energy and Energy Density within the constraints including the FCEPS mass, volume, and required power. Using this method, some surprising combinations appear as the winners. A combination of the 60% lithium hydride slurry system from Safe Hydrogen, LLC and CAN 33 chlorate candles from Molecular Products provides the best SE and PD at 0.44 kWh/kg and 0.48 kWh/L when used with the BZM 34 FCS from Siemens. A conservative design using compressed hydrogen and oxygen provides less than half of this SE and ED. A complete design would need to be carried out using the chosen options to determine the actual SE and ED.

References

Alexandra Baker and David Jollie, "Fuel Cell Market Survey: Military Applications," Fuel Cell Today, www.fuelcelltoday.com, 13-April-2005

Rob Baumert and Danny Epp, "Hydrogen storage for fuel cell powered underwater vehicles," proc. Oceans '93: Engineering in Harmony with the ocean, New York: IEEE, 1993, p. 166-171

David J. Bents, et al., "Hydrogen-Oxygen PEM Regenerative Fuel Cell Energy Storage System," 2004 Fuel Cell Seminar, San Antonio TX Nov 1-5, 2004, NASA TM 2005-213381

Roy Burcher and Louis Rydill, *Concepts in Submarine Design*, New York: Cambridge University Press, 1998

Gilbert W. Castellan, *Physical Chemistry*, Menlo Park, Calif.: Benjamin/Cummings Pub. Co., 3rd ed., 1983

Claus Hviid Christensena, et al., "Metal ammine complexes for hydrogen storage," Journal of Materials Chemistry, web publication, DOI: 10.1039/b511589b, 7-Sep-2005

Henry J. DeRonck, "Fuel cell power systems for submersibles," proc. Oceans 1994, Brest, France

Chris Egan, "UUV Power & Energy Requirements" presentation, DARPA UUV Energy Workshop, Newport, RI, 23 Nov 2004

Christopher P. Garcia, et al., "Round Trip Energy Efficiency of NASA Glenn Regenerative Fuel Cell System," 9th Grove Fuel Cell Symposium, October 4-6, 2005

Stefan Geiger, "Fuel Cell Powered Autonomous Underwater Vehicle (AUV)," Fuel Cell Today, www.fuelcelltoday.com, October 2002

Stefan Geiger and David Jollie, "Fuel Cell Market Survey: Military Applications," Fuel Cell Today, www.fuelcelltoday.com, 1-April-2004

R. Gitzendanner, et al., "High power and high energy lithium-ion batteries for under-water applications," Journal of Power Sources, Volume 136, Issue 2, 1 October 2004, p. 416-418

Gwyn Griffiths, et al., "Modeling Hybrid Energy Systems for Use in AUVs ", Proc. 14th Unmanned Untethered Submersible Technology, Durham, New Hampshire, August 21-24, 2005

Gwyn Griffiths, "Cost vs. performance for fuel cells and batteries within AUVs"
7th Unmanned Underwater Vehicle Showcase (UUVS 2005), Southampton, UK, September 28-29, 2005

M. S. Haberbusch, et al., "Rechargeable cryogenic reactant storage and delivery system for fuel cell powered underwater vehicles," IEEE, 2002, 0-7803-7572-6/02, p. 103-109

Albert Hammerschmidt, "PEM Fuel Cells for Air Independent Propulsion," ONR Workshop on Fuel Cells for Unmanned Underwater Vehicles, October 29, 2003

Albert Hammerschmidt and Josef Lersch, "PEM Fuel Cells for Submarines – New Highlights and Latest Experiences during Setting to Work," received by email from Albert Hammerschmidt on 28-Jun-2005

Peter Hauschildt and Albert Hammerschmidt, "PEM Fuel Cell Systems – An attractive energy source for submarines," *Naval Forces*, Mönch Publishing Group, Bonn, Germany, edition No. 5, October 2003, pp. 30-33

Willi Hornfeld, "DeepC the German AUV Development Project," http://www.deepc-auv.de/deepc/bibliothek/pdf/South_eng.pdf

Tadahiro Hyakudome, et al., "Key Technologies for AUV URASHIMA," IEEE, 0-7803-7534-3, 2002

Shojiro Ishibashi, et al., "An Ocean Going Autonomous Underwater Vehicle URASHIMA equipped with a Fuel Cell," IEEE, 0-7803-8541, 2004, p. 209-214

Brian D. James, "UUV Power System Overview," 2005 UUV Power System Workshop presentation, 20-April-2005

L. Joerissen, et al., "Fuel Cell System for an Autonomous Underwater Vehicle," *2003 Fuel Cell Seminar Abstracts*, November 3-7, 2003, Miami Beach, FL, p. 1012-1015

Hunter Keeter, "Ohio-class SSGNs Experimental Test Beds for Future Attack Subs," Navy League, http://www.navyleague.org/sea_power/aug_03_10.php, August 2003

Toshio Maeda, et al., "Development of Fuel Cell AUV URASHIMA," Mitsubishi Heavy Industries, Ltd. Technical Review Vol. 41 No. 6 (Dec. 2004)

Andrew W. McClaine, et al., "Hydrogen Transmission/Storage with Metal Hydride-Organic Slurry and Advance Chemical Hydride/Hydrogen for PEMFC Vehicles," Proc. 2000 U.S. DOE Hydrogen Program Review, NREL/CP-570-28890

Matthew E. Moran, et al., "Experimental Results of Hydrogen Slosh in a 62 Cubic Foot (1750 Liter) Tank," NASA Technical Memorandum AIA-94-3259, Presented at the 30th Joint Propulsion Conference, Indianapolis, IN, June 27-29, 1994

Perez-Davis, et al., "Energy Storage for Aerospace Applications," 36th Intersociety Energy Conversion Engineering Conference, Savannah, GA, July 29-August 2, 2001, NASA/TM—2001-211068

Joakim Pettersson and Ove Hjortsberg, "Hydrogen Storage Alternatives -- A Technological and Economic Assessment," KFB (The Swedish Transport and Communications Research Boarch), Stockholm, http://www.kfb.se/pdfer/M-99-27.pdf, December 1999

Frederick E. Pinkerton and Brian G. Wicke, "Bottling the hydrogen genie," The Industrial Physicist, February/March 2004, American Institute of Physics, p. 20-23

Laurie Powers, "Flexibly Fueled Storage Tank Brings Hydrogen-Powered Cars Closer to Reality," S&TR, Lawrence Livermore National Laboratory, June 2003, p. 24-26

G. T. Reader, et al., "Power and Oxygen Sources for a Diver Propulsion Vehicle," Oceans 2001 MTS/IEEE Conference and Exhibition, Honolulu, HI, ISBN: 0-933957-28-9, vol. 2, p. 880-887, November 5-8, 2001

Rosenfeld, "DARPA UUV Fuel Cell Program," ONR Workshop on Fuel Cells for Unmanned Undersea Vehicles, Naval Undersea Warfare Center, Newport, Rhode Island, October 30, 2003

K. Rutherford and D. Doerffel, "Performance of Lithium-Polymer Cells at High Hydrostatic Pressure," 14th International Symposium on Unmanned Untethered Submersible Technology, Durham, NH, August 21 - 24, 2005

Takao Sawa, et al., "Fuel Cell Power Will Open New AUV Generation," Underwater Intervention 2004, New Orleans

K. Strasser, "H2/O2-PEM-fuel cell module for an air independent propulsion system in a submarine," *Handbook of Fuel Cells – Fundamentals, Technology and Applications*, p. 1201-1214

Satoshi Tsukioka, et al., "Results of a Long Distance Experiment with the AUV 'Urashima'," OCEANS '04, MTS/IEEE TECHNO-OCEAN '04 Conference Proceedings, August 2004, Vol. 3, p. 1714 - 1719

Omourtag Velev, et al., "PEM Fuel Cell Based Energy Storage Concept for Unmanned Underwater Vehicles," Intelligent Ships Symposium VI, 1-2 June 2005, Villanova University, Villanova, Pennsylvania

Ikuo Yamamoto, et al., "Fuel Cell System of AUV Urashima," received by email from Kazuhisa Yokoyama on 30-Jun-2005

Hugh D. Young, *University Physics*, 7th Ed., Addison Wesley, 1992

Rosa C. Young, "Advances of Solid Hydrogen Storage Systems," National Hydrogen Association's 14th Annual U.S. Hydrogen Conference and Hydrogen Expo, March 4-6, 2003

Andreas Züttel, "Materials for Hydrogen Storage," Materials Today, September 2003, ISSN 1369 7021, Elsevier Ltd, p. 24-33

Appendix A: Equations

Storage Metrics

Assuming that all of the Storage System components (hydrogen storage, oxygen storage, product water storage) are sized to accommodate the same amount of energy (it would be wasteful in terms of mass and volume to do otherwise), then:

$$SE_{H2} = \frac{E_{SS}}{m_{H2}} \tag{19}$$

$$SE_{O2} = \frac{E_{SS}}{m_{O2}} \tag{20}$$

$$SE_{H2O} = \frac{E_{SS}}{m_{H2O}} \tag{21}$$

$$ED_{H2} = \frac{E_{SS}}{V_{H2}} \tag{22}$$

$$ED_{O2} = \frac{E_{SS}}{V_{O2}} \tag{23}$$

$$ED_{H2O} = \frac{E_{SS}}{V_{H2O}} \tag{24}$$

Combining the SE of the Storage System components:

$$SE_{SS} = \frac{E_{SS}}{m_{H2} + m_{O2} + m_{H2O}} = \frac{1}{\frac{m_{H2}}{E_{SS}} + \frac{m_{O2}}{E_{SS}} + \frac{m_{H2O}}{E_{SS}}} = \frac{1}{\frac{1}{SE_{H2}} + \frac{1}{SE_{O2}} + \frac{1}{SE_{H2O}}} \tag{25}$$

Combining the ED of the Storage System components:

$$ED_{SS} = \frac{E_{SS}}{V_{H2} + V_{O2} + V_{H2O}} = \frac{1}{\frac{V_{H2}}{E_{SS}} + \frac{V_{O2}}{E_{SS}} + \frac{V_{H2O}}{E_{SS}}} = \frac{1}{\frac{1}{ED_{H2}} + \frac{1}{ED_{O2}} + \frac{1}{ED_{H2O}}} \tag{26}$$

If the product water storage is not necessary, then the equations can be simplified:

$$SE_{SS} = \frac{SE_{H2}SE_{O2}}{SE_{H2} + SE_{O2}} \tag{27}$$

$$ED_{SS} = \frac{ED_{H2}ED_{O2}}{ED_{H2} + ED_{O2}} \tag{28}$$

FCS Choice

Assume that the Storage System SE will not change with the selection of the new FCS:

$$\varepsilon_{FCS1} SE_{SS} \left(m_{SS0} + m_{FCS0} - m_{FCS1} \right) > \varepsilon_{FCS0} SE_{SS} m_{SS0} \tag{29}$$

$$\frac{\varepsilon_{FCS1}}{\varepsilon_{FCS0}} > \frac{m_{SS0}}{m_{SS0} + m_{FCS0} - m_{FCS1}} \tag{30}$$

$$\frac{\varepsilon_{FCS0}}{\varepsilon_{FCS1}} < 1 + \frac{m_{FCS0} - m_{FCS1}}{m_{SS0}} \tag{31}$$

$$\frac{\varepsilon_{FCS1} - \varepsilon_{FCS0}}{\varepsilon_{FCS1}} > \frac{m_{FCS1} - m_{FCS0}}{m_{SS0}} \tag{32}$$

Assume that the Storage System ED will not change with the selection of the new FCS:

$$\varepsilon_{FCS1} ED_{SS} \left(V_{SS0} + V_{FCS0} - V_{FCS1} \right) > \varepsilon_{FCS0} ED_{SS} V_{SS0} \tag{33}$$

$$\frac{\varepsilon_{FCS1}}{\varepsilon_{FCS0}} > \frac{V_{SS0}}{V_{SS0} + V_{FCS0} - V_{FCS1}} \tag{34}$$

$$\frac{\varepsilon_{FCS0}}{\varepsilon_{FCS1}} > 1 + \frac{V_{FCS0} - V_{FCS1}}{V_{SS0}} \tag{35}$$

$$\frac{\varepsilon_{FCS1} - \varepsilon_{FCS0}}{\varepsilon_{FCS1}} > \frac{V_{FCS1} - V_{FCS0}}{V_{SS0}} \tag{36}$$

If both the inequalities in Equation 32 and Equation 36 are met, then the FCS1 will provide a net energy benefit over FCS0. If $D_{FCS1} = D_{FCS0} = D_{SS}$, then the inequalities express the same condition. If one inequality is met and the other is not, the FCS1 will not have a benefit over FCS0 because ballast or floats must be added to maintain the same overall FCEPS density with FCS1 as with FCS0.

Additional FCS Components

Mass of FCEPS must not change:

$$m_{New} = \left(m_{SS0} - m_{SS1} \right) + \left(m_{B0} - m_{B1} \right) \tag{37}$$

Volume of FCEPS must not change:

$$V_{New} = \left(V_{SS0} - V_{SS1} \right) + \left(V_{B0} - V_{B1} \right) \tag{38}$$

Assume Storage System density does not change:

$$D_{SS} = \frac{m_{SS1}}{V_{SS1}} = \frac{m_{SS0}}{V_{SS0}} \tag{39}$$

Assume ballast/float density does not change:

$$D_B = \frac{m_{B1}}{V_{B1}} = \frac{m_{B0}}{V_{B0}} \tag{40}$$

The density of the new component is:

$$D_{New} = \frac{m_{New}}{V_{New}} \tag{41}$$

Determine new energy storage volume:
Equations 37, 39, 40→

$$m_{New} = D_{SS}\left(V_{SS0} - V_{SS}\right) + D_B\left(V_{B0} - V_{B1}\right) \tag{42}$$

$$V_{B0} - V_{B1} = \frac{m_{New} - D_{SS}\left(V_{SS0} - V_{SS1}\right)}{D_B} \tag{43}$$

Equation 43 →

$$V_{SS0} - V_{SS1} = V_{New} - \left(\frac{m_{New} - D_{SS}\left(V_{SS0} - V_{SS1}\right)}{D_B}\right) \tag{44}$$

$$V_{SS0} - V_{SS1} = V_{New} - \frac{m_{New}}{D_B} + \frac{D_{SS}}{D_B}\left(V_{SS0} - V_{SS1}\right) \tag{45}$$

$$\left(V_{SS0} - V_{SS1}\right)\left(1 - \frac{D_{SS}}{D_B}\right) = V_{New} - \frac{m_{New}}{D_B} \tag{46}$$

$$\left(V_{SS0} - V_{SS1}\right)\left(1 - \frac{D_{SS}}{D_B}\right) = V_{New}\left(1 - \frac{D_{New}}{D_B}\right) \tag{47}$$

$$V_{SS1} = V_{SS0} - V_{New}\frac{\left(1 - \frac{D_{New}}{D_B}\right)}{\left(1 - \frac{D_{SS}}{D_B}\right)} \tag{48}$$

$$V_{SS1} = V_{SS0} - V_{New}\frac{\left(D_B - D_{New}\right)}{\left(D_B - D_{SS}\right)} \tag{49}$$

If this condition is met, then the new component or system enhancement will provide an energy storage benefit:

$$\varepsilon_{FCS1} E_{SS1} > \varepsilon_{FCS0} E_{SS0} \tag{50}$$

Assume Energy Density of Storage System does not change:

$$\frac{E_{SS1}}{V_{SS1}} = \frac{E_{SS0}}{V_{SS0}} \tag{51}$$

Rewrite the condition in Equation 50:

$$\frac{\varepsilon_{FCS1}}{\varepsilon_{FCS0}} > \frac{E_{SS0}}{E_{SS1}} \tag{52}$$

Equations 51, 52 →

$$\frac{\varepsilon_{FCS1}}{\varepsilon_{FCS0}} > \frac{V_{SS0}}{V_{SS1}} \tag{53}$$

Equations 49, 53→

$$\frac{\varepsilon_{FCS1}}{\varepsilon_{FCS0}} > \frac{V_{SS0}}{V_{SS0} - V_{New}\dfrac{(D_B - D_{New})}{(D_B - D_{SS})}} \tag{54}$$

$$\frac{\varepsilon_{FCS1}}{\varepsilon_{FCS0}} > \frac{1}{1 - \dfrac{V_{New}}{V_{SS0}}\dfrac{(D_B - D_{New})}{(D_B - D_{SS})}} \tag{55}$$

$$1 - \frac{V_{New}}{V_{SS0}}\frac{(D_B - D_{New})}{(D_B - D_{SS})} > \frac{\varepsilon_{FCS0}}{\varepsilon_{FCS1}} \tag{56}$$

$$1 - \frac{\varepsilon_{FCS0}}{\varepsilon_{FCS1}} > \frac{V_{New}}{V_{SS0}}\frac{(D_B - D_{New})}{(D_B - D_{SS})} \tag{57}$$

Equivalent Specific Energy and Energy Density at Desired Density

$$D_B = \frac{m_B}{V_B} \tag{58}$$

$$D_{SS} = \frac{ED_{SS}}{SE_{SS}} \tag{59}$$

$$D_{SS} = \frac{m_{SS}}{V_{SS}} \tag{60}$$

Define the D_{SS_B} as the combined density of the Storage System and the required ballast/floats to bring the FCEPS to the desired density:

$$D_{SS\_B} = \frac{m_{SS} + m_B}{V_{SS} + V_B} \tag{61}$$

$$D_{SS\_B} = \frac{\frac{ED_{SS}}{SE_{SS}} V_{SS} + D_B V_B}{V_{SS} + V_B} \tag{62}$$

$$D_{SS\_B} = \frac{\frac{ED_{SS}}{SE_{SS}} + D_B \frac{V_B}{V_{SS}}}{1 + \frac{V_B}{V_{SS}}} \tag{63}$$

$$D_{SS\_B}\left(1 + \frac{V_B}{V_{SS}}\right) = \frac{ED_{SS}}{SE_{SS}} + D_B \frac{V_B}{V_{SS}} \tag{64}$$

$$\frac{V_B}{V_{SS}}\left(D_{SS\_B} - D_B\right) = \frac{ED_{SS}}{SE_{SS}} - D_{SS\_B} \tag{65}$$

$$\frac{V_B}{V_{SS}} = \frac{\frac{ED_{SS}}{SE_{SS}} - D_{SS\_B}}{D_{SS\_B} - D_B} \tag{66}$$

Define the SE_{SS_B} as the Specific Energy of the combined Storage System and the ballast/floats required to bring the FCEPS to the desired density:

$$SE_{SS\_B} = \frac{SE_{SS} \cdot m_{SS}}{m_{SS} + m_B} \tag{67}$$

Equations 58, 59, 60, 67→

$$SE_{SS\_B} = \frac{SE_{SS} \cdot m_{SS}}{\frac{ED_{SS}}{SE_{SS}} V_{SS} + D_B V_B} \tag{68}$$

Equations 59, 60, 68→

$$SE_{SS\_B} = \frac{ED_{SS}}{\frac{ED_{SS}}{SE_{SS}} + D_B \frac{V_B}{V_{SS}}} \tag{69}$$

Equations 66, 69→

$$SE_{SS\_B} = \frac{ED_{SS}}{\frac{ED_{SS}}{SE_{SS}} + D_B \frac{\frac{ED_{SS}}{SE_{SS}} - D_{SS\_B}}{D_{SS\_B} - D_B}} \tag{70}$$

$$SE_{SS\_B} = \frac{ED_{SS}\left(D_{SS\_B} - D_B\right)}{D_{SS}\left(D_{SS\_B} - D_B\right) + D_B\left(D_{SS} - D_{SS\_B}\right)} \tag{71}$$

$$SE_{SS\_B} = \frac{ED_{SS}\left(D_{SS\_B} - D_B\right)}{D_{SS}D_{SS\_B} - D_B D_{SS\_B}} \tag{72}$$

$$SE_{SS\_B} = \frac{ED_{SS}\left(1 - \frac{D_B}{D_{SS\_B}}\right)}{\left(D_{SS} - D_B\right)} \tag{73}$$

Make the following substitution, since D_{SS_B} is the desired Storage System density (it is desirable to have no ballast or floats required):

$$D_{SS\_Desired} = D_{SS\_B} \tag{74}$$

Equations 73, 74→

$$SE_{SS\_B} = \frac{ED_{SS}\left(1 - \frac{D_B}{D_{SS\_Desired}}\right)}{\left(D_{SS} - D_B\right)} \tag{75}$$

Equations 75, 3→

$$ED_{SS\_B} = SE_{SS\_B}D_{SS\_Desired} \tag{76}$$

Ballast/Float Sizing

$$m_{FCEPS} = m_{FCS} + m_O + m_B + m_{SS} \tag{77}$$

$$V_{FCEPS} = V_{FCS} + V_O + V_B + V_{SS} \tag{78}$$

Equations 58, 60, 77, 78→

$$m_{FCEPS} = m_{FCS} + m_O + D_B V_B + D_{SS}\left(V_{FCEPS} - V_{FCS} - V_O - V_B\right) \tag{79}$$

$$D_{SS}V_B - D_B V_B = m_{FCS} + m_O + D_{SS}\left(V_{FCEPS} - V_{FCS} - V_O\right) - m_{FCEPS} \tag{80}$$

$$V_B = \frac{m_{FCS} + m_O + D_{SS}\left(V_{FCEPS} - V_{FCS} - V_O\right) - m_{FCEPS}}{D_{SS} - D_B} \tag{81}$$

$$m_B = V_B D_B \tag{82}$$

Appendix B: Storage System Options

Symbol	Specific Energy (kWh/kg)	Energy Density (kWh/L)
A1	3.73	1.30
A2	3.73	1.24
A3	3.73	1.08
A4	3.69	1.32
A5	3.53	1.97
A6	3.00	1.05
A7	2.68	1.20
A8	2.67	1.06
A9	2.66	1.07
A10	2.40	1.19
A11	2.35	1.32
A12	2.28	1.28
A13	1.81	0.63
A14	1.79	1.08
A15	1.60	0.66
A16	1.53	0.93
A17	1.53	0.80
A18	1.49	1.11
A19	1.32	1.04
A20	1.26	0.65
A21	1.22	0.95
A22	1.13	0.75
A23	0.87	0.49
A24	0.86	0.44
A25	0.75	0.54
B1	3.73	1.15
B2	3.73	1.11
B3	3.73	0.98
B4	3.69	1.17
B5	3.53	1.65
B6	3.00	0.95
B7	2.68	1.08
B8	2.67	0.96
B9	2.66	0.97
B10	2.40	1.07
B11	2.35	1.17
B12	2.28	1.14
B13	1.81	0.59
B14	1.79	0.98
B15	1.60	0.62
B16	1.53	0.85
B17	1.53	0.75
B18	1.49	1.00
B19	1.32	0.95
B20	1.26	0.61
B21	1.22	0.87
B22	1.13	0.70
B23	0.87	0.47
B24	0.86	0.42
B25	0.75	0.51
C1	3.73	0.81
C2	3.73	0.79
C3	3.73	0.72
C4	3.69	0.82
C5	3.53	1.03
C6	3.00	0.70
C7	2.68	0.77
C8	2.67	0.71
C9	2.66	0.72
C10	2.40	0.77
C11	2.35	0.82
C12	2.28	0.80
C13	1.81	0.49
C14	1.79	0.72
C15	1.60	0.51
C16	1.53	0.65
C17	1.53	0.59
C18	1.49	0.73
C19	1.32	0.70
C20	1.26	0.50
C21	1.22	0.66
C22	1.13	0.55
C23	0.87	0.40
C24	0.86	0.37
C25	0.75	0.43
D1	3.73	0.77
D2	3.73	0.76
D3	3.73	0.69
D4	3.69	0.78
D5	3.53	0.97
D6	3.00	0.68
D7	2.68	0.74
D8	2.67	0.68
D9	2.66	0.69
D10	2.40	0.74
D11	2.35	0.78
D12	2.28	0.77
D13	1.81	0.47
D14	1.79	0.69
D15	1.60	0.49
D16	1.53	0.63
D17	1.53	0.57
D18	1.49	0.70
D19	1.32	0.68
D20	1.26	0.48
D21	1.22	0.64
D22	1.13	0.54
D23	0.87	0.39
D24	0.86	0.36
D25	0.75	0.42
E1	2.30	1.43
E2	2.30	1.37
E3	2.30	1.18
E4	2.29	1.47
E5	2.23	2.30
E6	2.00	1.13
E7	1.86	1.32
E8	1.85	1.15
E9	1.84	1.17
E10	1.72	1.31
E11	1.69	1.46
E12	1.65	1.41
E13	1.39	0.66
E14	1.38	1.17
E15	1.26	0.70
E16	1.22	1.00
E17	1.22	0.86
E18	1.19	1.21
E19	1.08	1.13
E20	1.04	0.68
E21	1.01	1.03
E22	0.95	0.79
E23	0.76	0.51
E24	0.76	0.46
E25	0.67	0.56
F1	1.87	1.05
F2	1.87	1.01
F3	1.87	0.90
F4	1.86	1.06
F5	1.82	1.44
F6	1.67	0.88
F7	1.56	0.98
F8	1.56	0.89
F9	1.55	0.90
F10	1.46	0.98
F11	1.44	1.06
F12	1.42	1.04
F13	1.22	0.56
F14	1.21	0.90
F15	1.12	0.59
F16	1.09	0.79
F17	1.09	0.70
F18	1.06	0.92
F19	0.98	0.88
F20	0.94	0.58
F21	0.92	0.81
F22	0.87	0.66
F23	0.71	0.45
F24	0.70	0.41
F25	0.63	0.49
G1	1.83	1.44
G2	1.83	1.38
G3	1.83	1.18
G4	1.82	1.47
G5	1.78	2.32
G6	1.63	1.14
G7	1.53	1.33
G8	1.53	1.16
G9	1.52	1.17
G10	1.44	1.31

G11	1.42	1.47	I5	1.53	1.75	J24	0.63	0.42	L18	0.88	0.49
G12	1.39	1.42	I6	1.42	0.98	J25	0.57	0.50	L19	0.82	0.48
G13	1.20	0.66	I7	1.35	1.12	K1	1.38	1.02	L20	0.80	0.38
G14	1.19	1.18	I8	1.34	1.00	K2	1.38	0.99	L21	0.78	0.46
G15	1.11	0.70	I9	1.34	1.01	K3	1.38	0.88	L22	0.74	0.41
G16	1.07	1.00	I10	1.27	1.11	K4	1.37	1.04	L23	0.62	0.32
G17	1.07	0.86	I11	1.26	1.22	K5	1.35	1.39	L24	0.62	0.30
G18	1.05	1.21	I12	1.24	1.19	K6	1.26	0.86	L25	0.56	0.34
G19	0.97	1.14	I13	1.08	0.61	K7	1.20	0.96	M1	1.27	0.47
G20	0.93	0.68	I14	1.08	1.01	K8	1.20	0.87	M2	1.27	0.46
G21	0.91	1.03	I15	1.00	0.64	K9	1.20	0.88	M3	1.27	0.44
G22	0.86	0.79	I16	0.98	0.88	K10	1.14	0.95	M4	1.27	0.47
G23	0.70	0.51	I17	0.98	0.77	K11	1.13	1.03	M5	1.25	0.53
G24	0.70	0.46	I18	0.96	1.04	K12	1.11	1.01	M6	1.17	0.43
G25	0.62	0.56	I19	0.89	0.98	K13	0.99	0.56	M7	1.12	0.45
H1	1.76	1.39	I20	0.86	0.62	K14	0.98	0.88	M8	1.12	0.43
H2	1.76	1.33	I21	0.84	0.90	K15	0.92	0.58	M9	1.12	0.44
H3	1.76	1.15	I22	0.79	0.71	K16	0.90	0.78	M10	1.07	0.45
H4	1.75	1.43	I23	0.66	0.48	K17	0.90	0.69	M11	1.06	0.47
H5	1.72	2.21	I24	0.65	0.43	K18	0.89	0.90	M12	1.04	0.47
H6	1.58	1.11	I25	0.59	0.52	K19	0.82	0.86	M13	0.93	0.34
H7	1.49	1.29	J1	1.41	1.11	K20	0.80	0.57	M14	0.93	0.44
H8	1.48	1.13	J2	1.41	1.07	K21	0.78	0.79	M15	0.87	0.35
H9	1.48	1.14	J3	1.41	0.95	K22	0.74	0.65	M16	0.85	0.41
H10	1.40	1.27	J4	1.41	1.13	K23	0.62	0.45	M17	0.85	0.38
H11	1.38	1.42	J5	1.39	1.57	K24	0.62	0.40	M18	0.84	0.44
H12	1.35	1.38	J6	1.30	0.92	K25	0.56	0.48	M19	0.78	0.43
H13	1.17	0.65	J7	1.23	1.04	L1	1.37	0.53	M20	0.76	0.34
H14	1.17	1.15	J8	1.23	0.93	L2	1.37	0.52	M21	0.75	0.41
H15	1.08	0.69	J9	1.23	0.95	L3	1.37	0.49	M22	0.71	0.37
H16	1.05	0.98	J10	1.17	1.03	L4	1.37	0.53	M23	0.60	0.29
H17	1.05	0.84	J11	1.16	1.13	L5	1.35	0.71	M24	0.60	0.28
H18	1.03	1.18	J12	1.14	1.10	L6	1.26	0.48	M25	0.54	0.31
H19	0.95	1.11	J13	1.01	0.58	L7	1.20	0.51	N1	1.26	0.60
H20	0.92	0.67	J14	1.00	0.95	L8	1.20	0.48	N2	1.26	0.59
H21	0.89	1.01	J15	0.94	0.61	L9	1.20	0.49	N3	1.26	0.55
H22	0.84	0.78	J16	0.92	0.83	L10	1.14	0.51	N4	1.26	0.61
H23	0.69	0.51	J17	0.92	0.73	L11	1.13	0.53	N5	1.24	0.59
H24	0.69	0.45	J18	0.90	0.97	L12	1.11	0.53	N6	1.16	0.54
H25	0.62	0.56	J19	0.84	0.92	L13	0.99	0.37	N7	1.11	0.58
I1	1.57	1.20	J20	0.81	0.60	L14	0.98	0.49	N8	1.11	0.55
I2	1.57	1.15	J21	0.79	0.85	L15	0.92	0.38	N9	1.11	0.55
I3	1.57	1.01	J22	0.75	0.68	L16	0.90	0.46	N10	1.06	0.58
I4	1.56	1.22	J23	0.63	0.46	L17	0.90	0.42	N11	1.05	0.61

N12	1.04	0.60
N13	0.93	0.40
N14	0.92	0.55
N15	0.87	0.42
N16	0.85	0.51
N17	0.85	0.47
N18	0.84	0.56
N19	0.78	0.54
N20	0.76	0.41
N21	0.74	0.52
N22	0.71	0.45
N23	0.60	0.34
N24	0.59	0.32
N25	0.54	0.36
O1	1.24	1.01
O2	1.24	0.98
O3	1.24	0.88
O4	1.24	1.03
O5	1.22	1.38
O6	1.15	0.85
O7	1.10	0.95
O8	1.10	0.86
O9	1.10	0.87
O10	1.05	0.95
O11	1.04	1.02
O12	1.03	1.00
O13	0.92	0.55
O14	0.91	0.87
O15	0.86	0.58
O16	0.84	0.77
O17	0.84	0.68
O18	0.83	0.89
O19	0.77	0.85
O20	0.75	0.57
O21	0.74	0.79
O22	0.70	0.64
O23	0.59	0.45
O24	0.59	0.40
O25	0.54	0.48
P1	1.23	0.47
P2	1.23	0.47
P3	1.23	0.44
P4	1.23	0.48
P5	1.21	0.54

P6	1.14	0.44
P7	1.09	0.46
P8	1.09	0.44
P9	1.09	0.44
P10	1.04	0.46
P11	1.03	0.48
P12	1.02	0.47
P13	0.91	0.34
P14	0.91	0.44
P15	0.85	0.35
P16	0.84	0.41
P17	0.84	0.39
P18	0.82	0.45
P19	0.77	0.44
P20	0.75	0.35
P21	0.73	0.42
P22	0.70	0.37
P23	0.59	0.30
P24	0.59	0.28
P25	0.53	0.31
Q1	1.22	0.45
Q2	1.22	0.44
Q3	1.22	0.42
Q4	1.21	0.45
Q5	1.19	0.51
Q6	1.13	0.41
Q7	1.08	0.44
Q8	1.08	0.42
Q9	1.07	0.42
Q10	1.03	0.44
Q11	1.02	0.45
Q12	1.01	0.45
Q13	0.90	0.33
Q14	0.90	0.42
Q15	0.85	0.34
Q16	0.83	0.39
Q17	0.83	0.37
Q18	0.82	0.42
Q19	0.76	0.41
Q20	0.74	0.33
Q21	0.73	0.40
Q22	0.69	0.36
Q23	0.59	0.29
Q24	0.58	0.27

Q25	0.53	0.30
R1	1.17	0.79
R2	1.17	0.77
R3	1.17	0.71
R4	1.17	0.80
R5	1.15	1.00
R6	1.09	0.69
R7	1.04	0.76
R8	1.04	0.70
R9	1.04	0.70
R10	1.00	0.75
R11	0.99	0.80
R12	0.97	0.79
R13	0.88	0.48
R14	0.87	0.71
R15	0.82	0.50
R16	0.81	0.64
R17	0.81	0.58
R18	0.79	0.72
R19	0.74	0.69
R20	0.72	0.49
R21	0.71	0.65
R22	0.68	0.55
R23	0.58	0.40
R24	0.57	0.36
R25	0.52	0.43
S1	1.07	0.89
S2	1.07	0.86
S3	1.07	0.78
S4	1.07	0.90
S5	1.05	1.16
S6	1.00	0.76
S7	0.96	0.84
S8	0.96	0.77
S9	0.96	0.78
S10	0.92	0.84
S11	0.91	0.90
S12	0.90	0.88
S13	0.82	0.52
S14	0.82	0.78
S15	0.77	0.54
S16	0.76	0.70
S17	0.76	0.63
S18	0.75	0.80

S19	0.70	0.76
S20	0.68	0.53
S21	0.67	0.71
S22	0.64	0.59
S23	0.55	0.42
S24	0.55	0.38
S25	0.50	0.45
T1	0.88	0.37
T2	0.88	0.36
T3	0.88	0.35
T4	0.88	0.37
T5	0.87	0.41
T6	0.84	0.34
T7	0.81	0.36
T8	0.81	0.35
T9	0.81	0.35
T10	0.78	0.36
T11	0.78	0.37
T12	0.77	0.37
T13	0.71	0.28
T14	0.70	0.35
T15	0.67	0.29
T16	0.66	0.33
T17	0.66	0.31
T18	0.65	0.35
T19	0.62	0.34
T20	0.60	0.29
T21	0.59	0.33
T22	0.57	0.30
T23	0.50	0.25
T24	0.49	0.24
T25	0.46	0.26
U1	0.79	1.55
U2	0.79	1.48
U3	0.79	1.26
U4	0.79	1.59
U5	0.78	2.63
U6	0.75	1.21
U7	0.73	1.42
U8	0.73	1.23
U9	0.73	1.24
U10	0.71	1.40
U11	0.70	1.58
U12	0.69	1.53

U13	0.64	0.69
U14	0.64	1.25
U15	0.62	0.72
U16	0.61	1.06
U17	0.61	0.90
U18	0.60	1.29
U19	0.57	1.20
U20	0.56	0.71
U21	0.55	1.09
U22	0.53	0.82
U23	0.47	0.53
U24	0.46	0.47
U25	0.43	0.58
V1	0.65	0.34
V2	0.65	0.34
V3	0.65	0.32
V4	0.65	0.34
V5	0.64	0.37
V6	0.62	0.32
V7	0.61	0.33
V8	0.61	0.32
V9	0.61	0.32
V10	0.59	0.33
V11	0.59	0.34
V12	0.59	0.34
V13	0.55	0.27
V14	0.55	0.32
V15	0.53	0.27
V16	0.52	0.31
V17	0.52	0.29
V18	0.52	0.33
V19	0.49	0.32
V20	0.49	0.27
V21	0.48	0.31
V22	0.46	0.28
V23	0.41	0.24
V24	0.41	0.23
V25	0.39	0.25
W1	0.51	0.52
W2	0.51	0.51
W3	0.51	0.48
W4	0.51	0.52
W5	0.51	0.61
W6	0.49	0.47

W7	0.48	0.50
W8	0.48	0.47
W9	0.48	0.48
W10	0.47	0.50
W11	0.47	0.52
W12	0.47	0.51
W13	0.44	0.36
W14	0.44	0.48
W15	0.43	0.37
W16	0.43	0.45
W17	0.43	0.42
W18	0.42	0.48
W19	0.41	0.47
W20	0.40	0.37
W21	0.40	0.45
W22	0.39	0.40
W23	0.35	0.31
W24	0.35	0.29
W25	0.33	0.33
X1	0.46	0.96
X2	0.46	0.93
X3	0.46	0.84
X4	0.46	0.97
X5	0.46	1.28
X6	0.45	0.81
X7	0.44	0.91
X8	0.44	0.82
X9	0.44	0.83
X10	0.43	0.90
X11	0.43	0.97
X12	0.43	0.95
X13	0.41	0.54
X14	0.41	0.83
X15	0.40	0.56
X16	0.39	0.74
X17	0.39	0.66
X18	0.39	0.85
X19	0.38	0.81
X20	0.37	0.55
X21	0.37	0.76
X22	0.36	0.62
X23	0.33	0.44
X24	0.33	0.39
X25	0.31	0.47

Y1	0.35	0.70
Y2	0.35	0.68
Y3	0.35	0.63
Y4	0.34	0.70
Y5	0.34	0.85
Y6	0.34	0.62
Y7	0.33	0.67
Y8	0.33	0.62
Y9	0.33	0.63
Y10	0.33	0.67
Y11	0.33	0.70
Y12	0.33	0.69
Y13	0.31	0.44
Y14	0.31	0.63
Y15	0.31	0.46
Y16	0.30	0.58
Y17	0.30	0.52
Y18	0.30	0.64
Y19	0.30	0.62
Y20	0.29	0.45
Y21	0.29	0.58
Y22	0.28	0.50
Y23	0.26	0.37
Y24	0.26	0.34
Y25	0.25	0.40
Z1	0.28	0.57
Z2	0.28	0.56
Z3	0.28	0.53
Z4	0.28	0.58
Z5	0.28	0.68
Z6	0.28	0.52
Z7	0.27	0.55
Z8	0.27	0.52
Z9	0.27	0.53
Z10	0.27	0.55
Z11	0.27	0.58
Z12	0.27	0.57
Z13	0.26	0.39
Z14	0.26	0.53
Z15	0.26	0.40
Z16	0.25	0.49
Z17	0.25	0.45
Z18	0.25	0.53
Z19	0.25	0.52

Z20	0.25	0.40
Z21	0.24	0.49
Z22	0.24	0.43
Z23	0.23	0.33
Z24	0.23	0.31
Z25	0.22	0.35
AA1	0.26	0.79
AA2	0.26	0.77
AA3	0.26	0.70
AA4	0.26	0.80
AA5	0.26	0.99
AA6	0.26	0.69
AA7	0.25	0.75
AA8	0.25	0.69
AA9	0.25	0.70
AA10	0.25	0.75
AA11	0.25	0.79
AA12	0.25	0.78
AA13	0.24	0.48
AA14	0.24	0.70
AA15	0.24	0.50
AA16	0.24	0.64
AA17	0.24	0.57
AA18	0.24	0.71
AA19	0.23	0.69
AA20	0.23	0.49
AA21	0.23	0.65
AA22	0.22	0.54
AA23	0.21	0.40
AA24	0.21	0.36
AA25	0.20	0.42
AB1	1.98	1.01
AB2	1.98	0.97
AB3	1.98	0.87
AB4	1.97	1.02
AB5	1.92	1.37
AB6	1.76	0.85
AB7	1.64	0.95
AB8	1.63	0.86
AB9	1.63	0.87
AB10	1.53	0.94
AB11	1.51	1.02
AB12	1.48	1.00
AB13	1.27	0.55

AB14	1.26	0.87
AB15	1.16	0.58
AB16	1.13	0.77
AB17	1.13	0.68
AB18	1.10	0.89
AB19	1.01	0.85
AB20	0.97	0.57
AB21	0.95	0.79
AB22	0.89	0.64
AB23	0.72	0.45
AB24	0.72	0.40
AB25	0.64	0.48
AC1	3.73	0.93
AC2	3.73	0.90
AC3	3.73	0.81
AC4	3.69	0.94
AC5	3.53	1.22

AC6	3.00	0.79
AC7	2.68	0.88
AC8	2.67	0.80
AC9	2.66	0.81
AC10	2.40	0.87
AC11	2.35	0.94
AC12	2.28	0.92
AC13	1.81	0.53
AC14	1.79	0.81
AC15	1.60	0.55
AC16	1.53	0.72
AC17	1.53	0.64
AC18	1.49	0.83
AC19	1.32	0.79
AC20	1.26	0.54
AC21	1.22	0.74
AC22	1.13	0.61

AC23	0.87	0.43
AC24	0.86	0.39
AC25	0.75	0.46
AD1	3.73	1.42
AD2	3.73	1.36
AD3	3.73	1.17
AD4	3.69	1.45
AD5	3.53	2.26
AD6	3.00	1.12
AD7	2.68	1.31
AD8	2.67	1.14
AD9	2.66	1.16
AD10	2.40	1.29
AD11	2.35	1.45
AD12	2.28	1.40
AD13	1.81	0.66
AD14	1.79	1.16

AD15	1.60	0.69
AD16	1.53	0.99
AD17	1.53	0.85
AD18	1.49	1.20
AD19	1.32	1.12
AD20	1.26	0.68
AD21	1.22	1.02
AD22	1.13	0.79
AD23	0.87	0.51
AD24	0.86	0.45
AD25	0.75	0.56

APPENDIX D

One-Dimensional Time-Domain Model of Hydrate Sample Dissociation

Nomenclature

A	decomposition area (m^2)
c_p	specific heat of hydrate (J/mol-K)
c_{pi}	specific heat of methanol (J/kg-K)
c_{pw}	specific heat of water (J/kg-K)
E	molar activation energy for hydrate dissociation (J/mol)
f	methane fugacity (Pa)
H	turbulent convective heat transfer coefficient (W/m^2-K)
k	hydrate heat conductivity (W/m-K)
K_0	hydrate dissociation constant (mol/m^2-Pa-s)
K_d	hydrate dissociation constant (mol/m^2-Pa-s)
L	hydrate sample length (m)
L_0	initial hydrate sample length (m)
LC	load cell reading (N)
LV	water level (m)
M_w	molar mass of water (kg/mol)
n	hydrate number
N	mole of hydrate (composition $CH_4.nH_2O$)
N_{gas}	mole of methane (from dissociation)
p	pressure (Pa)
p_{atm}	atmospheric pressure (Pa)
$p_{chamber}$	pressure in load cell container (Pa)
p_{core}	pressure in hydrate sample container (Pa)
p_{eq}	three-phase methane hydrate equilibrium pressure (Pa)
q_{inj}	mass injection rate for methanol solution (kg/s)
R	gas constant (J/mol-K)
s	methanol mass fraction
s_0	initial methanol mass fraction
t	time (s)
T	hydrate temperature (K)
T_0	initial hydrate temperature (K)
T_{eq}	three-phase methane hydrate equilibrium temperature (K)
T_{ref}	reference temperature (K)
T_{inj}	temperature of injected methanol solution (K)
T_s	hydrate decomposition temperature (K)
V_{ref}	reference ideal-gas molar volume (m^3)
z	vertical coordinate (m)
z_i	pseudo-vertical coordinate depending on L (m)

Greek

α	hydrate thermal diffusivity (m^2/s)
δf	driving fugacity difference in intrinsic decomposition rate (Pa)
δLC	load cell correction from liquid injection effect (N)

δLV water level correction from liquid injection effect (m)
λ hydrate heat of dissociation (J/mol)
ρ hydrate density (mol/m^3)
ρ_{inj} density of injected methanol solution (mol/m^3)
θ bulk liquid temperature (K)
υ flow rate anomaly during liquid injection (m^3/s)

Approach

A cylindrical hydrate sample of molar composition $CH_4.nH_2O$ is assumed to be isolated except for its upper surface A. At time t = 0, injection of an inhibitor solution triggers hydrate dissociation on the surface A. Injection and the release of water initially bound in the hydrate will generate a bulk liquid phase overlying the shrinking hydrate sample. The modeled situation is illustrated in Figure 1. Since the side walls are assumed to be adiabatic and the sample has radial symmetry, it is reasonable to consider the problem with only one spatial variable (vertical coordinate z).

Kim *et al.* (1987) proposed an intrinsic hydrate dissociation mechanism taking place in a desorption layer at the hydrate surface. Accordingly, they defined a dissociation rate in well-stirred isothermal experiments where dissociation is induced by depressurization:

$$\frac{dN}{dt} = -K_d A\{f[p_{eq}(T_s;s),T_s] - f(p,T_s)\} \tag{1}$$

where $K_d = K_0 \exp(-\frac{E}{RT_s})$. Note that the equilibrium pressure is shown to parametrically depend on inhibitor mass fraction s if an inhibitor solution is used.

Clarke and Bishnoi (2001) recently improved the measurement procedure of Kim *et al.* (1987) for the two parameters needed in this formulation (a basic constant K_0 and a molar activation energy E).

Jamaluddin *et al.* (1989) suggested that the same formalism was applicable when hydrates are dissociated at constant pressure. The definition of the driving fugacity difference, shown as δf in Figure 2, leads to some ambiguity, however, since there is no obvious physical meaning for $p_{eq}(T_s)$ in this case. The approach of Jamaluddin *et al.* (1989) was nevertheless followed in the present analysis, even though its general applicability (when hydrates are not dissociated by depressurization) has never, to our knowledge, been verified.

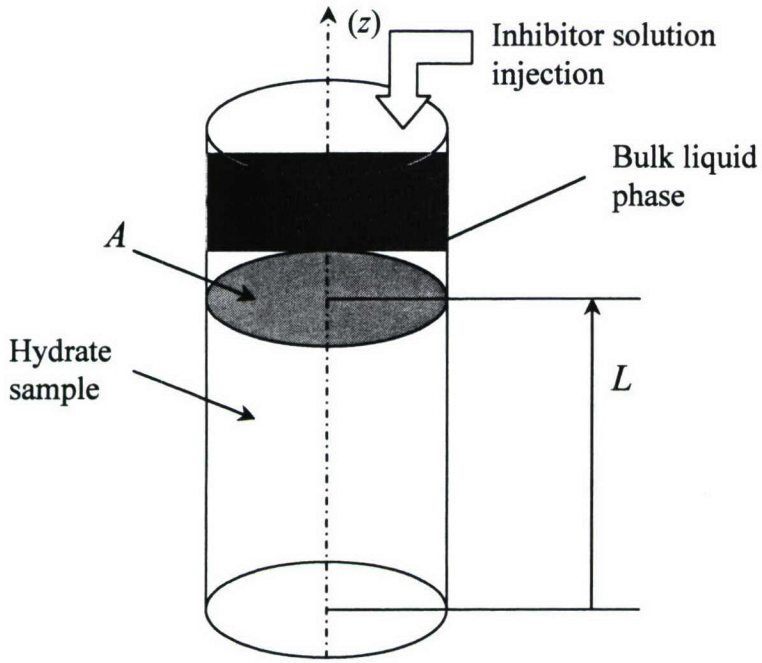

Figure 1. Schematic of the modeled experimental setup

Assuming that the hydrate decomposition area is the same as the sample geometric upper surface area, we also have the relationship:

$$\frac{dN}{dt} = \rho A \frac{dL}{dt} \tag{2}$$

Heat conduction within the hydrate sample is governed by the following partial differential equation:

$$\frac{\partial T}{\partial t} = \alpha \frac{\partial^2 T}{\partial z^2} \tag{3}$$

where the thermal diffusivity is $\alpha = \frac{k}{\rho c_p}$.

The boundary conditions are $\frac{\partial T}{\partial t}(0) = 0$ and $T(L) = T_s$.

The solution for Equation (3) and its boundary conditions requires knowledge of both unknowns L and T_s. Equations (1) and (2) provides a first relationship between L and T_s. Another may be derived from a heat balance at the hydrate decomposition front:

$$-k \frac{\partial T}{\partial z}(L) + H(\theta - T_s) = -\lambda \rho \frac{dL}{dt} \tag{4}$$

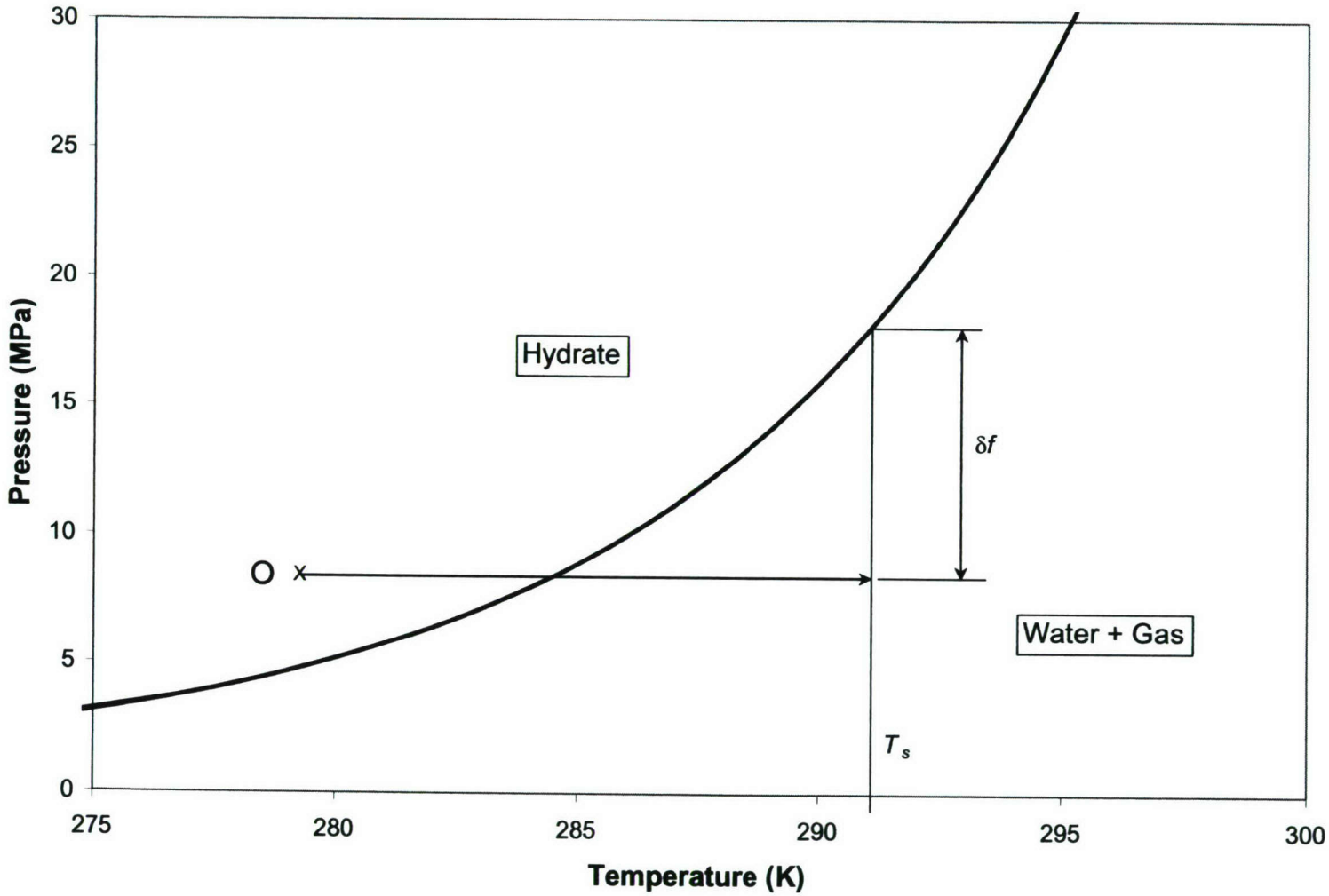

Figure 2. Definition of the driving fugacity difference δf in the intrinsic hydrate decomposition model

For practical numerical purposes, a combination of Equations (1), (2), and (4), shown below, is used as an implicit equation in T_s:

$$-k\frac{\partial T}{\partial z}(L)+H(\theta-T_s)-\lambda K_0\exp(-\frac{E}{RT_s})\{f[p_{eq}(T_s;s),T_s]-f(p,T_s)\}=0 \tag{5}$$

The bulk liquid phase is considered to be well mixed, and heat transfer with the hydrate decomposition surface is represented with a simple convective term $H(\theta - T_s)$.

The mass fraction of inhibitor (e.g., methanol) as a function of time is available from an elementary mass balance:

$$s=\frac{s_0\int q_{inj}dt}{\int q_{inj}dt+nM_w\rho A(L_0-L)} \tag{6}$$

To close the problem, the bulk temperature θ must be determined. At any time, the enthalpy of the bulk liquid phase is

$$\theta\{[c_{pi}s_0+c_{pw}(1-s_0)]\int q_{inj}dt+c_{pw}nM_w\rho A(L_0-L)\}$$

Its time derivative must be equal to the enthalpy change per unit time given by the expression below:

$$-c_{pw}nM_w\rho AT_s\frac{dL}{dt}+[c_{pi}s_0+c_{pw}(1-s_0)]q_{inj}T_{inj}$$

This procedure (considering the temperature dependence of the specific heats as negligible) leads to the following equation:

$$\frac{d\theta}{dt}=\frac{[c_{pi}s_0+c_{pw}(1-s_0)]q_{inj}(T_{inj}-\theta)-c_{pw}nM_w\rho A(T_s-\theta)\frac{dL}{dt}}{[c_{pi}s_0+c_{pw}(1-s_0)]\int q_{inj}dt+c_{pw}nM_w\rho A(L_0-L)} \tag{7}$$

The solution procedure is adapted from Jamaluddin *et al.* (1989) who considered hydrate decomposition from a constant supply of radiant heat. It involves a discretization of Equation (3) using pseudo-coordinates z_i proportional to L within the hydrate sample. This yields a number of (time) first-order ordinary differential equations (ODEs). Replacing z with the pseudo-coordinates, however, gives rise to advective terms of the

form $\frac{dz_i}{dt}\frac{\partial}{\partial z_i}$ in the right-hand-sides of the ODEs. This was not accounted for in Jamaluddin *et al.* (1989). An ODE for L is available, e.g., as a combination of Equations (1) and (2), and Equation (7) is an ODE for θ. At each time step, s is given by Equation (6) and T_s by solving Equation (5). The complete system of ODEs can be solved with a standard fourth-order Runge-Kutta scheme.

Initial conditions, sample geometry and injection characteristics must be provided. Other parameters are typical estimates from the literature. No attempt has yet been made to constrain the heat transfer coefficient H (inferred order of magnitude from 100s to 1000s).

The value measured by the Coriolis flow meter in our destabilization experiments is proportional1 to $\frac{dN_{gas}}{dt} = -\frac{dN}{dt}$ while the cumulative values derived from both water level and load cell are proportional[1] to $N_{gas} = \rho A(L_0 - L)$.

Data Reduction Protocol

One of the features of our hydrate destabilization apparatus is the redundancy provided for measurement of the amount of evolved gas released during hydrate dissociation. This is done directly by a Coriolis flow meter and indirectly via water level and load cell measurements. A primary objective of the experiments conducted during the present reporting period was to elucidate the kinetics of hydrate dissociation in the presence of thermodynamic inhibitors such as methanol. Ideally, modeling activities can help formalize underlying physical processes. In the previous Section, a simple analytical model conceived for such a purpose was described in some detail. Before any attempt is made to compare data and model predictions, however, raw data must be reduced to a proper form.

One issue with the injection of a liquid methanol solution is that when q_{inj} is not zero, a volume of gas is displaced from the headspace overlying the hydrate sample. This occurs *per se*, whether concurrent hydrate dissociation takes place or not. Such an extraneous contribution must be evaluated precisely and subtracted from the data records. To complicate matters, the range of direct measurements from the Coriolis flow meter could not exceed about 1.1 standard2 liter per minute (slpm). Therefore, information from this instrument was not available at times of higher cumulative gas release which roughly coincided with methanol injection.

---

1 Methane absorbed in any undersaturated liquid phase is neglected

2 standard conditions correspond to atmospheric pressure p_{atm} = 101325 Pa and to a temperature T_{ref} = 273.15 K; this yields an ideal-gas molar volume V_{ref} of 22.414 liters.

The calibration to correct for displaced gas is greatly facilitated by the existence of data collected on November 8, 2005 (Record # 051108) when distilled water was injected and no detectable hydrate dissociation took place. The response of the load cell and level indicator can entirely be ascribed to the gas displacement effect from liquid injection. Neglecting small temperature differences between the container holding the hydrate core sample and the chamber where the load cell and water level indicator are located, the volume flow rate anomaly υ corresponding to liquid injection simply is:

$$\upsilon = \frac{q_{inj}\, p_{core}}{\rho_{inj}\, p_{chamber}} \tag{8}$$

where ρ_{inj} is the density of the injected liquid.

Calling LV the water level time history, the following equality holds for Record # 051108:

$$LV(t)-LV(0) = \{LV(\infty)-LV(0)\}\frac{\int q_{inj}\,dt}{\int^{\infty} q_{inj}\,dt} \tag{9}$$

The same equation is valid for the load time history LC and Record # 051108.

Figure 3 shows excellent agreement between measured values of $LV(t)$ - $LV(0)$ and Equation (9). It should be noted, however, that a residual background injection signal of about 0.06 g/s must be removed from the injection data. This 'leakage' was observed for all records.

By virtue of Equations (8) and (9), the following water level correction term δLV should be subtracted from the water level time history of any record:

$$\delta LV(t) = [\frac{\{LV(\infty)-LV(0)\}\rho_{inj}\, p_{chamber}}{p_{core}\int^{\infty} q_{inj}\,dt}]_{051108}\frac{p_{core}}{\rho_{inj}\, p_{chamber}}\int q_{inj}\,dt \tag{10}$$

A similar formula is applicable to load cell data. In Equations (9) and (10), pressures are assumed steady enough to be 'averaged' out of the time integrals. Liquid density was linearly approximated between 786 kg/m^3 for pure methanol (MEOH) and 1000 kg/m^3 for pure water. Typical values of record parameters are shown in Table 1.

Figures 4a and 4b display the corrected water level and load cell time series obtained by subtracting δLV and δLC, respectively, from the raw data for Record # 051028. Figures 5a and 5b are similar for Record # 050930, and Figures 6a and 6b for Record # 051003.

Table 1. Selected Record Parameters

Record # (date)	MEOH (% volume)	s_0	ρ_{inj} (kg/m^3)	$p_{chamber} - p_{atm}$ (psig)	$p_{core} - p_{atm}$ (psig)	T_0 (°C)	T_{inj} (°C)
051108	0	0	1000	733	715	4	4
051028	25	0.208	946.5	734	730	4	4
051031	25	0.208	946.5	735	730	4	4
050930	50	0.440	893	732	800	4	7
051003	75	0.702	840	732	800	4	10
051012	100	1	786	736	730	4	10

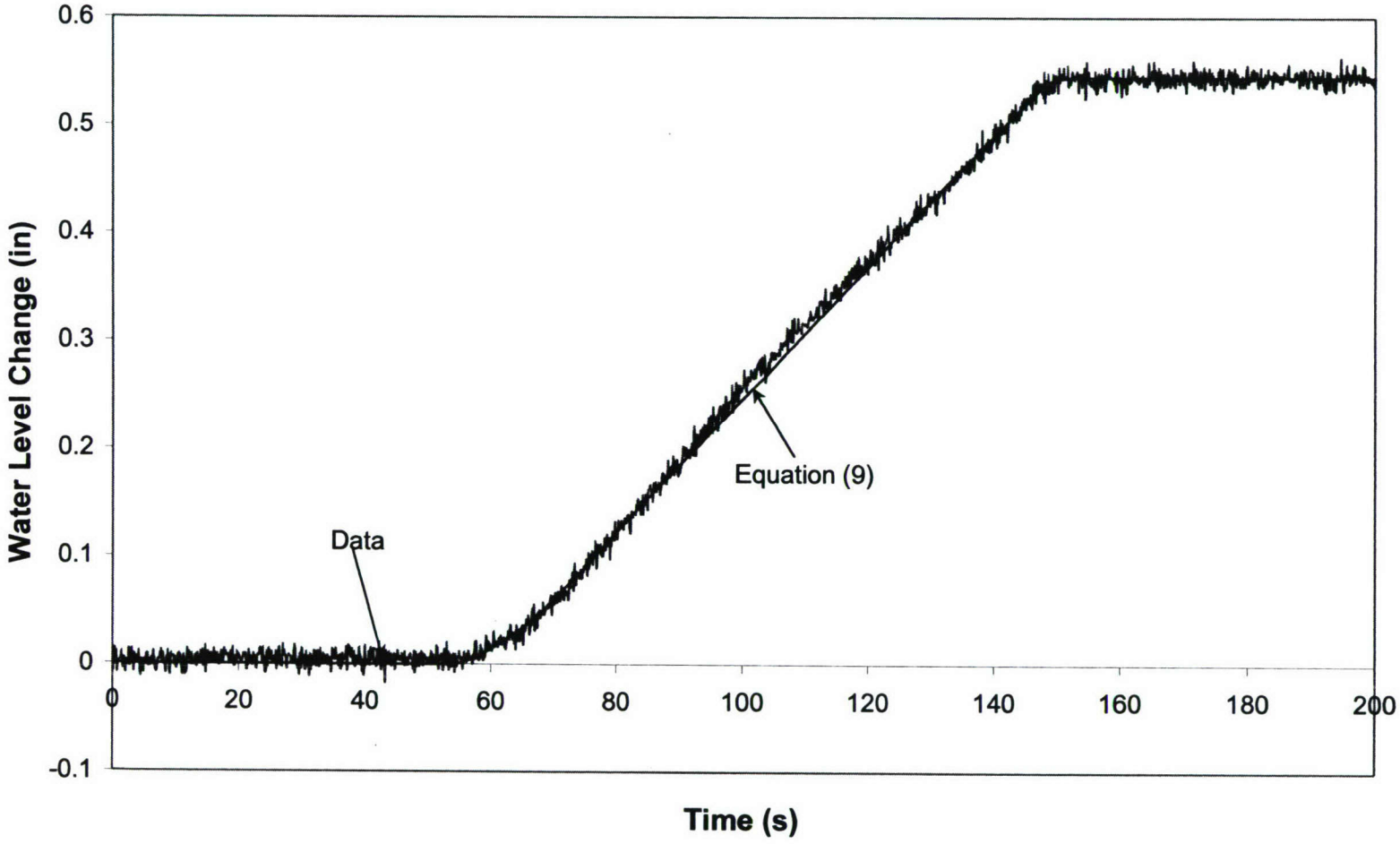
Record # 051108
Water Level Change (in)
0.6
0.5
0.4
0.3
0.2
0.1
0
-0.1
0
20
40
60
80
100
120
140
160
180
200
Time (s)
Data
Equation (9)

Figure 3

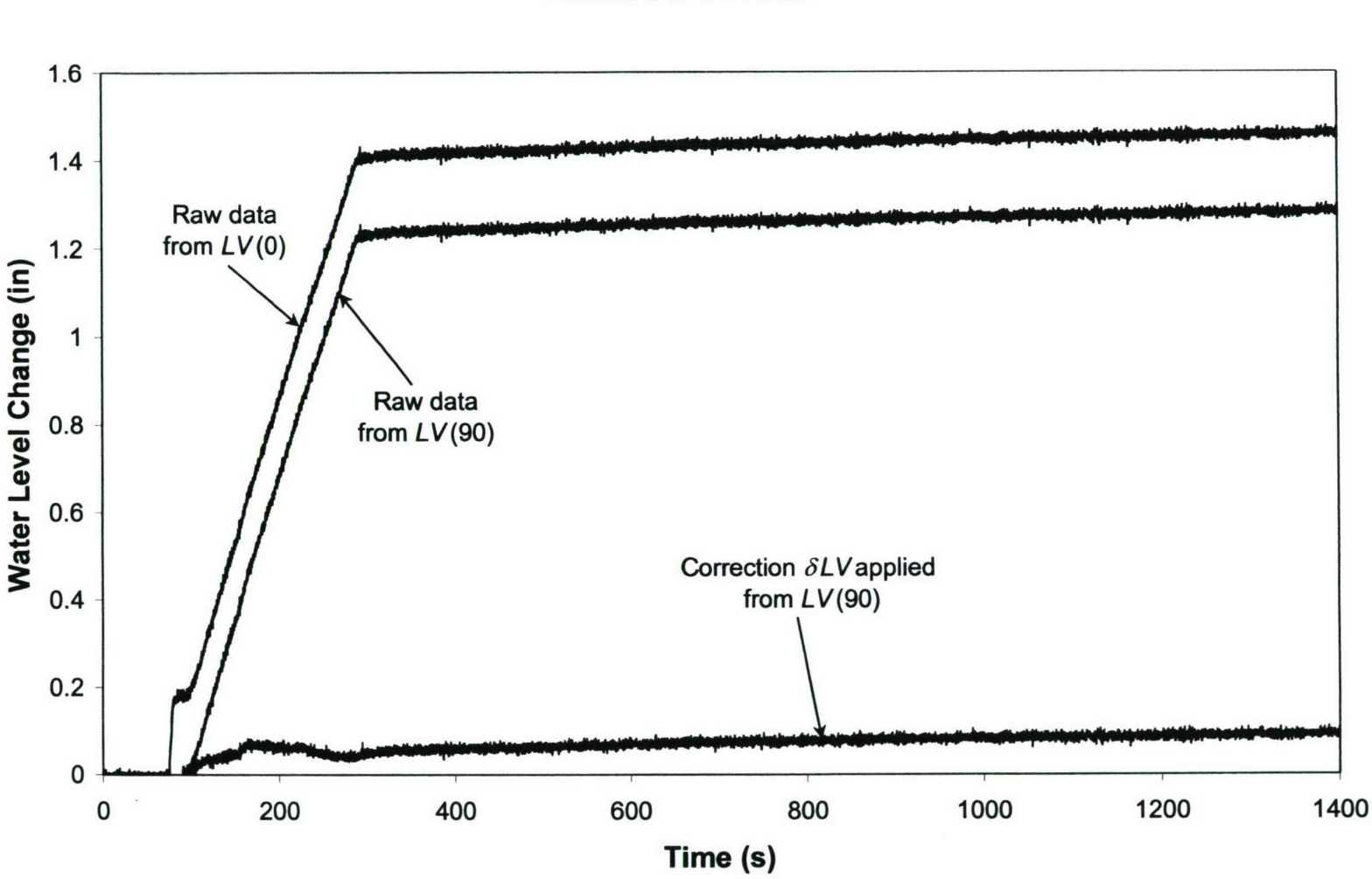
Record # 051028
Water Level Change (in)
Time (s)
Raw data from LV(0)
Raw data from LV(90)
Correction δLV applied from LV(90)
0
0.2
0.4
0.6
0.8
1
1.2
1.4
1.6
0
200
400
600
800
1000
1200
1400

Figure 4a

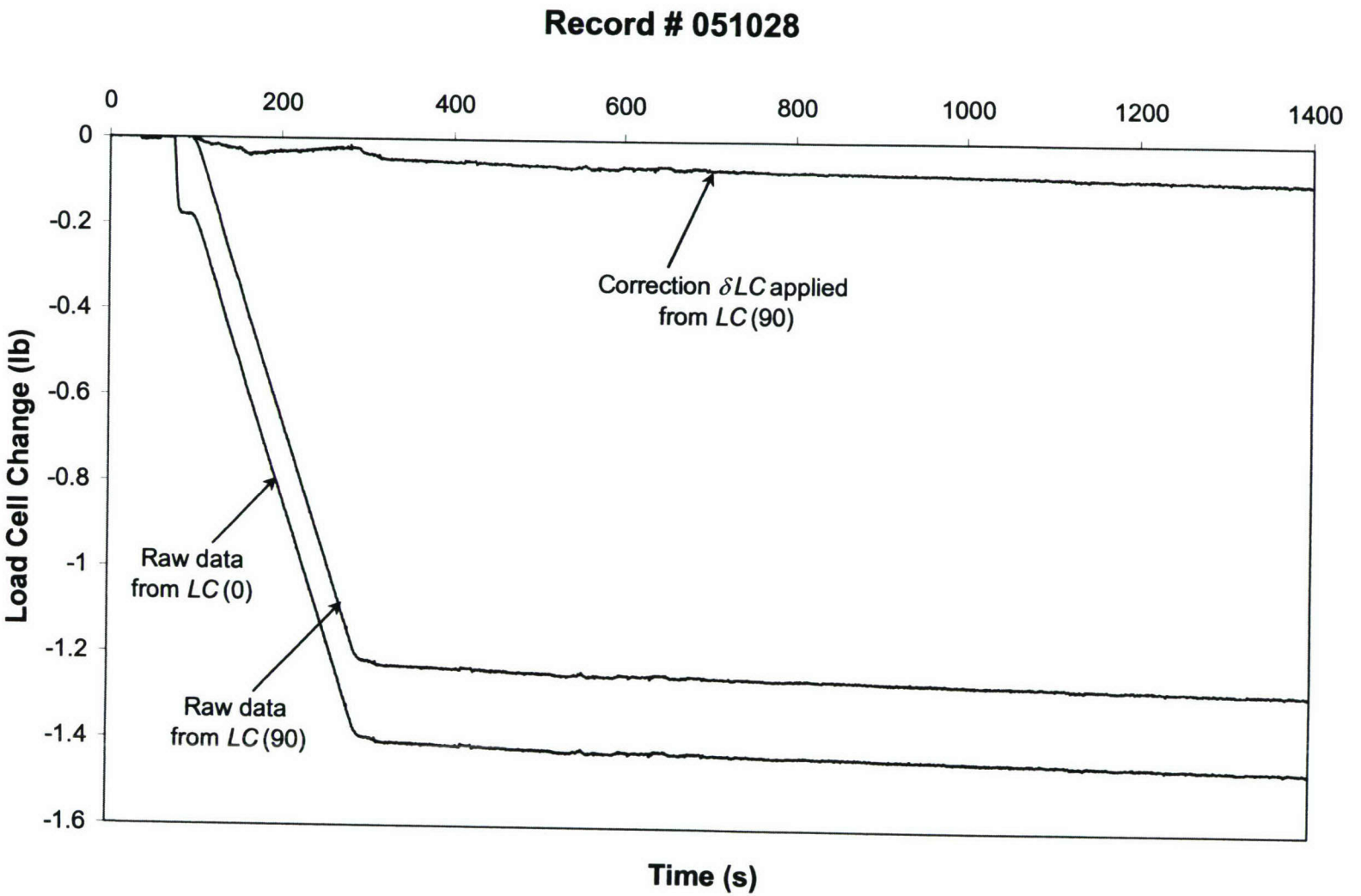
Record # 051028
0
200
400
600
800
1000
1200
1400
0
-0.2
-0.4
-0.6
-0.8
-1
-1.2
-1.4
-1.6
Load Cell Change (lb)
Correction δLC applied
from LC(90)
Raw data
from LC(0)
Raw data
from LC(90)
Time (s)

Figure 4b

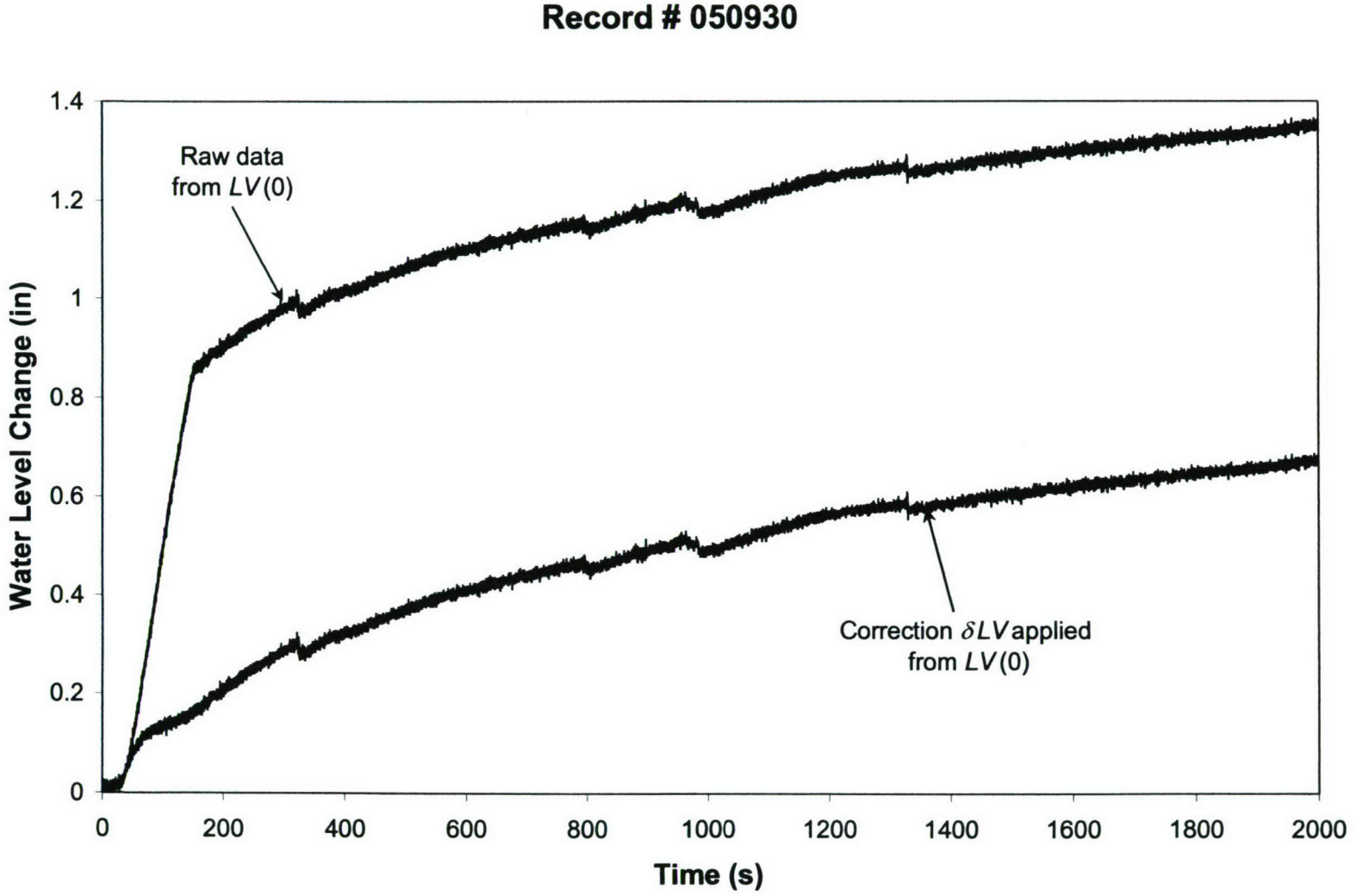
Record # 050930
Raw data
from LV(0)
Correction δLV applied
from LV(0)
Water Level Change (in)
Time (s)
0
0.2
0.4
0.6
0.8
1
1.2
1.4
0
200
400
600
800
1000
1200
1400
1600
1800
2000

Figure 5a

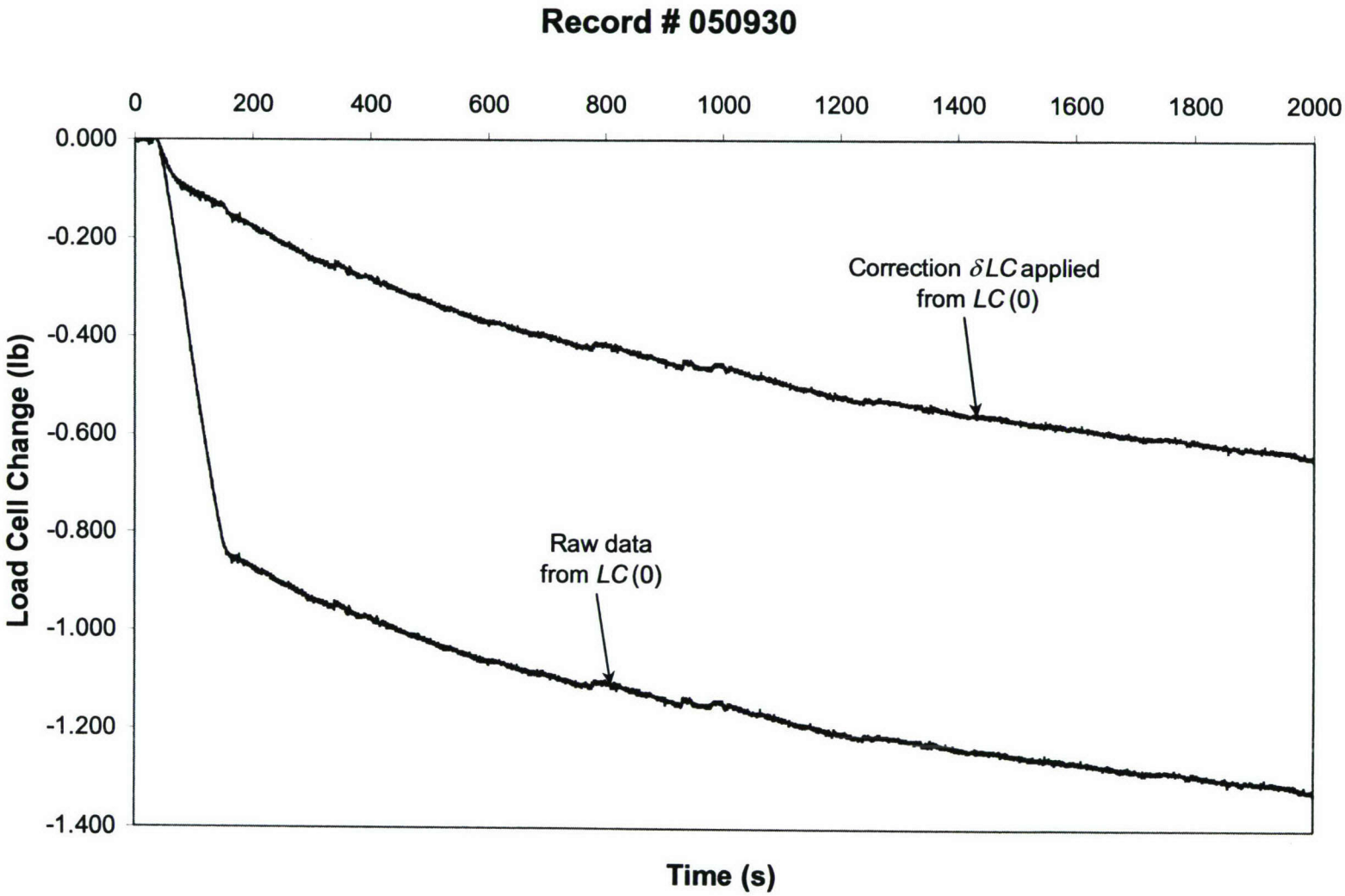
Record # 050930
0
200
400
600
800
1000
1200
1400
1600
1800
2000
0.000
-0.200
-0.400
-0.600
-0.800
-1.000
-1.200
-1.400
Load Cell Change (lb)
Correction δLC applied
from LC(0)
Raw data
from LC(0)
Time (s)

Figure 5b

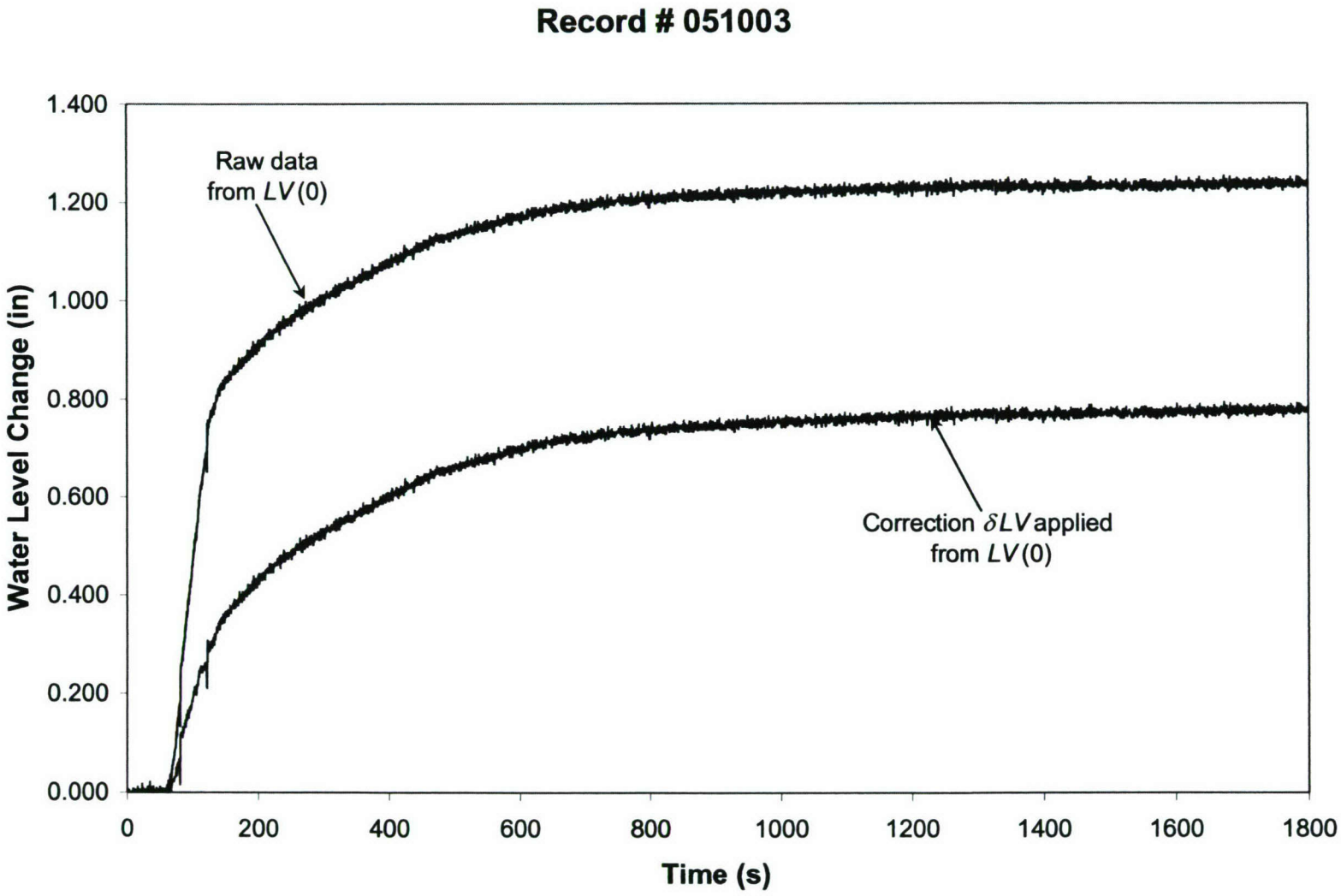
Record # 051003
Water Level Change (in)
1.400
1.200
1.000
0.800
0.600
0.400
0.200
0.000
Raw data
from LV(0)
Correction δLV applied
from LV(0)
0
200
400
600
800
1000
1200
1400
1600
1800
Time (s)

Figure 6a

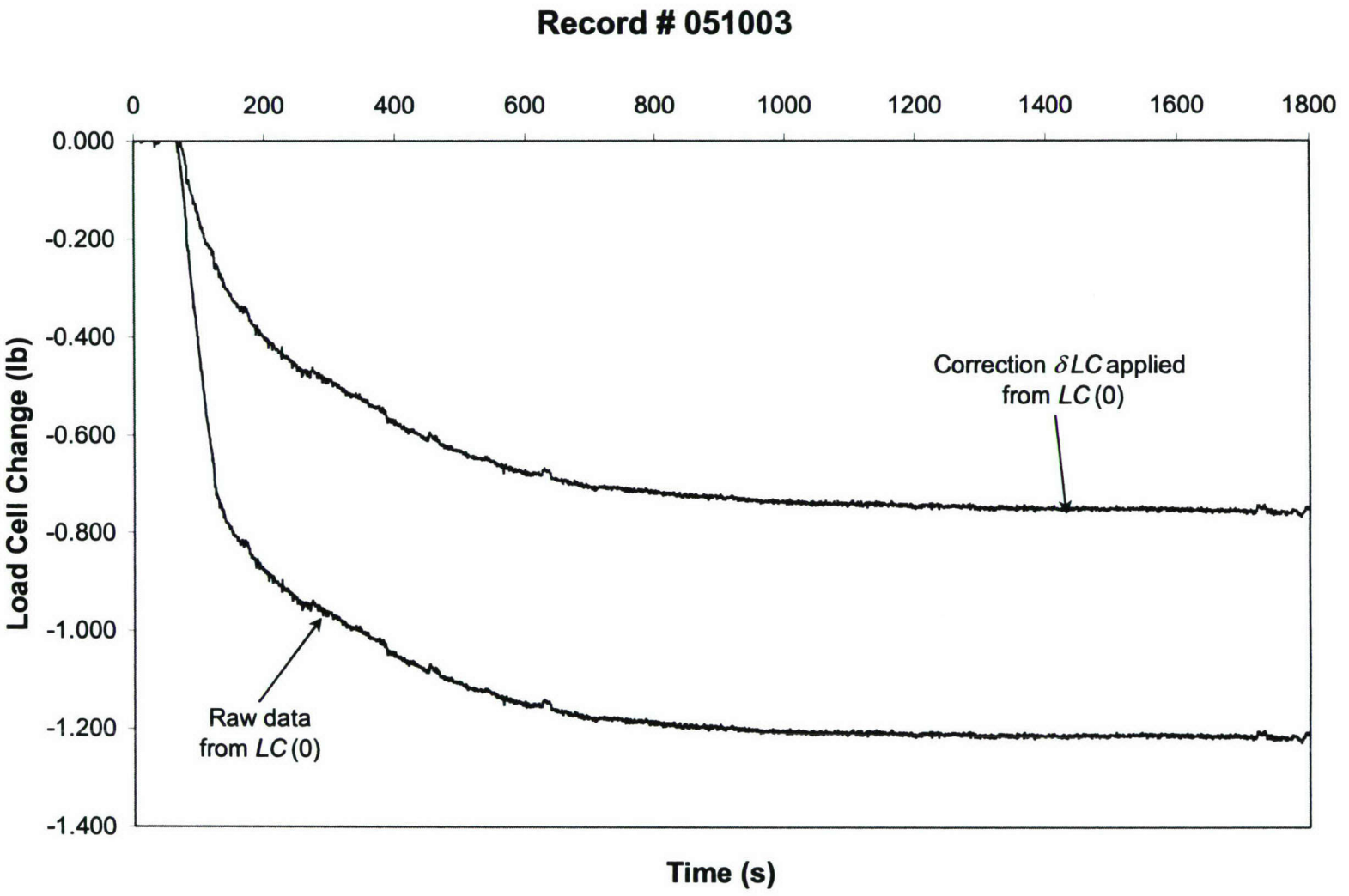
Record # 051003
0
200
400
600
800
1000
1200
1400
1600
1800
0.000
-0.200
-0.400
-0.600
-0.800
-1.000
-1.200
-1.400
Load Cell Change (lb)
Correction δLC applied
from LC(0)
Raw data
from LC(0)
Time (s)

Figure 6 b